Melting and Crystallization Behavior of Linear Low-Density Polyethylene

Lijun Feng

Department of Chemical Engineering
McGill University, Montreal, Quebec, Canada

August 2004

A thesis submitted to the Faculty of Graduate Studies and Research in partial fulfillment of the requirements for the Degree of Doctor of Philosophy

Library and
Archives Canada

Published Heritage
Branch

395 Wellington Street
Ottawa ON K1A 0N4
Canada

Bibliothèque et
Archives Canada

Direction du
Patrimoine de l'édition

395, rue Wellington
Ottawa ON K1A 0N4
Canada

Your file Votre référence
ISBN: 978-0-494-22810-4
Our file Notre référence
ISBN: 978-0-494-22810-4

NOTICE:
The author has granted a non-exclusive license allowing Library and Archives Canada to reproduce, publish, archive, preserve, conserve, communicate to the public by telecommunication or on the Internet, loan, distribute and sell theses worldwide, for commercial or non-commercial purposes, in microform, paper, electronic and/or any other formats.

The author retains copyright ownership and moral rights in this thesis. Neither the thesis nor substantial extracts from it may be printed or otherwise reproduced without the author's permission.

AVIS:
L'auteur a accordé une licence non exclusive permettant à la Bibliothèque et Archives Canada de reproduire, publier, archiver, sauvegarder, conserver, transmettre au public par télécommunication ou par l'Internet, prêter, distribuer et vendre des thèses partout dans le monde, à des fins commerciales ou autres, sur support microforme, papier, électronique et/ou autres formats.

L'auteur conserve la propriété du droit d'auteur et des droits moraux qui protège cette thèse. Ni la thèse ni des extraits substantiels de celle-ci ne doivent être imprimés ou autrement reproduits sans son autorisation.

In compliance with the Canadian Privacy Act some supporting forms may have been removed from this thesis.

While these forms may be included in the document page count, their removal does not represent any loss of content from the thesis.

Conformément à la loi canadienne sur la protection de la vie privée, quelques formulaires secondaires ont été enlevés de cette thèse.

Bien que ces formulaires aient inclus dans la pagination, il n'y aura aucun contenu manquant.

Canada

Foreword

According to the thesis preparation guideline of the Faculty of Graduates Studies and Research, McGill University, I choose the manuscript-based thesis option.

As an alternative to the traditional thesis format, the dissertation can consist of a collection of papers of which the student is an author or co-author. These papers must have a cohesive, unitary character making them a report of a single program of research. The structure for the manuscript-based thesis must conform to the following:

1. Candidates have the option of including, as part of the thesis, the text of one or more papers submitted, or to be submitted, for publication, or the clearly-duplicated text (not the reprints) of one or more published papers. These texts must conform to the "Guidelines for Thesis Preparation" with respect to font size, line spacing and margin sizes and must be bound together as an integral part of the thesis. (Reprints of published papers can be included in the appendices at the end of the thesis.)

2. The thesis must be more than a collection of manuscripts. All components must be integrated into a cohesive unit with a logical progression from one chapter to the next. In order to ensure that the thesis has continuity, connecting texts that provide logical bridges preceeding and following each manuscript are mandatory.

3. The thesis must conform to all other requirements of the "Guidelines for Thesis Preparation" in addition to the manuscripts.

The thesis must include the following:

1. *a table of contents;*
2. *a brief abstract in both English and French;*
3. *an introduction which clearly states the rational and objectives of the research;*
4. *a comprehensive review of the literature (in addition to that covered in the introduction to each paper);*
5. *a final conclusion and summary;*
6. *a thorough bibliography;*
7. *Appendix containing an ethics certificate in the case of research involving human or animal subjects, microorganisms, living cells, other biohazards and/or radioactive material.*

4. As manuscripts for publication are frequently very concise documents, where appropriate, additional material must be provided (e.g., in appendices) in sufficient detail to allow a clear and precise judgement to be made of the importance and originality of the research reported in the thesis.

5. In general, when co-authored papers are included in a thesis the candidate must have made a substantial contribution to all papers included in the thesis. In addition, the candidate is required to make an explicit statement in the thesis as to who contributed to *such work and to what extent. This statement should appear in a single section entitled "Contributions of Authors" as a preface to the thesis. The supervisor must attest to the accuracy of this statement at the doctoral oral defence. Since the task of the examiners is made more difficult in these cases, it is in the candidate's interest to clearly specify the responsibilities of all the authors of the co-authored papers.*

6. *When previously published copyright material is presented in a thesis, the candidate must include signed waivers from the publishers and submit these to the Graduate and Postdoctoral Studies Office with the final deposition, if not submitted previously. The candidate must also include signed waivers from any co-authors of unpublished manuscripts.*
7. *Irrespective of the internal and external examiners reports, if the oral defence committee feels that the thesis has major omissions with regard to the above guidelines, the candidate may be required to resubmit an amended version of the thesis. See the "Guidelines for Doctoral Oral Examinations," which can be obtained from the web (http://www.mcgill.ca/fgsr), Graduate Secretaries of departments or from the Graduate and Postdoctoral Studies Office, James Administration Building, Room 400, 398-3990, ext. 00711 or 094220.*
8. *In no case can a co-author of any component of such a thesis serve as an external examiner for that thesis.*

Chapters 2 to 8 of this thesis include and/or revise the texts of papers published, and/or submitted for publication. These papers were prepared under normal supervision of my research supervisor, Professor Musa R. Kamal, who is the coauthor in all of the papers. In Chapter 2, Dr. T. Huang gave me important suggestions, who is also the coauthor of the corresponding publication.

I, Musa R. Kamal, hereby give copyright clearance for inclusion of the following papers, of which I am the co-author, in the dissertation of Lijun Feng.

1. Kamal, Musa R.; Feng, Lijun; Huang, Tao "A Generalized Equation for the Prediction of Melting Temperatures of Homopolymers and Copolymers", *The Canadian Journal of Chemical Engineering* **2002**, 80(3), 432-442.
2. Feng, Lijun; Kamal, Musa R. "Distributions of Crystal Size from DSC Melting Traces for Polyethylenes", *The Canadian Journal of Chemical Engineering* **2004**, accepted for publication.
3. Feng, Lijun; Kamal, Musa R. "Melting Temperature Characteristics for Polyethylenes from Crystal Size Distribution", *Themochimica Acta* **2004**, submitted for publication.
4. Feng, Lijun; Kamal, Musa R. "Spherulitic Crystallization Behavior of Linear Low-Density Polyethylene", *Polymer Engineering and Science* **2004**, accepted for publication.
5. Kamal, Musa R.; Feng, Lijun "Non-linear Crystalline Spherulitic Growth Behavior for Linear Low-Density Polyethylene", *International Polymer Processing* **2004**, accepted for publication.
6. Feng, Lijun; Kamal, Musa R. "Crystallization and Melting Behavior of Homogeneous and Heterogeneous Linear Low-density Polyethylenes", *Polymer Engineering and Science* **2004**, submitted for publication.
7. Feng, Lijun; Kamal, Musa R. "Study on Morphology of Linear Low-Density Polyethylene with Polarized Light Microscopy", *Polymer* **2004**, submitted for publication.

2004/11/25

Professor Musa R. Kamal　　　　　　　　Date

Department of Chemical Engineering

McGill University, Montreal, Quebec, Canada

I, Tao Huang, hereby give copyright clearance for inclusion of the following papers, of which I am the co-author, in the dissertation of Lijun Feng.

1. Kamal, Musa R.; Feng, Lijun; Huang, Tao "A Generalized Equation for the Prediction of Melting Temperatures of Homopolymers and Copolymers", *The Canadian Journal of Chemical Engineering* **2002**, 80(3), 432-442.

July 16, 2004

Dr. Tao Huang
DuPont Central Research and Development
Information and Computing Technology
Wilmington, DE 19880, USA

Date

Abstract

The melting and crystallization behavior of linear low-density polyethylene (LLDPE) is of great scientific and industrial importance. It depends strongly on polymer molecular structural characteristics and processing conditions, and determines polymer application properties. In this work, we study three different types of LLDPE polymers: metallocene-based LLDPEs (m-LLDPEs), Ziegler-Natta-based LLDPEs (ZN-LLDPEs), and m-LLDPE blends.

A generalized equation is introduced to clarify conceptual definitions of polymer melting temperatures. It incorporates the effects of comonomer volume, crystal length, folding surface free energy and enthalpy of fusion. It is successful in describing the characteristic melting temperatures of various α-alkene-ethylene copolymers. The proposed equation is used, along with melting traces obtained by differential scanning calorimetry (DSC), to estimate the crystal size number distributions. Furthermore, the melting temperature characteristics are identified, using crystal size number distributions.

The crystallization behavior of LLDPEs is studied by polarized light microscopy (PLM) and DSC. A modified Hoffman-Lauritzen (MHL) expression is proposed for the linear crystallization kinetics by replacing the equilibrium melting temperature, T_m^0, with the melting temperature of the crystal stem with the maximum possible length, T_m^{C,n^*}. The concept of the effective nucleation induction time is introduced, in order to employ the Avrami equation to analyze the overall crystallization kinetics during the initial crystallization stage.

The MHL analysis suggests the presence of three crystallization regimes: regimes III and II, and a special regime IM. The Avrami exponents are respectively 2, 1.5, and 1 in these regimes. The typical optical morphology of LLDPEs is spherulitic. As the crystallization temperature increases, the morphology changes from spherulites without ring bands, to ring-banded spherulites and sometimes to irregular structure with rough ring bands. These structural characteristics seem to correspond to MHL regimes.

Non-linear spherulitic growth behavior is observed in regimes II and IM. This behavior is explained by the reduction of the concentration of crystallizable ethylene sequences in the melt phase. The MHL expression may be still used to analyze non-linear growth crystallization kinetics by employing a variable T_m^{C,n^*}.

Résumé

Le comportement en fusion et cristallisation du polyéthylène linéaire basse densité (LLDPE) est d'une importance scientifique et industrielle majeure. Il dépend fortement des caractéristiques moléculaires structurelles du polymère et des conditions de transformation, et détermine les propriétés d'application du polymère. Dans cette étude, trois différents types de polymères LLDPE sont considérés : metallocene-LLDPEs (m-LLDPEs), Ziegler-Natta LLDPESs (ZN-LLDPEs) et mélanges de m-LLDPE.

Une équation généralisée est présentée dans le but de clarifier les définitions conceptuelles de températures de fusion des polymères. L'équation considère les influences du volume de co-monomère, longueur du cristal, énergie libre de surface repliée et enthalpie de fusion. Elle décrit avec succès les températures caractéristiques de fusion de nombreux co-polymères α-alcène-éthylène. L'équation généralisée est utilisée, en combinaison avec les tracés de fusion obtenus par calorimétrie différentielle à balayage (DSC), pour estimer les distributions en nombre de taille de cristal. En outre, les caractéristiques de température de fusion sont identifiées, utilisant les distributions en nombre de taille de cristal.

Le comportement de cristallisation des LLDPEs est étudié par microscopie à lumière polarisée (PLM) et DSC. Une expression de Hoffman-Lauritzen modifiée (MHL) est proposée pour la cinétique de cristallisation linéaire en replaçant la température d'équilibre de fusion, T_m^0, par la température de fusion de la branche de cristal ayant la plus grande longueur possible, $T_m^{C,n*}$. Le concept de temps d'induction de nucléation effectif est introduit, dans le but d'utiliser l'équation d'Avrami pour analyser la cinétique de cristallisation globale lors de l'étape de cristallisation initiale.

L'analyse MHL suggère la présence de trois régimes de cristallisation : régimes III et II, et un régime spécial IM. Les exposants d'Avrami sont respectivement 2, 1.5 et 1 dans ces régimes. La morphologie optique typique des LLDPEs est sphérulitique. Alors que la température de cristallisation augmente, la morphologie passe de sphérulites sans anneaux, à sphérulites avec anneaux et parfois à une structure irrégulière avec anneaux plus ou moins distincts. Ces caractéristiques structurelles semblent correspondre aux régimes MHL.

Une croissance non-linéaire des spherulites est observée dans les régimes II et IM. Ce comportement s'explique par la réduction de la concentration de séquences d'éthylène cristallisable dans la phase fondue. L'expression MHL pourrait encore être utilisée pour analyser la cinétique de cristallisation par croissance non linéaire en faisant varier T_m^{C,n^*}.

Acknowledgments

In the first place, I would like to express my deepest gratitude to my research supervisor, Professor Musa R. Kamal, for his guidance, wisdom, understanding, and encouragement through the duration of this work.

I sincerely thank the following persons:

- Professor Juan H. Vera for teaching me the important principles of thermodynamics,
- Professor Alejandro D. Rey for introducing me to computational method in chemical engineering,
- Dr. Richard Lai-fook, Dr. Tao Huang, and other colleagues in my group for their scientific discussions and friendship
- Professor Mark Sutton and Mr. Khosrow Hassani from the Physics Department for the use of the X-ray equipment,
- Mr. Christian Lungu who introduced me to differential scanning calorimetry (DSC).

I am also indebted to Nova Chemicals Co. (Calgary, Canada) for supplying the materials used in this study and financial support, the Natural Sciences and Engineering Research Council of Canada (NSERC), la Formation de Chercheurs et l'Aide à la Recherche (FCAR), Government of the Province of Quebec and McGill University for financial support.

I would also like to thank Mr. Vincent Mollet for his help in the preparation of the French version of thesis abstract.

Finally, I want to express by deep appreciation for my family: my mother, Ruiyin, my father in memory, Xixiang, and especially my wife, Minya, and my children, Xiaojie, Angela and Sean, for their everlasting moral support, understanding and encouragement throughout the course of my studies.

Content

Foreword ..... **i**

Abstract ..... **v**

Résumé ..... **vii**

Acknowledgments ..... **ix**

Content ..... **x**

List of Figures ..... **xv**

List of Tables ..... **xx**

Nomenclature and Symbols ..... **xxi**

1 General Introduction **1**

- 1.1 Introduction 1
- 1.2 Linear Low-Density Polyethylene 2
  - 1.2.1 Polyolefins, polyethylene, and linear low-density polyethylene 2
  - 1.2.2 Three types of linear low-density polyethylenes 4
- 1.3 Melting and crystallization behavior and morphological characteristics 5
  - 1.3.1 Melting behavior 5
    - 1.3.1.1 Melting temperature 5
    - 1.3.1.2 Crystal size and melting temperature distributions 7
  - 1.3.2 Crystallization behavior 9
    - 1.3.2.1 Linear crystallization kinetics 10
    - 1.3.2.2 Overall crystallization kinetics 13
  - 1.3.3 Crystalline morphological characteristics 15
- 1.4 Experimental Techniques 18
  - 1.4.1 Polarized light microscopy (PLM) 19
  - 1.4.2 Differential scanning calorimetry (DSC) 19
  - 1.4.3 Small angle x-ray scattering (SAXS) 20
- 1.5 Objectives and Present Investigation 21
- 1.6 References 23

2 A Generalized Equation for the Prediction of Melting Temperatures of Polymers **27**

2.1 Introduction 28

2.2 Theoretical Analysis 30
  2.2.1 Flory's Equation 30
  2.2.2 The proposed equation 33

2.3 Discussion 36
  2.3.1 The Modified Gibbs-Thomson Equation 36
  2.3.2 Application to α-alkene-ethylene Copolymers 37
    2.3.2.2 Effect of Molecular Weight 40
    2.3.2.3 Effect of the Degree of Branching 43
    2.3.2.4 Effect of Branch Length 47

2.4 Conclusions 49

2.5 References 50

3 Distributions of Crystal size from DSC Melting Traces for Polyethylenes 52

3.1 Introduction 53

3.2 Theoretical Analysis 54
  3.2.1 Crystal Size Number Distribution and Characteristics 54
  3.2.2 Comparison with other equations 58

3.3 Experimental 60
  3.3.1 Materials 60
  3.3.2 Differential Scanning Calorimetry 62
  3.3.3 Small Angle X-ray Scattering 63

3.4 Results 63
  3.4.1 SAXS Intensities and Long Periods 63
  3.4.2 DSC Melting Traces 66

3.5 Discussion 68
  3.5.1 Crystal Size Number Distributions 68
  3.5.2 Heat of Fusion and Crystallinity 71
  3.5.3 Comparison of Average Crystal Sizes from DSC and SAXS 73
  3.5.4 Comparison of Different Crystal Size Distributions 75

3.6 Conclusions 78

3.7 References 80

3.8 Appendix 82

4 Melting Temperature Characteristics for Polyethylenes from Crystal Size Distribution 84

4.1 Introduction 85

4.2 Theoretical analysis 86

4.3 Experimental 89
  4.3.1 Materials 89

4.3.2 Differential Scanning Calorimetry 89
4.3.3 Small Angle X-ray Scattering 91

4.4 Results 91
4.4.1 SAXS 91
4.4.2 DSC melting traces 93

4.5 Discussion 95
4.5.1 Crystal sizes and distributions 95
4.5.2 Melting temperature characteristics 97
4.5.3 Melting temperature characteristics for different polyethylenes 99

4.6 Conclusions 102

4.7 References 104

5 Spherulitic Crystallization Behavior of Linear Low-Density Polyethylene 105

5.1 Introduction 106

5.2 Experimental 107
5.2.1 Materials and sample preparation 107
5.2.2 Observation and measurement of spherulitic growth during crystallization . 108

5.3 Results 109

5.4 Discussion 114
5.4.1 Modified Hoffman-Lauritzen expression 114
5.4.1.1 Crystallization regimes 119
5.4.1.2 Basal surface free energy 120
5.4.2 Basal surface free energy and short chain branching characteristics by TREF 121
5.4.3 Growth behavior in different regimes 125

5.5 Conclusions 128

5.6 References 129

6 Non-linear Crystalline Spherulitic Growth Behavior for Linear Low-Density Polyethylene 130

6.1 Introduction 131

6.2 Experimental 133
6.2.1 Materials 133
6.2.2 Two-step crystallization process by polarized light microscopy (PLM) 133

6.3 Results and Discussion 135
6.3.1 Uncrystallizable ethylene sequences (UCES) in different regimes 135
6.3.2 Diffusion layer 137
6.3.2.1 Effect of T_{1c} 138
6.3.2.2 Effect of SCBC 140
6.3.3 Crystallization kinetics in non-linear crystallization processes 141
6.3.3.1 Spherulitic growth rate in the 2nd crystallization step, G_2 142

6.3.3.2 Time dependence of $T_m^{C,n*}$ ... 143
6.3.3.3 Crystallization kinetics ... 146

6.4 Conclusions ... 148

6.5 References ... 149

7 Crystallization and Melting Behavior of Linear Low-density Polyethylene Resins ... 150

7.1 Introduction ... 151

7.2 Experimental ... 152
7.2.1 Materials ... 152
7.2.2 Differential scanning calorimetry ... 153
7.2.2.1 Nonisothermal stage in the initial isothermal process ... 153

7.3 Results and Discussion ... 155
7.3.1 Crystallization traces ... 155
7.3.1.1 Crystallization traces for different types of LLDPEs ... 155
7.3.1.2 Crystallization peak time and spherulitic growth time ... 159
7.3.2 Melting traces ... 160
7.3.2.1 Melting traces in regime III ... 161
7.3.2.2 Melting traces in regime II ... 165
7.3.2.3 Melting traces in regime IM ... 168
7.3.2.4 Melting peak positions ... 169
7.3.3 Induction time ... 172
7.3.4 Comparison between the linear and overall crystallization kinetics ... 176
7.3.5 Avrami crystallization constants and crystallization peaks ... 178

7.4 Conclusions ... 179

7.5 References ... 181

8 Study on Morphology of Linear Low-Density Polyethylene with Polarized Light Microscopy ... 182

8.1 Introduction ... 183

8.2 Experimental ... 183
8.2.1 Materials ... 183
8.2.2 Polarized light microscopy (PLM) with a hot stage ... 185

8.3 Results and Discussion ... 185
8.3.1 A Modification of Hoffman-Lauritzen Expression ... 185
8.3.2 Crystalline Morphology of LLDPEs ... 186
8.3.2.1 Morphology of ZN-LLDPEs ... 187
8.3.2.2 Morphology of m-LLDPEs ... 189
8.3.2.3 Morphology of m-LLDPE blends ... 190
8.3.3 Ring-banded spherulitic morphology ... 192
8.3.4 Ring-banded distances in different MHL regimes ... 195
8.3.4.1 Twist mechanism in regimes III and II ... 196

8.3.4.2 Branching mechanism in regime IM 198
8.3.5 The 3-dimensional growth behavior 198
8.4 Conclusions 200
8.5 References 202
9 General Conclusions, Contributions to Original Knowledge, and Suggestions for Future Work 203
9.1 General Conclusions 203
9.2 Contributions to Original Knowledge 206
9.3 Suggestions for Future Work 206
Bibliography 207
Appendix 219

List of Figures

Figure 1-1. The relationship among the material properties, processing conditions, melting and crystallization behavior, and application properties 2

Figure 1-2 Secondary and tertiary nuclei 10

Figure 1-3 Growth Regimes 11

Figure 1-4 Different growth regimes by Hoffman-Lauritzen equation 13

Figure 1-5 Polyethylene crystalline structure[70] 16

Figure 1-6 Regular chain folding (left) and irregular chain folding (right) 16

Figure 1-7 Model of Spherulite Growth Mechanism (Left: Hedgehog, Right: Pop-off).. 17

Figure 1-8 Model of spherulite morphology[74] 17

Figure 1-9 Ring-banded structure in Resin G spherulite. 17

Figure 1-10 Maltese Cross structure in resin G spherulite 18

Figure 2-1 Melting temperature vs. molecular weight of α-octene-ethylene homogeneous copolymers by theoretical equations 40

Figure 2-2 Melting temperature vs. branching degree of α-octene-ethylene homogeneous copolymers by theoretical equations 41

Figure 2-3 Three types of melting temperatures and the corresponding maximum possible and experimental crystal stem sizes for homogeneous LLDPEs with hexene comonomers 44

Figure 2-4 Melting temperature and lamellar thickness of α-octene-ethylene homogeneous copolymers 46

Figure 2-5 Melting temperature of α-butene-ethylene and α-octene-ethylene homogeneous copolymers vs. branching degree by theoretical equations. 48

Figure 2-6 Branching size effects on the melting temperatures for LLDPEs 49

Figure 3-1 The experimental SAXS curves 64

Figure 3-2 The Lorentz-corrected intensities of SAXS results ... 65
Figure 3-3 Long periods for different resins ... 65
Figure 3-4 Normalized heat flows of DSC melting traces ... 67
Figure 3-5 Melting peak positions of different resins ... 67
Figure 3-6 The crystal size number distributions for different resins ... 70
Figure 3-7 Crystal sizes for different resins ... 74
Figure 3-8 Comparison of normalized number distributions from Crist-Mirabella and the present work ... 76
Figure 3-9 The average number crystal sizes from Crist-Mirabella and the present work, and SAXS measurement for all LLDPE resins ... 77
Figure 3-10 The crystal size polydispersities from Crist-Mirabella and the present work78
Figure 3-11 The heating rate effects for resin I ... 82
Figure 3-12 the heating rate effects on number average crystal size for resins I and J 83
Figure 4-1 The Lorentz-corrected intensities of typical SAXS results ... 92
Figure 4-2 Long periods and volume crystallinities for isothermal samples ... 93
Figure 4-3 Normalized heat flows of DSC melting traces ... 94
Figure 4-4 The 1st peak positions of isothermal samples ... 95
Figure 4-5 The crystal-size number distribution ... 96
Figure 4-6 The average crystal sizes and crystal size polydispersities ... 97
Figure 4-7 The effective melting temperatures from different methods ... 98
Figure 4-8 The melting temperature polydispersities from different methods ... 99
Figure 4-9 The crystal size number distribution from DSC melting traces for non-isothermal experiments[8] ... 100
Figure 4-10 Number average melting temperatures from different methods and DSC main peak positions for different resins ... 101
Figure 4-11 Melting temperature polydispersity from different methods for different resins ... 102
Figure 5-1 Crystalline spherulites of resin J at 100°C ... 109
Figure 5-2 Spherulite radius vs. crystallization time for m-LLDPE resin J ... 110
Figure 5-3 Spherulite radius vs. crystallization time for m-LLDPE blend I3 (I/J:3/7)... 111
Figure 5-4 Spherulite radius vs. crystallization time for ZN-LLDPE resin C ... 111

Figure 5-5 Spherulitic growth rates vs. crystallization temperatures 112

Figure 5-6 Spherulitic growth rates of m-LLDPEs and their blends at 100°C 113

Figure 5-7 The description of crystallization kinetics by the MHL and HL equations .. 118

Figure 5-8 σ_e, $T_m^{C,\infty}$ and T_m^{C,n^*} for m-LLDPEs and their blends vs. resin I weight content 121

Figure 5-9 $T_{el,WN}$ vs. D_{branch} for different materials 123

Figure 5-10 The basal surface free energy and SCBP 124

Figure 5-11 The plots of radius vs. crystallization time in regime II 126

Figure 5-12 irregular crystallization morphologies in regime IM for resin G at 123°C. 127

Figure 6-1 The procedure of a two-step isothermal experiment for m-LLDPE resin J .. 134

Figure 6-2 Regular and irregular spherulitic morphologies in regimes III and IM for rein I 137

Figure 6-3 The growth of 1st kind of spherulites from different T_{1c} for resin J 138

Figure 6-4 The growth processes of old and new spherulites at T_{2c} for Blend I3 139

Figure 6-5 The spherulitic growth process at T_{2c} for ZN-LLDPE resin H 140

Figure 6-6 The thickness of diffusion layer for different resins 141

Figure 6-7 The linear growth behavior in isothermal crystallization after different t_{1c} at T_{1c} 108°C for resin J 142

Figure 6-8 G_{2c} vs. t_{1c} for resin J 143

Figure 6-9 T_m^{C,n^*} and D_{branch} (SCBC) vs. t_{1c} at 108°C for resin J 144

Figure 6-10 The application of the MHL equation to the crystallization kinetics of non-linear spherulitic growth for resin J 147

Figure 6-11 The application of the MHL equation to the crystallization kinetics of non-linear spherulitic growth for resin H 147

Figure 7-1 Isothermal crystallization curves after quenching from 180°C at 60°C/min for m-LLDPE blend I7 at 96°C 154

Figure 7-2 The crystallization traces at different temperatures for m-LLDPE resin I.... 156

Figure 7-3 The crystallization traces at different temperatures for m-LLDPE resin J ... 157

Figure 7-4 The crystallization traces at different temperatures for m-LLDPE blend I7 157

Figure 7-5 The crystallization traces at different temperatures for ZN-LLDPE resin G 158

Figure 7-6 Comparison of the crystallization peak time and the spherulite growth time 160
Figure 7-7 The melting traces after different crystallization times in regime III for m-LLDPEs 162
Figure 7-8 The melting traces after different crystallization times in regime III for m-LLDPE blend I7 163
Figure 7-9 The melting traces after different crystallization times in regime III for ZN-LLDPE resin G 164
Figure 7-10 The melting traces in regime II after different crystallization times for m-LLDPEs 166
Figure 7-11 The melting traces after different crystallization times in regime II 167
Figure 7-12 The melting traces after different crystallization times in regime IM for m-LLDPE resin I at 102°C. 168
Figure 7-13 The melting peak positions in melting traces at different crystallization times and temperatures for m-LLDPE resin I ($T_{II\text{-}IM}$= 100.8°C, $T_{III\text{-}II}$= 93.9°C) 169
Figure 7-14 The melting peak positions in melting traces at different crystallization times and temperatures for m-LLDPE resin J ($T_{III\text{-}II}$= 107.1°C) 170
Figure 7-15 The melting peak positions in melting traces at different crystallization times and temperatures for m-LLDPE blend I7 ($T_{III\text{-}II}$= 103.3°C) 170
Figure 7-16 The melting peak positions in melting traces at different crystallization times and temperatures for ZN-LLDPE resin G ($T_{III\text{-}II}$= 116.5°C) 171
Figure 7-17 Plots of $\ln[-\ln(1-x)]$ versus $\ln(t-t_0)$ for isothermal crystallization 174
Figure 7-18 The Avrami constants, and total crystallization induction time plotted against crystallization temperature 175
Figure 7-19 Comparison between the overall and linear crystallization kinetics 178
Figure 8-1 The morphologies of resin G in different regimes 187
Figure 8-2 The morphologies of resin H in different regimes 188
Figure 8-3 The morphologies of resin C in different regimes 189
Figure 8-4 The morphologies of resin J in different regimes 190
Figure 8-5 The morphologies of resin I in different regimes 190
Figure 8-6 The morphologies of blend I1 in different regimes 191

Figure 8-7 The morphology of blend I9 at 105°C, in regime IM. 192
Figure 8-8 Characteristic temperatures and SCBP for different LLDPEs. 193
Figure 8-9 The plots of ring-banded distance versus reciprocal supercooling degree ... 194
Figure 8-10 The ring-banded distances in the different MHL regimes for resin H........ 195
Figure 8-11 The transition temperatures between spherulites without and with ring bands in regime III for some resins, which are deducted from the MHL expression. 196
Figure 8-12 The irregular ring-banded spherulitic morphology in regime IM for resin H at 119°C 198
Figure 8-13 3-Dimensional characteristic of spherulites for different types of LLDPEs in regime II 199
Figure Appendix-1 GPC results of blends of resins I and J 219
Figure Appendix-2 TREF results of blends of resins I and J 219

List of Tables

Table 1-1 Avrami exponent and crystallization growth mechanism 14
Table 2-1 Melting temperature of α-hexene ethylene copolymers 45
Table 3-1 Polymer molecular characteristics 61
Table 3-2 Blend molecular characteristics 62
Table 3-3 Basal surface free energies, heats of fusion of samples and of finite-length crystals, and crystallinities 69
Table 4-1 Polymer molecular characteristics 90
Table 5-1 Polymer molecular characteristics 108
Table 5-2 The calculated parameters and results according to the MHL expression 117
Table 5-3 TREF calculation results 122
Table 5-4 Avrami exponents and corresponding growth characteristics in different regimes for heterogeneous nucleation mechanism 125
Table 6-1 Polymer molecular characteristics and characteristic temperatures 134
Table 6-2 Some temperature characteristics and parameters of the empirical equation for m-LLDPE resin J and ZN-LLDPE resin H 145
Table 7-1 Polymer characteristics 152
Table 7-2 The shift factors "*A*" 177
Table 8-1 Polymer molecular characteristics 184

Nomenclature and Symbols

CCES	concentration of crystallizable ethylene sequences
CES	crystallizable ethylene sequences
CUCES	concentration of uncrystallizable ethylene sequences
CRYSTAF	crystallization analysis fractionation
DSC	differential scanning calorimetry
ES	ethylene sequence
FTIR	Fourier transform infrared
GPC	gel permeation chromatography
HDPE	high-density polyethylene
HL	Hoffman-Lauritzen expression
LLDPE	linear low-density polyethylene
MHL	modified Hoffman-Lauritzen expression
MRR	melting-recrystallization-remelting
MW	molecular weight
MWD	molecular weight distribution
m-LLDPE	metallocene catalyzed LLDPE
m.s.u. (msu)	monomer structural unit
mb-LLDPE	metallocene catalyzed LLDPE blend
NMR	nuclear magnetic resonance
PLM	polarized light microscopy

SAXS	small angle x-ray scattering
SCBC	short chain branching content
SCBD	short chain branching distribution
SCBP	short chain branching polydispersity
TEM	transmission electronic microscopy
TREF	temperature rising elution fractionation
UCES	uncrystallizable ethylene sequence
WAXD	wide-angle x-ray diffraction
ZN-LLDPE	Ziegler-Natta catalyzed LLDPE

$^{\infty}$ (superscript) for crystal stems with infinite length

^{C} (superscript) for copolymers

^{H} (superscript) for homopolymers

(dN/dn)	derivative crystal stem number with respect to crystal size
(dN/dT)	derivative crystal stem number with respect to melting temperature
(dQ/dn)	derivatives heat of fusion with respect to crystal size
(dQ/dt)	heat flow from DSC experiments / derivatives heat of fusion with respect to time
(dT/dt)	experimental heating rate in DSC experiments
$(T_m^{C,n^*})^{\infty}$	T_m^{C,n^*} when t_{1c} is infinite

A	shift factor between the overall and linear crystallization kinetics (Chapter 7)
A_{II}	difference of the shift factors of the overall and linear crystallization kinetics between regimes III and II
A_{III}	shift factor of the overall and linear crystallization kinetics in regime III
A_{IM}	difference of the shift factors of the overall and linear crystallization kinetics between regimes II and IM
a	fitting parameter for T_m^{C,n^*} in non-linear spherulitic growth kinetics
b	fitting parameter for T_m^{C,n^*} in non-linear spherulitic growth kinetics
b_0	crystal layer thickness
c	fitting parameter for T_m^{C,n^*} in non-linear spherulitic growth kinetics
D	parameter defined by Eq.(2-9)
D_{Branch}	branching degree in copolymers
f	correction factor for the variation in the heat of fusion with the temperature, $2T_c/(T_m^0+T_c)$
$f_1(n)$	crystal size distribution by the direct DSC method
$f_2(n)$	crystal size distribution by the crystal size weight distribution
$f_3(n)$	crystal size distribution by the crystal size number distribution
G	spherulitic radial growth rate
G_0	pre-exponential parameter in the Hoffman-Lauritzen (HL) (the modified Hoffman-Lauritzen (MHL)) expression
G_1, G_2	spherulitic radial growth rate in the first and second isothermal crystallization steps, respectively
g	geometric factor
$I(s)$	experimental SAXS intensity

$I_C(s)$	Lorentz-corrected SAXS intensity, $I_C(s) = 4\pi s^2 I(s)$
K or K_{Avr}	crystallization constant in Avrami expression, $K = \sqrt[n]{k}$
K_{Der}	crystallization constant derivated from of the Avrami expression
K_g	nucleation constant in the HL expression
K_{gI}	nucleation constant for regime I in the HL expression
K_{gII}	nucleation constant for regime II in the HL expression
K_{gIII}	nucleation constant for regime III in the HL expression
K_{MgII}	nucleation constant for regime II in the MHL expression
K_{MgIII}	nucleation constant for regime III in the MHL expression
k	Boltzmann's constant
k	crystallization constant in Avrami expression
L	Bragg distances or long periods, $L = 1/s^*$
L_c	crystal size, $L_c = n\, l_u$
$L_{c,DSC}$	average crystal size from DSC experiment
$L_{c,SAXS}$	average crystal size from SAXS experiment
l_u	projected length per m.s.u in straight linear polymer chain
M_n	average number molecular weight
M_{nw}	average molecular weight, $M_{nw} = \sqrt{M_n M_w}$
M_{nw}^*	effective average molecular weight
M_w	average weight molecular weight
m	carbon number in comonomers
$\dot{N}$	crystallization nucleation density
N	crystal stem number

$N(n)$	number of crystal stems consisting of n m.s.u.
$N(T)$	crystal stem number with respect to melting temperature, T
N_{tC}	total number of crystal stems
n	Avrami exponent
n	actual number of m.s.u. in a crystal stem
n^*	maximum possible number of m.s.u. in a crystal stem / effective maximum possible number of m.s.u. for polymer resins
n_L	m.s.u. numbers in crystal stems having the largest crystal sizes in the whole crystal size distribution
$\overline{n}_n$	number average crystal size
n_S	m.s.u. numbers in crystal stems having the smallest crystal sizes in the whole crystal size distribution
n_t	total m.s.u. number in the sample
n_{tC}	total crystallized m.s.u. number in the sample
$\overline{n}_w$	weight average crystal size
p	sequence propagation probability that a monomer is succeeded by another monomer, i.e., the monomer mole fraction for homogeneous copolymers
$P_{n\#}$, P_n	crystal size polydispersity by No.# method, $P_n = \overline{n}_w / \overline{n}_n$
P_n^0	probability that the structural unit of melting polymer occupying a sequence initial site is a backbone structural unit at initial melting state
P_n^e	probability that the structural unit of melting polymer occupying a crystal stem initial site is a backbone structural unit at equilibrium state
$P_{T\#}$	melting temperature polydispersity by No.# method, $P_T = T_W / T_N$
$q(n)$	heat of fusion of a crystal stem with n m.s.u.
Q_D^*	activation energy for reptation and center-of-mass diffusion

R	gas constant
s	scattering vector in SAXS, $s = \frac{2\sin(\theta)}{\lambda}$
s^*	corresponding s value at the maximum $I_C(s)$
T_{1c}, T_{2c}	crystallization temperatures in the first and second isothermal crystallization steps, respectively
$T_{el,N}$	number average elution temperature in TREF experiments
$T_{el,W}$	weight average elution temperature in TREF experiments
$T_{el,WN}$	effective average elution temperature, $T_{el,WN} = \sqrt{T_{el,W}T_{el,N}}$
T_g	glass transition temperature
$T_{III\text{-}II}$	transition temperature between regimes III and II
$T_{II\text{-}IM}$	transition temperatures between regimes II and IM,
T_L	corresponding melting temperatures to n_L according to the proposed melting temperature equation
T_m	melting temperature
T_m^{∞}	melting temperature for a crystal with crystal stems of infinite length
$T_m^{C,\infty}$	melting temperature for the copolymer crystal with crystal stems of infinite length
$T_m^{C,n}$	melting temperature for the copolymer crystal with crystal stems containing n m.s.u.
T_m^{C,n^*}	melting temperature for the copolymer crystal with crystal stems containing n^* m.s.u.
$T_m^{H,\infty}$ or T_m^0	melting temperature for a homopolymer crystal with crystal stems of infinite length
$T_m^{H,n}$	melting temperature for the homopolymer crystal with crystal stems containing n m.s.u.

$T_m^{H,n*}$	melting temperature for the homopolymer crystal with crystal stems containing n^* m.s.u.
T_m^n	melting temperature for the crystal with crystal stems containing n m.s.u.
T_m^{n*}	melting temperature for the crystal with crystal stems containing n^* m.s.u.
T_{mp}	melting peak position
T_{mph}	melting peak position in the high melting temperature range
T_{mpl}	melting peak position in the low melting temperature range
$T_{N\#}$	number average melting temperatures by No.# method
$T_{NW\#}$	effective melting temperature by No.# method, $T_{NW} = \sqrt{T_N T_W}$
T_{nw} or T_{NW}	effective average melting temperature
T_{onset}	onset melting temperature in DSC
$T_{p\#}$	position of No.# melting peak.
T_S	corresponding melting temperatures to n_S according to the proposed melting temperature equation
T_W	weight average melting temperatures
$T_{W\#}$	weight average melting temperatures by No.# method
t_0	effective crystallization induction time in DSC (Chapter 7)
t_0	fitting parameter for $T_m^{C,n*}$ in non-linear spherulitic growth kinetics (chapter 6)
t_{1c}, t_{2c}	crystallization times in the first and second isothermal crystallization steps, respectively
t_{fs_PLM}	spherulitic growth time in PLM experiments
t_{p_DSC}	crystallization peak position in DSC melting crystallization trace
U^*	diffusive activation energy of chain reptation motion in the melt
w_1, w_2	weight fractions of components

X	crystallinity
X_∞	final crystallinity
X_A	monomer volume fraction in copolymers
X_{IC}, X_C	mole factions of comonomers in the crystalline phase and in the copolymer, respectively
X_v or X_V	volume crystallinity
X_w or X_W	weight crystallinity

Θ	relative crystallinity
ε	excess free energy by incorporating comonomers into the crystalline phase
ΔH_f	heat of fusion in DSC
ΔG_n	standard free energy of fusion per mole of crystal stems with n m.s.u.
ΔG_u	standard free energy of fusion per mole of m.s.u.
ΔH_e	heat of fusion per mole of end units
ΔH_u	heat of fusion per mole of m.s.u. in the perfect crystal
ΔS_e	entropy of fusion per mole of end units
ΔS_u	entropy of fusion per mole of m.s.u.
ΔT	degree of supercooling
λ	wavelength of x-ray in SAXS
ρ_a	density of amorphous phases
ρ_c	density of crystalline phases
σ	lateral surface free energy per mole of m.s.u
σ_e	basal surface free energy per mole of crystal stem ends

τ	crystallization nucleation induction time
θ_m	parameter defined by Eq.(2-13)
θ	parameter defined by Eq.(2-8)
τ_0	normal nucleation induction time
τ_1	nucleation induction time during quenching for isothermal DSC experiments
2θ	scattering angle in SAXS

Chapter 1

1 General Introduction

1.1 Introduction

Solid polymers can appear in amorphous or crystalline states. In the amorphous state, molecular chains are irregularly arranged. In the crystalline state, polymer chains or parts of them (segments) are fixed in certain conformations, such as, planar, zigzag and helical forms. They may be parallel to each other and packed regularly. Because crystalline and amorphous regions coexist in crystalline polymers, they are always called semicrystalline materials. Their crystallization capabilities depend on structure and regularity of molecular chains and on interactions among them.

Melting and crystallization are among the most important characteristics, which determine many of the final application and processing properties of semicrystalline polymers. However, these characteristics are very complex, because they do not depend on only molecular chemical composition and structural characteristics, but also on processing conditions, as illustrated in Figure 1-1. The melting temperature is a function of molecular structure and chemical composition. The melting temperature and processing parameters determine the kinetics of melting and crystallization during processing. Processing parameters include temperature, pressure, and stress, and their distributions in space and time. When there are density variations during processing, mass transport needs to be considered. Thus, processes can be very complex. Different processing conditions tend to form different morphologies and different final application properties (e.g. optical and mechanical properties).

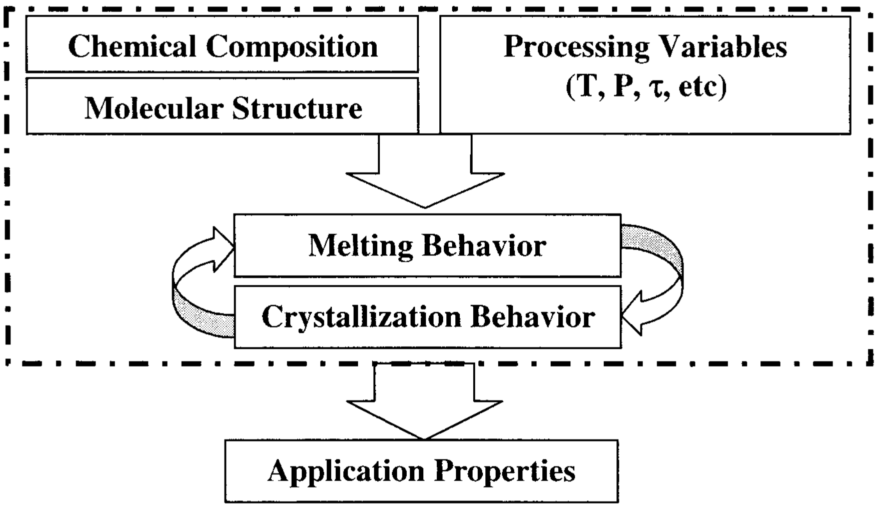

Figure 1-1. The relationship among the material properties, processing conditions, melting and crystallization behavior, and application properties

This thesis deals with the melting and crystallization behavior of polyethylene, especially linear low-density polyethylene copolymers (LLDPE), which are widely used for many important consumer and commercial applications, including packaging and agriculture application.

1.2 Linear Low-Density Polyethylene

1.2.1 Polyolefins, polyethylene, and linear low-density polyethylene

Polyolefins, which are generally semicrystalline, are the largest group of synthetic polymers produced today, They are widely used, because of their advantages, such as, low cost of production, light weight, and high chemical resistance. Polyolefin polymers are fully saturated hydrocarbon molecules, synthesized from olefins, such as ethylene, propylene, α-butene, α-hexene, α-octene, and isobutylene. Weak molecular interactions (van der Waals force) result in lower melting and crystallization temperatures than for polymers with strong interactions, such as polyamides with hydrogen bonds. Because melting temperatures are not very high, they can be processed relatively easily, but are unsuitable for high temperature applications. Furthermore, because of their saturated structures, they are highly chemically resistant to most solvents and liquids, and they are highly stable to oxidation.[1]

Although polyolefins were first produced in the 1930's, important advances are still being made in improving processes and performance, because of an abundant supply of cheap and simple monomers, advances in polymerization processes and catalysts, and the ability to blend them with fillers and other polymers. A wide range of mechanical properties is possible by the methods of co-polymerization, blending, and the use of additives. Products range from elastomers to thermoplastics, and in some cases cross-linked materials.

One of the most important polyolefins is polyethylene. It is based on the monomer, ethylene. The group includes high-density polyethylene (HDPE, density 0.94-0.97g/cm^3), low-density polyethylene (LDPE, 0.91-0.94), and very low-density polyethylene (VLDPE, 0.86-0.90).[2] Basically, the density depends on the content of short chain branches. Polyethylene with a lower density has a higher short chain branching content.

When ethylene is co-polymerized with α-olefins, such as α-butene, α-hexene, and α-octene, linear low-density polyethylene (LLDPE) (with ethyl, butyl or hexyl short chain branches, respectively), is produced. LLDPE contains linear polyethylene backbones with attached short alkyl groups at certain intervals. It has a higher short chain branching content than LDPE, and the density of LLDPE is in the range between those of LDPE and VLDPE.

1.2.2 Three types of linear low-density polyethylenes

There are two types of catalysts for producing LLDPE resins, i.e., metallocene and Ziegler-Natta catalysts. Metallocene type catalysts have a single type of active sites. The metallocene-LLDPE (m-LLDPE) product has, most probably, a narrow molecular weight distribution (~2.0) and a narrow short chain branch distribution.[3] The short-chain branches are expected to be distributed randomly in all molecules.[4] The m-LLDPEs show both inter- and intra-molecular homogeneity, in the molecular and structural characteristics (e.g. distributions of molecular weight and short chain branching). Therefore, the m-LLDPEs can be taken as model copolymers to study the dependence of properties on their molecular structure, since their molecular structural characteristics can be clearly identified.[5]

LLDPEs catalyzed by Zeigler-Natta type catalysts (ZN-LLDPE) exhibit broad and complex molecular weight distributions (MWD) and short chain branching distributions (SCBD), because Ziegler-Natta catalysts have multiple active sites. The short chain branching content (SCBC) in individual molecules varies with molecular weight.[6] The ZN-LLDPEs show heterogeneous behavior at both inter- and intra-molecular levels. Cross-fractionation methods, which include gel permeation chromatography (GPC) and temperature rising elution fractionation (TREF)[6] (or possibly crystallization analysis fractionation (Crystaf)[7]), can supply fractions with a narrow MWD and nominally narrow SCBD. However, SCBD in each fraction is neither fully uniform nor random, because TREF and Crystaf fractionate molecules according to their longest ethylene sequence. They do not provide information about the SCBD within individual molecules. Products provided by cross-fractionation cannot be taken as model materials to study the relationships among properties and molecular structure. Thus, it is difficult to explain explicitly and quantitatively the properties of heterogeneous LLDPEs (ZN-LLDPEs),in relation to their molecular structural characteristics.

One approach to understand the relationship among the properties and molecular structural characteristics might be to treat them as blends of homogeneous copolymers, or more correctly as the blends of homogeneous ethylene sequences. In such a case, it may be possible to estimate the properties of heterogeneous copolymers by use and extension of results obtained with homogeneous materials.

Since it is difficult to fully characterize and quantify the molecular structural characteristics of ZN-LLDPEs in detail, it is proposed to construct blends of various well-characterized homogeneous materials (m-LLDPEs). Such materials would be homogeneous at the intra-molecular level, but heterogeneous at the inter-molecular level. Thus, they are semi-homogeneous. They may represent a bridge between molecular characteristics of m-LLDPEs and ZN-LLDPEs.[8] Results for homogeneous copolymers can be applied and tested in the blends, then finally applied and tested in heterogeneous copolymers. If successful, such an approach should lead to improved opportunities for understanding and quantifying the melting and crystallization behavior of ZN-LLDPEs.

1.3 Melting and crystallization behavior and morphological characteristics

1.3.1 Melting behavior

1.3.1.1 Melting temperature

The melting temperature is one of the most important properties of semi-crystalline polymers, especially in the study of crystallization and melting processes. For metals, the melting peak is very narrow, thus, the melting temperature is easily identified from the peak position. However, for a semi-crystalline polymer, since it has generally a broad melting peak, even multi-peaks, it is difficult to represent the melting temperature by a peak position value. Moreover, the melting temperature does not only depend on polymer molecular structural parameters, but also on material processing history. Thus, for a specific material, different melting temperature characteristics are likely to be observed. Therefore, it is necessary to understand the melting behavior and identify the intrinsic melting temperature characteristics of semi-crystalline polymers.[9]

The equilibrium melting temperature refers to the melting temperature of a perfect and infinite crystal. Flory proposed an equation to estimate the equilibrium melting temperature of copolymers with excluded comonomers ($T_m^{C,\infty}$), in terms of the equilibrium melting temperature of the corresponding homopolymers, (T_m^0 or $T_m^{H,\infty}$), the enthalpy of fusion (ΔH_u) for monomers, and the monomer sequence perpetuation probability (p): [10,11]

$$\frac{1}{T_m^{C,\infty}}-\frac{1}{T_m^{H,\infty}\left(or\ T_m^0\right)}=-\frac{R}{\Delta H_u}\ln p \qquad (1\text{-}1)$$

where R is the gas constant.

Sanchez and Eby[12] employed Helfand and Lauritzen's equilibrium theory of copolymers with included comonomers[13] to derive $T_m^{C,\infty}$ for copolymers with included comonomer:

$$\frac{1}{T_m^{C,\infty}}-\frac{1}{T_m^{H,\infty}\left(or\ T_m^0\right)}=\frac{R}{\Delta H_u}\left[\frac{\varepsilon X_{IC}}{RT_m^{C,\infty}}+\left(1-X_{IC}\right)\ln\left(\frac{1-X_{IC}}{1-X_C}\right)+X_{IC}\ln\left(\frac{X_{IC}}{X_C}\right)\right] \qquad (1\text{-}2)$$

where ε is the excess free energy by incorporating comonomers into the crystalline phase, and X_{IC} and X_C refer to the mole factions of comonomers in the crystalline phase and in the copolymer, respectively.

When comonomer size is larger than propylene, LLDPE resins are generally copolymers that form crystals with excluded comonomers.[14,15,16] Therefore, the Flory equation is suitable for evaluating the equilibrium melting temperature of LLDPE resins.

Because the equilibrium melting temperature refers to a hypothetical state (for infinite size crystals), it should not be misused as the reference of the degree of supercooling. Because of the restriction of crystal size in real polymers, only the melting temperature for crystal stems with the maximum possible crystal length should be considered, T_m^{C,n^*}.[9] T_m^{C,n^*} depends on polymer molecular structural characteristics, independent of the processing conditions. It is a material constant. It could be observed under certain experimental conditions, although such experimental condition may be very difficult to attain for some polymers. It is possible to estimate this temperature for semicrystalline polymers with specified molecular structure.[9]

Experimentally determined melting temperatures are significantly lower than the equilibrium melting temperature. Moreover, melting temperatures obtained experimentally do not depend only on the molecular structural characteristics, but also on both processing history and measurement conditions. According to thermodynamic considerations, the experimental melting temperature should approach $T_m^{C,n*}$ under conditions approaching equilibrium. However, the crystal size generally does not reach the maximum possible crystal size.[17,18] For the crystals with length n of monomer structural units in the crystal stem, the melting temperature is normally estimated using the Gibbs-Thomson equation[19] for homopolymers or its modified form for copolymers with excluded comonomers (simplified from the Sanchez-Eby equation)[12] as Eqs.(1-3) and (1-4), respectively:

$$T_m^{H,n} = T_m^{H,\infty}\left(1 - \frac{2\sigma_e}{\Delta H_u n}\right) \tag{1-3}$$

$$T_m^{C,n} = T_m^{C,\infty}\left(1 - \frac{2\sigma_e}{\Delta H_u n}\right) \tag{1-4}$$

where $T_m^{H,n}$ and $T_m^{C,n}$ refer to the melting temperatures for homopolymers and copolymers, respectively, and σ_e is the basal surface free energy. However, since the above equations ignore some factors, such as comonomer volume effect in Eq.(1-4), they should be used with care.[9]

1.3.1.2 Crystal size and melting temperature distributions

The crystal size (lamellar thickness) distribution and the average crystal size, strongly depend on molecular structural characteristics and processing conditions. Thus, it is useful to understand and determine the relationships that govern crystal sizes and size distributions. There are several experimental techniques to determine the crystal size distribution, such as transmission electron microscopy (TEM),[20,21] atomic force microscopy (AFM),[21,22] small angle x-ray scattering (SAXS),[21,23,24] Raman longitudinal acoustic mode (Raman LAM),[25,26,27] and differential scanning calorimetry (DSC).[21,28,29]

TEM provides a direct method to observe the crystal size. However, this technique involves at least two weaknesses. Because of the requirement for material etching, the final observed structure is perhaps different from the original state. The crystalline lamellae are three-dimensional structures but TEM images only represent two-dimensional observations. There is a significant difference between 2-D and 3-D information. This is reflected in the non-uniform contrast of lamellae in TEM images. Therefore, the TEM histograms do not necessarily represent the real crystal size distribution.

Recently, AFM observation has become a popular method to evaluate morphological characteristics of film. Generally, it provides topological information, i.e., the surface structure. For thin film samples, it is acceptable to assume that the structure at the surface is similar to that in the center. However, for bulk samples, morphologies are quite different from those of films.[22,25,26] If cryo-microtomed samples are used, the knife produces scratch marks and brittle-fracture characteristics are observed on the surface. These make it difficult to analyze AFM images accurately. It is also difficult to determine the absolute dimensions, because of the lack of well-defined standard samples.[21] Finally, like TEM results, the 2-D and 3-D histograms yield possibly different conclusions. Therefore, care must be taken in using histograms from TEM and AFM to describe crystal size distributions.

SAXS is a well-established method for analyzing crystal size, based on volume average analysis. Although it seems possible to estimate the crystal size distribution, it is necessary to consider the crystalline lamellae as isotropic plates with sufficiently large extended lateral size.[23,24] Also, the corrected values have to be fitted to a certain model with a known distribution form.[30,31,32] Therefore, SAXS is not yet a good and accurate method to estimate crystal size distribution.

The Raman longitudinal acoustic mode (LAM) can be employed to determine the crystal size for high density-polyethylene and long paraffins. The wave number of the LAM mode is inversely proportional to the extended chain length in semicrystalline polymers.[33] It has been shown that the integrated intensity is proportional to the weight fraction of the stem length in the crystalline phase, when the amorphous part, the surface of crystalline part, and the folding loops are assumed to have no effects on the LAM intensity results.[26] For long crystal stems and regular folding structures, Raman LAM can give reasonable results. However, for crystalline polymers, such as linear low-density polyethylenes, with short crystal stems, a large number of irregular folding crystals, and a thick interfacial layer between amorphous and crystalline phases, the method is doubtful.[27]

Because it is the simplest and fastest method, the DSC technique has been widely used to determine crystal size distribution. Semi-crystalline polymers exhibit a broad melting peak or multi-peaks, mainly because of the broad crystal size distribution,[34] although some other factors, such as melting-recrystallization-remelting (MRR), thermal lag and secondary crystallization effects,[34] are also contributing factors. If the above factors can be neglected under certain experimental conditions, the melting traces can be directly employed to analyze the crystal size distribution and the average crystal size.[29,35] However, only the weight distribution forms have been mostly discussed, and the correction of the folding work for the heat of fusion is rarely considered. Thus, there is need to re-evaluate and upgrade the methodology.[8]

Although it has been generally recognized that the melting process for polymer semicrystalline materials is very complex,[34] only the melting peak position in the polymer melting trace has been suggested and accepted to describe the melting temperature characteristics. However, because broad or even multiple peaks exist in melting traces, one-point description by the melting peak position is doubtful. Thus, it is desirable to adopt a more comprehensive approach to obtain a description of melting temperature characteristics that correspond to the distribution of crystal size.[8,35]

1.3.2 Crystallization behavior

For semicrystalline polymers, a bulk crystallization process can occur at temperatures between the glass transition temperature and the melting temperature of crystal stems with the maximum possible crystal size. This process possibly involves three steps: (1) a nucleation step (the formation of active nuclei from the melting phase), (2) a growth step (the development of crystals from nuclei), and (3) a secondary crystallization step. Primary crystallization refers to the first two steps, whereas, secondary crystallization occurs in the already solidified phase and produces an increase of crystallinity.[36] The overall analysis of crystallization of semicrystalline polymers integrates the effects of the nucleation mechanism, growth mechanism, and growth geometry. There are two approaches to follow crystallization processes. One evaluates the evolution of the crystalline fraction (mass or volume),[37,38,39] and the other evaluates the evolution of volume (area) fraction transformed into semicrystalline forms, such as spherulites.[36,40] The former approach describes the overall crystallization characteristics, while the latter evaluates the linear crystallization behavior.

1.3.2.1 Linear crystallization kinetics

The crystal growth kinetic theory was developed by Lauritzen and Hoffman.[41,42] Crystal growth only appears on the nucleus lateral surface, and it follows a mechanism of two-dimensional growth. Crystal growth involves the chain segment deposition on the planar growth front. It forms a secondary nucleus. The secondary nucleus can accept other segments to form the tertiary nuclei. The crystal growth process involves sequential stages: the deposition of a secondary nucleus on the surface of the crystal that has existed, and the continuous deposition of a tertiary nucleus, shown in Figure 1-2. There are two rates, i.e., the surface nucleation rate (secondary nuclei, *i*) and the layer completion rate (tertiary nuclei, *g*). Depending on the difference between the two rates, the regime behavior of crystal growth can be determined.

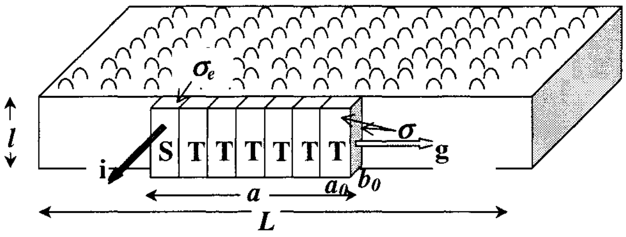

Figure 1-2 Secondary and tertiary nuclei

Hoffman and his coworkers[43,44] first suggested the regime behavior in polymer crystallization kinetics, shown in Figure 1-3. There are three regimes that depend on the crystallization temperature, or the supercooling degree. The supercooling degree is small in regime I. In this regime, the surface nucleation rate is much lower than the layer completion rate. The crystal growth rate is decided by the surface nucleation rate. As the supercooling degree increases, regime II appears. In regime II, the surface nucleation rate is similar to the layer completion rate. The crystal growth rate is determined by both rates. Multiple nuclei appear in the same layer. As the supercooling degree increases further, regime III can be expected.[45,46,47] In this regime, the surface nucleation rate is higher than the layer completion rate. The surface nucleation rate determines the overall crystal growth rate.

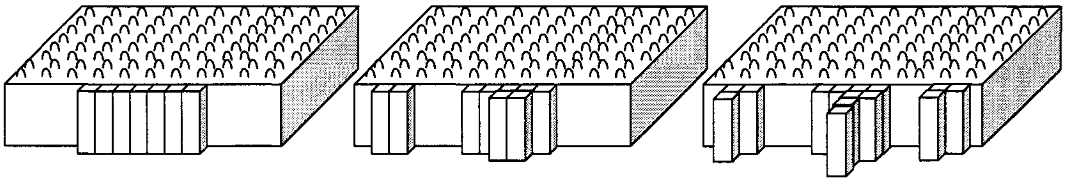

Regime I **Regime II** **Regime III**

Figure 1-3 Growth Regimes

Although it has been reported that the regime transition is a function of molecular weight,[48,49] polydispersity,[50] and chemical composition,[51,52] in addition to temperature, they cannot be taken as independent factors. These parameters can be related to the melting temperature of crystal stems with the maximum possible size.[9] Therefore, the regime transition may be only a function of temperature or degree of supercooling for a specific material.

According to the Hoffman-Lauritzen (HL) theory,[19,53] when the secondary nucleation rate and the layer completion rate are considered, the following kinetics relation is obtained:

$$G = G_0 \exp\left[-Q_D^* \middle/ RT_c \right] \exp\left[-K_g \middle/ T_c \Delta T f \right] \qquad (1\text{-}5)$$

where G_0 is a pre-exponential parameter containing quantities not strongly dependent on temperature, T_c represents the crystallization temperature, $\Delta T = T_m^0 - T_c$ is the supercooling degree (T_m^0 is the equilibrium melting temperature of the homopolymer), f is a correction factor for the variations of the heat of melting with temperature and is equal to $2T_c/(T_m^0+T_c)$, Q_D^* is the activation energy for reptation and center-of-mass diffusion, and is equal to 24 kJ/mol for polyethylenes,[53] and K_g is the nucleation constant, which depends on the regime behavior. For regimes III and I, K_g is given by:

$$K_{gIII} = K_{gI} = {4b_0\sigma\sigma_e T_m^0}\big/{k\Delta H_m} \tag{1-6}$$

and for regime II:

$$K_{gII} = {2b_0\sigma\sigma_e T_m^0}\big/{k\Delta H_m} \tag{1-7}$$

where σ and σ_e are the lateral and basal (folding) surface free energies, respectively, k is Boltzmann's constant, b_0 is the layer thickness, and ΔH_m is the heat of fusion.

For most polymers, when crystallization temperatures are equal to or less than T_g+100, where T_g is the glass transition temperature, $Q_D^*\big/RT_c \cong U^*\big/R(T - T_\infty)$. That is, the temperature dependence switches from the Arrhenius to WLF (Williams, Landel and Ferry) relations. Thus, Eq. (1-8) becomes:

$$G = G_0^* \exp\left[-U^*\big/R(T_c - T_\infty)\right]\exp\left[-K_g\big/T_c\Delta T f\right] \tag{1-8}$$

where U^* is the diffusive activation energy of chain reptation motion in the melt, and is a universal constant equal to 6.28 kJ/mol,[19] and $T_\infty = T_g$ -30.

As shown in Figure 1-4, the HL equation suggests three crystallization regimes. This indicated behavior is actually found in some polymers, such as polyethylene, poly(oxymethylene), polypropylene, and polybutene, when crystalline spherulite or axialite growth was observed. The existence of different growth regimes is often related to morphological changes. For example, for linear polyethylene, the morphologies are ring-banded spherulite, spherulite, and axialite in regimes III, II, and I, respectively.[53]

The HL equation cannot simply and directly be applied to calculate the overall crystallinity, or the overall crystallization kinetics, because it does not include the information about the amorphous part in spherulites or axialites. Also, it does not consider the effect of secondary crystallization. Furthermore, as discussed earlier in the melting temperature section, the equilibrium melting temperature represents a hypothetical state. Thus, the equilibrium melting temperature for homopolymers in the HL expression should be replaced by the melting temperature of crystal stems with the maximum possible size,[9] which is a function of molecular composition and molecular structure, especially for copolymer systems.

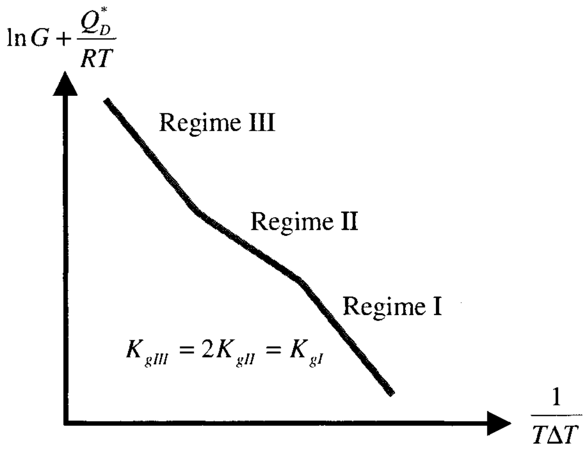

Figure 1-4 Different growth regimes by Hoffman-Lauritzen equation

1.3.2.2 Overall crystallization kinetics

The Avrami model is a classical expression to describe the overall crystallization kinetics in isothermal experiments.[54,55,56] It is effective only for the primary crystallization process. It leads to the following relation:

$$X(t) = 1 - \exp\left[-k(T)(t-\tau)^n\right] \tag{1-9}$$

where X is the crystallinity, τ is the induction time, n is the Avrami exponent, and k is the crystallization constant. From a plot of $\ln[-\ln(1-X)]$ vs. $\ln(t-\tau)$, coefficients n and k can be determined. The crystallization constant k contains cumulative information about the entire crystallization curve at T_c, and it can provide quantitative kinetic information of the crystallization mechanism. The Avrami exponent, n, indicates the growth mechanism, as shown in Table 1-1.[57,58] However, the total crystallization process generally includes several mechanisms. Therefore, different values for n are always obtained.

Table 1-1 Avrami exponent and crystallization growth mechanism

Avrami Exponent	Nucleation	Growth Habit	Growth Control
0.5	Instantaneous	Rod	Diffusion
1.0	Instantaneous	Rod	Interface
		Disc	Diffusion
1.5	Instantaneous	Sphere	Diffusion
	Homogeneous	Rod	Diffusion
2.0	Instantaneous	Disc	Interface
	Homogeneous	Disc	Diffusion
		Rod	Interface
2.5	Homogeneous	Sphere	Diffusion
3.0	Instantaneous	Sphere	Interface
	Homogeneous	Disc	Interface
4.0	Homogeneous	Sphere	Interface
5.0	Instantaneous	Sheaf	Interface
6.0	Homogeneous	Sheaf	Interface

Semicrystalline polymers cannot attain 100 percent crystallinity. Therefore, Mandelkern suggested that the relative crystallinity, Θ, should replace the absolute crystallinity, X.[59] Then, the generalized Avrami equation becomes:

$$\Theta(t)=\frac{X(t)}{X_\infty(T)}=1-\exp\left[k(T)(t-\tau)^n\right] \tag{1-10}$$

where X_∞ is the ultimate crystallinity obtained after long time at temperature T. Here, it is necessary to point out that X_∞ possibly depends on processing conditions. If secondary crystallization occurs, it could be very difficult to identify X_∞.

Because the Avrami model does not consider some factors, such as the secondary crystallization effect and the decrease of the growth rate, it generally fits data only in the initial crystallization stage. Some modified models have been proposed. For example, isothermal models have been proposed by Tobin,[60,61,62] Kim and Kim,[63] and Malkin.[64,65] Also, non-isothermal models have been proposed by Nakamura,[66] Ziabicki,[67] Dietz,[68] and Ozawa[69].

1.3.3 Crystalline morphological characteristics

Crystalline morphological characteristics of polymers include crystalline structure and crystalline morphology. The crystalline structure refers to the particular way in which the chains are packed. The crystalline morphology (or simply called morphology) refers to the shape and size, arrangement, and amorphous connection of crystallites.

The crystalline structure can be detected by X-ray, and electron and neutron diffraction. According to thermodynamic considerations, chains generally adopt conformations with a minimum free energy, such as a planar zigzag or a helical structure, which is mainly determined by the chemical structure of monomers and their linking forms. For polyethylene, the basic crystalline structure is the orthorhombic form. Chains form the planar zigzag conformation. The unit cell is shown in Figure 1-5.[70] Its dimensions are a = 0.742 nm, b = 0.493 nm, and c = 0.253 nm. In the amorphous phase, the conformation structure is random coiling, the same as that of melts and solutions.[71]

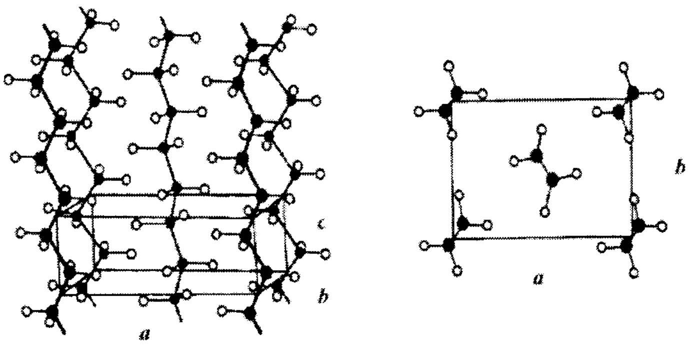

Figure 1-5 Polyethylene crystalline structure[70]

Polymer chains can take three basic forms in a polymer solid, i.e., amorphous, extended, and folded chains. The amorphous chains are similar to those in melts and glasses, i.e., chains are randomly arranged. The extended chains are the equilibrium crystals; and whole molecular chains extend to form the maximum size crystal. The folded chains are normal crystalline chain structures, and include regular and irregular folding structures, as shown in Figure 1-6. Semicrystalline polymers generally tend to form a combination structure, i.e., fringed micelle. For LLDPEs, because comonomers are excluded from the crystalline lattice of LLDPE crystals, the irregular folding chains are prevalent.

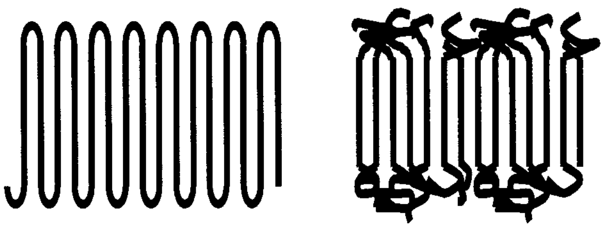

Figure 1-6 Regular chain folding (left) and irregular chain folding (right)

When polymers are crystallized from melts, spherulites are most frequently observed. This morphology has a spherical shape with aggregates of crystalline lamellae. There are two mechanisms that can produce a spherical morphology, i.e., hedgehog and pop-off models, shown in Figure 1-7.[72,73] Most polymer crystallizations follow the pop-off mechanism.

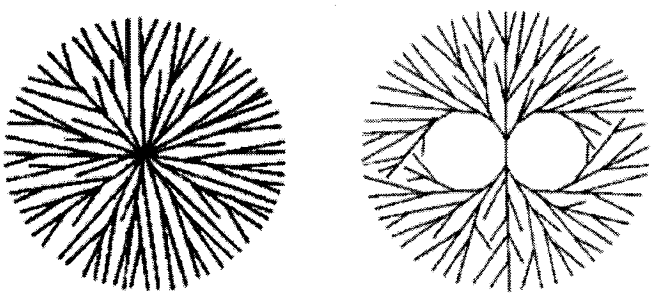

Figure 1-7 Model of Spherulite Growth Mechanism (Left: Hedgehog, Right: Pop-off)[74]

The lamellar arrangement in spherulites is shown in Figure 1-8. The lamellae open out into a fan from the center to the periphery along the radial direction. In some cases, the lamellae are twisted into spirals in radial directions, and then a regular ring-banded spherulite can be observed, as shown in Figure 1-9. The ring-banded distance decreases, as the crystallization temperature decreases.

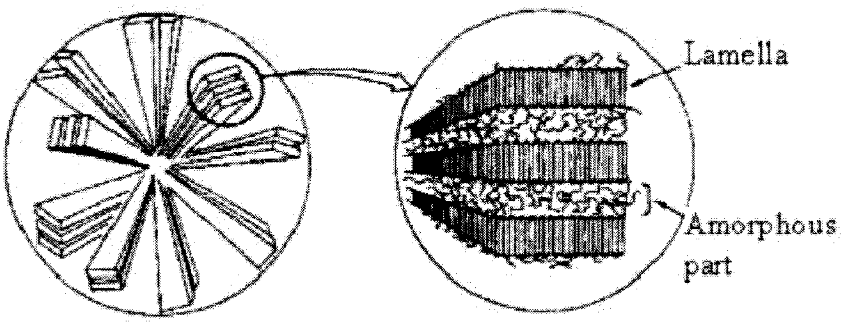

Figure 1-8 Model of spherulite morphology[74]

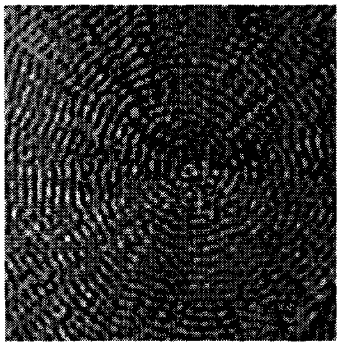

Figure 1-9 Ring-banded structure in Resin G spherulite.

Spherulites are optically anisotropic. The molecular chain orientation is generally perpendicular to spherulitic radius direction, as shown in Figure 1-8. Thus, they produce a birefringent Maltese cross when viewed by a polarized light microscope, as shown in Figure 1-10 for resin G. The diameters of spherulites range from several micrometers up to several millimeters.

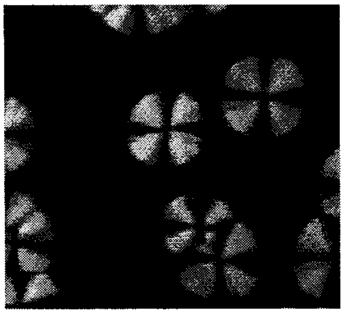

Figure 1-10 Maltese Cross structure in resin G spherulite

In addition to the crystalline phase with regular or ordered structures and the amorphous phase with irregular or disordered structure, there is an interfacial phase with partially regular or ordered phase, between the crystalline phase and amorphous phase. The contents of these phases can be quantitatively measured by using NMR[75], IR[76], and Raman[77] techniques.

1.4 Experimental Techniques

The molecular weight and distribution of LLDPE copolymers can be measured by gel permeation chromatography (GPC).[78] Nuclear magnetic resonance (NMR) is an effective method to measure the short chain branch content (SCBC).[79] Temperature rising elution fractionation (TREF),[6] crystallization analysis fractionation (CRYSTAF),[7] step crystallization (SC)[80], and successive self-nucleation and annealing (SSA)[81] by differential scanning calorimetry (DSC) can possibly identify the short chain branching distribution (SCBD).

The basic experimental techniques used for this work were polarized light microscopy (PLM), differential scanning calorimetry (DSC), and small angle x-ray scattering (SAXS). The polarized light microscope with a hot stage was used to study linear crystallization kinetics and morphologies. DSC was used to study melting behavior, overall crystallization kinetics, and crystal size and melting temperature distributions. SAXS was used to measure the average crystal size.

1.4.1 Polarized light microscopy (PLM)

Light microscopy is the most convenient method for morphological observation and size measurement. Because of the limitation of the wavelength, the image resolution is about 1μm. Thus, crystalline morphological features, such as spherulites and axialites, are easy to identify. However, individual lamella, with thickness usually less than 10nm, cannot be resolved.[57,82] Polymer spherulites under crossed polarization exhibit a Maltese cross image aligned with the polarizer and analyzer as shown in Figure 1-10.

A polarized light microscope (Olympus BH-2) equipped with a hot stage (Linkam TH600) and a digital camcorder (SONY DXC-950/1), was used in this research. The crystallization temperature is easily controlled by the hot stage (± 0.1°C). The heating or cooling rate can reach 130°C/min.

1.4.2 Differential scanning calorimetry (DSC)

Differential scanning calorimetry (DSC) is a commonly used thermal analysis technique. Heat flux to the sample is monitored against time or temperature, while a certain temperature program is imposed under a specific controlled atmosphere, for instance, nitrogen. The fundamental theory and application of DSC to polymer characterization have been reviewed in detail.[74]

For a first order transition process (melting-crystallization) of semicrystalline polymers, DSC can be used to measure accurately the heat of melting and crystallization and to determine the experimental melting and the crystallization temperature.

In this research, thermal analysis was performed in a Perkin-Elmer Pyris-1 Differential Scanning Calorimeter. The temperature and the heat flow were calibrated with pure indium (T_{onset} = 156.60°C, ΔH_f = 28.45 J/g). The contribution to the DSC curves by the empty aluminum specimen pan was subtracted from each measurement. All measurements were performed under nitrogen. The experimental baseline was selected as a sigmoid line, which was supplied by the Pyris software.

1.4.3 Small angle x-ray scattering (SAXS)

Small angle x-ray scattering (SAXS) is a widely used diffraction technique for detecting material structure. Semi-crystalline polymers have randomly oriented stack structures, in which crystalline lamellae are packed in parallel with alternating amorphous layers. Randomly oriented stacks produce isotropic scattering. The scattering data can be interpreted by the Lorentz-correction:[83]

$$I_c(s) = 4\pi s^2 I(s) \qquad (1\text{-}11)$$

where $I_c(s)$ is the correction intensity, $I(s)$ is the measured intensity after correction for background scattering, detector noise, and absorption,[84] and the scattering vector $s = \frac{2\sin(\theta)}{\lambda}$. The Lorenz-correction function complies with the average one-dimensional scattering intensity emitted by one stack. The first maximum, s^*, of the corrected function represents the reciprocal of the long period or Bragg distance, L:

$$L = 1/s^* \qquad (1\text{-}12)$$

The average lamellar thickness can be estimated by the product of L and volume crystallinity. This crystallinity value can be obtained from other experimental results, such as from DSC data.

In this research, SAXS experiments were performed in a high resolution diffractometer with a conventional 2.2Kw Cu-K$_\alpha$ x-ray tube source, built in the Physics Department at McGill University. The wavelength of x-ray, λ, was 0.154nm. The thickness of specimens was 6mm The scattering angle (2θ) was from 0.01 to 2.01°. The scattering intensities were corrected for the background and sample adsorption.

1.5 Objectives and Present Investigation

The research described in this thesis focuses on the melting and crystallization behavior of polyethylene materials, especially linear low-density polyethylene (LLDPE) copolymers (including homogeneous, semi-homogeneous, and heterogeneous LLDPE resins). The work involves theoretical analyses (physics and mathematics models) and experimental studies. Relationships among molecular structural parameters, processing conditions, and crystalline morphological characteristics are proposed. The objectives include:

- *Chapter 2*: Characterization of the melting temperature according to molecular structural parameters: ZN-LLDPE resins, m-LLDPE resins, and m-LLDPE blends

  As the melting temperature is one of the key points in this research, three types of melting temperatures are classified. A generalized melting temperature equation is proposed to estimate the melting temperatures from structural characteristics.

- *Chapter 3*: Prediction of crystal size number distributions from DSC melting traces for different LLDPEs

  The proposed melting temperature equation is employed, in conjunction with DSC melting traces, to determine crystal size number distributions. The predictions are validated experimentally.

- *Chapter 4*: Description of melting temperature distributions from DSC melting traces for different LLDPEs

  The melting temperature characteristics are discussed in more detail, based on the proposed melting temperature equation and crystal size number distributions. The melting temperature distribution is proposed to explain the melting behavior for semi-crystalline polymers.

- *Chapter 5*: Evaluation of crystallization kinetics by optical observation (linear)

  A modified form of the Hoffman-Lauritzen equation is proposed. It replaces the equilibrium melting temperature with the melting temperature of crystal stems with the maximum possible crystal size. The modified equation is employed to evaluate spherulitic growth kinetics for three types of linear low-density polyethylene: m-LLDPEs (homogeneous), m-LLDPE blends (semi-homogeneous), and ZN-LLDPEs (heterogeneous).

- *Chapter 6*: Explanation of crystalline non-linear spherulitic growth behavior

  The non-linear spherulitic growth behavior in the high crystallization temperature region (regimes II and IM) is explained for LLDPE materials. Diffusion of uncrystallizable ethylene sequences produces the non-linearity. Experimental data are used to validate the modified Hoffman-Lauritzen equation.

- *Chapter 7*: Evaluation of crystallization kinetics by DSC measurement (overall) and description of the relationship between overall and linear crystallization kinetics

  The overall crystallization kinetics are evaluated according to the Avrami equation. The effective nucleation induction time concept is introduced. The results of linear and overall crystallization kinetics are compared and explained.

- *Chapter 8*: Explanation of morphological characteristics

  The morphological characteristics of different LLDPEs are evaluated, and the factors influencing ring-banded distance are discussed. The morphological characteristics are related to the crystalline growth regime behavior.

1.6 References

1 Imuta J, Kashiwa N. In: Vasile, C. Editors, Handbook of Polyolefins, New York: Marcel-Dekker Press, 2000, p.71.

2 Peacock AJ. Handbook of Polyethylene: Structures, Properties, and Applications, New York: Marcel-Dekker Press, 2000.

3 Sehanobish K, Patel RM, Croft BA, Chum SP, Kao CI. J Appl Polym Sci 1994, 51:887.

4 Fu Q, Chiu FC, McCreight KW, Guo M, Tseng WW, Cheng SZD, Keating MY, Hsieh ET, DesLauriers PJ. J Macromol Sci, Phys 1997, B36:41.

5 Crist B, Howard PR. Macromolecules 1999, 32:3057.

6 Wild L, Ryle T, Knobeloch D, Peat I. J Polym Sci, B: Polym Phys 1982, 20:441.

7 Monrabal B. J Appl Polym Sci 1994, 52:491.

8 Feng L, Kamal MR. Can J Chem Eng 2004, accepted for publication (see Chapter 3 in this thesis).

9 Kamal MR, Feng L, Huang T. Can J Chem Eng 2002, 80:432. (see Chapter 2 of this thesis)

10 Flory PJ. Trans Faraday Soc 1955, 51:847.

11 Flory PJ. J Chem Phys 1949, 17:223.

12 Sanchez IC, Eby RK. Macromolecules 1975, 8:639.

13 Helfand E, Lauritzen JI. Jr. Macormolecules 1973, 6:631.

14 Jokela K, Väänänen A, Torkkeli M, Starck P, Serimaa R, Löfgren B, Seppälä J. J Polym Sci, B: Polym Phys 2001, 39:1860.

15 Marigo A, Zannetti R, Milani F. Eur Polym J 1997, 33:595.

16 Alamo RG, Mandelkern L. Thermochim Acta 1994, 238:155.

17 Stack GM, Mandelkern L, Kröhnke C, Wegner G. Macromolecules 1989, 22:4351.

18 Hoffman JD. Polymer 1991, 32:2828.

19 Hoffman JD, Davis GT, Lauritzen JI. In: Hannay NB. Editor, Treatise on Solid State Chemistry, Vol. 3, New York: Plenum Press, 1976 (Chapter 7).

20 Voigt-Martin IG, Alamo R, Mandelkern L. J Polym Sci, B: Polym Phys 1986, 24:1283.

21 Zhou H, Wilkes GL. Polymer 1997, 38:5735.

22 Eng LM, Fuchs H, Jandt KD, Petermann J. Helvetica Physica Acta 1992, 65:870.

23 Crist B. J Polym Sci, B: Polym Phys 1973, 11:635.

24 Crist B, Morosoff N. J Polym Sci, B: Polym Phys 1973, 11:1023.

25 Snyder RG, Scherer JR. J Polym Sci, B: Polym Phys 1980, 18:421.

26 Jandt KD, Buhk M, Miles MJ, Petermann J. Polymer 1994, 35:2458.

27 Villarreal N, Pastor JM, Perera R, Rosales C, Merino JC. Macromol Chem Phys 2002, 203:238.

28 Lu L, Alamo RG, Mandelkern L. Macromolecules 1994, 27:6571.

29 Crist B, Mirabella FM. J Polym Sci, B: Polym Phys 1999, 37:3131.

30 Lee YD, Phillips PJ, Lin JS. J Polym Sci, B: Polym Phys 1991, 29:1235.

31 Blundell DJ. Polymer 1978, 19:1258.

32 Marega C, Marigo A, Cingano G, Zannetti R, Paganetto G. Polymer 1996, 37:5549.

33 Mizushima S, Shimanouchi T. J Am Chem Soc 1949, 71:1320.

34 Wunderlich B. Macromolecular Physics, Vol.3. London: Academic Press, 1980.

35 Mirabella FM. J Polym Sci, B: Polym Phys 2003, 41: 235.

36 Haudin JM, Monasse E. NATO ASI Series Applied Sciences-Advanced Study Institue, 2000, 370:93.

37 Fatou JG, Marc C, Mandelkern L. Polymer 1990, 31:890.

38 Fatou JG, Marc C, Mandelkern L. Polymer 1990, 31:1685.

39 Tung LH. J Polym Sci 1967, 5A-2:391.

40 McMaster TJ, Hobbs JK, Barham PJ, Miles MJ. Probe Microscopy 1997, 1:43.

41 Lauritzen JI. Jr., Hoffman JD. J Res Natl Bur Stand 1960, 64A:73.

42 Hoffman JD, Lauritzen JI. Jr. J Res Natl Bur Stand 1961, 65A:297.

43 Lauritzen JI, Hoffman JD. J Appl Phys 1973, 44:4340.

44 Hoffman JD, Frolen LJ, Ross GS, Lauritzen JI. J Res Natl Bur Stand 1975, 79A:671.

45 Hoffman JD, Guttman CM, DiMarzio EA. Discuss Faraday Chem Soc 1979, 68:177.

46 Phillips PJ. Polym Prepr (Am Chem Soc Div Polym Chem) 1979, 20:483.

47 Hoffman JD. Polymer 1983, 24:3.

48 Hoffman JD, Miller RL. Macromolecules 1988, 21:3038.

49 Lambert WS, Phillips PJ. Polymer 1996, 37:3585.

50 Phillips PJ, Vatansever N. Macromolecules 1987, 20:2138.

51 Lovinger AJ, Davis DD, Padden FJ. Jr. Polymer 1985, 26:1595.

52 Lambert WS, Phillips PJ. Macromolecules 1994, 27:3537.

53 Hoffman JD, Miller RL. Polymer 1997, 38:3151.

54 Avrami M. J Chem Phys 1939, 7:1103.

55 Avrami M. J Chem Phys 1940, 8:212.

56 Avrami M. J Chem Phys 1941, 9:177.

57 Schultz JM. Polymer Crystallization: the Development of Crystalline Order in Thermoplastic Polymers, Oxford, New York: Oxford University Press, 2001 (Chapter10).

58 Flory PJ, McIntyre AC. J Polym Sci 1955, 18:592.

59 Mandelkern L. J Appl Phys 1955, 26:443.

60 Tobin MC. J Polym Sci, B: Polym Phys 1974, 12:399.

61 Tobin MC. J Polym Sci, B: Polym Phys 1976, 14:2253.

62 Tobin MC. J Polym Sci, B: Polym Phys 1977, 15:2269.

63 Kim SP, Kim SC. Polym Eng Sci 1991, 31:110.

64 Malkin AY, Beghishev VP, Kipin IA, Bolgov SA. Polym Eng Sci 1984, 24:1396.

65 Malkin AY, Beghishev VP, Kipin IA, Andrianova ZS. Polym Eng Sci 1984, 24:1402.

66 Nakamura K, Watanabe T, Katayama K, Amano T. J Appl Polym Sci 1972, 16:1077.

67 Ziabicki A. Polimery (Warsaw, Poland) 1967, 12:405.

68 Dietz W. Colloid Polym Sci 1981, 259:413.

69 Ozawa T. Polymer 1971, 12:150.

70 Bunn CW. Chemical Crystallography: An Introduction to Optical and X-ray Methods, (2nd ed.), London: Clarendon Press, Oxford (Oxford University Press), 1961.

71 Snyder RG, Schlotter NE, Alamo R, Mandelkern L. Macromolecules 1986, 19:621.

72 Keith HD, Padden FJ. J Appl Phys 1963, 34:2409.

73 Bassett DC, Vaughan AS. Polymer 1985, 26:717.

74 Wunderlich B. Thermal Analysis of Materials, downloadable: http://web.utk.edu/ ~athas/courses/ tham99.html.

75 Bergmann K, Nawotki K. Kolloid-Z. Z. Polym 1967, 219:132.

76 Keresztury G, Földes E. Polym Test 1990, 9:329.

77 Strobl GR, Hagedorn W. J Polym Sci, B: Polym Phys 1978, 16:1181.

78 Francuskiewicz F. Polymer Fractionation, Berlin: Springer-Verlag, 1994.

79 Randall JC, J Macromol Sci Rev: Macromol Chem Phys 1989, C29:201.

80 Schouterden P, Groeninckx G, Van der Heijden B, Jansen F. Polymer 1987, 28:2099.

81 Muller AJ, Hernandez ZH, Arnal ML, Sanchez JJ. Polym Bull 1979, 39:465.

82 Schultz JM. Polymer Materials Science, Englewood Cliffs, NJ: Prentice Hall, 1974.

83 Svergun DI, Feigin LA. X-ray and Neutron Low-Angle Scattering, New York: Plenum Press, 1987.

84 Androsch R, Blackwell J, Chvalun SN, Wunderlich B. Macromolecules 1999, 32:3735.

Chapter 2

2 A Generalized Equation for the Prediction of Melting Temperatures of Polymers

A generalized equation is introduced to clarify conceptual definitions of copolymer melting temperatures. This treatment incorporates the effects of comonomer volume, crystal length, folding surface free energy and enthalpy of fusion, when comonomers are excluded from the crystallite lattice. Both the Gibbs-Thomson Equation for homopolymers and a modified application to copolymers have also been derived from the proposed equation as two special cases. The melting temperature T_m in the Flory equation corresponds to the melting temperature $T_m^{C,\infty}$ of copolymer crystals with stems of infinite length. Also, $T_m^{C,n*}$, the melting temperature for copolymer crystals with stems containing the maximum possible number of structural units, n^*, should be used instead of T_m^0 as the basis of supercooling in crystallization. The proposed equation shows good agreement with experimental data for α-alkene-ethylene homogeneous copolymers.

2.1 Introduction

The melting temperature (T_m) is one of the most important properties of semi-crystalline polymers, especially in the study of crystallization and melting processes. In polymer processing, the energy requirements of the process, the behavior of the material during processing, and the morphology of the final product are strongly influenced by the melting and crystallization of the material. Therefore, it is useful to obtain dependable relationships or equations for the estimation of the melting temperatures of homopolymers and copolymers.

One of the commonly used melting parameters, T_m^0, refers to the thermodynamic equilibrium melting temperature of the polymer crystal with crystal stems containing an infinite number of structural units.[1] Obviously, this is a theoretical property, since it is not possible to achieve a polymer with infinite molecular weight. Usually, T_m^0 is estimated, for homopolymers, by extrapolation according to established relationships, such as the Gibbs-Thomson equation[2] and the Hoffman-Weeks equation[3], or by extrapolation according to the melting properties of a series of small molecules.[4] In this paper, we refer to T_m^0 for homopolymers as $T_m^{H,\infty}$. For copolymers, Flory[5] proposed theoretical calculation methods by consideration of crystals that excluded comonomers from the crystals. The treatment is based on analysis of the depression of T_m^0 ($T_m^{H,\infty}$) by the incorporation of the comonomers. Therefore, in this work, we shall refer to the melting temperature of a copolymer calculated following Flory's equation as $T_m^{C,\infty}$.

In real terms, one should consider finite dimensions of the crystal. Real crystal dimensions are finite, because of the finite molecular weights and the exclusion of branch units. So, T_m^∞ does not have real physical meaning in real crystals. It is more practical to consider the melting temperature of the crystal with crystal stems containing the maximum possible size or number of structural units (n^*), defined here as T_m^{n*}.

For homopolymers and copolymers with included comonomers, T_m^{n*} is the melting temperature of the molecular crystal. However, it is also very difficult to form molecular crystals, especially in high molecular weight polymers, because of limitations associated with chain flexibility, flow viscosity, etc. Therefore, this kind of melting temperature is difficult to achieve experimentally. For copolymers with excluded comonomers, because the excluded comonomer units become the lattice ends, the length of crystals of maximum possible size decreases substantially. Such a crystal would have a stem length equal to the length of the chain between comonomers. For such polymer, it is possible to form crystals with crystal stems having the maximum possible size under some special conditions. It is also possible to measure T_m^{n*} experimentally, especially in copolymers with high comonomer content.

For actual polymers, it is not possible to form crystals from the melt, if the crystallization temperature is higher than T_m^{n*}. Only when the crystallization temperature is lower than T_m^{n*}, crystals can form and develop. Therefore, T_m^{n*} should be the basis for determination of the degree of supercooling, which represents the crystallization driving force. The degree of supercooling governs polymer crystallization kinetics and even morphology. T_m^{n*} is a true material parameter, which is a property determined by material factors such as chemical composition, molecular weight, molecular weight polydispersity, branching degree, and branch distribution.

Some equations[4,6,7,8,9] have been employed to evaluate T_m^{n*} by considering molecular weight effects. Flory-Vrij[4] correctly measured and proposed an equation to estimate T_m^{n*} of paraffins. However, it is not necessarily valid to extrapolate their equation to linear polyethylene. Even if it is assumed that the Flory-Vrij equation[10,11] may be applied to estimate T_m^{n*} of linear polyethylene, the equation as it stands is not applicable for estimation of T_m^{n*} of the low-density polyethylene (LDPE) and linear low-density polyethylene (LLDPE). Furthermore, it is still difficult to predict T_m^{n*} for other polymers with more complex structures, due to the lack of experimental data similar to those available for paraffins.

The most commonly used melting temperature usually refers to the experimentally measured melting temperature, T_m^n, where n is the actual number of structural units in the real crystal stem. As in the case of T_m^0 and T_m^{n*}, T_m^n is also determined by material composition and structure. However, kinetic factors control various important aspects of polymer crystallization, such as growth rate, crystalline morphology, and lamellar thickness (i.e. crystal stem length).[2] Therefore, crystallization conditions have a great influence on T_m^n, and different crystallization conditions produce different T_m^n. Furthermore, since the crystallization of semi-crystalline polymers is not an equilibrium process, because of the high basal surface area of folding crystals, the lattices are continually evolving toward a more perfect crystalline state. The final melting temperature tends to approach T_m^{n*}, due to this evolution. Thus, the reported values of T_m^n are usually different for the same material. Although T_m^n is easy to obtain by experimental methods, such as differential scanning calorimetry (DSC), it is not truly a material property, since it is influenced by measurement conditions. However, because the evolution at room temperature is generally very slow for most polymers, some aspects of polymer behavior are related to T_m^n, even for long periods after solidification. As a result, some effective techniques have been used to modify semicrystalline polymer behavior by manipulating T_m^n. Thus, T_m^n is important in actual practice, although it is not generally a true equilibrium property.

In this paper, we propose equations to estimate T_m^∞, T_m^{n*} and T_m^n for homopolymers and copolymers, when comonomer structural units are excluded from the crystal. Starting with Flory's thermodynamic approach,[5] we derive a more general equation for the melting temperatures of polymers. The values of T_m^∞, T_m^{n*} and T_m^n for homopolymers and copolymers are evaluated, with special emphasis on α-alkene-ethylene copolymers and linear polyethylene homopolymers (including paraffins).

2.2 Theoretical Analysis

2.2.1 Flory's Equation

We start with Flory's thermodynamic treatment of the melting of copolymers,[5] in which all comonomers are excluded from lattices. Crystal longitudinal growth will be restricted by the appearance of comonomers in the chain.

In addition to the free energy requirements associated with the incorporation of structural units into crystals, formation of a crystal stem of a given size requires the availability in the melt of sequences containing a minimum number of consecutive structural units. Crystal stems of any length n are in equilibrium with the sequences of structural units available in the melt phase. Let P_n be the probability that the backbone structural unit of melting polymer occupying a crystal stem initial site is an A structural unit, which is within a sequence of at least n structural units. At equilibrium, P_n can be represented by the following equation:

$$P_n^e = \exp\left(-\Delta G_n / RT\right) \tag{2-1}$$

where the superscript e refers to the equilibrium condition, R is the gas constant, T is the temperature, and ΔG_n is the free energy of fusion of the crystal stem of n structural units. In turn, ΔG_n may be described in terms of the free energy of fusion per structural unit, ΔG_u, and the basal (folding) surface free energy, σ_e, as follows:

$$\Delta G_n = n\Delta G_u - 2\sigma_e \tag{2-2}$$

and

$$\Delta G_u = \Delta H_u - T\Delta S_u = \Delta H_u\left[1 - \left(T/T_m^0\right)\right] \tag{2-3}$$

where ΔH_u and ΔS_u are the heat of fusion and the entropy of fusion per repeat structural unit, respectively. It should be noted that Eq.(2-2) does not consider the lateral surface energy of the crystal stem. For the general case, crystal stems assemble together along the lateral surface to form the crystal. As a result, the area of the lateral surface will be greatly reduced. Therefore, no loss of precision occurs if the lateral surface effects are neglected.[2]

The melting temperature of the corresponding pure homopolymer, $T_m{}^0$, is:

$$T_m^0 = \frac{\Delta H_n}{\Delta S_n} = \frac{n\Delta H_u + \Delta H_e}{n\Delta S_u + \Delta S_e} = \frac{\Delta H_u + \dfrac{\Delta H_e}{n}}{\Delta S_u + \dfrac{\Delta S_e}{n}} \tag{2-4}$$

where ΔH_e and ΔS_e are the end-group contributions. When n tends to infinity or is large enough, Eq.(2-4) becomes:

$$T_m^0 = \frac{\Delta H_u}{\Delta S_u} \tag{2-5}$$

Thus, T_m^0 implies the melting temperature of a homopolymer crystal with crystal stems of infinite size,[12,13,14,15] although Flory had occasionally referred to it as the melting temperature of the pure polymer.[5] Hereafter, T_m^0 is referred to as $T_m^{H,\infty}$,

If $\Delta H_u/\Delta S_u$ has the same values at T and $T_m^{H,\infty}$, Eq.(2-2) becomes:

$$\Delta G_n = n\left[\Delta H_u\left(1-\frac{T}{T_m^{H,\infty}}\right)\right]-2\sigma_e \tag{2-6}$$

Finally, Eq.(2-1) can be rewritten as follows:

$$P_n^e = (1/D)\exp(-n\theta) \tag{2-7}$$

where

$$\theta = \frac{\Delta H_u}{R}\left(\frac{1}{T}-\frac{1}{T_m^{H,\infty}}\right) \tag{2-8}$$

and

$$D = e^{-2\sigma_e/RT} \tag{2-9}$$

Initially, when a crystal melts:

$$P_n^0 = X_A p^{n-1} \tag{2-10}$$

where the superscript 0 refers to zero time, X_A is the mole fraction of A structural units, (A is monomer), and p is the sequence propagation probability that a structural unit is succeeded by another structural unit. The latter is independent of the number of preceding structural units. For the case where the volume of the comonomer is the same as that of the backbone unit, for random copolymers, $p = X_A$; for block or ordered copolymers $p > X_A$; and $p < X_A$, if alternation of structural units is favored. If the volume of the comonomer is different from that of the backbone unit, then X_A should be replaced by the volume fraction.

A necessary and sufficient condition for crystallization is that $P_n^0 > P_n^e$, for one or more n-sequences. That is,

$$(X_A/p)p^n > (1/D)\exp(-n\theta) \tag{2-11}$$

Only when the number of these n-sequences is greater than zero, crystals can appear. In the general case, $(X_A/p) < (1/D)$, and if this is incorporated in Eq.(2-11), the following relationship is obtained:

$$p^n > \exp(-n\theta) \tag{2-12}$$

and

$$\theta > \theta_m = -\ln p \tag{2-13}$$

At the critical condition (melting condition), θ is replaced by θ_m. The melting temperature equation is:

$$\frac{1}{T_m} - \frac{1}{T_m^{H,\infty}\left(or\ T_m^0\right)} = -\frac{R}{\Delta H_u}\ln p \tag{2-14}$$

This is Flory's equation for estimating the melting temperature of copolymers. It describes the relationship between the melting temperature of a homopolymer ($T_m^{H,\infty}$) with an infinite crystal (i.e. a linear homopolymer of infinite molecular weight) and the melting temperature of a branched polymer or copolymer (T_m), with branches or comonomers excluded from the lattice.

2.2.2 The proposed equation

It should be noted that Eq.(2-14) involves a simplification of Eq.(2-11), where some terms have been neglected, thus leading to Eq.(2-12). In this section, we remove this simplification and introduce a more complete treatment of the melting temperature of copolymers with excluded comonomers. Starting with Eq.(2-11), the following equation is obtained:

$$\theta > \theta_m = -\left\{\ln p + \left[\ln\left(\frac{DX_A}{p}\right)\right]\Big/ n\right\} \tag{2-15}$$

At the critical condition, i.e. at the melting temperature, one obtains the following relationship:

$$\frac{1}{T_m^{C,n}} - \frac{1}{T_m^{H,\infty}} = -\left(\frac{R}{\Delta H_u}\right)\left\{\ln p + \left[\ln\left(\frac{DX_A}{p}\right)\right]\Big/ n\right\} \tag{2-16}$$

Another form of this equation is obtained by replacing *D*, using the expression in Eq.(2-9).

$$\frac{1}{T_m^{C,n}}\left(1 - \frac{2\sigma_e}{\Delta H_u n}\right) - \frac{1}{T_m^{H,\infty}} = -\left(\frac{R}{\Delta H_u}\right)\ln p - \frac{1}{n}\left(\frac{R}{\Delta H_u}\right)\ln\left(\frac{X_A}{p}\right) \tag{2-17}$$

Eq.(2-17) describes the relationship between $T_m^{H,\infty}$ and $T_m^{C,n}$. Compared with the Flory equation (Eq.(2-14)), Eq.(2-17) includes additional terms that incorporate the effects of the folding surface free energy, the crystal length (the number of structural units in the crystal stem), and the comonomer volume fraction. Eq.(2-17) provides a basis for the calculation of the melting temperature of real crystals with crystal stems of any structural unit number, *n*. The crystal length (i.e. the number of structural units in the crystal stems), *n*, is below its maximum possible crystal length (i.e. the maximum possible number of structural units in the crystal stems), n^*. When *n* reaches n^*, then Eq. (2-18) can be applied to describe $T_m^{C,n*}$:

$$\frac{1}{T_m^{C,n^*}}\left(1 - \frac{2\sigma_e}{\Delta H_u n^*}\right) - \frac{1}{T_m^{H,\infty}} = -\left(\frac{R}{\Delta H_u}\right)\ln p - \frac{1}{n^*}\left(\frac{R}{\Delta H_u}\right)\ln\left(\frac{X_A}{p}\right) \tag{2-18}$$

If n^* becomes infinite, that is, the sequence between two comonomers becomes infinite (the molecular chain length becomes infinitely large), then Eq.(2-18) simplifies to the form:

$$\frac{1}{T_m^{C,\infty}} - \frac{1}{T_m^{H,\infty}} \rightarrow -\frac{R}{\Delta H_u} \ln p \qquad (2\text{-}19)$$

where $T_m^{C,\infty}$ refers to the equilibrium melting temperature of the crystal with crystal stems of infinite structural unit number in the copolymer with excluded comonomers. This suggests that T_m in the Flory equation, Eq.(2-14), is actually $T_m^{C,\infty}$. Thus, $T_m^{C,\infty}$ is a hypothetical limiting parameter similar to $T_m^{H,\infty}$. Therefore, it is not expected that it would provide an accurate estimate of $T_m^{C,n}$ or T_m^{C,n^*}. This explains the observation that experimental data do not really fit the Flory prediction.

Starting with the Flory equation, Baur[15] introduced the "hindered equilibrium" concept to describe the quasi-eutectic behavior by considering the average sequence length. The predicted melting temperatures were in better agreement with experimental data than those obtained with the Flory's equation. Just as we discussed before, the Flory equation defines $T_m^{C,\infty}$, not T_m^n. Therefore, it is not expected to yield a good prediction of T_m^n. The Baur melting temperature is much like $T_m^{n^*}$. However, because Baur did not consider the effects of basal surface free energy and the comonomer volume effects, his equation is not expected to agree with real values, especially in copolymers with the high comonomer content. Wendling and Suter[16] combined the Baur and Sanchez-Eby[17] equations to predict the melting temperature of copolymers with included comonomers. When the comonomer content in crystals tends to zero, the equation become the Baur equation. Therefore, it is not expected to predict well the melting temperature of copolymers with excluded comonomers.

Hauser et al.[18] considered the work of removing the comonomer in front of the growth face, and made a series of simplifications to obtain an equation for predicting T_m^n. The method of comonomer removal applies only in the case of small molecules. The other simplifications can only apply in the case of low comonomer content. Compared with Eq.(2-17), their equation magnifies the branching degree effects, and neglects the comonomer volume effects, but considers the crystal stem length effect in a similar manner to Eq.(2-17). Therefore, while the Hauser-Schmidtke-Strobl expression[18] seems to satisfy their syndiotactic poly(propylene-co-octene) experimental data, it may not apply to other cases. Actually, the poly(propylene-co-octene) system does not satisfy the criterion of the perfect exclusion of comonomers from the crystal, since some side groups may be included in the polypropylene crystal. Thus, it may be more reasonable to employ a model dealing with copolymers with included comonomers.

2.3 Discussion

2.3.1 The Modified Gibbs-Thomson Equation

In the case of a random distribution of comonomers, if comonomer volume effects can be neglected, that is, n is large enough to neglect the effects of the difference between X_A and p, or if simply $p = X_A$ (e.g. the volume of B units is same as that of A units), Eq.(2-17) becomes:

$$\frac{1}{T_m^{C,n}}\left(1-\frac{2\sigma_e}{\Delta H_u n}\right)-\frac{1}{T_m^{H,\infty}}=-\frac{R}{\Delta H_u}\ln p \tag{2-20}$$

Goldbeck-Wood[19] obtained a similar result based on the extension[20] of the Sadler-Gilmer crystallization model,[21] and by considering entropy suppression by thickening:

$$\frac{1}{T_m^{C,n}}\left(1-\frac{2\sigma_e}{\Delta H_u n}\right)-\frac{1}{T_m^{H,\infty}}=-\frac{n-1}{2}\frac{R}{\Delta H_u}\ln p \tag{2-21}$$

Eq.(2-21) contains a factor of (n-1)/2 which is not found in Eq.(2-20). However, analysis of Eq.(2-21) shows that as crystal length increases, the melting temperature increases initially, but it decreases after reaching a maximum. The prediction that the melting temperature decreases after reaching a maximum as crystal length increases limits the utility of Eq.(2-21). On the other hand, Eqs.(2-17) and (2-20) do not show this tendency.

Substituting for $T_m^{C,\infty}$ from Eq.(2-19) into Eq.(2-20) yields:

$$T_m^{C,n} = T_m^{C,\infty}\left(1 - \frac{2\sigma_e}{\Delta H_u n}\right) \tag{2-22}$$

Eq.(2-22) has the same form as the Gibbs-Thomson equation,[2] except that $T_m^{H,\infty}$ is replaced with $T_m^{C,\infty}$. So, we shall refer to it as the modified Gibbs-Thomson equation. It was first suggested by Sanchez and Eby[17] by simplifying their comonomer inclusion model. Eq.(2-22) has been widely accepted and used for calculating melting temperature of copolymers with excluded comonomers. However, this was justified by empirical extension of the equation for homopolymers to copolymer systems[22,23,24]. The modified Gibbs-Thomson equation, Eq.(2-22), can be directly derived from Eq.(2-17) only when comonomer volume effects can be neglected. Generally, when comonomer content is low and comonomer volume is not very large compared with that of the structural unit, this condition can be easily satisfied. Thus, the modified Gibbs-Thomson equation, Eq.(2-22), may be considered as a special case form of our proposed equation, Eq.(2-17).

Eq.(2-22) can be used to calculate $T_m^{C,n}$, where n corresponds to the real crystal length. If n approaches n^*, then $T_m^{C,n*}$ can be obtained using the following simplified form of Eq.(2-17) or the modified Gibbs-Thomson equation, Eq.(2-22):

$$T_m^{C,n^*} = T_m^{C,\infty}\left(1 - \frac{2\sigma_e}{\Delta H_u n^*}\right) \tag{2-23}$$

Eq.(2-23) can be applied to calculate $T_m^{C,n*}$, only when comonomer volume effects can be neglected.

2.3.2 Application to α-alkene-ethylene Copolymers

α-alkene-ethylene copolymers are usually referred to as linear low-density polyethylene (LLDPE). Comonomers include propylene, α-butene, α-hexene, and α-octene etc. If comonomers are long enough, they may crystallize independently. This case will not be included in the following discussion. According to experimental observations,[25,26,27,28] α-alkene comonomers are excluded from the crystal lattice, except for the methyl branches.

Therefore, Eq.(2-17) can be used to describe the melting temperatures of these polymers, except for the propylene comonomer case.

For a heterogeneous copolymer system, the sequence propagation probability, p, is very difficult to identify. Due to the complexity of control and measurement of branch distribution and of molecular weight polydispersity, the determination of the distribution of maximum lengths of crystals is rather difficult. However, recent developments in metallocene and single site catalysts have made it easier to control molecular weight distribution and branch distribution. Thus, the preparation of homogeneous random copolymers has become more feasible. Furthermore, the development of the solvent-gradient elution fractionation (SGEF) and temperature-rise elution fractionation (TREF) techniques, coupled with advances in nuclear magnetic resonance (NMR) and gel permeation chromatography (GPC), has enhanced our ability to obtain more detailed and accurate characterization of molecular weight and branch distributions. Here, only the simplest copolymer systems, homogeneous random copolymers are discussed.

In homogeneous copolymers, the average comonomer content is the same in all macromolecules with different molecular weights. Furthermore, the comonomers are distributed randomly. Generally, the degree of branching is described by the number of branches per 1000 backbone carbons, D_{Branch}. For homogeneous random polymers, the relationship between D_{Branch} and p can be expressed as follows:

$$p = 1 - \frac{D_{Branch}}{500} \tag{2-24}$$

where 500 arises from the presence of two carbons in each ethylene repeat structural unit (CH_2CH_2). Normally, n^* should be described according to the actual comonomer separation distribution (or ethylene sequence length distribution). However, for simplicity, we assume that all comonomers are separated with an equal distance, that is, the branching distribution is uniform. Then, the effective n^* can be described as follows:

$$n^* = \frac{M^*_{nw}}{28.06} \Bigg/ \left(\frac{D_{Branch}}{500} \frac{M^*_{nw}}{28.06} + 1 \right) \tag{2-25}$$

where 28.06 is the molecular weight of the repeat structural unit, (C_2H_4), and M_{nw}^* is the effective average molecular weight of the main chain:

$$M_{nw}^* = \frac{M_{nw}}{1 + \frac{m-2}{2}\frac{D_{Branch}}{500}} \tag{2-26}$$

where m is the number of carbons in the comonomers, and M_{nw} represents the average molecular weight of the main chain. The latter can be described as:[29]

$$M_{nw} = \sqrt{M_n M_w} = M_w \Big/ \sqrt{\frac{M_w}{M_n}} \tag{2-27}$$

where M_n and M_w are the number and weight average molecular weights, respectively. Thus, M_{nw} contains, to some extent, the effect of molecular weight distribution.[29]

The volume fraction of ethylene structural units, X_A, is given by:

$$X_A = \frac{p}{\frac{m}{2}(1-p)+p} \tag{2-28}$$

For example, if the comonomer is octene, then $m=8$, and $X_A = \frac{p}{4-3p}$.

Therefore, for a homogeneous random α-alkene-ethylene copolymer, Eq.(2-17) yields $T_m^{C,n*}$:

$$\frac{1}{T_m^{C,n*}}\left(1 - \frac{2\sigma_e}{\Delta H_u n^*}\right) - \frac{1}{T_m^{H,\infty}} = -\left(\frac{R}{\Delta H_u}\right)\left\{\ln p - \frac{1}{n^*}\ln\left[\frac{m}{2}(1-p)+p\right]\right\} \tag{2-29}$$

or

$$T_m^{C,n*} = \frac{T_m^{H,\infty}\left(1 - \frac{2\sigma_e}{\Delta H_u n^*}\right)}{1 - \left(\frac{RT_m^{H,\infty}}{\Delta H_u}\right)\left\{\ln p - \frac{1}{n^*}\ln\left[\frac{m}{2}(1-p)+p\right]\right\}} \tag{2-30}$$

Thus, $T_m^{C,n*}$ is determined by the carbon number of the α-alkene comonomer, the effective molecular weight and the degree of branching.

Unless indicated otherwise, in the remaining discussion, we shall employ the following data: $T_m^{H,\infty} = 418.7$K;[29,30] the heat of fusion per repeat structural unit, ΔH_u = 8.1 kJ/mol (CH_2CH_2);[29] and the basal surface free energy per crystal stem end σ_e = 10.2 kJ/mol.[29]

2.3.2.2 *Effect of Molecular Weight*

Considering homogeneous random α-octene-ethylene copolymers as an example, we analyze molecular weight effects on $T_m^{C,\infty}$ from the Flory equation, Eq.(2-14), and $T_m^{C,n*}$ from Eq.(2-17), as modified in Eq.(2-30). The degrees of branching considered are: 0, 5, and 20 per 1000 carbons. Effective molecular weights vary from 2000 to 1024000. Theoretical predictions are shown in Figure 2-1.

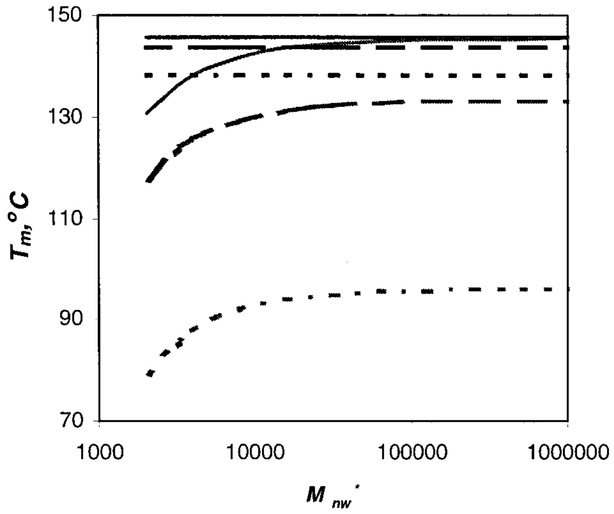

Figure 2-1 Melting temperature vs. molecular weight of α-octene-ethylene homogeneous copolymers by theoretical equations.

Horizontal lines: $T_m^{C,\infty}$ or $T_m^{H,\infty}$ from the Flory equation, curved lines: $T_m^{C,n*}$ or $T_m^{H,n*}$ from Eq.(2-30); branching degree: solid lines: 0 /kC, dashed lines: 5 /kC, dotted lines: 20 /kC.

Eq.(2-14) does not consider the effects of molecular weight. It only describes the melting temperature for an infinite crystal. Thus, for the polymers under consideration, it predicts a group of horizontal lines, in the plot of melting temperature vs. molecular weight for the different degrees of branching. The value of $T_m^{C,\infty}$ decreases almost linearly with the degree of branching in the region under consideration, as shown in Figure 2-2.

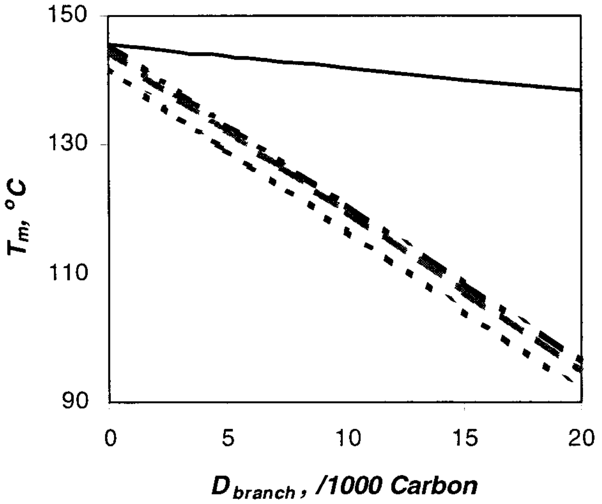

Figure 2-2 Melting temperature vs. branching degree of α-octene-ethylene homogeneous copolymers by theoretical equations.

The solid line: $T_m^{C,\infty}$ from the Flory equation; the line-dot-dot line: T_m^{C,n^*} from Eq.(2-30) when M_{nw}^* is 1024000; the dashed line: T_m^{C,n^*} from Eq.(2-30) when M_{nw}^* is 32000; the dotted line: T_m^{C,n^*} from Eq.(2-30) when M_{nw}^* is 8000.

On the other hand, application of Eq.(2-30) shows that as molecular weight decreases, T_m^{C,n^*} decreases, as seen in Figure 2-1. For example, at 0 branching, T_m^{C,n^*} is 145.5°C for M_{nw}^* 1024000, 144.6°C for 32000, and 141.8°C for 8000. At a degree of branching of 20, T_m^{C,n^*} is 96.0°C for M_{nw}^* 1024000, 95.0°C for 32000, and 91.5°C for 8000. The effect depends on the molecular weight range, being large when the molecular weight is less than 10,000. This is because n^* is affected substantially by M_{nw}^* in the low molecular weight region. As M_{nw}^* increases, the effect becomes smaller. Thus, when M_{nw}^* is higher than 100,000, T_m^{C,n^*} tends to a constant value, which is decided by the degree of branching. Actually, this observation can be deduced from Eq.(2-25). If M_{nw}^* is large enough, Eq.(2-25) becomes:

$$n^* = \frac{500}{D_{Branch}} \qquad (2\text{-}31)$$

Thus, when molecular weight is high, the molecular weight effect becomes negligible in determining the value of T_m^{C,n^*}. Under these conditions, Eq.(2-30) becomes:

$$\frac{1}{T_m^{C,n^*}}\left(1-\frac{2\sigma_e}{\Delta H_u}\Big/\frac{500}{D_{Branch}}\right)-\frac{1}{T_m^{H,\infty}}=-\left(\frac{R}{\Delta H_u}\right)\left\{\ln p-\frac{D_{Branch}}{500}\ln\left[\frac{m}{2}(1-p)+p\right]\right\} \qquad (2\text{-}32)$$

where p is also a function of only D_{Branch}.

If the reptation effect is considered,[29] then Eq.(2-25) is modified as follows:

$$n_{reptation}^* = \frac{2}{3}n^* = \frac{\frac{2}{3}\frac{M_{nw}^*}{28.06}}{\frac{D_{Branch}}{500}\left(\frac{M_{nw}^*}{28.06}\right)+1} \qquad (2\text{-}33)$$

where the constant 2/3 is used to modify the repeat structural unit by the reptation effect. Only when molecular weight is higher than about 3740 or the repeat structural unit number is higher than 133 for polyethylene, should the reptation effect be considered. However, because $T_m^{C,\infty}$ and T_m^{C,n^*} are thermodynamic equilibrium parameters, it is not necessary to consider kinetic factors. Thus, the reptation effect can be neglected in the calculation of $T_m^{C,\infty}$ or T_m^{C,n^*}. The reptation effect should be considered for the calculation of $T_m^{C,n}$ in the crystal with very long crystal stems. However, in Flory's thermodynamic approach, comonomers are not allowed to crystallize. The molecular chain is divided into sequences by comonomers. Crystallization is mainly determined by the movement of sequences, rather than by the movement of the whole molecular chain. Generally, the sequence length is shorter than the minimum for entanglement effects. Only when the degree of branching is very small, it is possible that chain sequences are larger than the minimum entanglement length. So, for copolymers with excluded comonomers, the reptation effect can usually be neglected when calculating the above three types of melting temperatures.

Generally, the dependence of $T_m^{C,n}$ on molecular weight should be similar to that of $T_m^{C,n*}$. However, it has been reported that $T_m^{C,n}$ decreases as molecular weight increases, when samples were quenched.[27] As pointed out earlier, $T_m^{C,n}$ depends strongly on crystallization conditions. Upon quenching, the crystal length decreases as molecular weight increases. This is because more time is required to array structural units for large molecules than for small molecules. Also, during quenching, melts do not have enough time to form many crystals before they are frozen. This will produce a larger amorphous part, which might explain the experimental observation[27] that crystallinity decreases as molecular weight increases.

2.3.2.3 Effect of the Degree of Branching

Again, taking homogeneous random α-octene-ethylene copolymers as an example, we analyze the effect of the degree of branching on $T_m^{C,\infty}$ from the Flory equation, and $T_m^{C,n*}$ from Eq.(2-30). Molecular weights are 8000, 32000, and 1024000, and the degrees of branching vary from 0 to 20 per 1000 carbons. The theoretical predictions are shown in Figure 2-2.

$T_m^{C,\infty}$ lines at different molecular weights collapse into one line for the Flory equation, because the effects of molecular weight are not considered in that equation. As the degree of branching increases, $T_m^{C,\infty}$ decreases almost linearly: e.g. 145.5°C for D_{Branch} = 0 /kC, 143.7°C for D_{Branch} = 5 /kC, and 138.3°C for D_{Branch} = 20 /kC. $T_m^{C,n*}$ also decreases almost linearly with increasing D_{Branch}. Application of Eq.(2-17) (or Eq.(2-30)) shows that, in the region under consideration, $T_m^{C,n*}$ values decrease faster than $T_m^{C,\infty}$ values. $T_m^{C,n*}$ involves the maximum possible crystal stem length that real molecules can form, which depends strongly on D_{Branch}. For example, when M_{nw}^* = 32000, $T_m^{C,n*}$ is 144.6°C for D_{Branch} = 0 /kC, 132.2°C for D_{Branch} = 5 /kC, and 95.0°C for D_{Branch} = 20 /kC.

The experimentally measured melting temperatures, $T_m^{C,n}$, reported by Hosoda[24] (1988) and Alamo and Mandelkern[31] (1989) are respectively shown in Figure 2-3 and Table 2-1, in comparison with calculated values of $T_m^{C,\infty}$ and T_m^{C,n^*}. Hosoda used *LLDPE* with α-butene comonomer, molecular weight 99300, and polydispersity of 1.2. GPC and TREF techniques were employed to fractionate the samples and to provide information about molecular weight and degree of branching for various fractions. The values of T_m^{C,n^*} and $T_m^{C,\infty}$ are calculated using Eq.(2-30) and the Flory equation, respectively. Table 2-1 gives the α-hexene comonomer results from Alamo and Mandelkern[31] (1989). Figure 2-3 and Table 2-1 show that the proposed approach yields melting temperature values in good agreement with these data. Given the $T_m^{C,n}$ value, it is easy to calculate the crystal stem length, and if the crystal stem length values are known, $T_m^{C,n}$ can be estimated from the general equation.

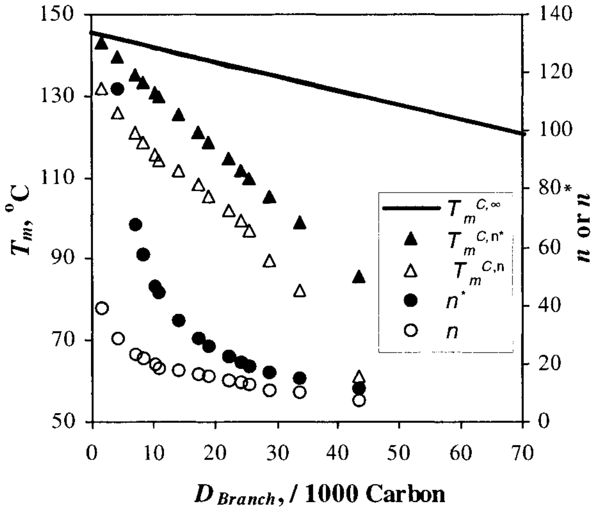

Figure 2-3 Three types of melting temperatures and the corresponding maximum possible and experimental crystal stem sizes for homogeneous LLDPEs with hexene comonomers

Experimental melting temperatures are from Hosoda (1988)[24]; σ_e is selected as 4.0 kJ/mol.

It is necessary to estimate or calculate the folding surface free energy, σ_e, which is a significant factor in the determination of T_m^{C,n^*}. One of the experimental methods to estimate σ_e is based on the melting temperature and crystal stem length, which can be detected by small angle X-ray scattering (SAXS). When the effects of differences between structural unit and comonomer volumes can be neglected, Eq.(2-17) is reduced to Eq.(2-22), the modified Gibbs-Thomson equation. The latter can be applied to extrapolate $T_m^{C,\infty}$ and σ_e according to the linear relationship between T_m^n and the reciprocal of lamellar thickness. If the comonomer volume effects cannot be neglected, Eq.(2-17) can be directly used to fit experimental data. Here, we directly applied Eq.(2-17) to fit the experimental results of Kim et al[9] shown in Figure 2-4(a) (b), and the experimental results of Heck et al[32] shown in Figure 2-4(C). A series of lines can be obtained. The intersections are $T_m^{C,\infty}$, which can be calculated from the Flory equation. The folding surface free energies can also be obtained from these lines. The experimental data can satisfactorily be fitted by the modified equation in the experimental error range.

Table 2-1 Melting temperature of α-hexene ethylene copolymers

M_w	M_w/M_n	D_{Branch} (/KC)	$T_m^{C,\infty}$(°C) [a]	$T_m^{C,n*}$(°C) [b]	n^* (m.s.u.)	$T_m^{C,n}$(°C)	n (m.s.u.)[c]
125000	~2	11.8	141.2	128.8	41.8	115.0	19.8
48800	1.87	12.1	141.1	128.1	40.0	114.0	19.1
104500	2.39	12.1	141.1	128.3	40.6	111.5	17.5
18875	2.39	14.3	140.3	124.2	32.2	113.0	19.0
239830	2.17	14.7	140.2	124.8	33.8	108.3	16.3
112000	~2	14.8	140.2	124.6	33.4	108.8	16.6
6500	2.85	17.4	139.2	117.1	23.5	112.0	19.1
80000	~2	17.4	139.2	120.9	28.3	100.1	13.3
88000	1.99	26.4	136.0	108.2	18.8	96.4	13.2
40000	~2	35.2	132.8	95.5	14.0	85.6	11.0

Experimental data $T_m^{C,n}$ from Alamo and Mandelkern,1989.[31] Assumed σ_e =5.0kJ/mol.
a: Calculation from the Flory equation.
b: Calculation from Eq.(2-30).
c: Calculation from Eq.(2-17), monomer structural unit.

According to the Flory equation, the degree of branching is the only variable influencing $T_m^{C,\infty}$. Eq.(2-17) also shows that the degree of branching has an important effect on $T_m^{C,n*}$, as in the case considered for homogeneous random α-alkene-ethylene copolymers. In fact, the effect of the degree of branching on $T_m^{C,n*}$ is larger than the effect of the molecular weight.[18]

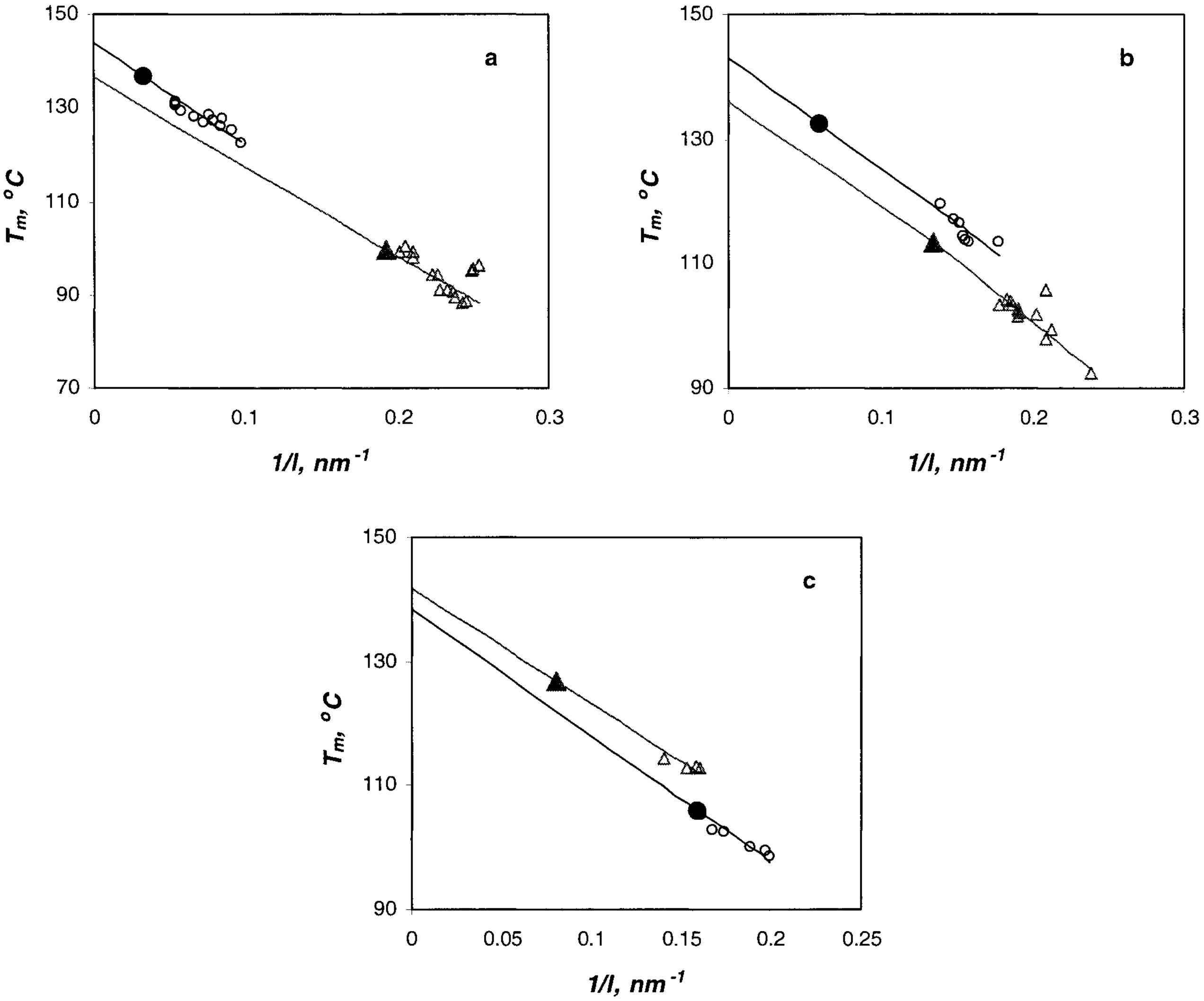

Figure 2-4 Melting temperature and lamellar thickness of α-octene-ethylene homogeneous copolymers.

Lines: theoretical value from the Eq.(2-30). Filled symbols represent $T_m^{C,n*}$; unfilled symbols represent experimental values from Kim et al. (a, b)[9] and Heck et al. (c)[32]

(a) circles: M_w 59900, M_w/M_n 2.149, D_{Branch} 3.98 /kC, $T_m^{C,\infty}$ 144.1°C, σ_e 8.27 kJ/mol;
triangles: M_w 46900, M_w/M_n 2.151, D_{Branch} 24.04 /kC, $T_m^{C,}$ 136.8°C, σ_e 7.25 kJ/mol;
(b) circles: M_w98400, M_w/M_n 2.196, D_{Branch} 7.32 /kC, $T_m^{C,\infty}$ 142.9°C, σ_e 6.68 kJ/mol;
triangles: M_w102700, M_w/M_n 2.108, D_{Branch} 16.92 /kC, $T_m^{C,\infty}$ 136.1°C, σ_e 7.32 kJ/mol;
(c) circles: Mw 90600, Mw/Mn 3, 20 /kC, $T_m^{C,\infty}$ 138.3°C, σ_e 7.69 kJ/mol;
triangles: Mw 86640, Mw/Mn 2.4, D_{Branch} 10 /kC, $T_m^{C,\infty}$ 141.9°C, σ_e 7.05 kJ/mol.

2.3.2.4 Effect of Branch Length

Computed branch length effects are shown in Figure 2-5, for $T_m^{C,n*}$ vs. the degree of branching. Comparing α-octene comonomers and α-butene comonomers, we find that $T_m^{C,n*}$ decreases slightly with increasing branch length, at the same degree of branching. The effect is larger for low molecular weight copolymers. At low degrees of branching (less than 10 per 1000 carbons), the effect of branch length is so small that the volume effect can be totally neglected. As D_{Branch} increases, the effect of branch length increases. When the degree of branching content is less than 10, the experimentally measured melting temperatures show no clear differences among comonomers of different lengths, as shown for $T_m^{C,n*}$ in Figure 2-5. When the degree of branching increases above 10, $T_m^{C,n*}$ decreases as comonomer length increases at the same branch content. Thus, the melting temperature for α-butene comonomer > α-octene comonomer > α-octadecene comonomer. The authors explained this as a dilution and steric effect that prevents crystal thickening. Here, the dilution effect can be explained according to the proposed equation, Eq.(2-17). The steric effect can be probably dealt with by a proper kinetic theory. However, the present results emphasize the importance of the difference in volume between comonomer and structural unit in predicting the melting temperature, especially in the case of a large volume difference and a high comonomer content. Clas et al.[33] reported experimental results that exhibit a similar effect on $T_m^{C,n}$ for ethylene copolymers with α-butene, α-octene, and α-octadecene comonomers. The experimental $T_m^{C,n}$ and the predicted $T_m^{C,n*}$ results are shown in Figure 2-6. The same tendency can be observed for the both types of the melting temperatures.

If the structural unit is propylene (PP), it is difficult to estimate the melting temperature according to the proposed method, since the structure of polypropylene is significantly more complex than that of polyethylene. Polypropylene can appear in isotatic and syndiotactic, as well as atactic structures. Also, there are a variety of crystalline phases. Only for iPP, there are five crystalline phases α, β, γ, δ, and a phase with intermediate crystalline order.[34,35] Therefore, the analysis would be more complex than in the case of polyethylene. Crystal defects appear frequently in polypropylene. Moreover, it has been suggested in many references that it is not accurate to assume that the comonomers are excluded from the lattice. Therefore, neither the Flory nor the proposed equation, Eq.(2-17), can effectively describe the melting temperature of polypropylene. However, if the crystal structure is known, the proposed equation, Eq.(2-17), can be used to predict the melting temperature of the crystal with the excluded comonomers. Unfortunately, existing experimental data do not identify the detailed structure of the polypropylene copolymers. In fact, there is significant disagreement in experimental results reported by various researchers regarding the melting/crystallization behavior of polypropylene.[36,37]

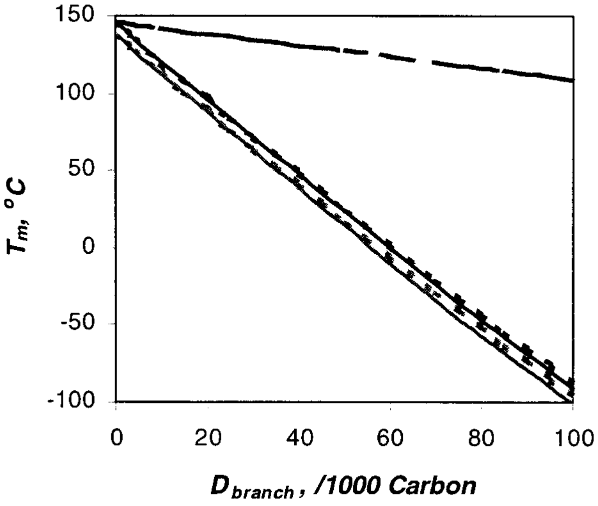

Figure 2-5 Melting temperature of α-butene-ethylene and α-octene-ethylene homogeneous copolymers vs. branching degree by theoretical equations.

The dashed line represents $T_m^{C,\infty}$ from the Flory equation. The upper and lower solid lines represent T_m^{C,n^*} of α-octene comonomers from Eq.(2-30), when the effective molecular weights are 1024000 and 4000, respectively. The upper and lower dotted lines represent T_m^{C,n^*} of α-butene comonomers from Eq.(2-30), when the effective molecular weights are 1024000 and 4000, respectively.

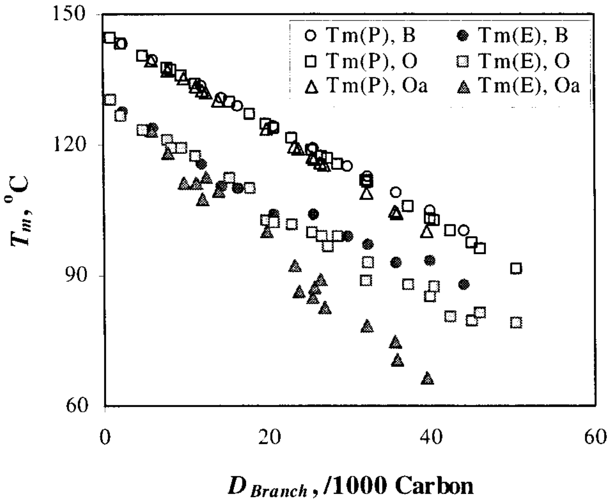

Figure 2-6 Branching size effects on the melting temperatures for LLDPEs

Experimental melting temperatures are from Clas et.al[33]; Tm(P) and Tm(E) refer respectively $T_m^{C,n*}$ and $T_m^{C,n}$; B, O, and Oa are the comonomers: Butene, Octene, and Octadecene, respectively. σ_e is selected as 3.2 kJ/mol.

2.4 Conclusions

A general treatment is proposed leading to equations for the calculation of various important melting temperature values for homopolymers and copolymers. It shows that the Flory equation for calculating the melting temperature of copolymer is a special limiting case of the proposed general equation. It also shows that the Flory equation provides a relationship between $T_m^{C,\infty}$ and $T_m^{H,\infty}$. The proposed generalized treatment leads to a more general equation, which provides a basis for the calculation of $T_m^{C,n*}$ and $T_m^{C,n}$ of a given copolymer, where $n \leq n^*$. It is proposed that $T_m^{C,n*}$ should be the basis for estimating the degrees of supercooling and superheating, and it should be distinguished from Flory's $T_m^{C,\infty}$, which applies only to hypothetical, infinite crystals. The treatment also provides a derivation of the Gibbs-Thomson equation for homopolymers and of a modified form of the Gibbs-Thomson equation for copolymers, when comonomer volume effects can be neglected. Experimental data from the literature regarding the melting behavior of linear low-density polyethylenes confirm the utility of the proposed approach.

2.5 References

1 Mandelkern L. Crystallization of Polymers, New York: McGraw-Hill, 1964.

2 Hoffman JD, Davis GT, Lauritzen JI. In: Hannay NB. Editor, Treatise on solid state chemistry, Vol. 3, New York: Plenum Press, 1976 (Chapter 7).

3 Hoffman JD, Weeks JJ. J Res Natl Bur Stand 1962, 66A:13.

4 Flory PJ, Vrij A. J Am Chem Soc 1963, 85:3548.

5 Flory PJ. Trans Faraday Soc 1955, 51:848.

6 Mandelkern L, Stack GM. Macromolecules1984, 17:871.

7 Kamide K, Ohno K, Kawai T. Makromol Chem 1970, 37:1.

8 Wunderlich B, Czornyj G. Macromolecules 1977, 10:906.

9 Kim M, Phillips PJ, Lin JS. J Polym Sci, B: Polym Phys 2000, 38:154.

10 Hoffman JD, Miller RL. Macromolecules 1988, 21:3038.

11 Hoffman JD, Miller RL. Macromolecules 1990, 23:3544.

12 Evans RD, Mighton HR, Flory PJ. J Am Chem Soc 1950, 72:2018.

13 Flory PJ, Mandelkern L, Hall HK. J Am Chem Soc 1951, 73:2532.

14 Mandelkern L, Flory PJ. J Am Chem Soc 1951, 73:3206.

15 Baur H, Baltorowicz M. Makromol Chem 1966, 98:297.

16 Wendling J, Suter UW. Macromolecules 1998, 31:2516.

17 Sanchez IC, Eby RK. Macromolecules 1975, 8:638.

18 Hauser G, Schmidtke J, Strobl GR. Macromolecules 1998, 31:6250.

19 Goldbeck-Wood G. Polymer 1992, 33:778.

20 Goldbeck-Wood G, Sadler DM. Polym Commun 1990, 31:143.

21 Sadler DM, Gilmer GH. Phys Rev Lett 1986, 56:2708.

22 Crist B, Howard PR. Macromolecules 1999, 32:3057.

23 Crist B, Mirabella FM. J Polym Sci, B: Polym Phys 1999, 37:3131.

24 Hosoda S. Polym J 1988, 20:383.

25 Jokela K, Väänänen A, Torkkeli M, Starck P, Serimaa R, Löfgren B, Seppälä J. J Polym Sci, B: Polym Phys 2001, 39:1860.

26 Marigo A, Zannetti R, Milani F. Eur Polym J 1997, 33:595.

27 Alamo RG, Mandelkern L. Thermochim Acta 1994, 238:155.

28 Richardson MT, Flory PJ, Jackson JB. Polymer 1963, 4:221.

29 Hoffman JD, Miller RL. Polymer 1997, 38:3151.

30 Mandelkern L, Alamo RG. In: Mark JE. Editor, Physical properties of polymers handbook, American Institute of Physics, New York: Woodbury, 1996 (Chapter11).

31 Alamo RG, Mandelkern L. Macromolecules 1989, 22:1273.

32 Heck B, Hugel T, Iijima M, Strobl, G. Polymer 2000, 41:8839.

33 Clas SD, McFaddin DC, Russell KE, Scammell-Bullock MV, Peat IR. J Polym Sci, A: Polym Chem 1987, 25:3105.

34 Turner-Jones A, Aizlewood JM, Beckett DR. Makromol Chem 1964, 75:134.

35 Varga J. J Mater Sci 1992, 27:2557.

36 Fatou JG. In: Vasile C, Seymour RB. editord, Handbook of polyolefins: synthesis and properties, New York: Marcel-Dekker 1993.

37 Janeschitz-Kriegl H, Fleischmann E, Geymayer W. In: Karger-Kocsis I. Editor, Polypropylene: structure, blends, and compositions, London: Chapman and Hall, 1995 (Chapter1).

Chapter 3

3 Distributions of Crystal size from DSC Melting Traces for Polyethylenes

Melting curves, obtained by differential scanning calorimetry, are used to estimate crystal size distributions. The proposed theoretical analysis is applied to different types of polyethylene, including high-density polyethylene (HDPE), metallocene catalyzed linear low-density polyethylenes (m-LLDPE), blends of m-LLDPEs, and Ziegler-Natta catalyzed LLDPEs (ZN-LLDPE). Theoretical predictions are in agreement with experimental results. A generalized melting temperature equation successfully predicts the melting temperatures of all the LLDPEs, although it was initially proposed for homogeneous copolymers with excluded comonomers. This heat of fusion can be calculated from the average crystal size or the crystal size number distribution.

3.1 Introduction

The crystal size (lamellar thickness) distribution and the average crystal size have significant effects on both the processing and application properties of semi-crystalline polymers. These crystalline properties are strongly dependent on molecular structure and processing conditions. Thus, it is useful to understand and determine the relationships that govern crystalline sizes and size distributions. Furthermore, it would be both desirable and useful to solve the inverse problem of determination of the melting characteristics of a polymer with a specified crystal size distribution.

Because it is the simplest and fastest method, differential scanning calorimetry (DSC) has been widely used to determine the crystal size distribution. Although the melting process is a non-equilibrium process, it may be treated as a sequence of pseudo-equilibrium states, by dividing the process into a series of small steps when the scanning rate is not high. Generally, there are two methods to analyze the DSC traces. One method is to analyze DSC endothermic results directly, in conjunction with a certain relationship, such as the Gibbs-Thomson equation.[1] The normalized heat flow at a given temperature in the endothermic curve is assumed to be proportional to the weight fraction of crystalline lamellae that melt at that temperature. The second method employs a differential approach, where the mass fraction of the crystalline phase is calculated by the normalized heat of fusion.[2]

In this paper, we examine the relationship between the crystal size distribution and DSC melting traces, and propose a new method to calculate the crystal size number distribution. A detailed calculation method is proposed according to the recently proposed generalized melting temperature equation.[3] The new method is used to calculate the number average crystal sizes (lamellar thickness) for several linear low-density polyethylenes (LLDPEs) with different types of molecular structures, and one linear polyethylene. The calculated average crystal sizes are compared with small angle x-ray scattering (SAXS) results. The crystal size polydispersity is evaluated from the number average crystal size and the weight average crystal size.

3.2 Theoretical Analysis

3.2.1 Crystal Size Number Distribution and Characteristics

The DSC melting curves indicate the heat flow as a function of time. In non-isothermal experiments, they can be converted into temperature functions. Furthermore, they can be converted into crystal size (lamellar thickness) functions, if no other factors are involved, such as the crystal multiphase transitions and crystal melting-recrystallization-remelting (MRR).

If it can be assumed that there is a direct simple relationship between the crystal size and the heat of fusion, then it is possible to write the following equation:

$$\left(\frac{dQ}{dn}\right)=K\left(\frac{dQ}{dt}\right) \tag{3-1}$$

dQ/dn and *dQ/dt* are the derivatives of the heat of fusion functions with respect to crystal size and time, respectively, K is a constant, t is time, and n is the number of monomer structural units (m.s.u.) in the crystal stem which melts at time t. n also represents the crystal size, the crystal stem length, or the lamellar thickness, because these properties represent the product of n and the m.s.u. projected length along the crystal c axis, when the tilt angle between the crystal stem and the surface is zero. This method (referred to here as "direct method") has been employed widely for homopolymers[4,5,6] and copolymers.[6,7]

Crist and Mirabella[8] and Mirabella[9] pointed out that the parameter K is not a constant but a temperature function. In order to obtain the melting point for a stem consisting of n m.s.u, they employed the Gibbs-Thomson equation[1] for homopolymers and the modified Gibbs-Thomson equation[10] for copolymers with excluded comonomers, respectively. They obtained the following equation.

$$\left(\frac{dQ}{dn}\right)=K_2\left(\frac{dQ}{dt}\right)\left(T_m^x-T\right)^2 \tag{3-2}$$

T_m^x is the equilibrium melting temperature of the perfect crystal for homopolymers or copolymers, $T_m^{H,\infty}$ (T_m^0) or $T_m^{C,\infty}$, respectively. Minick et al.[11] obtained similar results for homopolymers. Both the direct method and the Crist-Mirabella method[8] are based on the weight distribution function. Here, we start with the crystal size number distribution.

From the experimental DSC melting trace of a semi-crystalline polymer, *dQ/dt* vs. *t*, the heat of fusion between *t* and *t+dt* is *(dQ/dt)dt*. From the curve of *dQ/dn* vs. *n*, the heat of fusion in the interval *dn*, which corresponds to *dt*, can be described as *(dQ/dn)dn*. Then:

$$\left(\frac{dQ}{dn}\right)dn = \left(\frac{dQ}{dt}\right)dt \tag{3-3}$$

The above equation can be expressed as follows:

$$\begin{aligned}\left(\frac{dQ}{dn}\right) &= \left[\left(\frac{dT}{dt}\right)^{-1}\left(\frac{dT}{dn}\right)\right]\left(\frac{dQ}{dt}\right) \\ &= \left(\frac{dT}{dn}\right)\left(\frac{dQ}{dT}\right)\end{aligned} \tag{3-4}$$

where *dT/dt* is the experimental heating rate, which is generally a constant in DSC experiments. *dT/dn* can be calculated from the melting temperature equation.

For copolymers with excluded comonomers, the following equation was derived for the melting temperature, *T*, of a crystal stem with *n* m.s.u.[3]

$$\frac{1}{T}\left(1-\frac{2\sigma_e}{\Delta H_u n}\right)-\frac{1}{T_m^{H,\infty}} = -\left(\frac{R}{\Delta H_u}\right)\ln p - \frac{1}{n}\left(\frac{R}{\Delta H_u}\right)\ln\left(\frac{X_A}{p}\right) \tag{3-5}$$

where σ_e is the basal surface free energy, ΔH_u is the heat of fusion per mole m.s.u. for the perfect crystal, *R* is the gas constant, X_A is the monomer volume fraction, and *p* is the sequence propagation probability that a monomer is succeeded by another monomer, i.e., the monomer mole fraction for homogeneous copolymers. The difference between Eq.(3-5) and the Gibbs-Thomson equation is in the final term.[3] When the comonomer size is similar to that of the monomer, and if comonomer content is not high, the branch volume effect can be neglected. Then, Eq.(3-5) becomes the Gibbs-Thomson equation. In the following discussion, Eq.(3-5) is used to analyze the crystal size distribution in LLDPE resins. In other systems, when the assumptions employed in deriving Eq.(3-5) are not applicable, the equation may be modified to accommodate their behavior.

Eq.(3-5) is correct only for the completely melted specimen, because p should be the same for solid and completed melted specimen.[12] In this work, it is assumed that the value of p does not change during melting, because the short chain branching content is considered to be the same in both the solid and molten phases. However, it is possible that the value of p could vary during melting.

Eqs.(3-4) and (3-5), may be combined to obtain:

$$\left(\frac{dQ}{dn}\right)=\frac{\left(\frac{dQ}{dt}\right)T_m^0\left[2\Delta H_u\sigma_e-2R\sigma_eT_m^0\ln p-\Delta H_uRT_m^0\ln\left(\frac{X_A}{p}\right)\right]}{\left(\frac{dT}{dt}\right)\left[-\Delta H_un+nRT_m^0\ln p+RT_m^0\ln\left(\frac{X_A}{p}\right)\right]^2} \tag{3-6}$$

Generally, the heat of fusion depends on temperature. It is the difference between temperature-dependent enthalpy values for the liquid and crystalline phases.[13] For the lamellar crystal structure, the lateral surface energy can be neglected, because the area is very small compared to the basal surface. After the effect of the heat capacity is removed, the heat of fusion of a crystal stem with n m.s.u. is given by:[8,12]

$$q(n)=n\Delta H_u-2\sigma_e \tag{3-7}$$

Since n is related to the temperature as indicated in Eq.(3-5), the heat of fusion (Eq.(3-7)) is still a temperature-dependent function.

If $N(n)$ represents the number of crystal stems consisting of n m.s.u., the derivative crystal number with respect to crystal size, dN/dn, can be described by the following equation ,

$$\left(\frac{dN}{dn}\right)=\left(\frac{dQ}{dn}\right)\Big/q(n) \tag{3-8}$$

Finally,

$$\left(\frac{dN}{dn}\right)=\frac{\left(\frac{dQ}{dt}\right)}{\left(\frac{dT}{dt}\right)}\frac{T_m^0\left[2\Delta H_u\sigma_e-2R\sigma_e T_m^0\ln p-\Delta H_u RT_m^0\ln\left(\frac{X_A}{p}\right)\right]}{(n\Delta H_u-2\sigma_e)\left[-n\Delta H_u+nRT_m^0\ln p+RT_m^0\ln\left(\frac{X_A}{p}\right)\right]^2} \tag{3-9}$$

Eq.(3-9) describes the curve of *dN/dn* vs. *n* from the DSC curve (*dQ/dt* vs. *t*) for copolymers with excluded comonomers. According to Eq.(3-9), the crystal size characteristics, such as the number and weight average crystal sizes and the crystal size polydispersity, can be calculated.

The total number of crystal stems is

$$N_{tc}=\int_{n_0}^{n_\infty}\left(\frac{dN}{dn}\right)dn \tag{3-10}$$

where n_0 and n_∞ are, respectively, the minimum and maximum m.s.u. numbers in crystal stems. The total crystallized m.s.u. number is

$$n_{tc}=\int_{n_0}^{n_\infty}n\left(\frac{dN}{dn}\right)dn \tag{3-11}$$

The number and weight average crystal sizes are respectively

$$\overline{n}_n=\frac{n_{total}}{N_{total}}=\frac{\int_{n_0}^{n_\infty}n\left(\frac{dN}{dn}\right)dn}{\int_{n_0}^{n_\infty}\left(\frac{dN}{dn}\right)dn}, \tag{3-12}$$

and $$\overline{n}_w=\frac{\int_{n_0}^{n_\infty}n^2\left(\frac{dN}{dn}\right)dn}{\int_{n_0}^{n_\infty}n\left(\frac{dN}{dn}\right)dn} \tag{3-13}$$

The polydispersity of crystal size (lamellar thickness distribution) is

$$P_n = \frac{\bar{n}_w}{\bar{n}_n} \tag{3-14}$$

It should be pointed out that Eq.(3-5) applies mainly to lamellar crystal structure, because it neglects the lateral surface free energy. Therefore, the above analysis is only suitable for lamellar crystals, not for other crystal morphologies with large lateral surface, such as granular morphology. However, if a suitable melting temperature relationship with *n* can be obtained, this concept of crystal size number distribution may be employed for all crystal forms.

3.2.2 Comparison with other equations

The Flory equation[14] gives a method to calculate the equilibrium melting temperature of copolymer with excluded comonomers:

$$\frac{1}{T_m^{C,\infty}} - \frac{1}{T_m^{H,\infty}} = -\frac{R}{\Delta H_u} \ln p \tag{3-15}$$

When it is combined with Eq.(3-5),

$$\frac{1}{T}\left(1 - \frac{2\sigma_e}{\Delta H_u n}\right) = \frac{1}{T_m^{C,\infty}} - \frac{1}{n}\left(\frac{R}{\Delta H_u}\right)\ln\left(\frac{X_A}{p}\right) \tag{3-16}$$

Therefore, *dT/dn* can be expressed as:

$$\left(\frac{dT}{dn}\right) = \frac{\Delta H_u \left[2\sigma_e - RT_m^{C,\infty} \ln\left(\frac{X_A}{p}\right)\right] T_m^{C,\infty}}{\left[n\Delta H_u - RT_m^{C,\infty} \ln\left(\frac{X_A}{p}\right)\right]^2} \tag{3-17}$$

When the comonomer volume effect can be neglected, $X_A/p = 1$, Eq.(3-17) becomes:

$$\left(\frac{dT}{dn}\right) = \frac{2T_m^{C,\infty}\sigma_e}{n^2 \Delta H_u} = \frac{\left(T_m^{C,\infty} - T\right)^2 \Delta H_u}{2T_m^{C,\infty}\sigma_e} \tag{3-18}$$

Actually, this expression can also be directly obtained from the modified Gibbs-Thomson equation,[10]

$$T = T_m^{C,\infty}\left(1 - \frac{2\sigma_e}{n\Delta H}\right) \tag{3-19}$$

Therefore,

$$\left(\frac{dQ}{dn}\right) = \left[\frac{2T_m^{C,\infty}\sigma_e}{\Delta H_u\left(\frac{dT}{dt}\right)}\right]\frac{\left(\frac{dQ}{dt}\right)}{n^2} = \frac{K_n}{n^2}\left(\frac{dQ}{dt}\right) \tag{3-20}$$

or

$$\left(\frac{dQ}{dn}\right) = \left[\frac{\Delta H_u}{2T_m^{C,\infty}\sigma_e\left(\frac{dT}{dt}\right)}\right]\left(T_m^{C,\infty} - T\right)^2\left(\frac{dQ}{dt}\right) = K_T\left(T_m^{C,\infty} - T\right)^2\left(\frac{dQ}{dt}\right) \tag{3-21}$$

The constants K_n and K_T only depend on materials and experimental heating rate.

It suggests that Eq.(3-21) is a simplified form of Eq.(3-6) when the comonomer volume effect is neglected. The dependence of heat of fusion on crystal size is a function of the heat flow and the second power of the degree of super-cooling based on the equilibrium melting temperature, $T_m^{C,\infty}$. Crist and Mirabella[8] obtained a similar result.

According to Eq.(3-8), the derivative crystal number function with respect to crystal size is

$$\left(\frac{dN}{dn}\right) = \frac{K_n}{n^2\left(n\Delta H_u - 2\sigma_e\right)}\left(\frac{dQ}{dt}\right) \tag{3-22}$$

When the crystal size is large enough, the basal surface free energy can be neglected.

$$\left(\frac{dN}{dn}\right) = \frac{K_n'}{n^3}\left(\frac{dQ}{dt}\right) \tag{3-23}$$

where K_n' is a new constant. When the comonomer volume effect can be neglected, n can be calculated by the following equation from Eqs. (3-5) and (3-15).

$$n = \frac{2\sigma_e T_m^{C,\infty}}{\Delta H_u \left(T_m^{C,\infty} - T\right)} \tag{3-24}$$

Then,

$$\left(\frac{dN}{dn}\right) = K_T^{'} \left(T_m^{C,\infty} - T\right)^3 \left(\frac{dQ}{dt}\right) \tag{3-25}$$

Therefore, *dN/dn* is a function of the heat flow and the third power of the degree of super-cooling based on the equilibrium melting temperature, $T_m^{C,\infty}$.

The approximate equations, i.e., Eqs. (3-21) and (3-25), cannot be employed for LLDPEs, especially when the degrees of branching are high, because the crystal stems are not sufficiently long to satisfy the approximation conditions. In the following discussion, only Eq.(3-9) is employed.

3.3 Experimental

3.3.1 Materials

The polyethylene resins employed in this study were provided by the Nova Chemical Co. (Calgary, Canada) in pellet form, including one commercial HDPE (Sclair 2907), two experimental m-LLDPEs (polymers I and J), and four experimental ZN-LLDPEs (polymers H, C, G, and L). The material characteristics are listed in Table 3-1. The molecular structure parameters were also provided by Nova Chemical Co. The branching degrees were measured by nuclear magnetic resonance (NMR), and molecular weights were measured by gel permeation chromatography (GPC).

In homogeneous copolymers, comonomers appear randomly along the molecular chains. m-LLDPEs have homogeneous molecular structure, considering both inter- and intra-molecular comparisons. Thus, they are useful in the determination of relationships between properties and molecular structures. In heterogeneous copolymers, comonomers appear non-randomly. ZN-LLDPEs have heterogeneous molecular structure, considering inter- and intra-molecular comparisons. Thus, it is difficult to explain directly and quantitatively their properties in relation to molecular structural characteristics. Furthermore, it is difficult to characterize and quantify their molecular structural characteristics in detail. However, it may be possible to treat them as blends of homogeneous copolymers, or more correctly as the blends of homogeneous ethylene sequences. In such a case, it would be possible to estimate some of the properties of heterogeneous copolymers. This possibility has been examined in this work by studying the behavior of blends of m-LLDPEs. Five new LLDPEs were obtained by blending two m-LLDPEs. The molecular structure of the blends is homogeneous at the intra-molecular scale, and heterogeneous at the inter-molecular scale. The melting temperatures and crystal size distributions of the blends are estimated using relationships designed for m-LLDPEs. The treatment is extended to estimate these properties for ZN-LLDPEs. In both cases, the predictions are compared to experimental results.

Table 3-1 Polymer molecular characteristics

Resin	Com[a]	Type[b]	D_{Branch} (Per 1000C)	M_n (kg/mol)	M_w (kg/mol)
H	B	ZN	18.9	29.5	123.0
C	H	ZN	18.9	33.3	102.0
L	O	ZN	14.0	25.9	114.0
G	O	ZN	15.8	23.1	98.6
I	O	m	24.8	21.9	52.9
J	O	m	15.8	38.2	70.2
HDPE		Sclair2907		20.6	69.2

All copolymers were polymerized in solution.
a: Com is comonomer; B is butene, H is hexene, and O is octene.
b: ZN is Zeigler-Natta catalyst, and m is metallocene catalyst.

Table 3-2 lists the blend ratios and molecular characteristics obtained by calculating the weight average based on the properties of the pure resins. After copolymers were dissolved and strongly stirred in xylene (1%w/v) at 120°C for around two hours, the blends were immediately precipitated in a large amount of cold methanol. After filtering, they were dried under vacuum at about 50°C for more than one week. The same procedure was applied to the pure m-LLDPEs. The experimental results showed that there was no effect of the solution process on the properties of the polymers.

Table 3-2 Blend molecular characteristics

Blend	I wt	D_{Branch} (Per 1000C)	M_n (kg/mol)	M_w (kg/mol)
I0 (J)	0.0	15.8	38.2	70.2
I1	0.1	16.7	35.5	68.5
I3	0.3	18.5	31.2	65.0
I5	0.5	20.3	27.9	61.5
I7	0.7	22.1	25.1	58.1
I9	0.9	23.9	22.9	54.6
I10 (I)	1.0	24.8	21.9	52.9

3.3.2 Differential Scanning Calorimetry

Thermal analysis was performed in a Perkin-Elmer Pyris-1 differential scanning calorimeter (DSC), with an ice bath. The thermal lag, temperature, and heat of fusion were calibrated before experiments with pure indium standard (T_{onset} = 156.60°C, ΔH_f = 28.45J/g), which was supplied by Perkin-Elmer.

All thermal analysis samples were compressed into 0.3mm thick films at 180°C. The weights of DSC specimens varied from 4 to 8mg. They were heated to 180°C, kept at this temperature for 10min to remove previous memory, and cooled at –2°C/min to room temperature. After the thermal treatment, they were heated at 10°C/min to obtain the melting traces from 50°C to 180°C. The effects of heating rates and the reason for selecting 10°C/min in this study are discussed in the Appendix. LLDPE samples may start crystallization at the glass transition temperature, mainly when the short chain branching content is high. In this work, the branching degree was not very high, the maximum being 24.8/KC for resin I. The crystallization process is completed at relatively high temperatures. Therefore, the experimental temperature range (from 50°C to 180°C) is sufficient to record the whole melting process for lamellar crystals under the experimental conditions employed. The contribution of the empty aluminum pan to the DSC curves was subtracted from each measurement. All measurements were performed under nitrogen protection.

3.3.3 Small Angle X-ray Scattering

Small angle x-ray scattering (SAXS) experiments were performed in a high resolution diffractometer with a conventional 2.2Kw Cu-K_α x-ray tube source, built in the Physics Department at McGill University. The apparatus was used to measure the average crystal size. The wavelength of x-ray, λ, was 0.154nm. All SAXS samples were compressed into discs with 15mm diameter and 2mm thickness by compression molding. The discs were sandwiched between two round aluminum foils. Subsequently, they were put in a shear stage (Linkam CSS 450). Then, they were exposed to the first heating and cooling step exactly as for the DSC samples. After this treatment, four layers of the same sample were stacked to produce specimens with 6mm thickness for each x-ray measurement. The scattering angle (2θ) was from 0.01 to 2.01°. The scattering intensities were corrected for the background and sample adsorption.

3.4 Results

3.4.1 SAXS Intensities and Long Periods

If semicrystalline polymers are considered to be isotropic two-phase systems, the SAXS intensity will depend on the electron density difference between crystalline and amorphous phases. If crystals are too small to form lamellar structures but small fringed-micelles in the crystalline phase, they cannot be detected by SAXS. Only the lamellar crystal structures can be detected. The degrees of branching of polymers used in this work are not very high. Under the experimental conditions employed, polarized light microscopy experiments showed that the morphology of the samples is spherulitic.[15] Thus, these polymers exhibit orthorhombic crystal structure, and they are lamellar crystals.[16]

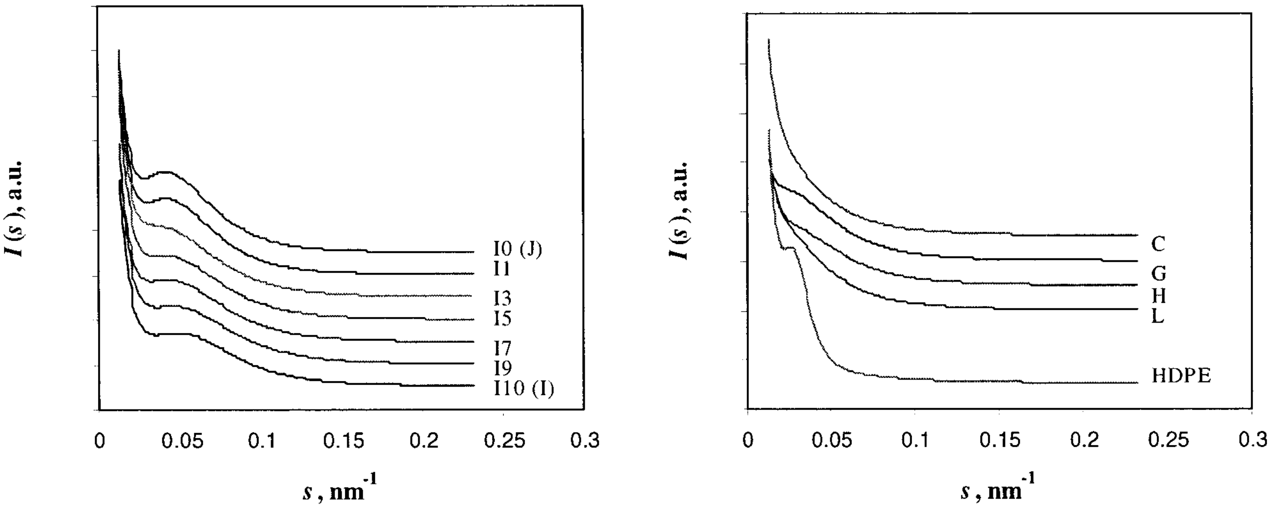

(a) m-LLDPEs and their blends (b) ZN-LLDPEs and HDPE

Figure 3-1 The experimental SAXS curves

The experimental SAXS intensities, $I(s)$, are shown in Figure 3-1. s is the scattering vector, $s = 2\sin(\theta)/\lambda$. Figure 3-1(a) shows the intensity curves for m-LLDPEs and their blends, Figure 3-1(b) is for HDPE and ZN- LLDPEs. It is necessary to make the Lorentz-correction for analysis by a one-dimensional stack model for semicrystalline polymers, $I_C(s) = 4\pi s^2 I(s)$. The corrected intensities, $I_C(s)$, are shown in Figure 3-2. They have maximum points at s^*. From these points, Bragg distances or long periods, L, which represent the average length of the amorphous layer plus the crystalline layer, can be calculated as $L = 1/s^*$. Figure 3-3 shows the long periods for different polymers. The linear polyethylene has the maximum value among all the polymers. The heterogeneous copolymers (ZN-LLDPEs) have higher long periods than m-LLDPEs and their blends. For example, resin G (ZN-LLDPE) and resin J (m-LLDPE) have same short chain branching content (15.8/KC) and the same comonomer (1-octene). Their long periods are, respectively, 17.0nm for resin G and 15.2nm for resin J.

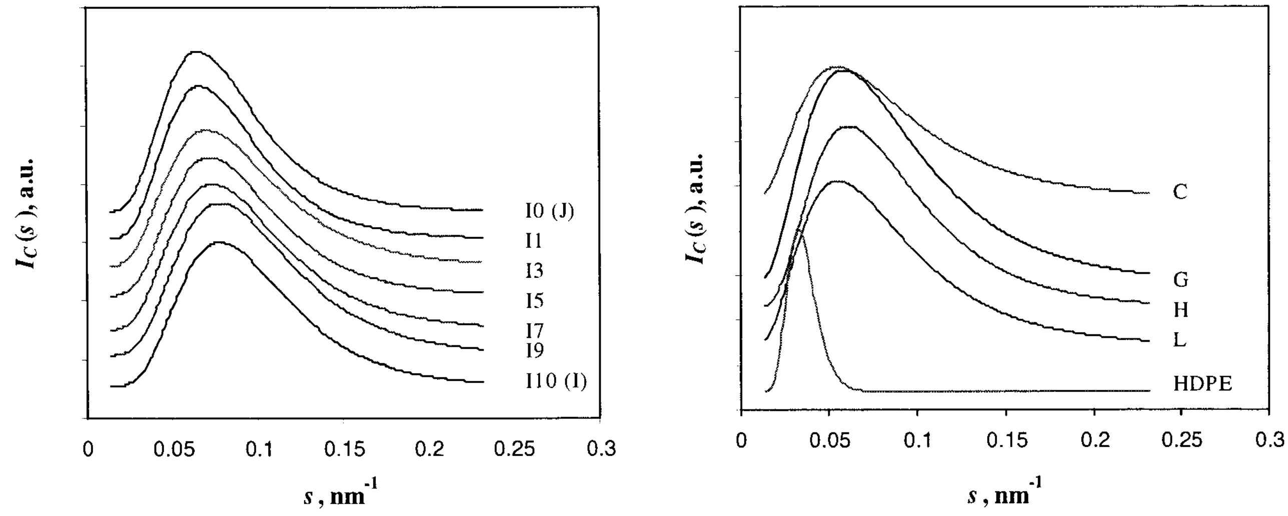

(a) m-LLDPEs and their blends (b) ZN-LLDPEs and HDPE

Figure 3-2 The Lorentz-corrected intensities of SAXS results

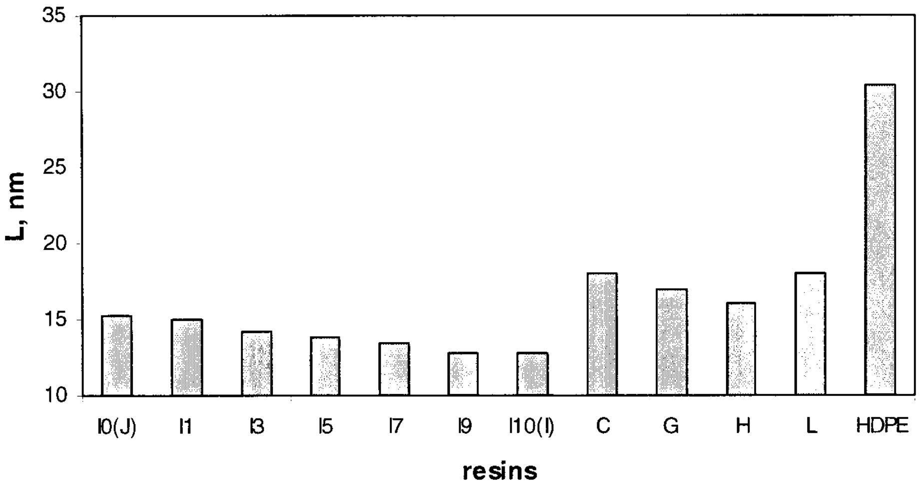

Figure 3-3 Long periods for different resins

For the two m-LLDPEs (resins I and J), the resin with higher short chain branch content (SCBC) has a shorter long period: 15.2nm for resin J with 15.8/KC SCBC and 12.8nm for resin I with 24.8/KC SCBC. The same tendency can also be found in ZN-LLDPE resins G and L with octene comonomers, 18.0nm for resin L with 14.0/KC SCBC and 17.0nm for resin G with 15.8/KC SCBC. The blends of m-LLDPEs also show a similar tendency. As resin I content increases from 0.1 to 0.9wt, the long period gradually decreases from 15.0nm to 12.8nm.

3.4.2 DSC Melting Traces

The melting trace baselines had a sigmoidal form. The sigmoidal baseline is an empirical method to separate the effect of the heat capacity from the latent heat. Ideally, the separation may be obtained by using the actual values of the heat capacities. However, if other factors, such as sample preparation, operator differences, and apparatus (surrounding) stability are considered, the sigmoidal baseline compensates for these effects, in addition to the effect of the heat capacities. Therefore, this approach was employed to obtain the heat of fusion, under the experimental conditions of this study. After subtracting the sigmoid baselines, the final DSC curves were normalized relative to the mole content. The curves of the final normalized heat flow vs. temperature are shown in Figure 3-4. In Figure 3-4(a), the melting trace of m-LLDPEs and their blends are shown. It is expected that the two m-LLDPE resins I and J are miscible, because they have similar molecular structures. The melting peaks of their blends appear between the melting peaks of the pure resins, and move to lower temperatures, as resin I (with the low melting temperature) content increases, i.e., as the SCBC increases.

Two melting peaks are observed in the endothermic curves. At low content of resin I, the small low temperature peak has not been fully explained. Various researchers have reported the presence of two melting peaks in DSC measurements for low-density polyethylene (LDPE),[17] heterogeneous LLDPE[18,19] and homogeneous LLDPE.[20,21,22] Crist and Claudio[23] considered them to indicate two crystal populations corresponding to long and short ethylene sequences. The endothermic curves of ZN-LLDPEs and HDPE are shown in Figure 3-4(b). Only one melting peak can be observed in their DSC curves.

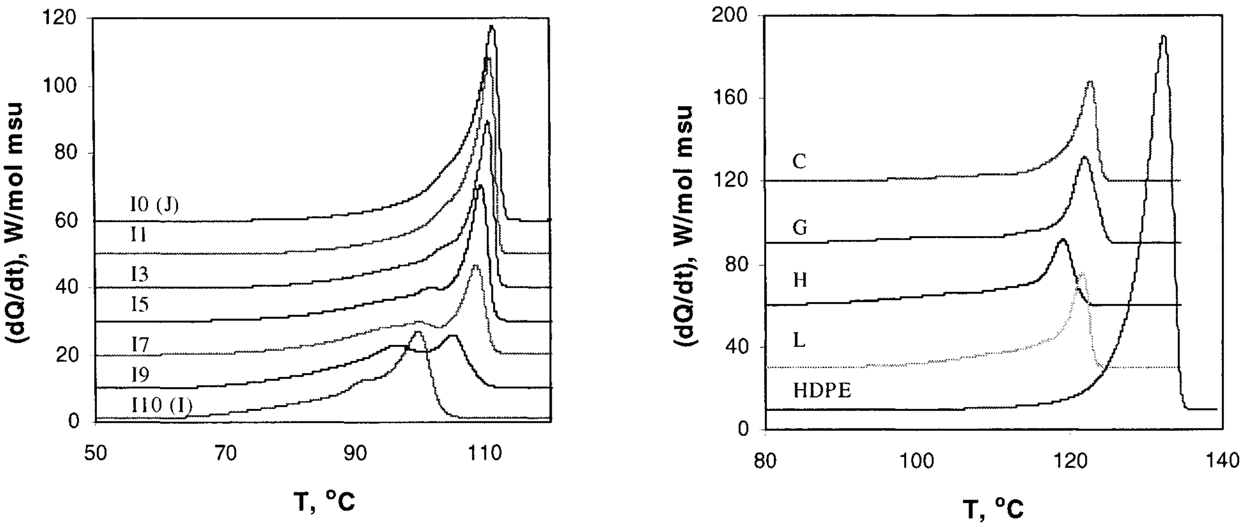

(a)m-LLDPEs and their blends (b) ZN-LLDPEs and HDPE

Figure 3-4 Normalized heat flows of DSC melting traces

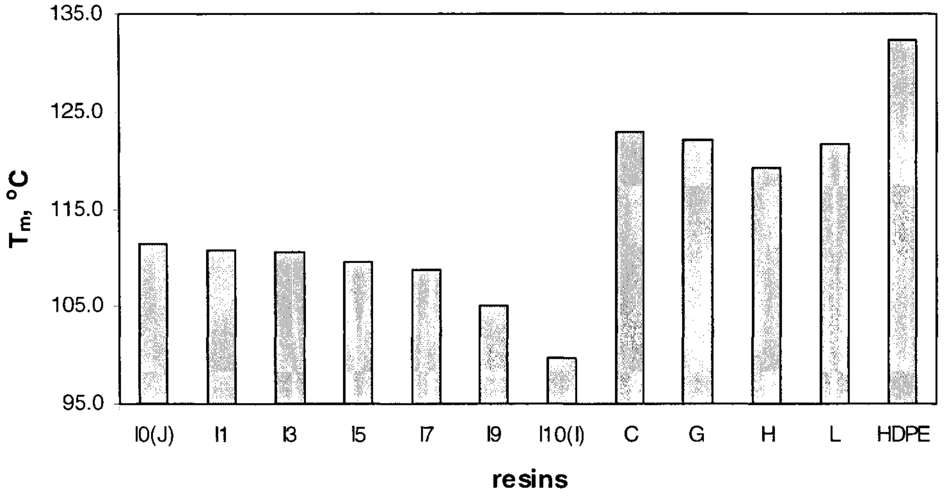

Figure 3-5 Melting peak positions of different resins

The main melting peak positions for different polyethylenes are shown in Figure 3-5. HDPE has the highest value among all resins, as expected. In general, the melting peak positions of ZN-LLDPEs are higher than those of m-LLDPEs. For m-LLDPEs and their blends, as SCBC decreases, the experimental melting position increases, from 99.7°C for resin I to 111.3°C for resin J. In ZN-LLDPEs, there is a similar tendency, 122.1°C for resin G and 121.7°C for resin L. However, as pointed out earlier,[3] one cannot expect to obtain a direct relationship between the melting peak and SCBC, because other factors also influence the melting peak. Similarly, the melting peak alone does not represent a characteristic crystal size, because the size distribution form should also be considered.

3.5 Discussion

3.5.1 Crystal Size Number Distributions

Semi-crystalline polymers exhibit a broad melting peak, mainly because of the broad crystal size distribution,[24] although some other factors, such as multiphase transitions, melting-recrystallization-remelting (MRR), secondary crystallization,[24] and lag effects,[4,5] are contributing factors. For ethylene copolymers, although the (pseudo) hexagonal phase was observed[25] and possibly also the monoclinic phase,[26] they were only observed under relatively high comonomer content and under quenching experimental conditions.[27] As a result, the morphology of the crystals changes from the lamellar structure to the fringed-micellar structure with high defect content.[16] However, under moderate experimental conditions, only the orthorhombic phase has been observed. Reorganization can be generally neglected in copolymers during heating.[6,28] Also, the lag effect in the case of broad peaks is not important, because the change in heat of fusion corresponding to the lag is small.[8] Therefore, the melting traces can be directly employed to analyze the crystal size distribution and the average crystal size, under moderate experimental conditions. In this study, we focus on the lamellar structure (orthorhombic phase). The crystal size distribution for hexagonal and monoclinic phases may also be determined, if the corresponding relevant parameters are employed. However, when there are multi-phases (including the case that the intermediate phase has a different structure) in the system, different parameters for different phases should be employed. This will make the problem more complex and difficult to solve. However, it might be possible to obtain a solution using peak-separation methods.

Table 3-3 Basal surface free energies, heats of fusion of samples and of finite-length crystals, and crystallinities

Resin	σ_e (J/mol)[a]	ΔH_f (J/mol msu)	ΔH^0 (J/mol msu)	X_w	X_v
I0 (J)	5200	2257	7443	0.305	0.273
I1	4870	2119	7430	0.287	0.256
I3	4300	1950	7409	0.264	0.235
I5	3970	1798	7376	0.244	0.217
I7	3920	1681	7335	0.230	0.203
I9	4300	1746	7267	0.244	0.216
I10 (I)	4660	1823	7200	0.254	0.216
C	2340	1427	7666	0.187	0.164
G	2730	1551	7588	0.205	0.181
H	3060	1603	7516	0.214	0.182
L	3270	1630	7603	0.215	0.198
HDPE	10200	5494	7798	0.710	0.677

a: details of determination of σ_e, see reference 15.

All LLDPE crystals are orthorhombic, under the experimental conditions employed in this work. Therefore, the DSC traces depend only on the crystal size distribution. The crystal size number distributions are calculated from Eq.(3-9). The calculation parameters are: the equilibrium melting temperature for perfect crystals $T_m{}^0 =$ 418.7K (145.5°C);[29,30] the heat of fusion per repeat structural unit ΔH_u = 8.106kJ/mol ethylene m.s.u. (289J/g);[30] the ethylene m.s.u. length projected along the c axis l_u = 0.2546 nm.[30] The basal surface free energy is strongly dependent on the molecular structure. For HDPE, σ_e = 10.2kJ/mol crystal stem end (90erg/cm^2) is used.[30] For copolymers with excluded comonomers, molecular chains fold more easily at branching points. Their basal surface free energies are lower than the value for linear polyethylene.[31] The basal surface free energies of all samples are listed in Table 3-3, based on the modified Hoffman-Lauritzen equation.[15] The basal surface free energy decreases as the ethylene sequence polydispersity increases. For the different types of

LLDPE resins, the values of σ_e follow the following order: m-LLDPE> blends of m-LLDPE> ZN-LLDPE.

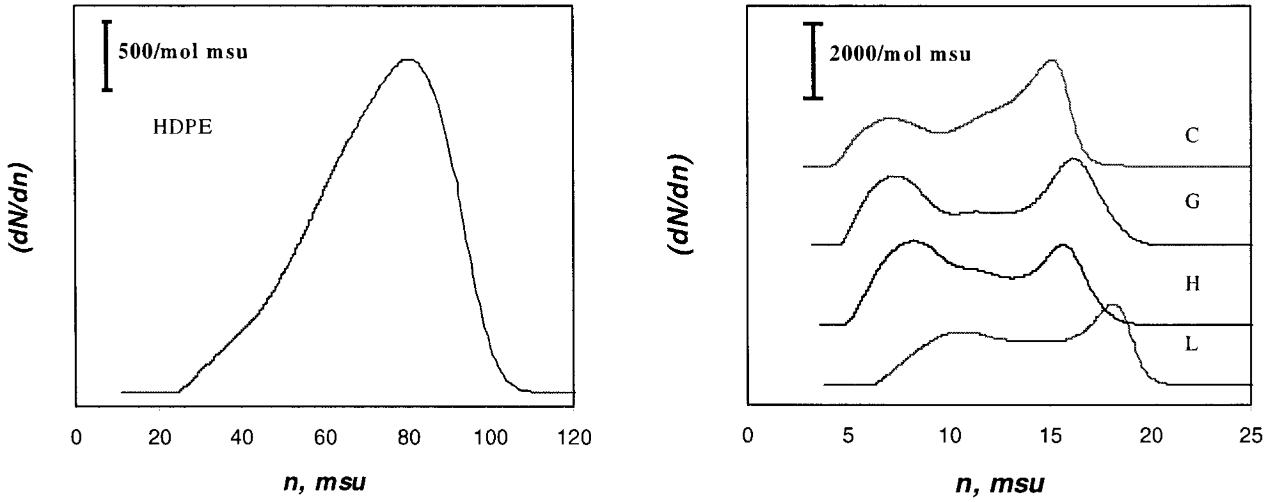

(a) HDPE (LPE)

(b) ZN-LLDPEs

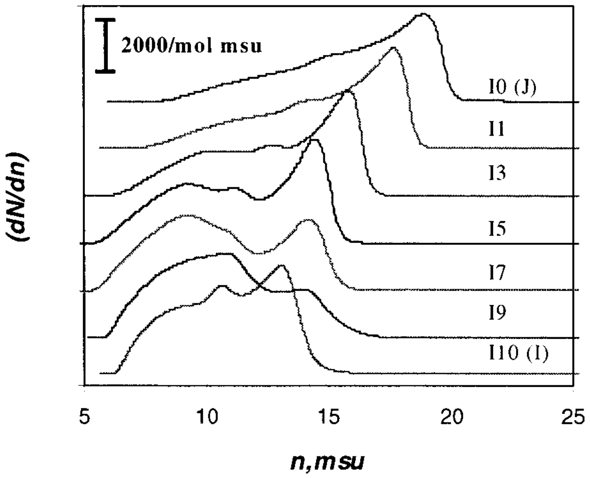

(c) m-LLDPEs and their blends

Figure 3-6 The crystal size number distributions for different resins

Figure 3-6 shows the curves for *dN/dn* vs. crystal size, as calculated from Eq.(3-9). Figure 3-6(a) shows that there is only one peak for HDPE, i.e., one crystal size population. For ZN-LLDPEs, although only one peak appears in the DSC melting curves, multiple peaks appear in the crystal size number distribution, as shown in Figure 3-6(b).

This suggests that there are multiple crystal size populations in ZN-LLDPEs. It is interesting that the crystal sizes at the high peaks are around twice the values at the low peaks. Thus, some of the long ethylene sequences are folded once to form the small crystal population. The high peaks correspond to the long ethylene sequences. The results for m-LLDPEs and their blends are shown in Figure 3-6(c). The top and bottom curves are, respectively, for resin J and I. For resin J, although the peak is very broad, there is only one clear peak, while resin I shows multiple peaks. The small peak perhaps arises from the secondary crystallization at the experimental conditions prevailing in this work, because it did not appear in a simple heating-cooling-heating cycle. Blends of resins I and J exhibit multi-peaks. All peak positions decrease as resin I content increases. In blends I7 (I/J:7/3) and I9 (I/J:9/1), the relative populations at the peaks corresponding to small crystal size are higher than for resin I. This suggests that some of long ethylene sequences (around 18 m.s.u. in resin J) are folded once into small crystals (around 9 m.s.u. in the blends).

There are possibly three factors that produce multiple peaks in LLDPE crystal size distribution curves. One reason is that there are multiple populations of ethylene sequences in the material. This can occur in ZN-LLDPEs and blends of m-LLDPEs. Another factor is that some of the long ethylene sequences are folded and produce new crystal size populations. This can occur in all types of LLDPE. Thirdly, some crystals correspond to part of a long ethylene sequence. Such crystals tend to assume the extended crystal form under certain conditions, such as annealing. Thus, the third factor is strongly dependent on processing conditions. It can operate in all types of LLDPE. Therefore, it is normal to observe multiple crystal size populations in LLDPEs.

3.5.2 Heat of Fusion and Crystallinity

From DSC endothermic peaks, the weight crystallinity can be calculated by the heat of fusion, ΔH_f, according to the following equation,

$$X_w = \frac{\Delta H_f}{\Delta H^0} \tag{3-26}$$

where ΔH^0 is the heat of fusion for 100 percent crystalline samples. Generally, the value for perfect crystals, ΔH_u, is applied. However, calculations based on perfect crystals do not consider the influence of basal surface free energy. Thus, for finite-length crystals, ΔH^0 is overestimated. The actual ΔH^0 can be estimated according to the crystal size number distribution,

$$\Delta H^0 = \Delta H_u - \frac{2\sigma_e}{N_{tc}} \int_{n_0}^{n_\infty} \left[\frac{1}{n} \left(\frac{dN}{dn} \right) \right] dn \tag{3-27}$$

The basal surface free energy is also called folding work (Hoffman and Miller 1997). Eq.(3-27) includes both the heat of fusion and the folding work.[8] The values of ΔH^0 for the different resins are shown in Table 3-3. It is necessary to point out that ΔH^0 is not only dependent on molecular structure but also on processing. From the crystal size number distribution function, the weight crystallinity can be easily calculated,

$$X_w = \frac{n_{tc}}{n_t} \tag{3-28}$$

where n_t is the total m.s.u. number in both the crystalline and amorphous phases., the volume crystallinity, X_v, can be calculated from the weight crystallinity as follows:

$$X_v = \frac{X_w / \rho_c}{X_w / \rho_c + (1 - X_w) / \rho_a} \tag{3-29}$$

where the amorphous density, ρ_a, is assumed to be 0.85g/cm^3.[32] If the density difference between the crystalline and amorphous phases is assumed to be 0.145g/cm^3,[33] the crystalline density ρ_c is 0.995g/cm^3. The calculated volume crystallinities are also listed in Table 3-3.

As shown in Table 3-3, HDPE has the highest crystallinity among all polyethylenes. Compared to m-LLDPEs and their blends, the crystallinities of ZN-LLDPEs are lower, at the same level of short chain branching content (SCBC). For example, $X_v = 0.181$ for resin G and 0.273 for resin J. Under the experimental conditions, the crystallinity tends to decrease, as the short chain branching polydispersity (SCBP) increases. Kuwabara et al. found the interfacial thickness for ZN-LLDPE is a little higher than that of m-LLDPE.[34] In the interfacial layer, there are some partial regular structures, which are difficult to detect by DSC.[35] Thus, the effect of SCBD can also be partially explained by the interfacial thickness. For m-LLDPEs and their blends, the crystallinity decreases as resin I content increases, i.e., SCBC decreases. It tends to a minimum at 0.7wt resin I, and then increases, as resin I content continues to increase. As SCBC increases, the thickness of the interfacial layer between the amorphous and crystalline phases tends to increase. Also, as SCBC increases, the average ethylene sequence size tends to decrease, and the uncrystallizable ethylene sequence content tends to increase under a high crystallization temperature. Then, the crystallinity tends to decrease. The appearance of the minimum can be partially explained by the SCBP. Blend I7 has the largest SCBP in blend systems.[15]

3.5.3 Comparison of Average Crystal Sizes from DSC and SAXS

The average crystal size can be calculated from the long period obtained from SAXS and the volume crystallinity,

$$L_{c,SAXS} = X_v L \tag{3-30}$$

Eq.(3-29) was used to calculate X_v obtained from DSC data.

Also, the number average crystal size can be calculated from DSC traces,

$$L_{c,DSC} = \bar{n}_n l_u \tag{3-31}$$

The crystal sizes are shown in Figure 3-7 for different resins. Generally, for LLDPEs, the average crystal sizes from DSC are in accordance with the results from SAXS. For HDPE, there is a small difference between the average crystal sizes from the two methods. This can be explained by the assumptions regarding SCBC or T_m^0. SCBC in HDPE is assumed to be zero. However, it is possible that there are some branches in HDPE. If it is assumed that SCBC = 5/KC, the results from both experiments become comparable: $L_{c,SAXS}$ = 20.5nm, and $L_{c,DSC}$ = 20.8nm. Moreover, if the Flory-Vrij expression[36] is applied to calculate the equilibrium melting temperature, then T_m^0 = 416.4K instead of 417.2K; the results are then: $L_{c,DSC}$ = 20.2nm and $L_{c,SAXS}$ = 20.6nm.

Because the results from DSC and SAXS are almost the same, there is no need to consider a tilt angle, in the calculation of average crystal size from the crystal size number distribution. However, although the peak positions of DSC traces are normally taken as the melting characteristics, the crystal sizes at peak positions are much larger than the average crystal sizes for all polyethylenes, as shown in Figure 3-7. Thus, it does not appear appropriate, even for HDPE, to choose the peak position to describe all melting behavior. Interestingly, if a tilt angle between crystal sequence direction and crystal surface direction is introduced, and assumed to be 30°,[37] the corrected results of crystal sizes from peak positions become comparable to the average crystal sizes measured by SAXS.

Figure 3-7 shows that in m-LLDPEs and their blends, the average crystal size decreases as resin I content increases (as SCBC increases). After 0.7wt resin I, it tends to remain constant. The average crystal size of ZN-LLDPE (such as resin G) is less than that of m-LLDPE (such as resin J), when SCBC is the same. As indicated earlier, some long ethylene sequences in ZN-LLDPE are folded. Accordingly, the fraction of small crystal sizes in ZN-LLDPEs tends to be higher than that in m-LLDPEs. Therefore, the average crystal size of ZN-LLDPE is relatively smaller at the same SCBC.

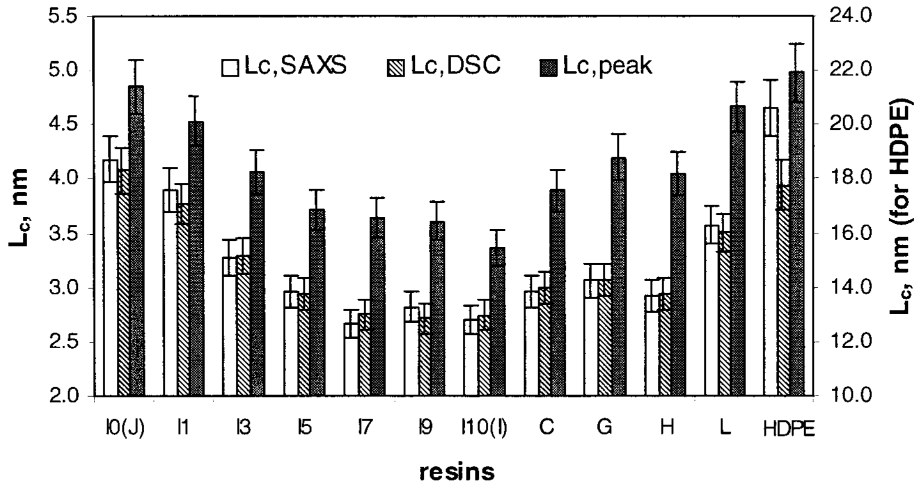

Figure 3-7 Crystal sizes for different resins

Although Eq.(3-5) was introduced for homogeneous copolymers with excluded comonomers,[3] this equation was extended here to non-homogeneous LLDPEs (blends of m-LLDPEs and ZN-LLDPEs). Assuming that these non-homogeneous LLDPEs are the blends of homogeneous ethylene sequences, the number average molecular structure properties, such as short chain branching and molecular weight characteristics, can be represented by mean values. Experimental results indicate that this extension is acceptable. The main molecular structure difference is due to the basal surface free energy, which is strongly dependent on SCBC and SCBD. For copolymers with excluded comonomers, the basal surface free energy decreases, as SCBC and SCBP increase.[15]

3.5.4 Comparison of Different Crystal Size Distributions

As indicated above, there are three possible methods to estimate the crystal size distribution forms. These methods suggest the following three normalized expressions for the crystal size distribution functions:

Direct DSC: $$f_1(n)=\frac{\left(\frac{dQ}{dT}\right)}{\int_{n_0}^{n_\infty}\left(\frac{dQ}{dT}\right)dn}\overset{\frac{dT}{dt}=CONSTANT}{\Rightarrow}\frac{\left(\frac{dQ}{dt}\right)}{\int_{n_0}^{n_\infty}\left(\frac{dQ}{dt}\right)dn}\tag{3-32}$$

Crist-Mirabella: $$f_2(n)=\frac{\left(\frac{dQ}{dn}\right)}{\int_{n_0}^{n_\infty}\left(\frac{dQ}{dn}\right)dn}\tag{3-33}$$

Present work: $$f_3(n)=\frac{\left(\frac{dN}{dn}\right)}{\int_{n_0}^{n_\infty}\left(\frac{dN}{dn}\right)dn}\tag{3-34}$$

$f_1(n)$ is directly based on the relationship of the heat of fusion vs. temperature or time. $f_2(n)$ and $f_3(n)$ are, respectively, based on the relationships between the heat of fusion and crystal size and between the crystal number and crystal size. Because crystal sizes estimated from f_1 have no physical significance, the function f_1 is not useful for estimation of crystal size distribution. The average crystal size obtained from f_3 is the number average size, while the average crystal size obtained from f_2 is actually the weight average size. However, Crist and Mirabella[8] employed a single value for the basal surface free energy value, based on the value for linear polyethylene (10.2kJ/mol msu).

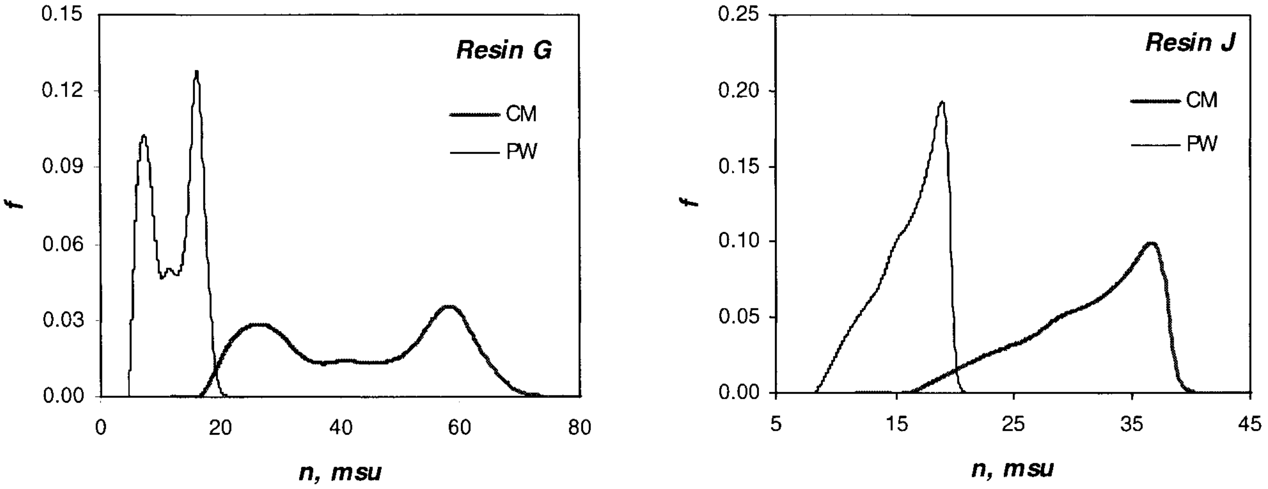

(a) ZN-LLDPE resin G

(b) m-LLDPE resin J

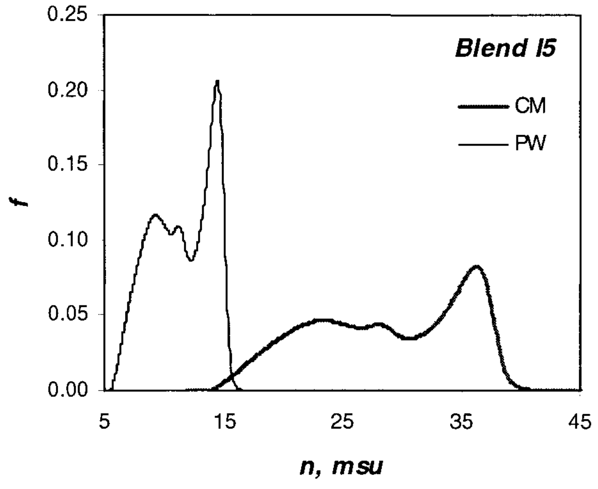

(c) m-LLDPE blend I5

Figure 3-8 Comparison of normalized number distributions from Crist-Mirabella and the present work

Figure 3-8 shows the comparison between the normalized number distribution results obtained with the Crist-Mirabella (CM) method and the present work for ZN-LLDPE resin G, m-LLDPE resins I and J, and m-LLDPE blend I5. The predictions from the two functions are significant different. For all LLDPE resins in this study, the estimation using the CM method indicates much longer crystal sizes than values estimated in the present work, as shown in Figure 3-9. Compared with SAXS results, the estimation from CM is too high.

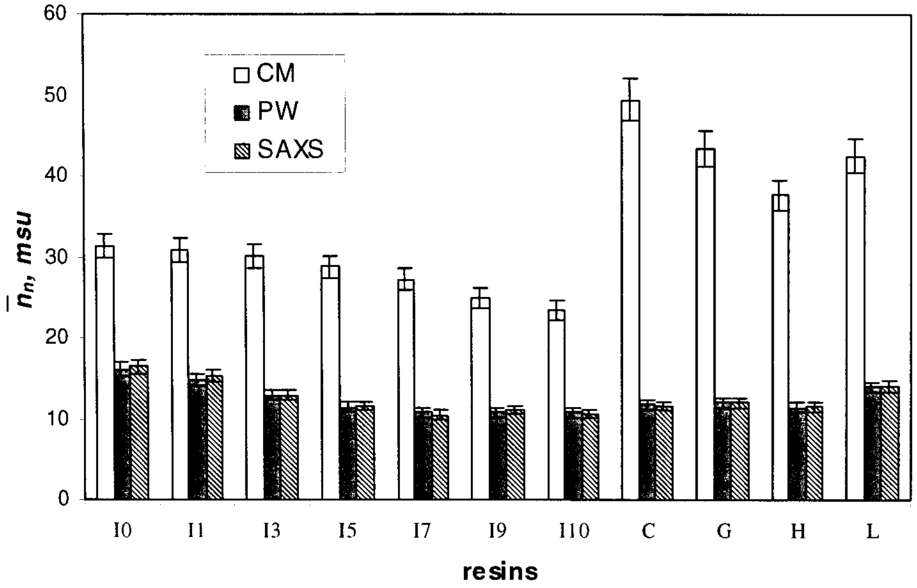

Figure 3-9 The average number crystal sizes from Crist-Mirabella and the present work, and SAXS measurement for all LLDPE resins

Figure 3-10 shows that the crystal size polydispersities obtained from CM and the present work are quite similar. There are only small differences. For the different resins, polydispersity decreases as follows: ZN-LLDPEs > blends of m-LLDPEs > m-LLDPEs and HDPE. Because there are several active sites in Ziegler-Natta catalysts, ZN-LLDPEs are heterogeneous, considering intra- and inter-molecular branching. Their short chain branching distributions (SCBD) are expected to be broader than those of blends of two m-LLDPEs, which may be treated as products from a catalyst with two active sites. Because m-LLDPEs are polymerized using single active site catalysts, their polydispersities should be the lowest. The crystal size polydispersity is also influenced by SCBC. It tends to increase as the SCBC increases. For linear polyethylene, there are no or few branches in the molecular chains. Therefore, although it is produced with a Ziegler-Natta type catalyst, the crystal size polydispersity is still small. For m-LLDPEs and their blends, the crystal size polydispersity shows a maximum value at 0.7wt resin I. A similar maximum point was also obtained in the polydispersities of elution temperatures by temperature-rising elution fractionation (TREF) experiments.[15]

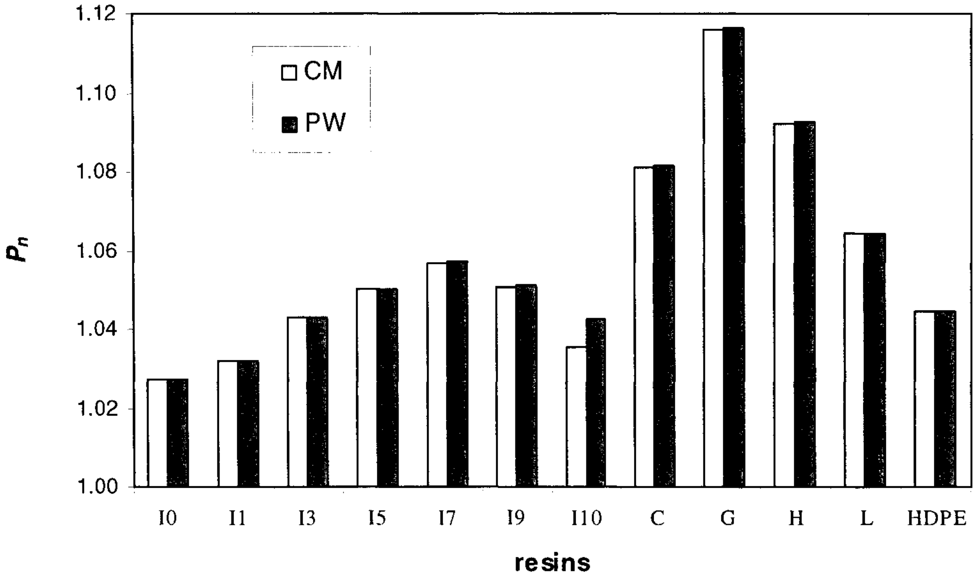

Figure 3-10 The crystal size polydispersities from Crist-Mirabella and the present work

3.6 Conclusions

A calculation method was described to estimate the crystal size number distribution from DSC melting traces. LLDPE resins were used to test this method. The proposed method provides a realistic estimation of crystal size distribution for finite-length crystals.

A method was proposed to estimate the heat of fusion of non-perfect (finite-length) crystals, which is not only dependent on the molecular structure characteristics, but also on processing history. The heat of fusion may be calculated from the average crystal size or the distribution of crystal sizes. The heat of fusion of finite-length crystals is lower than that of perfect crystals, because of the contribution of the basal surface free energy.

DSC and SAXS experimental results for different types of polyethylenes were analyzed, using the proposed distribution form. The results suggest that the generalized melting temperature equation can be extended to non-homogeneous copolymers with excluded comonomers, by treating them as blends of homogeneous ethylene sequences.

For the polyethylene resins considered in this study, linear polyethylene has the highest crystallinity, the largest average crystal size, and the lowest crystal size polydispersity. For LLDPEs, there are multiple populations of crystal sizes. As SCBC increases, the crystallinity and the average crystal size decrease, while the crystal size polydispersity increases. As SCBP increases, the basal surface free energy decreases; then, the crystallinity and the average crystal size decrease, while the crystal size polydispersity increases.

3.7 References

1 Hoffman JD, Davis GT, Lauritzen JI. In: Hannay NB. Editor, Treatise on solid state chemistry, Vol. 3, New York: Plenum Press, 1976 (Chapter 7)

2 Alberola N, Cavaille J, Perez J. J Polym Sci, B: Polym Phys 1990, 28:569.

3 Kamal MR, Feng L, Huang T. Can J Chem Eng 2002, 80: 432.

4 Wlochowicz A, Eder M. Polymer 1984, 25:1268.

5 Plummer CJG, Kausch HH. Polym Bull 1996, 37:393.

6 Lu L, Alamo RG, Mandelkern L. Macromolecules 1994, 27:6571

7 Hosoda S, Kojima K, Furuta M. Macromol Chem 1986, 187:1501.

8 Crist B, Mirabella FM. J Polym Sci, B: Polym Phys 1999, 37:3131.

9 Mirabella FM. J Polym Sci, B: Polym Phys 2003, 41: 235.

10 Sanchez IC, Eby RK. Macromolecules 1975, 8:638.

11 Minick J, Moet A, Hiltner A, Baer E, Chum SPJ. J Appl Polym Sci 1995, 58:1371.

12 Crist B. Polymer 2003, 44:4563.

13 Hoffman JD, Weeks JJ. J Chem Phys 1962, 37:1723.

14 Flory PJ. Trans Faraday Soc 1955, 51:848.

15 Feng L, Kamal MR. Polym Eng Sci 2004, accepted for publication (see Chapter 5 of this thesis).

16 Bensason S, Nazarenko S, Chum S, Hiltner A, Baer E. Polymer 1997, 38:3513.

17 Maderek E, Strobl GR. Colloid Polym Sci 1983, 261:471.

18 Alamo R, Mandelkern L. J Polym Sci, B: Polym Phys 1986, 24:2087.

19 Schouterden P, Groenickx G, Van der Heijden B, Jansen F. Polymer 1987, 28:2099.

20 Kim MH, Phillips PJ. J Appl Polym Sci 1998, 70:1893.

21 Androsch R. Polymer 1999, 40:2805.

22 Alizadeh A, Richardson L, Xu J, McCartney S, Marand H, Cheung W, Chum S. Macromolecules 1999, 32:6221.

23 Crist B, Claudio ES. Macromolecules 1999, 32:8945.

24 Wunderlich B. Macromolecular Physics, Vol.3. London: Academic Press, 1980.

25 Androsch R, Blackwell J, Chvalun SN, Wunderlich B. Macromolecules 1999, 32:3735.

26 McFaddin DC, Russell KE, Wu G, Heyding RD. J Polym Sci, B: Polym Phys 1993, 31:175.

27 Androsch R, Wunderlich B. Macromolecules 2000, 33:9076.

28 Mathot VBF. In: Mathot VBF. Editor, Calorimetry and Thermal Analysis of Polymers, New York: Hanser Publishers, 1994 (Chapter 9).

29 Mandelkern L, Alamo RG. In: Mark JE. Editor, Physical Properties of Polymers Handbook, American Institute of Physics, New York: Woodbury, 1996 (Chapter11).

30 Hoffman JD, Miller RL. Polymer 1997, 38:3151.

31 Lambert WS, Phillips PJ. Macromolecules 1994, 27:3537.

32 Defoor F, Groeninckx G, Reynaers H, Schouterden P, Van der Heijden, B. Macromolecules 1993, 26:2575.

33 Jokela K, Väänänen A, Torkkeli M, Starck P, Serimaa R, Löfgren B, Seppälä J. J Polym Sci, B: Polym Phys 2001, 39:1860.

34 Kuwabara K, Kaji H, Horii F, Bassett DC, Olley RH. Macromolecules 1997, 30:7516.

35 Alamo RG, Mandelkern L. Thermochim Acta 1994, 238:155.

36 Flory PJ, Vrij A. J Am Chem Soc 1963, 85:3548.

37 Voigt-Martin IG, Mandelkern L. J Polym Sci, B: Polym Phys 1984, 22:1901.

3.8 Appendix

In this study, the heating rate was 10°C/min. The heating rate may affect the DSC melting traces, thus, different heating rates may yield different traces and produce different crystal size number distributions and average crystal sizes.

The heating rate can possibly produce two effects: thermal lag and crystal melting-recrystallization-remelting (MRR), which influences melting traces seriously at low and high heating rates. In order to avoid these effects, a reasonable heating rate between 5 and 20°C/min is recommended. Experimental results confirm this point, as shown in Figure 3-11. The DSC traces and crystal number distributions are almost identical at heating rates between 5 and 20°C/min.

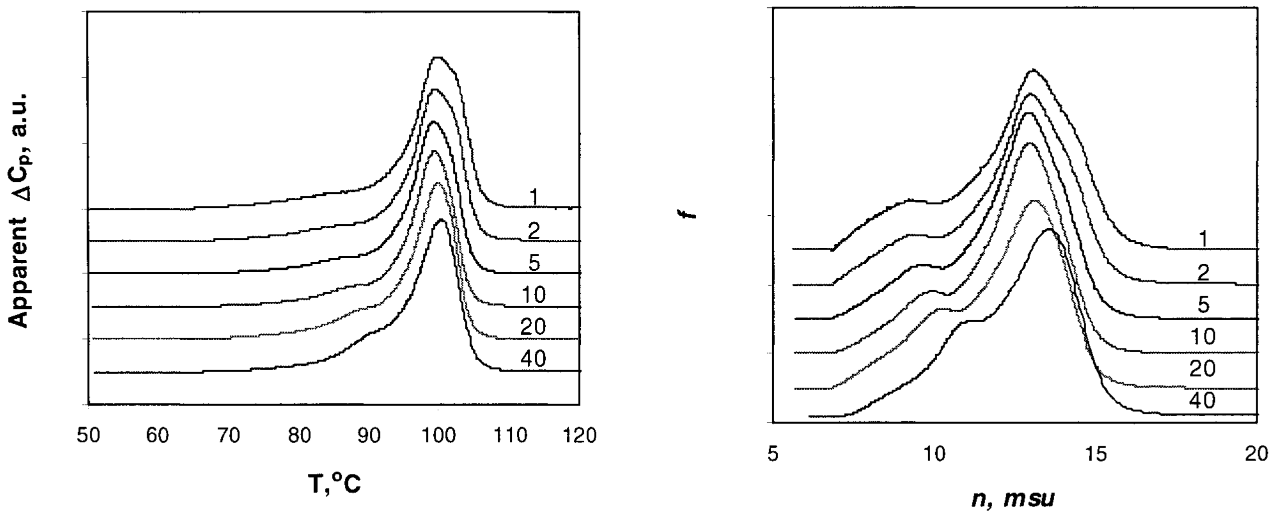

(a) DSC traces (b) Crystal size number distributions

Figure 3-11 The heating rate effects for resin I

The heating rates are identified near the corresponding curves. The experimental procedure: kept for 5min at 180°C, then cooled to 50°C at –10°C/min, and heated at 1, 2, 5, 10, 20, and 40°C/min, respectively.

Because LLDPE shows a broad crystal size distribution, the average crystal size is not sensitive to the heating rate. The differences among the average crystal sizes at different heating rates are very small, as shown in Figure 3-12. Relatively high average crystal sizes appear at low heating rates (1 and 2°C/min) and high heating rate (40°C/min). This is due to MRR and thermal lag. Therefore, heating rates between 5 and 20°C/min appear to produce reasonable results under the experimental conditions employed.

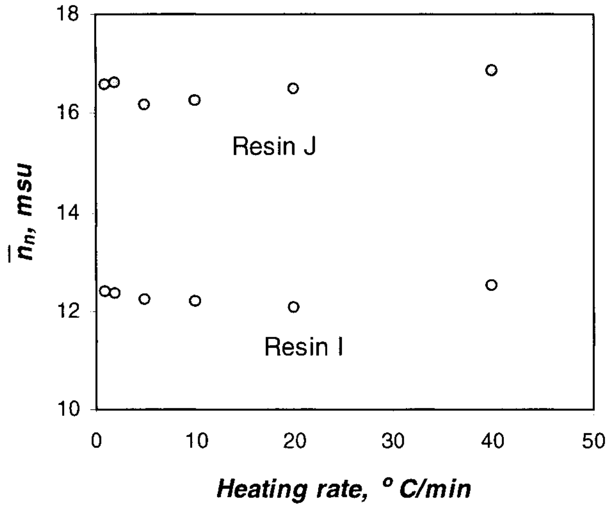

Figure 3-12 the heating rate effects on number average crystal size for resins I and J

Chapter 4

4 Melting Temperature Characteristics for Polyethylenes from Crystal Size Distribution

Because semi-crystalline polymers exhibit broad and multiple peaks in their melting traces, the melting temperature characteristics should consider both melting peak positions and melting temperature polydispersity. The melting temperature characteristics were calculated from the crystal size number distribution and the melting temperature equation. Three methods are proposed for calculating melting temperature characteristics, respectively, according to the value of average crystal size, the crystal stem number distribution function, and the monomer structural unit distribution function. They are applied to analyze the isothermal and non-isothermal experimental results for polyethylene polymers, especially for linear low-density polyethylene copolymers. The first method, based on the value of average crystal size, gives the most reasonable results.

4.1 Introduction

The melting temperature is one of the most important properties of semicrystalline polymers. Generally, it refers to only one point: the melting peak position in the DSC endothermic trace. For small molecules, because the crystals are generally identical, only one narrow melting peak can be observed in their DSC traces. Therefore, it is acceptable for the melting peak position to represent the melting temperature characteristics. However, semicrystalline polymers generally show a broad peak or multiple peaks during melting. The melting traces depend on polymer molecular structure and thermal history.[1] The characteristics of melting temperature distribution need to be considered, as well as the melting peak positions.

For a specific polymer crystal, the melting temperature is determined by the crystal size.[2,3,4,5] As the crystal size increases, the corresponding melting temperature increases. Thus, for a given crystal size distribution, the corresponding melting temperature characteristics need to be identified.

In this paper, we discuss the melting temperature characteristics for polyethylenes, especially for linear low-density polyethylenes (LLDPEs). For these polymers, the molecular characteristics include, not only molecular weight (MW) and molecular weight distribution (MWD), but also short chain branching content (SCBC) and short chain branching distribution (SCBD). Their complex molecular characteristics result in complex melting traces. Generally, they show broad and multiple melting peaks.[2,6,7] Starting with the DSC melting trace, the crystal size number distribution can be predicted.[8] The inverse problem is considered here. Thus, starting with the molecular characteristics, it is desired to predict the corresponding DSC trace or the melting temperature characteristics.

4.2 Theoretical analysis

The melting temperature for a specified crystal stem depends on the crystal length. A generalized melting temperature equation has been proposed for a crystal stem with n monomer structural units (m.s.u.):[1]

$$\frac{1}{T}\left(1-\frac{2\sigma_e}{\Delta H_u n}\right)-\frac{1}{T_m^{H,\infty}}=-\left(\frac{R}{\Delta H_u}\right)\ln p-\frac{1}{n}\left(\frac{R}{\Delta H_u}\right)\ln\left(\frac{X_A}{p}\right) \qquad (4\text{-}1)$$

where σ_e is the basal surface free energy, ΔH_u is the heat of fusion per mole of m.s.u. in the perfect crystal, $T_m^{H,\infty}$ is the equilibrium melting temperature of the perfect crystal of the homopolymer, R is the gas constant, X_A is the monomer volume fraction, and p is the sequence propagation probability that a monomer is succeeded by another monomer, i.e., the monomer mole fraction for homogeneous copolymers. Eq.(4-1) mainly applies to lamellar crystal structure, because it neglects the lateral surface free energy. Therefore, the above analysis is only suitable for lamellar crystals, not for other crystal morphologies with large lateral surface, such as granular morphology. However, the proposed treatment may be applied to such systems, if an equation comparable to Eq.(4-1) may be obtained to describe the melting temperature dependence on structural characteristics.

Semi-crystalline polymers exhibit a broad melting peak, mainly because of the broad crystal size distribution,[2] although some other factors, such as multiphase transitions, melting-recrystallization-remelting (MRR), secondary crystallization,[2] and lag effects[9,10] are contributing factors. For ethylene copolymers, although the (pseudo) hexagonal phase was observed,[11] and possibly also the monoclinic phase,[12] they were only observed for relatively high comonomer content and under quenching experimental conditions.[13] As a result, the morphology of the crystals changes from the lamellar structure to the fringed-micellar structure with high defect content.[14] However, under moderate experimental conditions, only the orthorhombic phase has been observed. Reorganization can be generally neglected in copolymers during heating.[15,16] Also, the lag effect is not important in the case of broad peaks, because the change in heat of fusion corresponding to the lag is small.[4] Therefore, the melting traces can be employed directly to analyze the crystal size distribution and the average crystal size, under moderate experimental conditions.[8] When Eq.(4-1) is employed, the crystal size number distribution can be described by the following equation.[8]

$$\left(\frac{dN}{dn}\right)=\frac{\left(\frac{dQ}{dt}\right)T_m^0\left[2\Delta H_u\sigma_e-2R\sigma_eT_m^0\ln p-\Delta H_uRT_m^0\ln\left(\frac{X_A}{p}\right)\right]}{\left(\frac{dT}{dt}\right)\left(n\Delta H_u-2\sigma_e\right)\left[-\Delta H_un+nRT_m^0\ln p+RT_m^0\ln\left(\frac{X_A}{p}\right)\right]^2} \tag{4-2}$$

where $\left(\frac{dN}{dn}\right)$ is the derivative of crystal stem number, $N(n)$, with respect to crystal size, n; $\left(\frac{dQ}{dt}\right)$ is the heat flow from DSC experiments; $\left(\frac{dT}{dt}\right)$ is the heating rate (it is generally a constant for DSC experiments). Thus, Eq.(4-2) may be used to calculate the basis for obtaining the curve of $\left(\frac{dN}{dn}\right)$ vs. n from the DSC melting traces. According to Eq.(4-2), the crystal size characteristics, such as the number and weight average crystal sizes and the crystal size polydispersity.[8]

As in the case of crystal size characteristics, it is possible to describe the melting temperature characteristics in terms of the number and weight average melting temperatures, T_N and T_W, respectively, and the melting temperature polydispersity, $P_T=T_W/T_N$. The effective melting temperature, T_{NW}, may also be defined:

$$T_{NW}=\sqrt{T_NT_W} \tag{4-3}$$

As in the case of the effective molecular weight,[17] T_{NW} considers both the average melting temperature and the melting temperature distribution.

Three methods are proposed here to describe the melting temperature characteristics, starting with the DSC traces. The simplest method is the direct utilization of the number and weight average crystal sizes, $\bar{n}_n$ and $\bar{n}_w$, to calculate the corresponding melting temperatures, using Eq.(4-1)

$$T_{N1} = T(\bar{n}_n) \tag{4-4}$$

$$T_{W1} = T(\bar{n}_w) \tag{4-5}$$

The other two methods employ the whole crystal size distribution. The 2nd method is based on the crystal stem number distribution for the sample. Eqs.(4-6) and (4-7) describe, respectively, the calculation of number and weight average melting temperatures according to the 2nd method:

$$T_{N2} = \frac{\int_{T_S}^{T_L} T\left(\frac{dN}{dT}\right)dT}{N_{total}} = \frac{\int_{n_S}^{n_L} T(n)\left(\frac{dN}{dn}\right)dn}{\int_{n_S}^{n_L}\left(\frac{dN}{dn}\right)dn} \tag{4-6}$$

$$T_{W2} = \frac{\int_{T_S}^{T_L} T^2\left(\frac{dN}{dT}\right)dT}{\int_{T_S}^{T_L} T\left(\frac{dN}{dT}\right)dT} = \frac{\int_{n_S}^{n_L} [T(n)]^2\left(\frac{dN}{dn}\right)dn}{\int_{n_S}^{n_L} T(n)\left(\frac{dN}{dn}\right)dn} \tag{4-7}$$

where $\left(\frac{dN}{dT}\right)$ is the derivative of crystal stem number, $N(T)$, with respect to melting temperature, T; n_S and n_L are, respectively, the m.s.u. numbers in crystal stems having the smallest and largest crystal sizes in the whole crystal size distribution; and T_S and T_L are, respectively, the melting temperatures corresponding to n_S and n_L according to Eq.(4-1).

The 3rd method is based on the m.s.u. number distribution in the whole sample. Eqs.(4-8) and (4-9) describe the number and weight average melting temperatures, respectively, according to the 3rd definition:

$$T_{N3} = \frac{\int_{T_S}^{T_L} T\left(\frac{dn_{tc}}{dT}\right)dT}{n_{tc}} = \frac{\int_{T_S}^{T_L} T\left(\frac{dn_{tc}}{dT}\right)dT}{\int_{T_S}^{T_L}\left(\frac{dn_{tc}}{dT}\right)dT} = \frac{\int_{n_S}^{n_L} T(n)\left[n\left(\frac{dN}{dn}\right)\right]dn}{\int_{n_S}^{n_L}\left[n\left(\frac{dN}{dn}\right)\right]dn} \tag{4-8}$$

$$T_{W3} = \frac{\int_{T_S}^{T_L} T^2 \left(\frac{dn_{tC}}{dT} \right) dT}{\int_{T_S}^{T_L} T \left(\frac{dn_{tC}}{dT} \right) dT} = \frac{\int_{n_S}^{n_L} [T(n)]^2 \left[n \left(\frac{dN}{dn} \right) \right] dn}{\int_{n_S}^{n_L} T(n) \left[n \left(\frac{dN}{dn} \right) \right] dn} \qquad (4\text{-}9)$$

where n_{tC} is the total crystallized m.s.u. number in the sample. Because all monomer structural units have the same weight, the m.s.u. number reflects the weight of the crystals. Therefore, the 3rd method involves the crystal weight distribution.

In the following discussion, we compare the above three methods for polyethylenes, especially for linear low-density polyethylenes (LLDPEs).

4.3 Experimental

4.3.1 Materials

The materials employed in this study were provided by Nova Chemical Co. (Calgary, Canada) in pellet form, including one commercial high density polyethylene (HDPE) (Sclair 2907), two experimental metallocene-based LLDPE (m-LLDPEs) (resins I and J), four experimental Ziegler-Natta based LLDPE (ZN-LLDPEs) (resins H, C, G, and L), and five solvent-mixed blends of m-LLDPE resins I and J (blends I1, I3, I5, I7, and I9). The material characteristics are listed in Table 4-1. The molecular structure parameters were also provided by Nova Chemical Co. The branching degrees were measured by nuclear magnetic resonance (NMR), and molecular weights were measured by gel permeation chromatography (GPC).

4.3.2 Differential Scanning Calorimetry

Thermal analysis was performed in a Perkin-Elmer Pyris-1 differential scanning calorimeter (DSC). The lag compensation, temperature and the heat flow were calibrated with pure indium standard (T_{onset} = 156.60°C, ΔH_f = 28.45 J/g, as provided by the DSC manual). All thermal analysis samples were compressed into 0.3 mm thick films at 180°C. The DSC sample weights varied from 4 to 8 mg. They were heated to 180°C, and kept at this temperature for 10 min to remove previous memory. Then, for isothermal experiments (only m-LLDPE resins I and J were tested), they were quenched to the set crystallization temperature at –30°C/min, and held at that temperature to complete isothermal crystallization. Subsequently, they were cooled at –2°C/min to room temperature. For non-isothermal experiments (all materials were tested), they were directly cooled to room temperature at –2°C/min. Finally, after the above thermal treatment, the samples were heated again to 180°C at 10°C/min to obtain their melting traces. The contribution to the DSC curves by the empty aluminum pan was subtracted from each measurement. All measurements were performed under nitrogen.

Table 4-1 Polymer molecular characteristics

Material	Com [a]	Type [b]	D_{Branch} (/1000C)	M_n (kg/mol)	M_w (kg/mol)	σ_e (J/mol) [c]
H	B	ZN	18.9	29.5	123.0	3060
C	H	ZN	18.9	33.3	102.0	2340
L	O	ZN	14.0	25.9	114.0	3270
G	O	ZN	15.8	23.1	98.6	2730
J (I0)	O	m	15.8	38.2	70.2	5200
I1	O	mb (0.1 I wt)	16.7	35.5	68.5	4870
I3	O	mb (0.3 I wt)	18.5	31.2	65.0	4300
I5	O	mb (0.5 I wt)	20.3	27.9	61.5	3970
I7	O	mb (0.7 I wt)	22.1	25.1	58.1	3920
I9	O	mb (0.9 I wt)	23.9	22.9	54.6	4300
I (I10)	O	m	24.8	21.9	52.9	4660
HDPE		Sclair2907		20.6	69.2	10200

a: *Com* is comonomer; B, H, and O are, respectively, butene, hexene, and octene.
b: ZN, m, and mb are, respectively, ZN-LLDPE, m-LLDPE, m-LLDPE blend.
c: The basal surface free energies were estimated from the Hoffman-Lauritzen secondary nucleation crystallization kinetics analysis for LLDPEs;[18] for HDPE, the reference value is applied.[17]

4.3.3 Small Angle X-ray Scattering

Small angle x-ray scattering (SAXS) experiments were performed in a high resolution diffractometer with a conventional 2.2Kw Cu-K_α x-ray tube source, built in the Physics Department at McGill University. SAXS was used to measure the average crystal size.[8] The wavelength of x-ray, λ, was 0.154nm. All SAXS samples were compressed into discs with 15mm diameter and 2mm thickness by compression molding. The discs were sandwiched between two round aluminum foils. Subsequently, they were put in a Linkam shear stage (CSS 450). Then, they were exposed to the same thermal treatment as the corresponding DSC samples. Four layers of the same sample were stacked to produce a sample with 6mm thickness for each measurement. The scattering angle (2θ) was from 0.01 to 2.01°. The scattering intensities were corrected for the background and sample adsorptions.

4.4 Results

4.4.1 SAXS

It is necessary to make the Lorentz-correction for a one-dimensional stack model for semicrystalline polymers, $I_C(s) = 4\pi s^2 I(s)$.[19,20] $I(s)$ is the experimental SAXS intensity; s is the scattering vector, $s = \dfrac{2\sin(\theta)}{\lambda}$.

Typical experimental Lorentz-corrected results are shown in Figure 4-1. SAXS patterns are similar for different crystallization temperatures. They have maximum points at s^*. From these points, Bragg distances or long periods, L, which represent the average length of the amorphous layer plus the crystalline layer, can be calculated as $L = 1/s^*$.

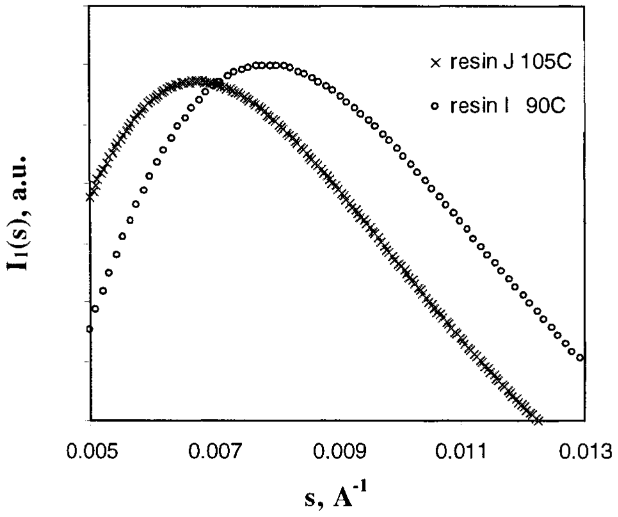

Figure 4-1 The Lorentz-corrected intensities of typical SAXS results
Samples of resin J crystallized at 105°C and resin I crystallized at 90°C.

As shown in Figure 4-2, the magnitudes of the long periods from SAXS, *L*, for resins I and J are almost independent of temperature: around 12.4 and 15.0nm, respectively. Their volume crystallinities from DSC, X_v, are also almost independent of temperature: around 0.22 and 0.28 for resins I and J, respectively. Therefore, their average crystal sizes are also similar, according to $L_{c.SAXS} = X_v L$, where $L_{c.SAXS}$ is the average crystal size. The volume crystallinity, X_v, can be calculated from the weight crystallinity, X_w,

$$X_v = \frac{X_w/\rho_c}{X_w/\rho_c + (1-X_w)/\rho_a} \qquad (4\text{-}10)$$

where the amorphous density, ρ_a, is assumed to be 0.85g/cm^3.[21] If the density difference between the crystalline and amorphous phases is assumed to be 0.145g/cm^3,[22] the crystalline density ρ_c is 0.995g/cm^3. X_w can be easily predicted from the total numbers of m.s.u. in the crystalline phase, n_{tC}, over the total m.s.u. number in both the crystalline and amorphous phases, n_t.

$$X_w = \frac{n_{tC}}{n_t} \qquad (4\text{-}11)$$

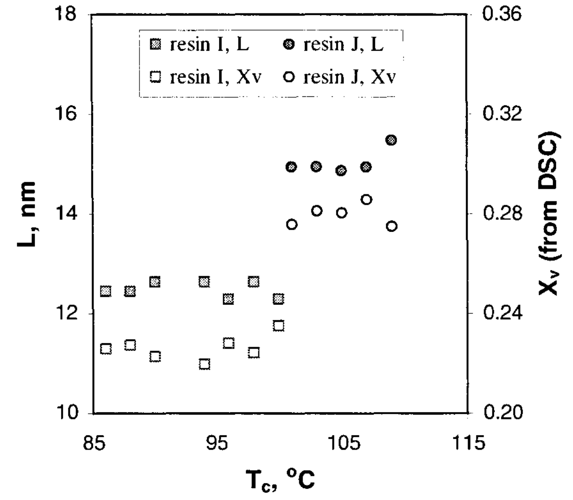

Figure 4-2 Long periods and volume crystallinities for isothermal samples

If n_t is normalized to 1 mole,

$$X_w = n_{tc} / mol \tag{4-12}$$

4.4.2 DSC melting traces

The experimental results of DSC melting traces are shown in Figure 4-3. Three melting peaks are observed under the experimental conditions employed. As the temperature increases, they are, respectively, referred to as the 1st, 2nd, and 3rd peaks in the following discussion.

The 1st peak appears at a temperature lower than the corresponding crystallization temperature. Therefore, it relates to the crystallization process after the isothermal crystallization. The uncrystallizable ethylene sequences (UCES) are solidified in the amorphous part in the solid phase during the isothermal crystallization, because they are not long enough. Some crystallizable ethylene sequences (CES) can also possibly be solidified in the amorphous part, because of kinetic factors. When the crystallization temperature is lowered after the isothermal crystallization, they become gradually crystallizable. Generally, this produces the 1st melting peak. Eq.(4-1) indicates that for higher isothermal crystallization temperature, there are larger amounts of UCES. The sizes of these UCES are larger than those obtained at lower crystallization temperatures. Therefore, both the area and position of the 1^{st} peak increase, as the crystallization temperature increases, as shown in Figure 4-3.

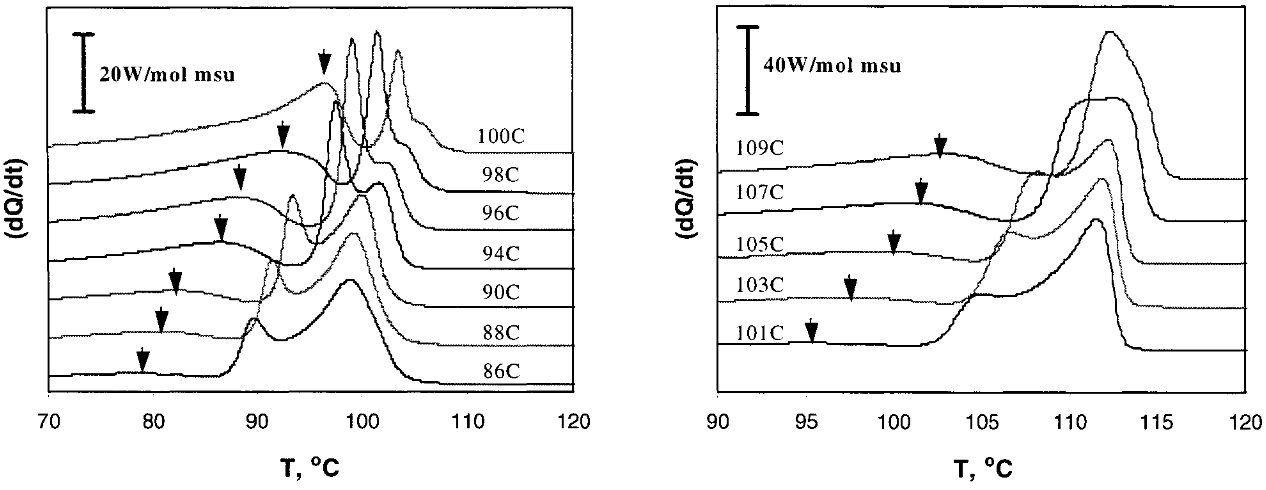

(a) resin I (b) resin J

Figure 4-3 Normalized heat flows of DSC melting traces

Crystallization temperatures are indicated for each trace. The arrows mark the 1st peak positions for each trace.

The relation between the 1^{st} peak positions and the corresponding crystallization temperatures is shown in Figure 4-4. As T_c increases, T_{p1} increases linearly, although the results are for two different resins. The linear fit shows that T_{p1} is 6.6 ± 1.1^{o}C lower than the corresponding T_c. If the result for resin I at 100^{o}C is excluded , the fit shows a high r-square coefficient. Perhaps, resin I was not completely crystallized at 100^{o}C under the experimental conditions employed. This should be reflected in the crystal size distribution, as will be shown in the following discussion.

The positions of the other two peaks (2^{nd} and 3^{rd}) are higher than the corresponding crystallization temperatures. They should relate to the crystals that are formed during the isothermal condition. As the isothermal crystallization temperature increases, their positions move to higher temperatures. The relative intensities of the 2nd peaks increase, and those of the 3rd peaks decrease.

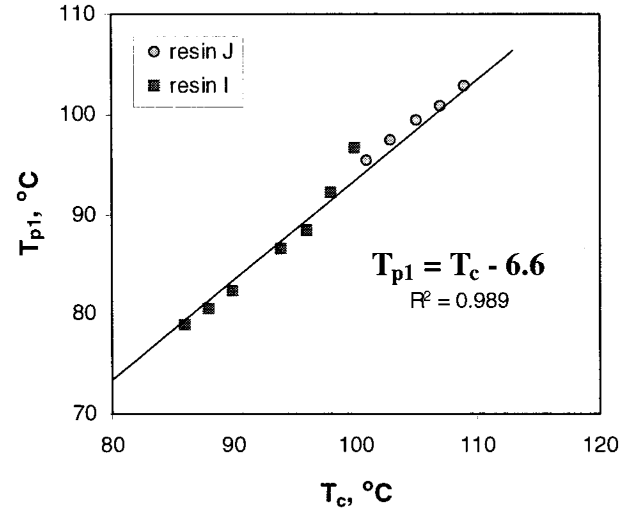

Figure 4-4 The 1st peak positions of isothermal samples

Based on analysis of the crystallization growth regime behavior, the regime transition temperatures between regimes III and II, T_{III-II}, are 93.9 and 107.1°C for resins I and J, respectively.[18] It is interesting to note that these temperatures are roughly equal to the temperatures at which the inversion is observed in the relative intensities between the 2nd and 3rd peaks, as shown in Figure 4-3. Before T_{III-II}, the intensities of the 2nd peaks are lower than those of the 3rd peaks. After T_{III-II}, the intensities of the 3rd peaks are lower than those of the 2nd peaks.

4.5 Discussion

4.5.1 Crystal sizes and distributions

The crystal size number distribution can be obtained from Figure 4-3, using Eq.(4-2). The results are shown in Figure 4-5.

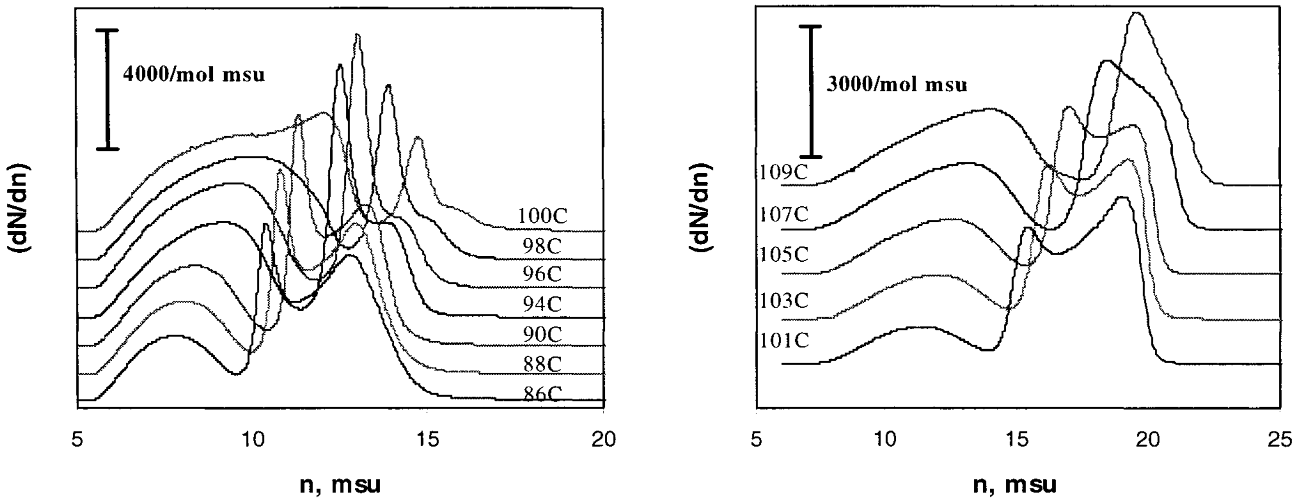

(a) resin I (b) resin J

Figure 4-5 The crystal-size number distribution

Crystallization temperatures are indicated for each trace.

Basically, there are three populations of crystal sizes, corresponding to the three peaks in the DSC melting traces, as shown in Figure 4-5. However, for the sample of resin I at 100°C, it can be clearly observed that two populations of crystal sizes correspond to the 1st melting peak, rather than one population as for the other isothermal samples. It was suggested above that the isothermal crystallization may not have been completed at 100°C under the experimental conditions employed, because this temperature is close to regime IM, according to analysis of linear crystalline growth behavior.[18] Thus, some long ethylene sequences (ES) remained in the melt phase, before the crystallization temperature was lowered. These ES form a population of relatively long crystal sizes, with respect to the 1st melting peak. Therefore, as shown in Figure 4-4, the sample of resin I at 100°C has a higher 1st melting position than the expected value.

With the crystal size number distributions in hand, it is possible to estimate the number and weight average crystal sizes, $\overline{n}_n$ and $\overline{n}_w$, and crystal size polydispersity, P_n ($P_n = \overline{n}_w / \overline{n}_n$). The number average crystal size can also be represented by crystal length, $L_{c,DSC}$. $L_{c,DSC} = \overline{n}_n l_u$, where the ethylene m.s.u. length projected along the c axis l_u = 0.2546 nm.[17] The calculation results are shown in Figure 4-6. Although the distributions of crystal sizes are totally different for different isothermal crystallization temperatures, the average crystal sizes are independent of temperature for both resins: 2.8 and 4.2 nm for resins I and J, respectively. SAXS results confirm the calculation results from DSC experiments. The non-isothermal experiments also gave almost the same values of the number average crystal sizes: 2.70 and 4.18nm for resins I and J, respectively.[8] So, for the experimental conditions employed, the average crystal size is not very sensitive to the crystallization temperature. Although the differences of average crystal sizes are small, the crystal size polydispersities increase as the crystallization temperature increases, as shown in Figure 4-6.

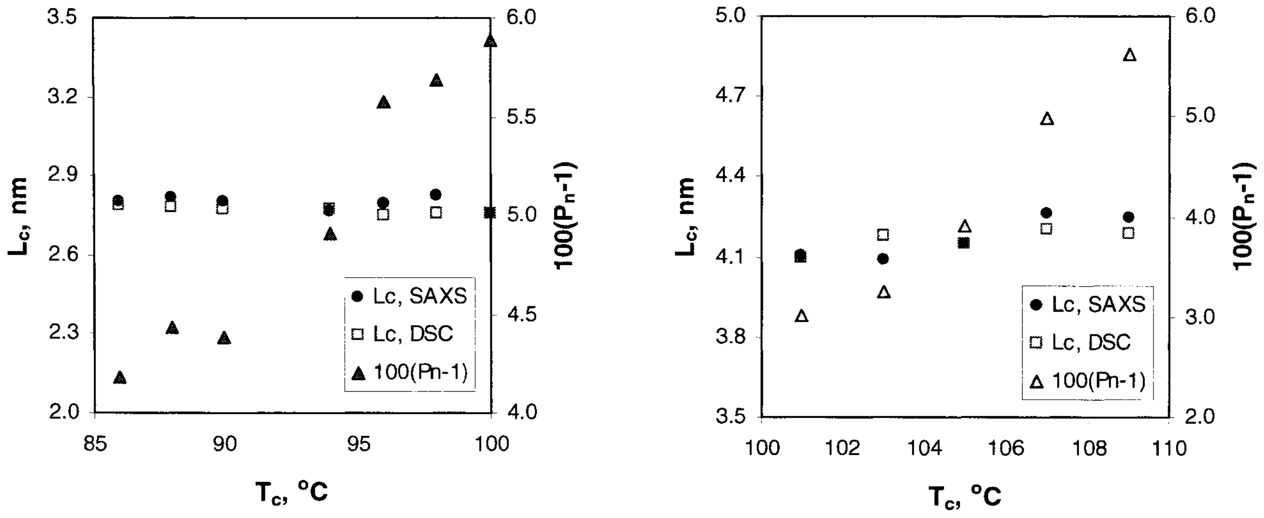

(a) resin I (b) resin J

Figure 4-6 The average crystal sizes and crystal size polydispersities

4.5.2 Melting temperature characteristics

The melting temperature characteristics can be calculated by three methods from the crystal size number distributions, as discussed above. The calculation results are shown in Figure 4-7 for the effective melting temperatures and Figure 4-8 for the melting temperature polydispersities. Figure 4-7 shows that the effective melting temperature from the 1st method, T_{NW1}, is the highest. T_{NW3} is a little lower than T_{NW1}. T_{NW2} is the lowest effective melting temperature. Just like its effect on the average crystal size, the crystallization temperature effect on the effective melting temperature is small, under the experimental conditions considered. Generally, as the crystallization temperature increases, the effective melting temperature decreases slightly in regime III, and increases slightly in regime II, by the 1st and 2nd methods, as shown in Figure 4-7. T_{NW2} keeps decreasing slightly as the crystallization temperature increases.

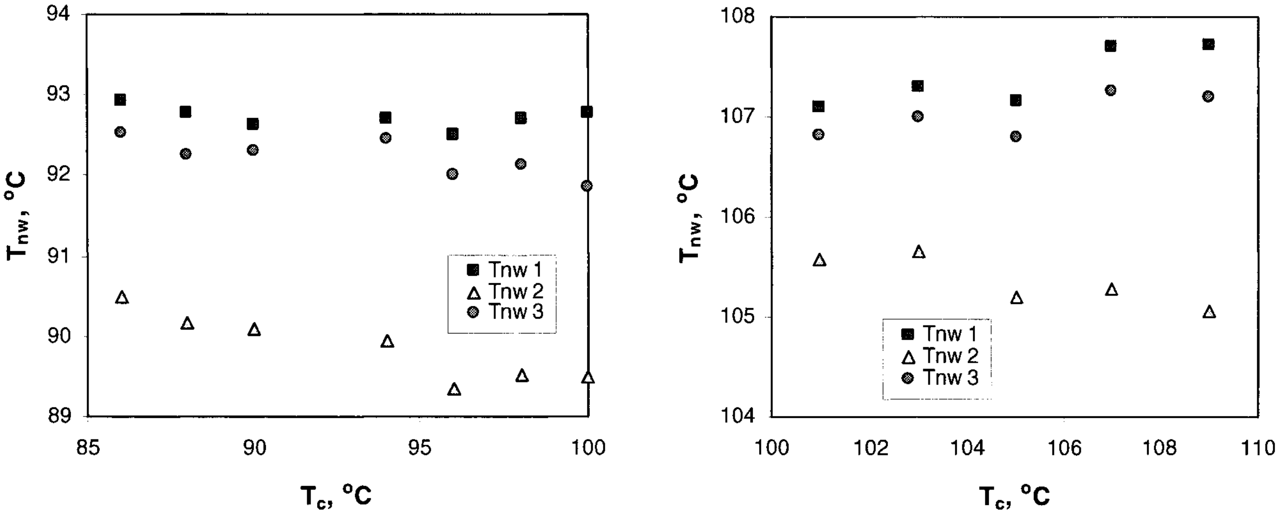

(a) resin I (b) resin J

Figure 4-7 The effective melting temperatures from different methods

Figure 4-8 shows that the melting temperature polydispersity, P_T, increases, as the crystallization temperature increases. The 1st method gives the highest value, and the 3rd method gives the lowest value. The increasing tendency of P_T with the crystallization temperature is not so pronounced with the 2nd and 3rd methods in resin J. P_{T2} and P_{T3} for resin I do not show clear temperature dependence. As shown in Figure 4-3, the DSC melting traces show that as the crystallization temperature increases, the occurrence of the multiple peaks becomes more pronounced. Therefore, the 2nd and 3rd methods may not appropriate to characterize the melting temperature polydispersity.

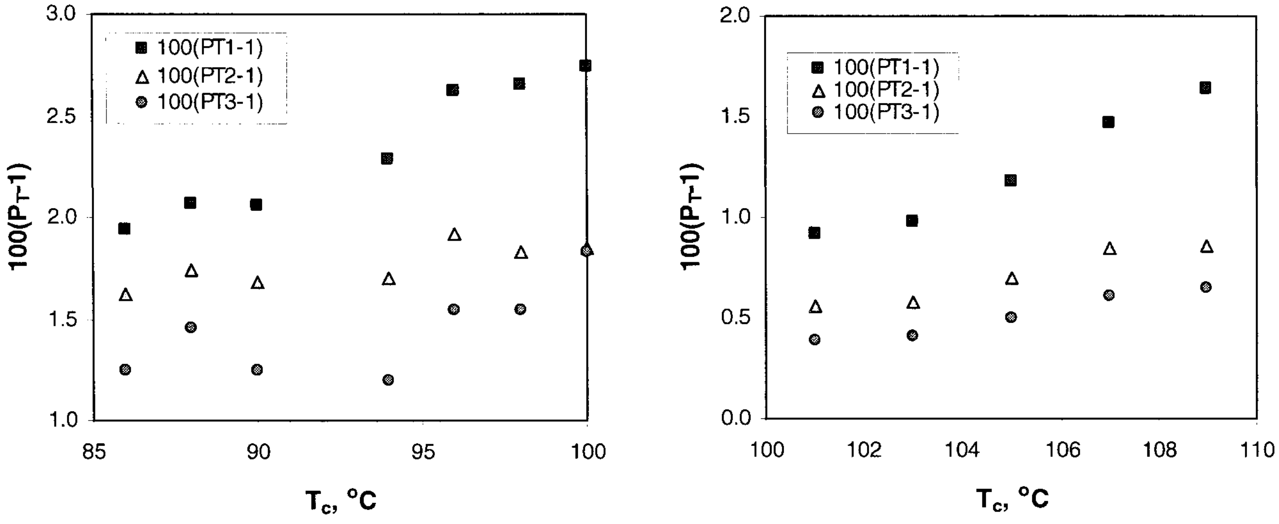

(a) resin I (b) resin J

Figure 4-8 The melting temperature polydispersities from different methods

4.5.3 Melting temperature characteristics for different polyethylenes

The experimental and calculation results for non-isothermal crystallization[8] are employed to compare the melting temperature characteristics for different polyethylenes. The crystal size number distributions obtained from non-isothermal experiments for the different resins are shown in Figure 4-9 (a) for HDPE, (b) for ZN-LLDPEs, and (c) for m-LLDPEs and their blends.[8]

Figure 4-10 shows the effective average melting temperatures, as calculated by the three methods (Eqs.(4-4)-(4-9)). The maximum melting peak positions are also shown in the same figure. They are significantly higher than the average melting temperatures. The above analysis shows that the conventional melting temperatures (i.e., main melting peak positions) are higher than all the three effective temperatures. Just like the results from isothermal experiments, T_{NW1} is only slightly higher than T_{NW3}. T_{NW2} is the lowest among the calculated average melting temperatures.

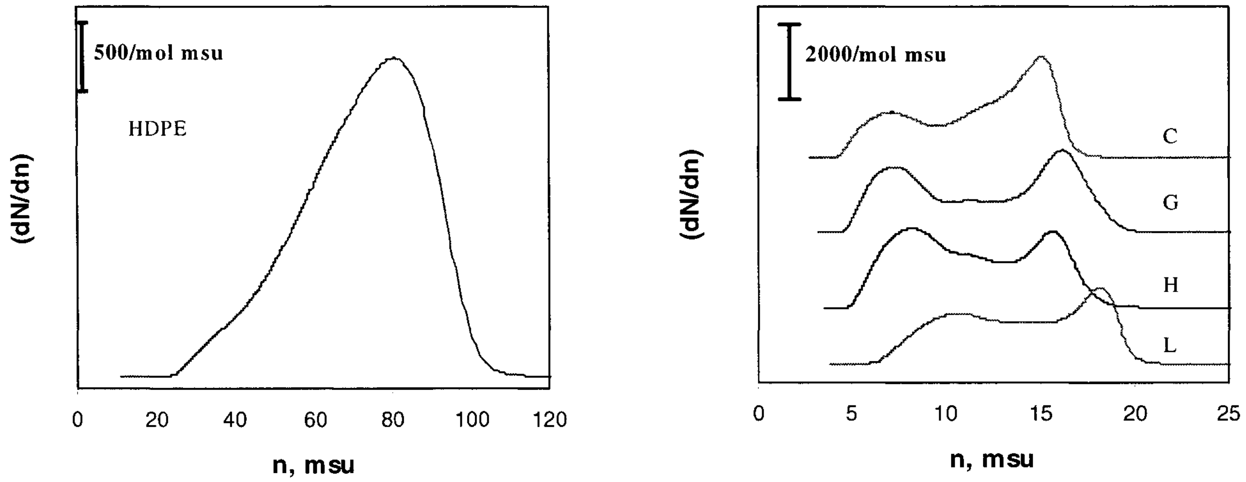

(a) HDPE (LPE)

(b) ZN-LLDPEs

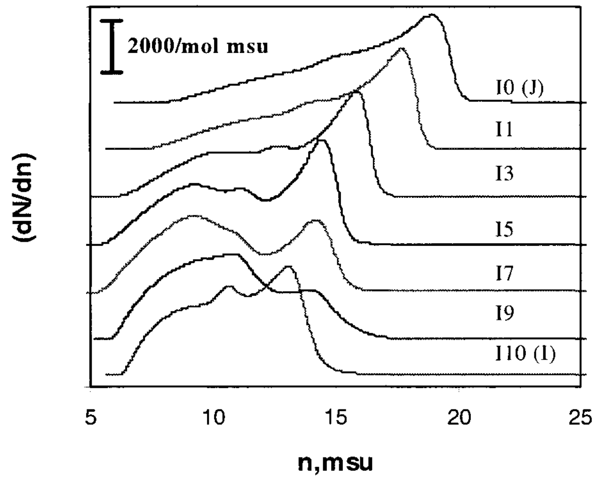

(c) m-LLDPEs and their blends

Figure 4-9 The crystal size number distribution from DSC melting traces for non-isothermal experiments[8]

Among the different materials studied, HDPE has the highest melting temperature, then ZN-LLDPEs, and finally m-LLDPEs and their blends. Although the average crystal size of resin G (ZN-LLDPE) is lower than that of resin J (m-LLDPE),[8] the average melting temperature of the former is higher, because the basal surface free energy of ZN-LLDPE is lower than that of m-LLDPE,[18] when their short chain branching contents (SCBC) are the same. In m-LLDPEs and their blends, the average melting temperature decreases as SCBC increases (as resin I weight content increases).

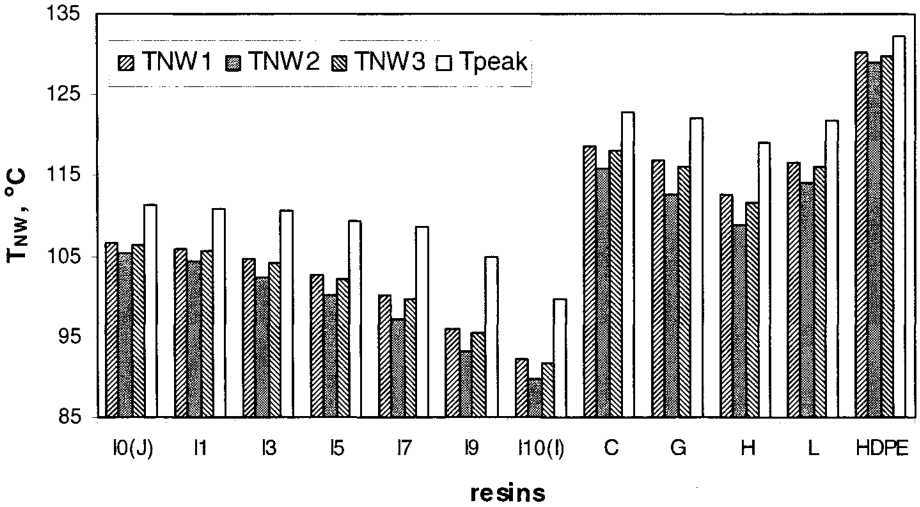

Figure 4-10 Number average melting temperatures from different methods and DSC main peak positions for different resins

The melting temperature polydispersities, P_T, obtained by the different calculation methods are shown for the different resins in Figure 4-11. Generally, just as in the isothermal experiments, P_{T1} are the highest and then P_{T2}. P_{T3} are the lowest. Among all the resins, HDPE has the lowest values of P_T. The melting temperature peak for HDPE is rather sharp, because there is no branching. P_T for ZN-LLDPE (resin G) is much higher than P_T for m-LLDPE (resin J). P_T for m-LLDPE with high SCBC (resin I) is higher than that for m-LLDPE with low SCBC (resin J). Also, P_T for ZN-LLDPE with high SCBC (resin G) is higher than that for ZN-LLDPE with low SCBC (resin L). In m-LLDPEs and their blends, P_{T1} increases as resin I content increases, and reaches a maximum at 0.7 ~ 0.9 wt resin I. This pattern interestingly corresponds to the pattern of the short chain branching polydispersity vs. resin I content. However, P_{T2} and P_{T3} do not show maximum values; they keep increasing, as resin I content increases.

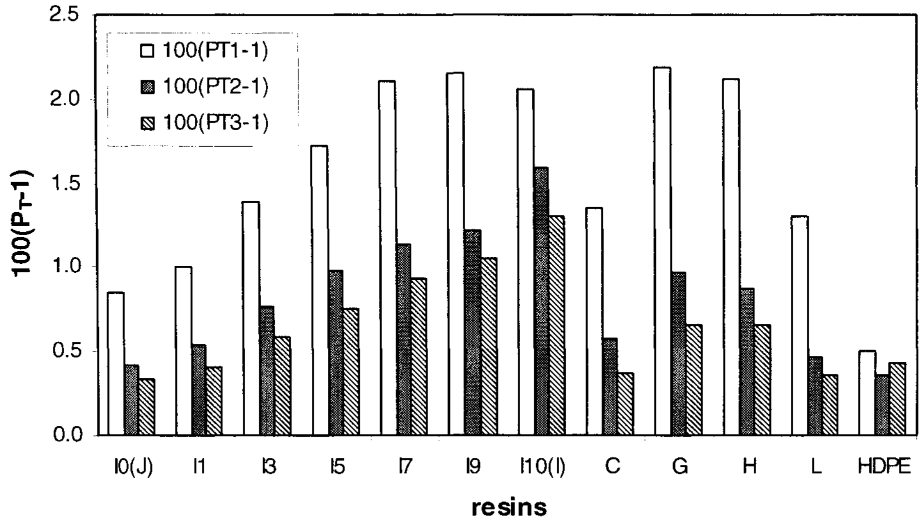

Figure 4-11 Melting temperature polydispersity from different methods for different resins

4.6 Conclusions

The melting temperature and melting temperature polydispersity are defined according to the crystal size number distribution. The melting temperatures may be characterized by the number and weight average melting temperatures, and the effective melting temperature. Three calculation methods are proposed and compared. They are based on the value of average crystal size, the crystal stem number function, and the monomer structural unit function, respectively.

The melting temperature characteristics are applied to polyethylene polymers, with special emphasis on LLDPEs in isothermal and non-isothermal experiments. The calculation results of average crystal sizes are confirmed by SAXS experiments.

Under the conditions used in the isothermal experiments, the effective melting temperatures decrease slightly in regime III and increase slightly in regime II, as the crystallization temperature increases. The melting temperature polydispersity increases as the crystallization temperature increases.

For different materials, HDPE has the highest average melting temperature and the lowest melting temperature polydispersity. For LLDPEs, there are multiple populations of crystal sizes. As the short chain branching content (SCBC) increases, the average melting temperature decreases, while the melting temperature polydispersity increases. As the short chain branching distribution becomes broader, the melting temperature polydispersity decreases, while the average melting temperature increases.

4.7 References

1 Kamal MR, Feng L, Huang T. Can J Chem Eng 2002, 80: 432.

2 Wunderlich B. Macromolecular Physics, Vol.3. London: Academic Press, 1980.

3 Sanchez IC, Eby RK. Macromolecules 1975, 8:638.

4 Crist B, Mirabella FM. J Polym Sci, B: Polym Phys 1999, 37:3131.

5 Hoffman JD, Weeks JJ. J Res Natl Bur Stand 1962, 66A:13.

6 Mirabella FM. J Polym Sci, B: Polym Phys 2001, 39:2800.

7 Kim MH, Phillips PJ. J Appl Polym Sci 1998, 70:1893.

8 Feng L, Kamal MR. Can J Chem Eng 2004, accepted for publication (see Chapter 3 in this thesis).

9 Wlochowicz A, Eder M. Polymer 1984, 25:1268.

10 Plummer CJG, Kausch HH. Polym Bull 1996, 36:355.

11 Androsch R, Blackwell J, Chvalun SN, Wunderlich B. Macromolecules 1999, 32:3735.

12 McFaddin DC, Russell KE, Wu G, Heyding RD. J Polym Sci, B: Polym Phys 1993, 31:175.

13 Androsch R, Wunderlich B. Macromolecules 2000, 33:9076.

14 Bensason S, Minick J, Moet A, Chum S, Hiltner A, Baer E. J Polym Sci, B: Polym Phys 1996, 34:1301.

15 Lu L, Alamo RG, Mandelkern L. Macromolecules 1994, 27:6571.

16 Mathot VBF. In: Mathot VBF. Editor, Calorimetry and Thermal Analysis of Polymers, New York: Hanser Publishers, 1994 (Chapter 9).

17 Hoffman JD, Miller RL. Polymer 1997, 38:3151.

18 Feng L, Kamal MR. Polym Eng Sci 2004, accepted for publication (see Chapter 5 in this thesis)

19 Svergun DI, Feigin LA. X-ray and Neutron Low-Angle Scattering, New York: Plenum Press, 1987.

20 Crist B. J Polym Sci, B: Polym Phys 1973, 11:635.

21 Defoor F, Groeninckx G, Reynaers H, Schouterden P, Van der Heijden, B. Macromolecules 1993, 26:2575.

22 Jokela K, Väänänen A, Torkkeli M, Starck P, Serimaa R, Löfgren B, Seppälä J. J Polym Sci, B: Polym Phys 2001, 39:1860.

Chapter 5

5 Spherulitic Crystallization Behavior of Linear Low-Density Polyethylene

The crystallization behavior of linear low-density polyethylenes (LLDPE) (ethylene-α-olefin copolymers) is studied by polarized light microscopy. A modified Hoffman-Lauritzen expression is proposed by replacing the equilibrium melting temperature, $T_m^{H,\infty}$ (T_m^0), of the melting temperature of the crystal stem with the maximum possible stem length, T_m^{C,n^*}. It successfully describes the crystalline spherulitic growth kinetics for both homogeneous and heterogeneous LLDPEs. Besides regimes III and II, another regime (IM) is found in the high crystallization temperature range. Linear growth behavior of crystalline spherulites is observed in regime III; non-linear growth behavior is found in regime II and regime IM. The basal surface free energy can be estimated from the short chain branching polydispersity (SCBP) for LLDPEs with excluded comonomers.

5.1 Introduction

The crystallization kinetics of linear low-density polyethylenes (LLDPEs) depends on the molecular structure, such as molecular weight (MW) and molecular weight distribution (MWD), short chain branching content (SCBC) and short chain branching distribution (SCBD), and crystallization processing conditions.[1,2,3] Spherulitic morphology is commonly observed in polyethylenes. Spherulitic growth is used to study and analyze the linear crystallization kinetics of LLDPEs.[4,5,6] Spherulitic growth rates of linear polymers during isothermal crystallization processes have been described by the Hoffman-Lauritzen theory (HL)[7,8] according to the secondary nucleation mechanism,

$$G = G_0 \exp\left[-\frac{Q_D^*}{RT_c}\right]\exp\left[-\frac{K_g}{T_c\left(T_m^0 - T_c\right)f}\right] \tag{5-1}$$

G refers to the spherulitic radial growth rate; the first exponent term refers to the diffusion across the interface of crystals and melts; the second term represents the deposition of crystal stems; G_0 is a pre-exponential parameter containing quantities not strongly dependent on the temperature. Q_D^* is the diffusion activation energy; T_c refers to the crystallization temperature; (T_m^0-T_c) is the degree of supercooling. T_m^0 ($T_m^{H,\infty}$) is the equilibrium melting temperature of perfect homopolymer crystals with infinite crystal size; $f = 2T_c/(T_m^0+T_c)$ is a correction factor for the variation in the heat of fusion with the temperature. The nucleation constant K_g is the net activation energy for layer growth. It depends on the spherulitic growth regime behavior. According to the HL theory, the regime behavior passes from regimes III to II, and I, as the crystallization temperature increases, (the degree of supercooling decreases)[7,8,9] In regimes III and I, K_g can be expressed by:

$$K_{gIII} = K_{gI} = \frac{4b_0\sigma\sigma_e}{k\Delta H_u}T_m^0 \tag{5-2}$$

In regime II, K_g is:

$$K_{gII} = \frac{2b_0\sigma\sigma_e}{k\Delta H_u}T_m^0 \tag{5-3}$$

where σ and σ_e are, respectively, the lateral and basal (folding) surface free energies, k is Boltzmann's constant, b_0 is the layer thickness, and ΔH_u is the heat of fusion.

In this paper, we propose a modification of the HL equation based on the generalized melting temperature equation,[10] and apply it to homogeneous LLDPEs (metallocene catalyzed LLDPE: m-LLDPEs), then extend it to m-LLDPE blends, and finally to heterogeneous LLDPEs (Ziegler-Natta catalyzed LLDPEs: ZN-LLDPEs). The regime behavior and other properties are discussed according to the modified HL equation.

5.2 Experimental

5.2.1 Materials and sample preparation

The LLDPE virgin resins used in this work were described elsewhere.[11] They were provided by Nova Chemical Co. (Calgary, Canada) in pellet form, including two experimental m-LLDPEs (resins I and J), and four experimental ZN-LLDPEs (resins H, C, G, and L). The material characteristics are listed in Table 5-1. The molecular structural parameters were also provided by Nova Chemical Co. The branching degrees were measured by nuclear magnetic resonance (NMR), and molecular weights were measured by the gel permeation chromatography (GPC). Five blends of m-LLDPE resins I and J (blends I1, I3, I5, I7, and I9) were prepared by solvent-mixing.[11] The blend characteristics were estimated from the pure m-LLDPE resins. They are also listed in Table 5-1.

The pellets of LLDPE resins (m-LLDPEs and ZN-LLDPEs) were pressed at about 180°C into 2mm thick plates by compression molding and quenched to room temperature. Then, the plates were cut into small 3~5μm thick films, using a microtome under liquid nitrogen, for microscopy experiments.

Table 5-1 Polymer molecular characteristics

Material	Com [a]	Type [b]	D_{Branch} (/1000C)	M_n (kg/mol)	M_w (kg/mol)
H	B	ZN	18.9	29.5	123.0
C	H	ZN	18.9	33.3	102.0
L	O	ZN	14.0	25.9	114.0
G	O	ZN	15.8	23.1	98.6
J (I0)	O	m	15.8	38.2	70.2
I1	O	mb (0.1 I wt)	16.7	35.5	68.5
I3	O	mb (0.3 I wt)	18.5	31.2	65.0
I5	O	mb (0.5 I wt)	20.3	27.9	61.5
I7	O	mb (0.7 I wt)	22.1	25.1	58.1
I9	O	mb (0.9 I wt)	23.9	22.9	54.6
I (I10)	O	m	24.8	21.9	52.9

a: Com is comonomer; B is butene, H is hexene, and O is octene.
b: ZN is ZN-LLDPE, and m is m-LLDPE, and mb is m-LLDPE blend

The m-LLDPE blend samples were prepared by the solution method. After copolymers were dissolved in xylene (1%w/v) at 120°C and strongly stirred for around 1 hour, a droplet of the hot solution was sprayed on a clean circular microscopic glass cover. A thin film (about 2~3μm) formed after the solvent evaporated. Then, it was dried under vacuum at about 50°C for more than one week. The same procedure was applied to the pure m-LLDPEs. The experimental results showed that there was no effect of the solution process on the properties of the polymers.

5.2.2 Observation and measurement of spherulitic growth during crystallization

A thin film specimen was fixed on a circular microscopic glass cover. Then, the glass cover was placed on a hot stage (Linkam TH600). The hot stage was used in conjunction with a polarized light microscope (Olympus BH-2), equipped with a digital camcorder system (SONY DXC-950/1). The temperature can be controlled within 0.1 degree. The film specimen was heated to 180°C and kept for 10 min to remove thermal history effects. Subsequently, the melted film was quenched to the set crystallization temperature, and kept at that temperature until the crystallization process was terminated. The quenching rate was about 130°C/min, which was achieved by direct flow of compressed air through the hot stage sample holder. The spherulitic growth with time was recorded and saved in a computer by the Linkam software. The whole experimental process was conducted under nitrogen atmosphere.

Under the experimental conditions employed, the crystalline morphology is the spherulitic structure, as shown in Figure 5-1. The spherulite is a typical structure of polymer crystallization from bulk melts. As the crystallization temperature increases, the spherulitic structure deteriorates. The Linkam software provides a method to measure the spherulitic size directly. If the spherulite was too small to detect directly, especially in the initial crystallization stage, the image was enlarged before application of the image analysis software. The measurement precision is about 0.05μm.

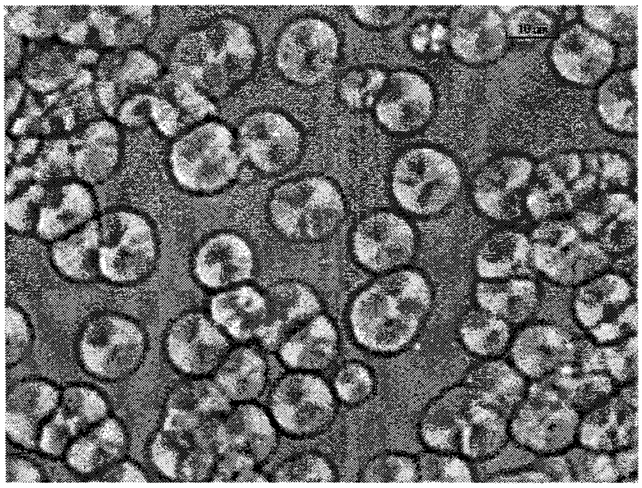

Figure 5-1 Crystalline spherulites of resin J at 100°C

5.3 Results

Typical plots of spherulitic radius versus crystallization time under isothermal conditions are shown in Figure 5-2 for m-LLDPE resin J, in Figure 5-3 for m-LLDPE blend I3, and in Figure 5-4 for ZN-LLDPE resin C. As shown in these figures, for all three different types of LLDPE, when crystallization temperature is relatively low, the spherulitic radius, *R*, increases linearly with the crystallization time, t_c; and, the spherulitic radial growth rate, *G*, is constant during the whole crystallization process. When the crystallization temperature is relatively high, the spherulitic radius increases non-linearly with t_c, and *G* decreases with t_c. The non-linear growth characteristic becomes more obvious, as the crystallization temperature increases. Although non-linear spherulitic growth has already been observed in blend systems with crystalline and amorphous components,[12,13,14] here it is observed in LLDPE in the high crystallization temperature range.

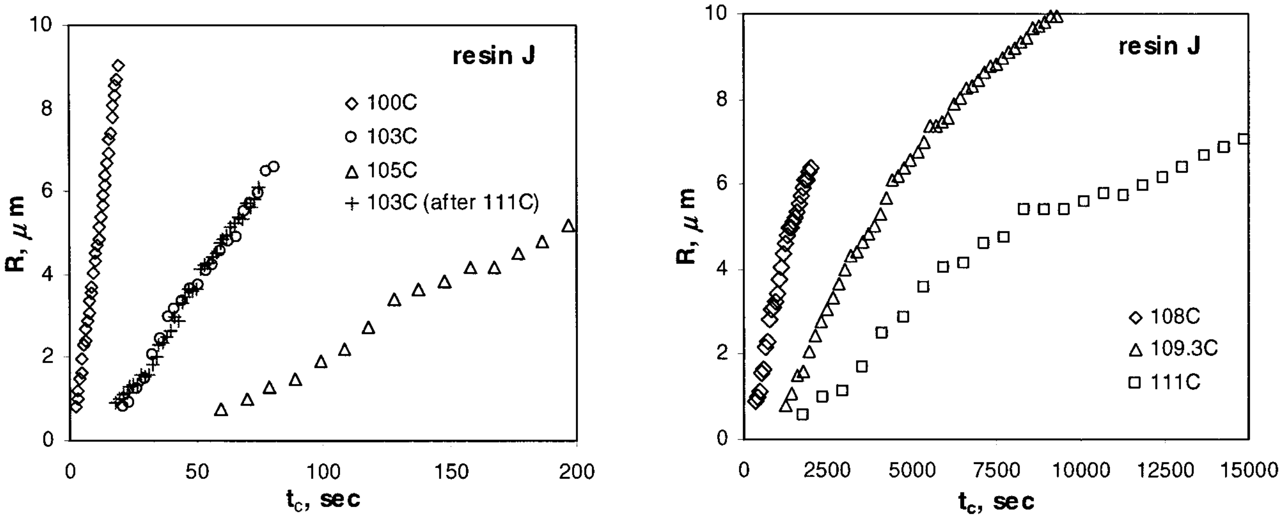

(a) linear growth (b) non-linear growth

Figure 5-2 Spherulite radius vs. crystallization time for m-LLDPE resin J

In order to confirm that the non-linear spherulitic growth was not caused by possible degradation, some samples that experienced non-linear growth were melted and allowed to crystallize again at relatively low temperature. The experimental results reproduced the expected linear behavior obtained previously at the low temperature. This is illustrated in Figure 5-2(a) for crystallization of resin J at 103°C after exhibiting non-linear crystallization at 111°C. Therefore, under the experimental conditions employed, the degradation effects appear to be negligible.

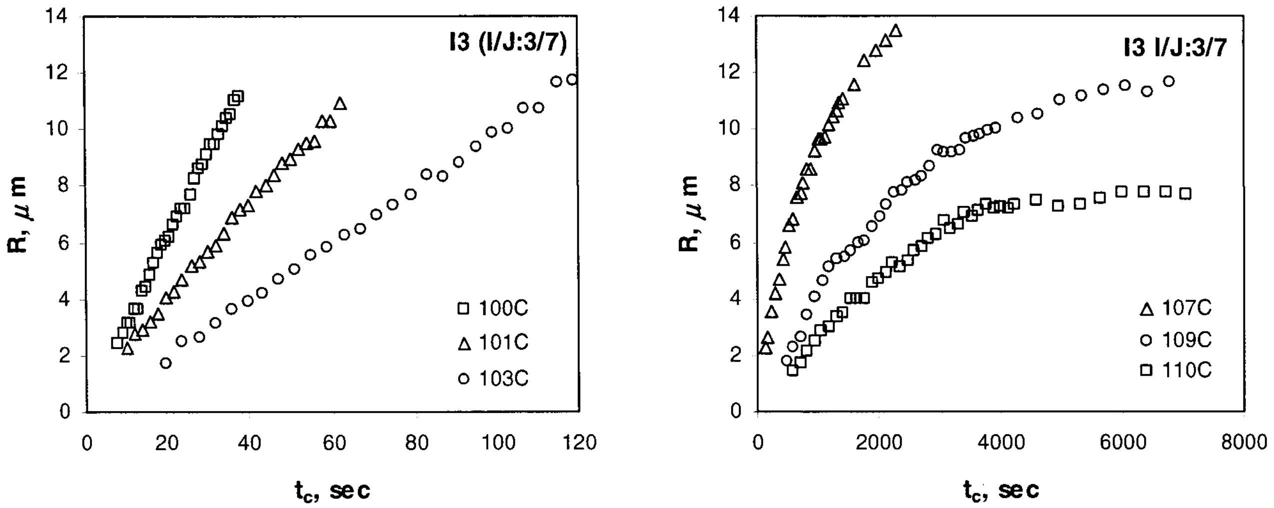

(a) linear growth (b) non-linear growth

Figure 5-3 Spherulite radius vs. crystallization time for m-LLDPE blend I3 (I/J:3/7)

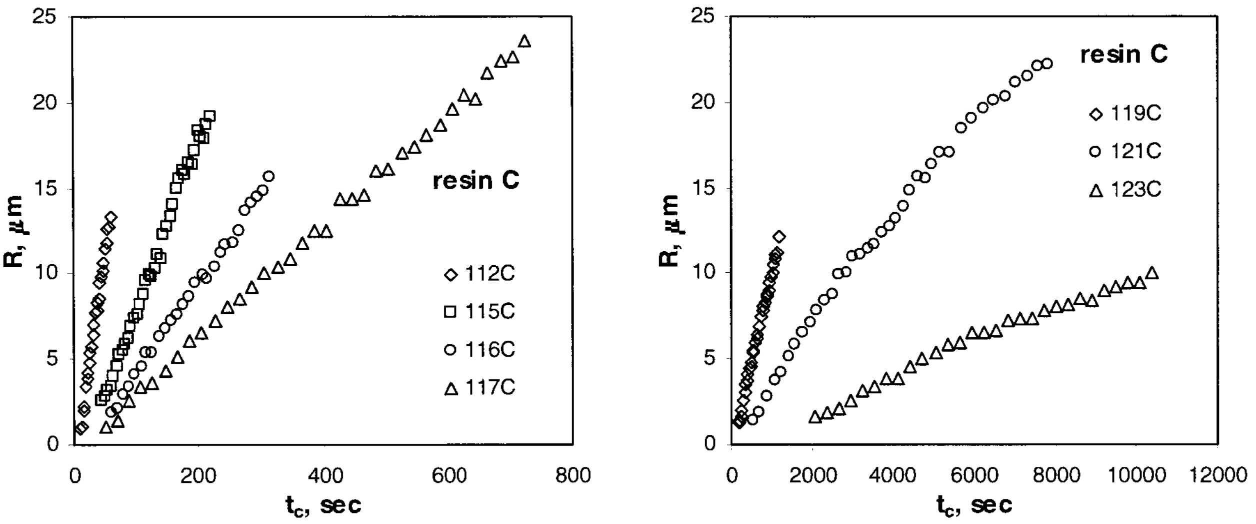

(a) linear growth (b) non-linear growth

Figure 5-4 Spherulite radius vs. crystallization time for ZN-LLDPE resin C

The spherulitic growth rate, *G*, was calculated from data on the variation of spherulitic radius with crystallization time. In the linear growth region, the spherulitic growth rate was the slope of the straight line. In the non-linear growth region (including irregular spherulites), the growth rate was determined from the slope of the linear portion (in the initial crystallization stage), by using linear regression for at least the first 15 experimental points. Generally, R^2 was higher than 0.985. For irregular spherulites, the crystal morphology could roughly maintain the spherulitic structure in the early crystallization stage. Thus, it is also possible to measure the spherulitic sizes. The results are shown in Figure 5-5. For all three types of LLDPE, the crystallization temperature, T_c, has a significant effect on the spherulitic growth rate. As the crystallization temperature increases, the growth rate decreases rapidly. For example, for m-LLDPE resin J, it decreases from 0.45μm/sec to 0.00076μm/sec, when T_c increases from 100°C to 111°C.

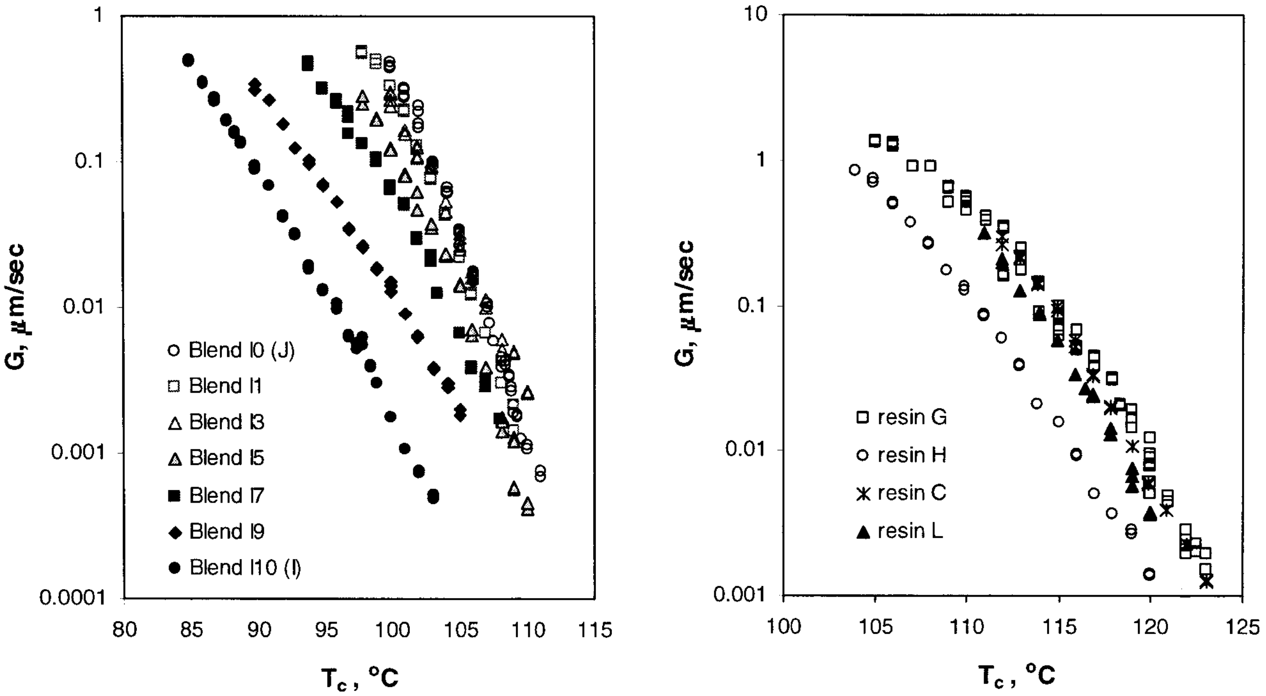

(a) m-LLDPEs and their blends

(b) ZN-LLDPEs

Figure 5-5 Spherulitic growth rates vs. crystallization temperatures

Under the experimental conditions employed in this study, the experimental crystallization temperature range is restricted by spherulitic growth rate: from about 0.0001 to 1 μm/sec. At high temperatures, such long times are required, that other factors, such as degradation, become significant. On the other hand, at low temperatures, the growth rates are so fast that the growth is completed before the temperature stabilizes.

For m-LLDPE resins and their blends, as shown in Figure 5-5(a). Under experimental conditions, as resin I weight content increases, the experimental crystallization temperature range become lower. For example, it goes from 100-111°C for resin J (I0, 0wt resin I), to 85-103°C for resin I (I10). At the same crystallization temperature, the spherulitic growth rate increases as the ratio of resin I decreases, as shown in Figure 5-6 for 100°C isothermal experiments. This is mainly because resin J has a lower short chain branching content (SCBC) than resin I and thus a higher melting temperature for the crystal stem with a maximum possible crystal size, $T_m^{C,n*}$. However, as shown in Figure 5-5(a), when the crystallization temperature is higher than 107°C, the growth rates crossover for blends I1, I3 and resin J. The spherulitic growth rates of blend I3 are higher than those of blend I1 and resin J. Therefore, there should be other factors, which also affect the spherulitic growth rates. According to the Hoffman-Lauritzen (HL) equation, the growth rates are not only dependent on the SCBC, but also on the basal surface free energy, σ_e, which can be taken as a material constant. For different materials, σ_e is a function of chemical composition and molecular structure. For LLDPEs with excluded comonomers, it mainly depends on the branching characteristics. A low basal surface free energy is expected for polymers with a high short chain branching polydispersity (SCBP), because a high SCBP produces high irregularity of the basal surface, which provides more space for holding branching units, which have relatively large volume.

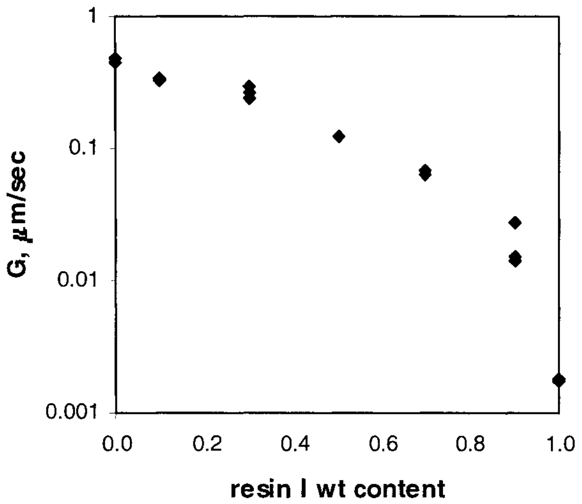

Figure 5-6 Spherulitic growth rates of m-LLDPEs and their blends at 100°C

Figure 5-5(b) shows the results for ZN-LLDPE resins. Resins G and L incorporate α–octene comonomer, and the SCBC of resin L is lower than that of resin G. However, at the same crystallization temperature, the growth rate of resin L is lower than that of resin G. Therefore, it is expected that the basal surface free energy of resin L is higher than that of resin G. For resins H and C, the short chain branch contents are similar, but the growth rate of resin H is much less than that of resin C. So, it would be expected that the basal surface free energy of resin H is much larger than that of resin C, if the difference between α-hexene and α-butene comonomers can be neglected. These observations will be discussed in a later section.

5.4 Discussion

5.4.1 Modified Hoffman-Lauritzen expression

Because it was initially proposed for linear crystalline polymers, the Hoffman-Lauritzen (HL) equation has to be modified, when it is applied to copolymers. For copolymers with excluded comonomers, such as LLDPE, we suggest that T_m^0 be replaced by the melting temperature of the crystal stem with the maximum possible length, $T_m^{C,n*}$.[10] $T_m^{C,n*}$ is a function of the short chain branching content (SCBC), the short chain branching polydispersity (SCBP), the comonomer volume, the basal (folding) surface free energy, and the molecular weight characteristics. It may be obtained from the following equation:

$$\frac{1}{T_m^{C,n^*}}\left(1-\frac{2\sigma_e}{\Delta H_u n^*}\right)-\frac{1}{T_m^0}=-\left(\frac{R}{\Delta H_u}\right)\ln p-\frac{1}{n^*}\left(\frac{R}{\Delta H_u}\right)\ln\left(\frac{X_A}{p}\right) \qquad (5\text{-}4)$$

where R is the gas constant, X_A is the volume fraction of monomer units, n^* is the maximum possible number of monomer units in the crystal stem, and p is the sequence propagation probability that a monomer is succeeded by another monomer. For random copolymers, it is equal to the monomer mole fraction.

In homogeneous copolymers, the comonomers are distributed randomly. Furthermore, the comonomer content can be assumed to be uniform in all molecules, even though their molecular weights are different. Generally, for LLDPE, the branching degree is represented by the number of branches per 1000 backbone carbons, D_{Branch}. For random systems (m-LLDPE), the following relationship is obtained between D_{Branch} and p:

$$p = 1 - D_{Branch}/500 \tag{5-5}$$

where 500 arises from the presence of two carbons in each ethylene repeat structural unit (CH_2CH_2).

For an ethylene sequence with length n^* between two branches, the maximum possible crystal length is n^*. Since the detail mole weight distribution and short chain branching distribution are rather complex, the actual value of n^* for a LLDPE resin is difficult to identify exactly. Therefore, in this work, an effective n^* is identified to correspond to an effective molecular weight with a corresponding effective homogeneous SCBD, as shown in the following equation:

$$n^* = \left(\frac{M_{nw}^*}{28.06}\right) \Bigg/ \left(\frac{D_{Branch}}{500}\frac{M_{nw}^*}{28.06} + 1\right) \tag{5-6}$$

where 28.06 is the molecular weight of the repeat structural unit, (C_2H_4), and M_{nw}^* is the effective molecular weight of the main chain:

$$M_{nw}^* = M_{nw} \Bigg/ \left(1 + \frac{m-2}{2}\frac{D_{Branch}}{500}\right) \tag{5-7}$$

where m is the number of carbons in the comonomer, and M_{nw} represents the molecular weight of the main chain. The latter can be described as,[8]

$$M_{nw} = \sqrt{M_n M_w} = M_w \Bigg/ \sqrt{\frac{M_w}{M_n}} \tag{5-8}$$

where M_n and M_w are the number and weight average molecular weights, respectively. Thus, M_{nw} contains, to some extent, the effect of molecular weight distribution. The volume fraction of ethylene structural units, X_A, is

$$X_A = \frac{p}{\frac{m}{2}(1-p)+p} \tag{5-9}$$

Therefore, for homogeneous random α-alkene-ethylene copolymers, T_m^{C,n^*} is given by,[10]

$$\frac{1}{T_m^{C,n^*}}\left(1-\frac{2\sigma_e}{\Delta H_u n^*}\right)-\frac{1}{T_m^{H,\infty}} = -\left(\frac{R}{\Delta H_u}\right)\left\{\ln p-\frac{1}{n^*}\ln\left[\frac{m}{2}(1-p)+p\right]\right\} \tag{5-10}$$

From Eq.(5-10), T_m^{C,n^*} of m-LLDPEs can be calculated according to their molecular structures.

In this work, m-LLDPE blends are mixtures of two m-LLDPEs. We assume that Eq.(5-10) can be applied to m-LLDPEs blends by employing average molecular structural parameters calculated from the weighted contributions of the parameters for the indicated resins. Moreover, we assume that heterogeneous LLDPEs (ZN-LLDPEs) may be considered as blends of several m-LLDPEs or of several ethylene sequences with different length. Thus, Eq.(5-10) is also extended for ZN-LLDPEs. The molecular structural parameters are represented by their corresponding averages. The different types of LLDPE have different values of the basal surface free energy. With the help of the average molecular structural parameters, it is possible to estimate. T_m^{C,n^*} values for m-LLDPE blends and ZN-LLDPEs, using Eq.(5-10). In the following discussion, the predictions of Eq.(5-10) are compared to the experimental results.

As suggested above, the HL equation is modified as follows for copolymers with excluded comonomers, such as LLDPE, or their mixtures:

$$G = G_0 \exp\left[-\frac{Q_D^*}{RT_c}\right]\exp\left[-\frac{K_{Mg}}{T_c\left(T_m^{C,n^*}-T_c\right)f}\right] \tag{5-11}$$

where $(T_m^{C,n^*}-T_c)$ is the effective degree of supercooling. The correction factor for the variation of the heat of fusion with the temperature, f, remains the same, $2T_c/(T_m^0+T_c)$, since the correction is applied to the heat of fusion at T_m^0. The plots of $(\ln G+Q_D^*/RT_c)$ vs. $1/(T_c\Delta Tf)$ are straight lines. In different regimes, the slopes are,

$$K_{MgIII} = K_{MgI} = \frac{4b_0\sigma\sigma_e}{k\Delta H_u} T_m^{C,n^*} \tag{5-12}$$

for regimes I and III, and

$$K_{MgII} = \frac{2b_0\sigma\sigma_e}{k\Delta H_u} T_m^{C,n^*} \tag{5-13}$$

for regime II. Theoretically, the ratio of the slopes in regimes III (or I) and II equals 2. In the following discussion, the following parameter values are used: $T_m^0 = 145.5$°C[15], $Q_D^* =$ 24 kJ/mol,[16] $b_0 = 0.415$ nm, l_u (projected length per CH_2) = 0.1273 nm, $\Delta H_u = 8.106$ kJ/mol (CH_2CH_2), and $\sigma = 11.8$ mJ/m^2.[8]

Table 5-2 The calculated parameters and results according to the MHL expression

Resin	σ_e [a] (J/mol)	$T_m^{C,n*}$ (K)	K_{MgIII} (10^4 K^2) Theoretical	K_{MgIII} (10^4 K^2) Experimental	$\frac{K_{MgIII}}{K_{MgII}}$	σ_e (J/mol) [b] from $T_m^{C,\infty}$	$T_{II\text{-}IM}$ [c] (°C)	$T_{III\text{-}II}$ [c] (°C)
H	3060	401.0	5.45	5.45	1.97	7870	117.4	112.5
C	2340	403.5	4.20	4.20	2.00	5220	122.5	118.5
L	3270	404.6	5.91	5.91	1.97	6980	-	117.3
G	2730	403.9	4.93	4.89	1.92	6140	122.0	116.5
I0 (J)	5200	396.4	9.20	9.20	1.97	17100	-	107.1
I1	4870	396.3	8.60	8.60	1.82	16900	-	107.2
I3	4300	396.0	7.60	7.60	1.98	14400	-	105.8
I5	3970	395.1	6.99	6.99	2.01	13600	-	107.6
I7	3920	393.3	6.88	6.88	1.97	12900	-	103.3
I9	4300	389.5	7.48	7.48	2.04	15700	103.0	96.0
I10 (I)	4660	386.7	8.04	8.00	2.05	19800	100.8	93.9

a: σ_e were estimated using a trial-and-error method by comparing theoretical values of K_{gIII} obtained from Eq.(5-12) with slopes from experimental results.

b: σ_e from $T_m^{C,\infty}$ are calculated from the slopes according to the HL expression.

c: $T_{III\text{-}II}$ and $T_{II\text{-}IM}$ are the regime transition temperatures from regimes III, II and IM, respectively.

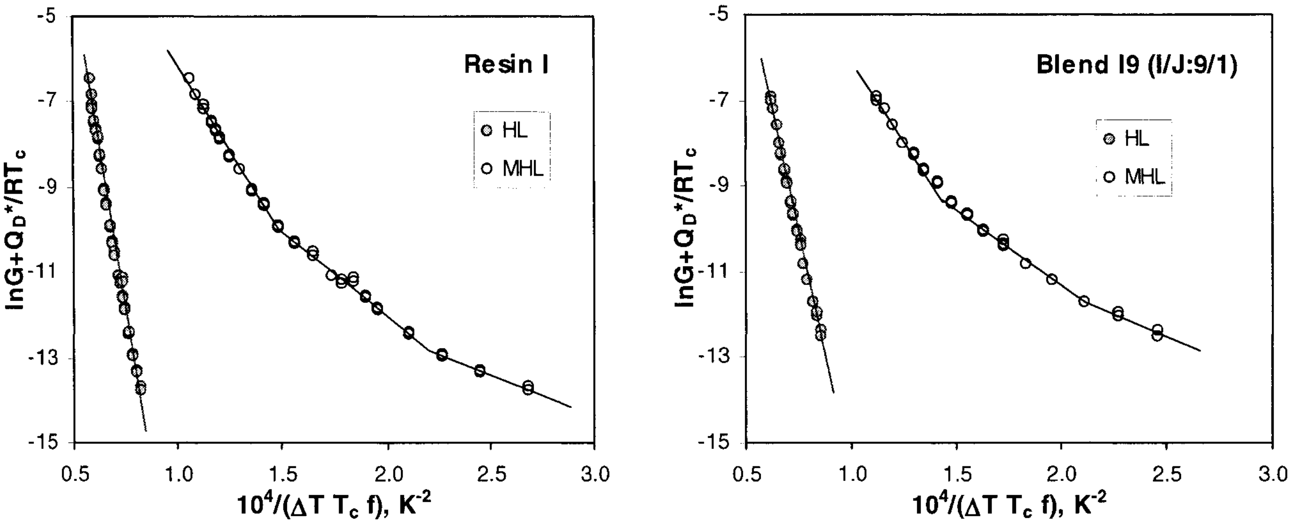

(a) m-LLDPE resin I

(b) m-LLDPE blend I9 (I/J:9/1)

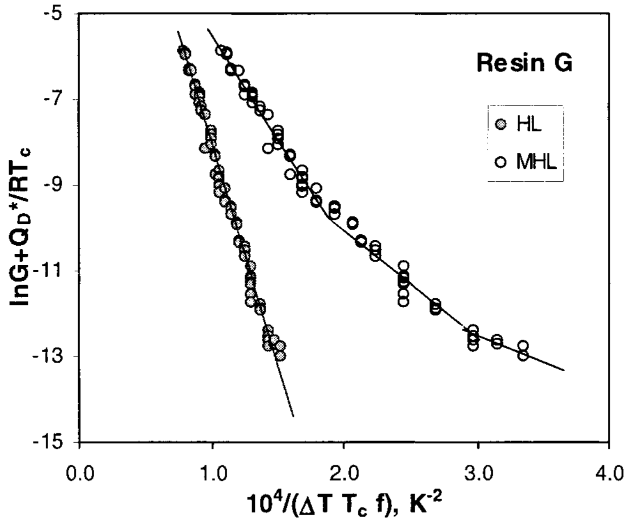

(c) ZN-LLDPE resin G

Figure 5-7 The description of crystallization kinetics by the MHL and HL equations

Figure 5-7 shows typical results of the application of Eq.(5-11) to three types of LLDPE: (a) m-LLDPE resin I, (b) m-LLDPE blend I9, and (c) ZN-LLDPE resin G. The results of application of the HL equation are also shown in Figure 5-7 for comparison. As shown in Figure 5-7, the linear crystallization kinetics for all three types of LLDPE can be described by the MHL equation. Under the experimental conditions employed in this study, regimes III and II are observed for all LLDPEs. The estimated characteristic parameters based on the experimental results are listed in Table 5-2. σ_e values were estimated using a trial-and–error method by comparing theoretical values of K_{gIII} obtained from Eq.(5-12) with slopes from experimental results. A value was guessed for σ_e, then $T_m^{C,n}$ was calculated. Subsequently, the theoretical value of K_{gIII} was calculated. The right σ_e is obtained, when the theoretical K_{gIII} value matches the experimental value obtained from plotting the experimental data, using the MHL equation. The slope ratios between regime III and regime II are about 2, as theoretically expected. This suggests that Eq. (5-4) and (5-11) provide a reasonable description of the linear crystallization kinetics of the three types of LLDPE.

5.4.1.1 Crystallization regimes

Figure 5-7 shows that, in addition to regimes III and II, a special regime is observed in the high crystallization temperature range for m-LLDPE resin I, m-LLDPE blend I9, and ZN-LLDPE resin G. In this regime, the slopes deviate from those for regime II, yet they do not increase to the expected values for regime I (the same as the values for regime III). In fact, the slopes in this regime are lower than the slope values for regime II. Because the slope in this regime is different from those obtained for regimes II or I (or III), we should refer to it as regime IM (I Modified). Similar behavior was also observed for ZN-LLDPE resins H and C.

It is difficult to observe regime I in LLDPEs. According to the HL secondary nucleation growth mechanism, the crystallization growth rate is determined by the co-operation between the secondary nucleation rate and the substrate completion rate.[7,8] In regime I, the crystallization temperature is high. The substrate completion rate is so fast that the growth rate does not depend on the substrate completion rate, but depends only on the secondary nucleation rate. However, due to the branching, more time is needed for ethylene sequences to fit into niches on the crystal substrates. Thus, the substrate completion rate in LLDPEs is too low to reach the requirements of regime I, especially when the short chain branching content (SCBC) is high. This behavior is similar to that of linear polyethylenes with high molecular weights. Entanglement effects are large in such polymers. Thus, the chain folding time is increased, and the substrate completion rate cannot reach sufficient levels to exhibit regime I behavior.[8]

5.4.1.2 Basal surface free energy

If the HL expression is directly employed to describe the spherulite growth kinetics, $T_m^{H,\infty}$ (T_m^0) has to be replaced by the melting temperature of the crystal stem with infinite length, $T_m^{C,\infty}$, for copolymers with excluded comonomers. Kamal et al.[10] pointed out that $T_m^{C,\infty}$ can be estimated from the Flory equation. [10,17]

$$\frac{1}{T_m^{C,\infty}} - \frac{1}{T_m^{H,\infty}} = -\frac{R}{\Delta H_u} \ln p \tag{5-14}$$

It only depends on the comonomer content for LLDPEs. As shown in Figure 5-7, based on the HL expression, all experimental data can be fitted into one straight line for the different LLDPEs. The regime behavior is difficult to identify, under the experimental conditions employed in this study. However, the different regimes are more easily distinguished according to the modified HL expression. The slopes are much higher when using the HL equation than those obtained with the MHL expression. Based on the HL slopes, the basal surface free energies are estimated and listed in Table 5-2. The values for m-LLDPEs and their blends are much higher than for linear polyethylene (10.2kJ/mol).[8] This is unreasonable. So, the method appears to be inconsistent with expectations. Furthermore, because of weak resolution of the differences among slopes of the different regimes, the estimated parameters cannot be compared, and the application of the equation for this purpose is limited.

The melting temperatures of crystal stems with possible maximum length, T_m^{C,n^*}, and the corresponding basal surface free energies, σ_e, estimated with Eq.(5-10) and Eq.(5-11), are also listed in Table 5-2 for the various resins. According to Eq.(5-10), there are two factors that have a significant influence on T_m^{C,n^*}: SCBC and σ_e. T_m^{C,n^*} decreases as the SCBC increases, and it increases as σ_e increases. For m-LLDPEs and their blends, Figure 5-8 shows that as resin I content increases, the SCBC increases. Thus, T_m^{C,n^*} decreases. Although the low basal surface free energy could involve a higher T_m^{C,n^*}, according to Eqs.(5-10) and (5-14), the reduction of p has a more important effect on T_m^{C,n^*} by causing a reduction in the equilibrium melting temperature of copolymers, $T_m^{C,\infty}$.[10] So, the SCBC has a dominant effect on T_m^{C,n^*}. As the SCBC increases, p

decreases. $T_m^{C,\infty}$ and $T_m^{C,n*}$ also tend to decrease. For ZN-LLDPEs, $T_m^{C,n*}$ has the same tendency as that of m-LLDPEs and their blends. For example, $T_m^{C,n*}$ of resin L (octene comonomer, D_{branch} 14.0) is higher than that of resin G (octene comonomer, D_{branch} 15.8).

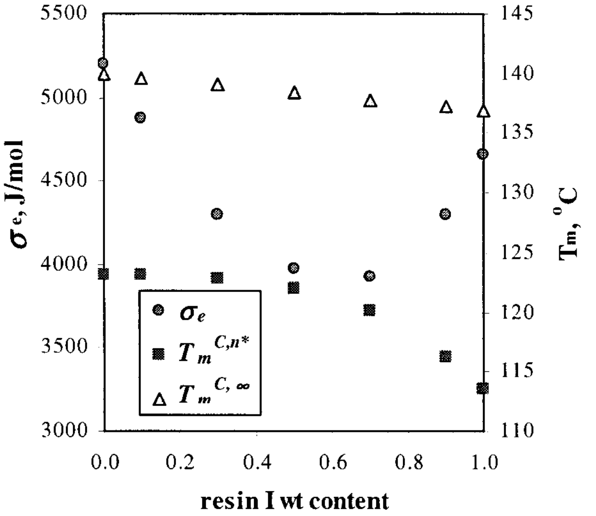

Figure 5-8 σ_e, $T_m^{C,\infty}$ and $T_m^{C,n*}$ for m-LLDPEs and their blends vs. resin I weight content

5.4.2 Basal surface free energy and short chain branching characteristics by TREF

Although Eqs.(5-4) and (5-10) were derived for homogeneous copolymers, they were shown to be also suitable for describing the behavior of heterogeneous copolymers and blends of homogeneous copolymers.[11] One of the important parameters in these equations that differentiates various types of LLDPE is the basal surface free energy, σ_e. This material property depends mainly on the short chain branching content (SCBC) and distribution (SCBD). The SCBC may be determined by techniques, such as FTIR and NMR. However, it is difficult to measure the short chain branching polydispersity (SCBP) directly. Generally, the SCBP may be deduced from temperature rising elution fractionation (TREF) experiments. Table 5-3 shows the elution temperature characteristics determined by TREF for the resins of interest. The elution temperature characteristics are designated in the same manner as for molecular weight characteristics. $T_{el,W}$ and $T_{el,N}$ are defined as the weight and number average elution temperatures, respectively. The effective average elution temperature is defined as $T_{el.WN} = \sqrt{T_{el.W}T_{el.N}}$. The elution temperature distribution (polydispersity) is given by $T_{el,W}/T_{el,N}$. TREF results were provided by Nova Chemical Co. (Calgary, Canada). For m-LLDPE blends, they were calculated according to their weight fraction.

Table 5-3 TREF calculation results

Resin	$T_{el,W}$ (°C)	$T_{el,N}$ (°C)	$T_{el,WN}$ (°C)	$T_{el,W}/T_{el,N}$
I0 (J)	78.4	77.9	78.1	1.0064
I1	76.8	75.8	76.3	1.0125
I3	73.6	72.1	72.8	1.0213
I5	70.4	68.6	69.5	1.0258
I7	67.2	65.5	66.4	1.0259
I9	64.0	62.7	63.4	1.0216
I10 (I)	62.5	61.4	61.9	1.0178
G	80.7	76.6	78.6	1.0542
C	79.0	74.2	76.6	1.0647
H	76.6	74.3	75.4	1.0316

$T_{el,W}$ and $T_{el,N}$ are defined as the weight and number average elution temperatures, respectively. The effective average elution temperature is defined as $T_{el.WN} = \sqrt{T_{el.W}T_{el.N}}$. The elution temperature distribution (polydispersity) is given by $T_{el,W}/T_{el,N}$.

$T_{el,WN}$ is an indicator of SCBC. As shown in Figure 5-9, $T_{el,WN}$ increases, as SCBC decreases. However, because the elution temperature in TREF experiments directly corresponds only to the longest ethylene sequence of individual molecules, it is not possible to find a direct relationship between the SCBC and the elution temperature.[18] TREF results for LLDPEs with octene comonomers can be fitted in one curve (Figure 5-9). However, the results for ZN-LLDPE resin C (hexene comonomers) and resin H (butene comonomers) do not follow the same curve. ZN-LLDPEs are heterogeneous from both inter- and intra-molecular considerations. Because of the intra-molecular heterogeneity, they have higher possibility of containing long ethylene sequences than m-

LLDPEs or m-LLDPE blends. Therefore, for ZN-LLDPEs, $T_{el,WN}$ are higher than those for m-LLDPEs and their blends at the same SCBC, as shown in Figure 5-9.

The results in Table 5-3 and Figure 5-9 (excluding resins C and H) may be fitted to the following equation:

$$T_{el,WN} = 118.2\exp\left(-0.0261 D_{Branch}\right)\ ^{\circ}\mathrm{C} \qquad (R^2 = 0.9995) \qquad (5\text{-}15)$$

where the maximum effective average elution temperature in the TREF solvent is 118.2°C. Actually, it is the equilibrium melting/dissolution temperature for a polyethylene chain with infinite chain length in a dilute solution, T_s^0. The reported value is 118.6±2°C in xylene, when $T_m^{H,\infty}$ (T_m^0) is 145.5±2°C.[19,20] Thus, the prediction is consistent with reported results.

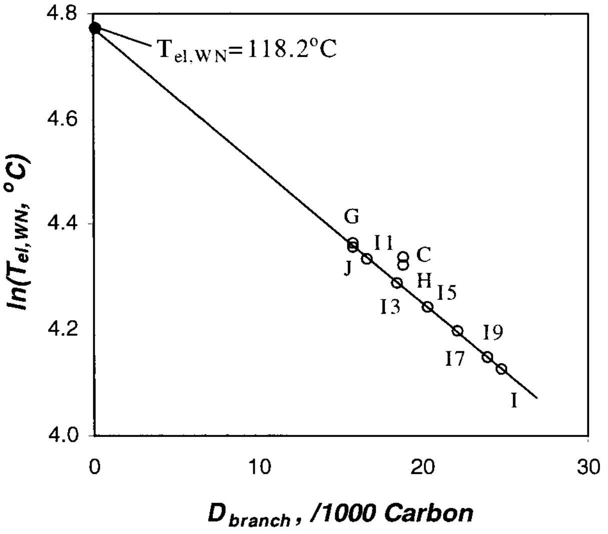

Figure 5-9 $T_{el,WN}$ vs. D_{branch} for different materials

For LLDPEs with excluded comonomers, the short branch units (comonomers) become the ends of crystal stems, because they are not crystallizable. In such polymers, the folds are large and only loose folds are obtained. The folding work is much lower than the regular tight folds. Thus, the short chain branches reduce σ_e. The content of loose loops increases, as the SCBC increases, although it is difficult to find a direct and simple relation between σ_e and the SCBC. However, when the SCBC reaches a certain high value, only loose folding crystals occur in the crystalline phase, because all ethylene sequences between branches may not be long enough to fold at a certain crystallization temperature. Then, the SCBC has little effect on σ_e. Therefore, the SCBC effect on σ_e is not significant, when the SCBC is not very small, as under the experimental conditions employed in this study.

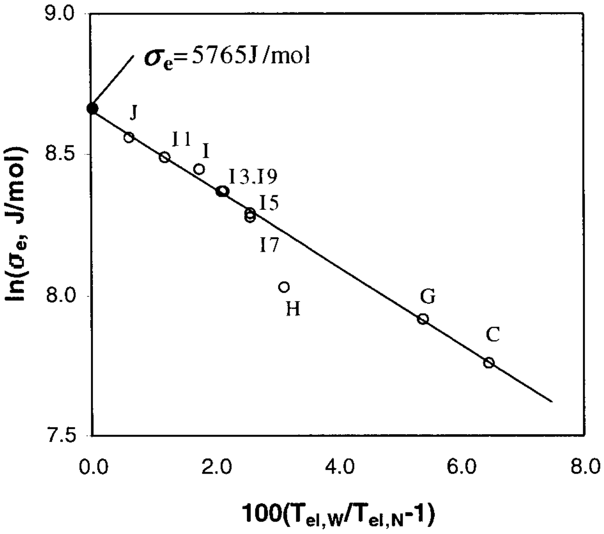

Figure 5-10 The basal surface free energy and SCBP

The SCBD has more important effects on the basal surface free energy than the SCBC, under the experimental conditions employed in this study. It can be described by the elution temperature distribution, $T_{el,W}/T_{el,N}$, from the TREF experimental results. The minimum value of $T_{el,W}/T_{el,N}$ is 1. The higher it is, the broader is the SCBD. As shown in Table 5-3, ZN-LLDPEs have higher SCBP values than m-LLDPEs and their blends, and the SCBP of m-LLDPEs are the smallest values, as expected. As the SCBD becomes broader, the irregularity of the basal surface increases. The irregular basal surface can easily hold comonomers with larger volume. Therefore, as the SCBD becomes broader, σ_e decreases. Under the experimental conditions employed, the relationship between σ_e and SCBP, shown in Figure 5-10, may be described by the following equation except resin H:

$$\sigma_e = 5765 \exp\left[-13.92\left(T_{el,W}/T_{el,N} - 1\right)\right] \qquad (R^2 = 0.996) \qquad (5\text{-}16)$$

Data for all the resins evaluated, except resin H, can be satisfactorily fit to the above equation. In resin H, the comonomer is α–butene. Because the ethyl branching size is rather small, it may be partially included in crystal lattices in TREF experiments. So, the apparent SCBP is probably smaller than the real value, as indicated in Figure 5-10. If $T_{el,W}/T_{el,N}$ takes the minimum value, 1, the length of the longest ethylene sequences in different molecules would be the same. Thus, for the case when all ethylene sequences have approximately the same length, σ_e = 5765 J/mol. The difference between this value and the value respected for linear polyethylenes (10.2 kJ/mol)[8] reflects the effect of the branching units.

5.4.3 Growth behavior in different regimes

As shown in the results, linear growth behavior is observed in regime III. On the other hand, non-linear growth behavior is observed in regimes II and IM. The regime transition points between regimes III and II appear to be the transition points between linear and non-linear spherulitic growth behavior. Application of the Avrami equation to overall crystallization kinetics (by DSC),[21] yields Avrami exponents equal to 2, 1.5, and 1 for regimes III, II and IM, respectively. The different exponents correspond to specific growth mechanisms,[22] as shown in Table 5-4. Under the experimental conditions employed in this study, the nucleation mechanism is heterogeneous.

Table 5-4 Avrami exponents and corresponding growth characteristics in different regimes for heterogeneous nucleation mechanism[22,23]

Regime	Avrami Exponent	Growth Habit	Growth Control
IM	1.0	Rod	Interface
		Disc	Diffusion
II	1.5	Sphere	Diffusion
III	2.0	Disc	Interface

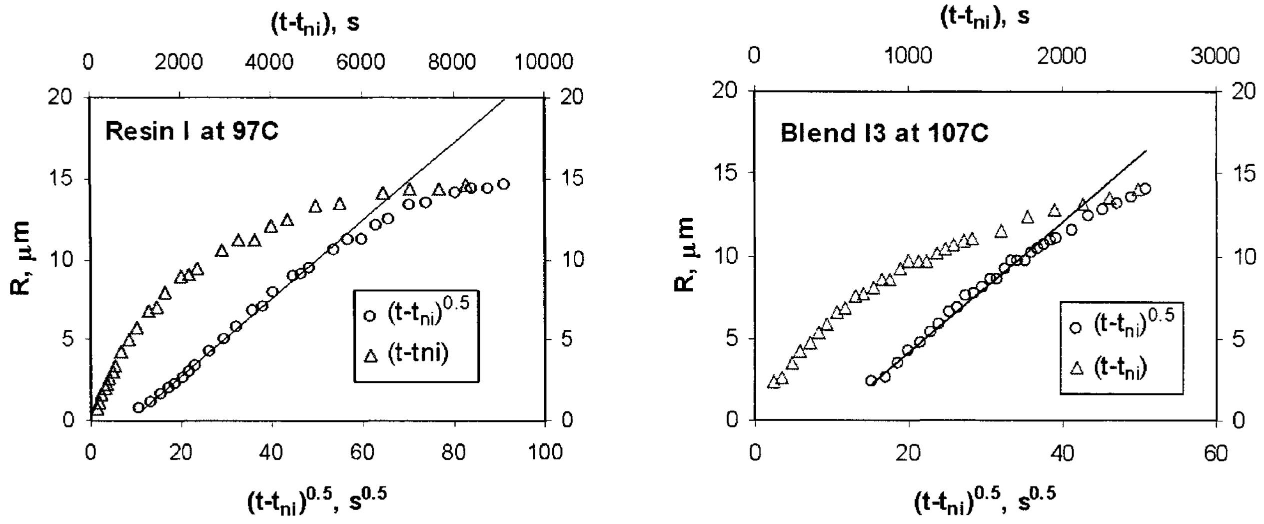

(a) m-LLDPE resin I at 97°C (b) m-LLDPE blend I3 at 107°C

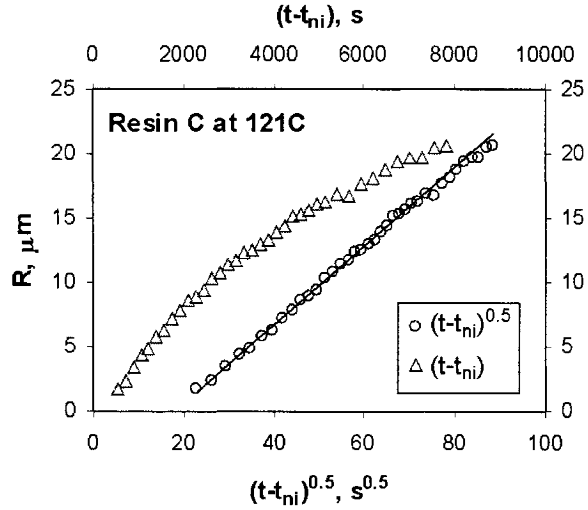

(c) ZN-LLDPE resin C at 121°C

Figure 5-11 The plots of radius vs. crystallization time in regime II

In regimes III and II, the growth habits are disc and sphere, respectively. So, in PLM experiments, the spherulitic structure is observed, as shown in Figure 5-1. For regime III, the interface mechanism controls the crystallization process. The growth rate is constant. So, the spherulite shows linear growth behavior. For regime II, the diffusion mechanism controls spherulitic growth. Although radial growth becomes slower with time, linear growth with $t^{0.5}$ is expected, if it follows the model of a moving boundary.[23] As shown in Figure 5-11, the spherulitic radius increases linearly with $t^{0.5}$ during most of regime II of the crystallization period for all three types of LLDPE. In the final stage, because of the impingement effect, the linear relationship cannot be maintained. Therefore, diffusion growth results in the non-linear growth behavior observed in regime II.

Table 5-4 shows that the Avrami exponent is 1 in regime IM. Thus, there are two possible growth habits, i.e., rod and disc forms, which are controlled, respectively, by the interface and diffusion mechanisms. Because the crystal morphology can roughly maintain the spherulitic structure in the early stages of crystallization, it is possible to measure the spherulitic growth rates. The propagation of rods in the melt phase helps to dissipate the self-created mechanical, thermal, and compositional fields at the growth front.[23] Therefore, the growth rate is higher than the expected value for the disc form. The characteristic slopes to fit experimental data, as obtained using the modified HL equation, are higher than the theoretical values. This leads to regime IM. As the crystallization continues, because of the competition between interface and diffusion mechanisms and the fluctuation of the concentration of crystallizable ethylene sequences in the melt phase, irregular morphologies are observed, as shown in Figure 5-12. Because of the diffusion mechanism, the non-linear growth behavior is also observed in regime IM, even in the early crystallization stages of that regime. However, because of the complex growth habit, it is difficult to find a direct generalized relationship between the spherulitic radius and the crystallization time.

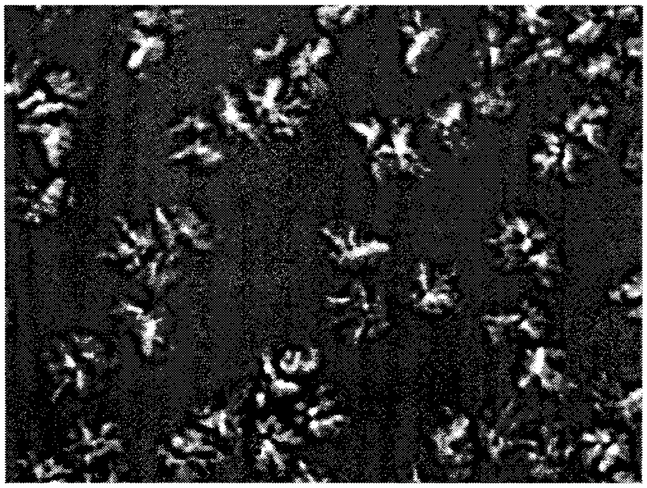

Figure 5-12 irregular crystallization morphologies in regime IM for resin G at 123°C

5.5 Conclusions

Although Eqs.(5-4) and (5-10) were originally proposed for homogeneous copolymer with excluded commoners, they can be extended to non-homogeneous LLDPEs, which may be considered as blends of homogeneous LLDPEs. These equations can thus be employed to calculate the melting temperatures of the crystal stem with the maximum possible length, $T_m^{C,n*}$ for both homogeneous and heterogeneous LLDPEs.

It is proposed to modify the Hoffman-Lauritzen (HL) equation for copolymers by replacing the equilibrium melting temperature, T_m^0, by $T_m^{C,n*}$. The modified Hoffman-Lauritzen equation provides satisfactory descriptions of the spherulitic growth kinetics for m-LLDPEs, m-LLDPE blends, and ZN-LLDPEs. The regime behavior was observed and analyzed according to the MHL equation. In addition to regimes III and II, regime IM was observed for ZN-LLDPEs, m-LLDPE resin I, and m-LLDPE blend I9. Non-linear growth behavior of spherulites was observed in regimes II and IM. Non-linear growth behavior and morphological characteristics may be explained by the crystallization growth habits and mechanisms indicated by the Avrami exponents, obtained from bulk crystallization kinetics experiments.

The basal surface free energy is strongly dependent on the short chain branching characteristics. The latter can be qualitatively described by the TREF results for LLDPEs.

5.6 References

1 Alamo RG, Mandelkern L. Thermochim Acta 1994, 238:155.

2 Bensason S, Minick J, Moet A, Chum S, Hiltner A, Baer E. J Polym Sci, B: Polym Phys 1996, 34:1301.

3 Bensason S, Stepanov EV, Chum S, Hiltner A, Baer E. Macromolecules 1997, 30:2436.

4 Lambert WS, Phillips PJ. Macromolecules 1994, 27:3537.

5 Lambert WS, Phillips PJ. Polymer 1996, 37:3585.

6 Wagner J, Phillips PJ. Polymer 2001, 42:8999.

7 Hoffman JD, Davis GT, Lauritzen JI. In: Hannay NB. Editor, Treatise on solid state chemistry, Vol. 3, New York: Plenum Press, 1976 (Chapter 7).

8 Hoffman JD, Miller RL. Polymer 1997, 38:3151.

9 Phillips PJ. Polym Prepr (Am Chem Soc Div Polym Chem) 1979, 20:483.

10 Kamal MR, Feng L, Huang T. Can J Chem Eng 2002, 80: 432.

11 Feng L, Kamal MR. Can J Chem Eng 2004, accepted for publication (see Chapter 3 in this thesis).

12 Keith HD, Padden FJ. Jr. J Appl Phys 1964, 35:1286.

13 Okada T, Saito H, Inoue T. Polymer 1994:35:5699.

14 Wu L, Lisowski M, Talibuddin S, Runt J. Macromolecules 1999, 32:1576.

15 Mandelkern L, Alamo RG. In: Mark JE. Editor, Physical Properties of Polymers Handbook, American Institute of Physics, New York: Woodbury, 1996 (Chapter11).

16 Fletcher DP, Klein J. Polym Commun 1985, 26:2.

17 Flory PJ. Trans Faraday Soc 1955, 51:848.

18 Soares JBP. Chem Eng Sci 2001, 56:4131.

19 Jackson JF, Mandelkern L, Long OC. Macromolecules 1968, 1:218.

20 Jackson JF, Mandelkern L. Macromolecules 1968, 1:546.

21 Feng L, Kamal MR. Polym Eng Sci 2004, submitted for publication (see Chapter 7 in this thesis).

22 Flory PJ, McIntyre AC. J Polym Sci 1955, 18:592.

23 Schultz JM. Polymer Crystallization: the Development of Crystalline Order in Thermoplastic Polymers, Oxford, New York: Oxford University Press, 2001 (Chapter10).

Chapter 6

6 Non-linear Crystalline Spherulitic Growth Behavior for Linear Low-Density Polyethylene

Non-linear growth behavior was observed in two crystallization regimes, depending on the temperature. Non-linearity may be explained by the reduction of the concentration of crystallizable ethylene sequences (CES) in the melt phase. In the two regimes, the concentration of uncrystallizable ethylene sequences (UCES) increases, as the crystallization time increases, because UCES are continuously excluded from the crystal lattice into the melt phase. An empirical equation is proposed to describe the melting temperature of the crystal stem with the maximum possible length, $T_m^{C,n*}$, in non-linear growth processes, assuming that the diffusion layer is negligible. A modified form of the Hoffman-Lauritzen equation (MHL) describes well the crystallization growth kinetics of LLDPE spherulites in the non-linear growth region.

6.1 Introduction

The Hoffman-Lauritzen nucleation mechanism has been widely used to explain crystalline spherulitic growth behavior during polymer crystallization.[1,2,3] In order to extend the utility of the Hoffman-Lauritzen (HL) equation from linear homopolymers to copolymers with excluded commoners, a modified equation was proposed. In this equation, the equilibrium melting temperature, T_m^0, is replaced with the melting temperature, T_m^{C,n^*}, of the crystal stem with the maximum possible length, n^*.[4,5] Thus, the modified Hoffman-Lauritzen (MHL) equation takes the form:

$$G = G_0 \exp\left[-\frac{Q_D^*}{RT_c}\right]\exp\left[-\frac{K_{Mg}}{T_c\left(T_m^{C,n^*}-T_c\right)f}\right] \tag{6-1}$$

where G_0 is a pre-exponential parameter containing quantities not strongly dependent on the temperature, R is the gas constant, Q_D^* is the diffusion activation energy, the nucleation constant K_{Mg} relates to the net activation energy for layer growth, T_c refers to the crystallization temperature, $\left(T_m^{C,n^*}-T\right)_c$ is the degree of supercooling (ΔT) (it replaces $\left(T_m^0 - T_c\right)$ in the HL equation), f is the correction factor for variation of the heat of fusion with the temperature and is equal to $2T_c/(T_m^0+T_c)$, and T_m^0 is the melting temperature of the crystal stem with infinite crystal length for homopolymers.

The plots of $\ln G+Q_D^*/RT_c$ vs. $1/(T_c\Delta Tf)$ are straight lines. In different crystallization regimes, the slopes, i.e., K_{Mg}, are different. Thus, in regimes III and I,

$$K_{MgIII} = K_{MgI} = \frac{4b_0\sigma\sigma_e}{k\Delta H_u}T_m^{C,n^*} \tag{6-2}$$

and in regime II,

$$K_{MgII} = \frac{2b_0\sigma\sigma_e}{k\Delta H_u}T_m^{C,n^*} \tag{6-3}$$

where σ and σ_e are, respectively, the lateral and basal (folding) surface free energies, k is Boltzmann's constant, b_0 is the layer thickness, and ΔH_u is the heat of fusion of monomer structural unit (m.s.u) in the perfect crystal. Theoretically, the slopes in regimes III and I are equal. Each of these slope equals twice the slope of regime II.

The melting temperature of crystals is dependent on the crystal size, n (represented by the number of m.s.u.), according to the following equation:[4]

$$\frac{1}{T_m}\left(1-\frac{2\sigma_e}{\Delta H_u n}\right)-\frac{1}{T_m^0}=-\left(\frac{R}{\Delta H_u}\right)\ln p-\frac{1}{n}\left(\frac{R}{\Delta H_u}\right)\ln\left(\frac{X_A}{p}\right) \tag{6-4}$$

where R is the gas constant, X_A is the monomer volume fraction, and p is the sequence propagation probability that a monomer is succeeded by another monomer, i.e., the monomer mole fraction for homogeneous copolymers. $T_m^{C,n*}$ may be estimated from Eq.(6-4) by replacing n with the maximum possible length, n^*.[4,5]

The regime behavior was observed for linear low-density polyethylenes (LLDPE), and analyzed according to Eq.(6-1).[5] In addition to regimes III and II, a special regime (regime IM) was found in the high crystallization temperature range. Non-linear spherulitic growth behavior was observed in regimes II and IM.[5]

Non-linear crystalline growth behavior has been reported in miscible blends of crystalline and amorphous polymers, such as blends of isotactic polypropylene and atactic polypropylene,[6] blends of isotactic polypropylene and liquid paraffin,[7,8] mixtures of isotactic polystyrene and atactic polystyrene,[9] and blends of poly(ethylene oxide) and PEO melt-miscible amorphous polymers.[10] It has been suggested that non-linear growth behavior depends on the interaction between the crystalline component and the amorphous component,[10] the molecular weight of the amorphous component,[6,8,9] and the content of the amorphous component.[11] Strong interaction between the two components, high molecular weight of the amorphous component, and high content of the amorphous component tend to produce non-linear growth behavior. A two-step diffusion mechanism has been proposed to explain the crystallization kinetics.[11]

Non-linear growth behavior was not only observed in miscible blend system, but it was also observed in LLDPEs[12] and syndiotactic polypropylene[13] in the high crystallization temperature range. However, it was ignored and treated similarly to the linear cases. [12,13] Bassett et al.[14,15] applied reflection optics to observe a series of quenched and etched samples, and predicted the non-linear crystalline spherulitic growth behavior in LLDPEs. However, their experiments were not real-time observations. Because polyethylene is a fast crystallizing polymer, crystal morphologies obtained during crystallization are possibly different from those observed in quenched samples.

In this paper, the non-linear spherulitic growth behavior of LLDPEs is observed in-situ using polarized light microscopy. The effects of crystallization temperature, crystallization time and concentration of uncrystallizable ethylene sequences (UCES) are discussed.

6.2 Experimental

6.2.1 Materials

Two experimental metallocene-based LLDPE (m-LLDPEs) (resins I and J) and one experimental Ziegler-Natta-based LLDPE (ZN-LLDPE) (resin H) were provided by the Nova Chemical Co. (Calgary, Canada) in pellet form. Material characteristics are listed in Table 6-1. The molecular structural parameters were also provided by the company. The branching degrees were measured by nuclear magnetic resonance (NMR), and molecular weights were measured by gel permeation chromatography (GPC). Three blends of m-LLDPE resins I and J (blends I1, I3, and I5) were prepared by solvent-mixing.[16] Blend characteristics were estimated from the pure m-LLDPE resins, and they are listed in Table 6-1. The characteristic temperatures of the resins are also listed.

6.2.2 Two-step crystallization process by polarized light microscopy (PLM)

As shown in Figure 6-1, a two-step isothermal experimental procedure was employed. After a thin film specimen was fixed on a circular microscopy glass cover, the glass cover was moved to a hot stage (Linkam TH600), which could control temperature within 0.1 degree. The hot stage was installed on a polarized light microscope (Olympus BH-2) equipped with a digital camcorder system (SONY DXC-950/1).

Table 6-1 Polymer molecular characteristics and characteristic temperatures

Material	Com [a]	Type [b]	D_{branch} (/1000C)	M_n (kg/mol)	M_w (kg/mol)	σ_e (J/mol)[c]	$(T_{el,W}/T_{el,N}$ -1)×100 [d]	$T_m^{C,n*}$ (°C)	$T_{II\text{-}IM}$ (°C) [e]	$T_{III\text{-}II}$ (°C) [e]
J (I0)	O	m	15.8	38.2	70.2	5200	0.64	123.2	-	107.1
I1	O	mb(0.1Iwt)	16.7	35.5	68.5	4870	1.25	123.1	-	107.2
I3	O	mb(0.3Iwt)	18.5	31.2	65.0	4300	2.13	122.8	-	105.8
I5	O	mb(0.5Iwt)	20.3	27.9	61.5	3970	2.58	121.9	-	107.6
I (I10)	O	m	24.8	21.9	52.9	4660	1.78	113.5	100.0	93.9
H	B	ZN	18.9	29.5	123.0	3060	3.16	127.8	117.4	112.5

a: *Com* is comonomer; O is octene, B is butene.

b: ZN is ZN-LLDPE, and m is m-LLDPE, and mb is m-LLDPE blend.

c: The basal surface free energies were calculated from the MHL secondary nucleation crystallization kinetics analysis for LLDPEs.[5]

d: The short chain branching polydispersities (SCBP) are calculated from the TREF results.[5] It is represented by $(T_{el,W}/T_{el,N} - 1)\times100$. $T_{el,W}$ and $T_{el,N}$ are defined as the weight and number average elution temperatures, respectively.

e: The regime transition temperatures from regime III to II, $T_{III\text{-}II}$, and from regime II to IM, $T_{II\text{-}IM}$, were based on MHL analysis.[5]

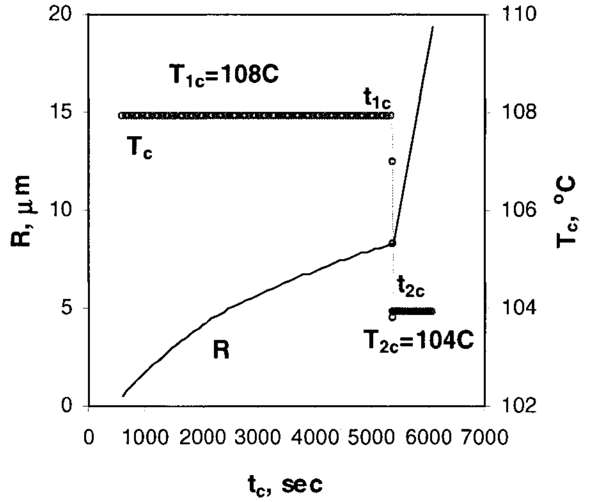

Figure 6-1 The procedure of a two-step isothermal experiment for m-LLDPE resin J T_{1c} = 108°C in regime II, T_{2c} = 104°C in regime III, t_{1c} = 90 min

The film specimen was heated to 180°C and kept for 10 minutes to remove the thermal history memory. Subsequently, the melted film was quenched to crystallize for a certain time, t_{1c}, at a high temperature, T_{1c}. At T_{1c}, the crystalline spherulitic growth behavior was non-linear. Then, the specimen was quenched to a lower temperature, T_{2c}, to finish the crystallization. Generally, T_{2c} is chosen in the temperature range of regime III. The growth behavior was linear at T_{2c}, if the specimen was cooled down directly from the melt to T_{2c} (one-step crystallization). Also, some of the T_{2c} values for ZN-LLDPE resin H were chosen in regime II. The crystallization time in the second step at T_{2c} was t_{2c}. The quenching rate was about 130°C/min, which was achieved by direct flow of compressed air through the hot stage sample holder. The spherulitic growth with time was recorded and saved in a personal computer by the Linkam software. The whole experimental process was conducted under nitrogen atmosphere.

6.3 Results and Discussion

6.3.1 Uncrystallizable ethylene sequences (UCES) in different regimes

When the size of the comonomer unit in LLDPE is larger than propylene, comonomers are generally excluded from the crystal lattice.[17] Comonomers separate the molecular chain into a series of ethylene sequences (ES). The ethylene sequence size is not uniform, but shows a distribution, which depends on the short chain branching distribution (SCBD). Thus, as indicated by Eq.(6-4), some ethylene sequences are perhaps not long enough to crystallize, at some crystallization temperatures. The amount of uncrystallizable ethylene sequences (UCES) depends on the crystallization temperature and the molecular structure. The concentration of UCES (CUCES) increases, as the crystallization temperature increases. During the crystallization process, not only UCES are excluded from the crystal lattices, but also some crystallizable ethylene sequences (CES) are possibly excluded, because of kinetic factors. If they are trapped in the solid amorphous part, they can undergo secondary crystallization.

The variation of CUCES in the melt phase, as crystallization time increases, determines the variation of spherulitic growth rate with time. Because, in a chain, ethylene sequences are connected, only a group of contiguous UCES can form a large loop and diffuse from the solid phase into the melt phase, i.e., those UCES are untrapped. If UCES are directly attached to crystallized CES, they cannot diffuse, but they are trapped between crystalline lamellae as the solid amorphous part. Therefore, diffusion depends on the probability of appearance of the contiguous UCES. When the crystallization temperature increases, this probability increases. As the crystallization time increases, the CUCES in the melt phase increases, because the amount of untrapped UCES increases. Therefore, the crystalline spherulitic growth rate decreases, and non-linear growth behavior is observed.

The regime transition temperatures can be determined by employing an analysis based on Eq.(6-1). In regime III, the degree of supercooling is high, and the CUCES is low. During the crystallization process, the UCES form small folds, which are fixed in the solidified amorphous part. Thus, the CUCES is constant in the melt phase. Therefore, the spherulitic growth rate is constant, and linear growth behavior is observed.

In regime II, a number of ethylene sequences are not long enough to crystallize. The probability that a group of contiguous UCES are untrapped from the solid phase increases. Thus, non-linear growth behavior may be observed in regime II. As the crystallization temperature increases, this probability increases, thus, non-linear growth behavior becomes more obvious.

In regime IM, the probability that a group of contiguous UCES are untrapped from the solid phase is higher than in regime II. As the amount of amorphous part untrapped from the solid phase and diffuses into melt phase increases, the spherulitic morphology in the solid phase becomes less stable. Therefore, the crystalline spherulitic morphology deteriorates, and irregular crystalline structure could appear. Figure 6-2 shows that while the regular spherulitic morphology is obtained in regimes III and II (Figure 6-2(a)), the crystalline morphology in regime IM is irregular (Figure 6-2(b)). Because the CUCES in the melt phase in regime IM increases faster than that in regime II, the non-linear growth behavior is more obvious in regime IM.

Therefore, in the different regimes, because of the variation of the CUCES in the melt phase, the crystalline growth behavior and morphological characteristics are different.

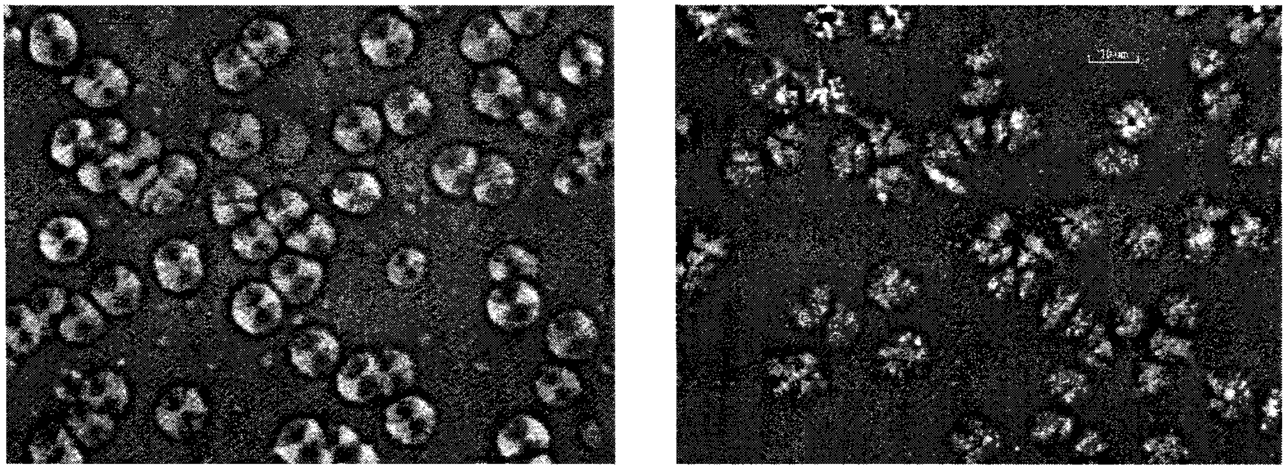
(a) 90°C (regime III) (b) 101°C (regime IM)

Figure 6-2 Regular and irregular spherulitic morphologies in regimes III and IM for rein I

6.3.2 Diffusion layer

As discussed above, the concentration of crystallizable ethylene sequences (CCES) in the melt phase decreases with time during isothermal experiments in regimes II and IM, because uncrystallizable ethylene sequences (UCES) are untrapped from the solid. If the untrapped UCES cannot diffuse immediately into the melt phase, a diffusion layer appears. If a diffusion layer exists in a crystallizing system, three phases may co-exist, i.e., solid (spherulite), melt, and diffusion layer (between spherulite and melt). The diffusion layer is part of the melt phase. It is the result of delay of UCES diffusion, and it hinders the free diffusion of ethylene sequences. The CCES is lower than that in the melt phase. The CCES increases along the direction from the diffusion layer/solid interface to the melt. As t_{1c} increases, the thickness of the layer increases, and the spherulitic growth rate decreases gradually to zero. Because it is difficult to measure the distribution of the CCES (or SCBC) in the diffusion layer, it is also difficult to provide quantitative description of the crystallization kinetics.

If the untrapped UCES can diffuse immediately into the melt phase, the diffusion layer does not exist. However, the CCES in the melt phase decreases with crystallization time. Non-linear growth behavior can be observed. Also, it is easier to describe the growth crystallization kinetics, quantitatively.

The diffusion layer for LLDPEs depends on the crystallization temperature and material structural parameters, such as short chain branching. The thickness of the diffusion layer depends on the amount of UCES that has to diffuse through it and the diffusion rate of UCES. As the amount of UCES increases and the diffusion rate decreases, the thickness of the diffusion layer increases.

6.3.2.1 Effect of T_{1c}

The thickness of the diffusion layer is sensitive to the 1st step crystallization temperature, T_{1c}. The crystallization temperature has two effects on the thickness of the diffusion layer. As T_{1c} decreases, the CUCES decreases. Thus, the amount of UCES that has to diffuse through the diffusion layer at T_{1c} decreases. So, the thickness of the diffusion layer tends to decrease, as T_{1c} decreases. However, because the diffusion rate also decreases as T_{1c} decreases, the thickness of the diffusion layer could increase. Under the experimental conditions employed, the effect of the diffusion rate on the thickness of the diffusion layer seems to be somewhat weaker than the effect of CUCES. As the crystallization temperature decreases, the thickness of the diffusion layer seems to decrease or disappear.

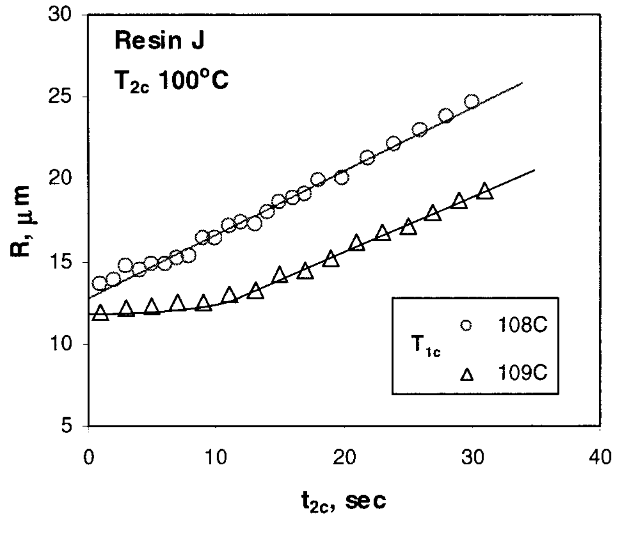

Figure 6-3 The growth of 1st kind of spherulites from different T_{1c} for resin J T_{2c} = 100°C, t_{1c} = 2 hrs, and t_{2c} starts to count when T_c reaches T_{2c}.

The diffusion layer can be identified from the slope change in the plot of spherulitic radius vs. the crystallization time, during the 2nd crystallization step, as shown in Figure 6-3. Figure 6-3 shows that the diffusion layer for resin J is clearly observed for T_{1c} 109°C, while it is not observed for T_{1c} 108°C. The development of a diffusion layer at T_{1c} = 109°C causes the initial growth rate to be low and to rise slowly to the steady level associated with T_{2c}.

The low slope, in the early crystallization region at T_{2c}, could be due to a delay in reaching the crystallization temperature (T_{2c}). Figure 6-4 shows that the observed behavior is not caused by this effect. When T_c is lowered to T_{2c}, some new nucleated spherulites appear. The growth processes of old (nucleated at T_{1c}) and new (nucleated at T_{2c}) spherulites are shown in Figure 6-4. The new spherulites show the same linear growth slope at T_{2c} during the whole spherulitic growth process as the slope exhibited by the old spherulites during the late stage of crystallization. No low slopes were observed during the early crystallization stage at T_{2c} for the new spherulites. Thus, the low slope during the early stage of crystallization of the old spherulites at T_{2c} is due to diffusion layer effect.

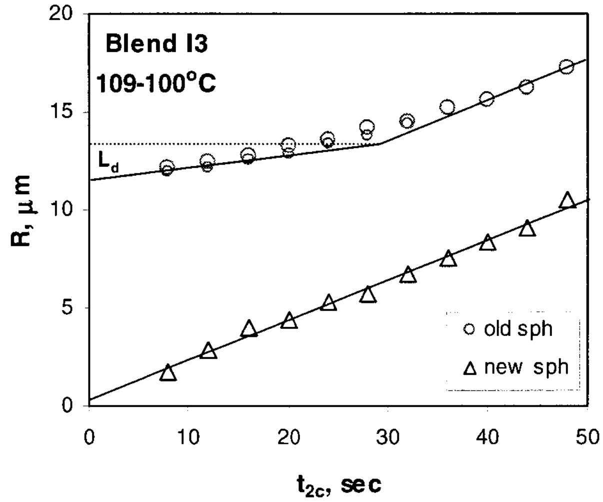

Figure 6-4 The growth processes of old and new spherulites at T_{2c} for Blend I3 T_{1c} = 109°C in regime II, T_{2c} = 100°C in regime III and t_{1c} = 2 hrs for 2-step experiments, t_{2c} starts to count when T_c reaches T_{2c}.

The above results show that m-LLDPE resin and m-LLDPE blends produce a diffusion layer in the high crystallization temperature range in regime II. On the other hand, ZN-LLDPE resin H shows that the diffusion layer seems to be negligible, even if T_{1c} is as high as the highest isothermal experimental temperature, 120°C (in regime IM), as shown in Figure 6-5.

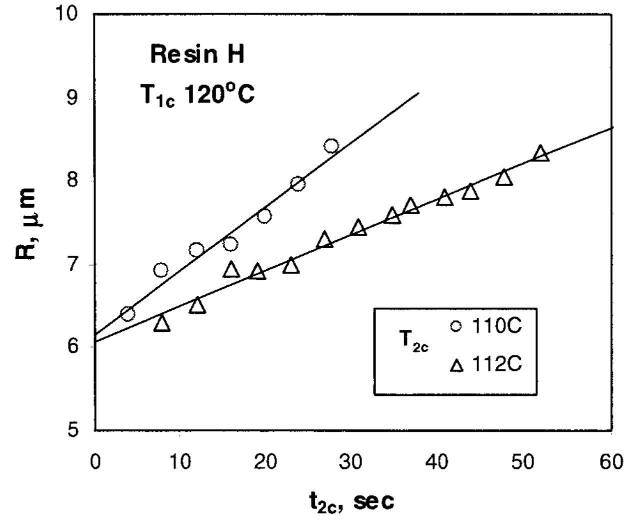

Figure 6-5 The spherulitic growth process at T_{2c} for ZN-LLDPE resin H T_{1c} = 120°C in regime IM, T_{2c} = 110 and 112°C in regime III and t_{1c} = 1 hr for 2-step experiments, t_{2c} starts to count when T_c reaches T_{2c}.

6.3.2.2 Effect of SCBC

When the crystallization temperature is higher than a certain value, the diffusion layer becomes important. The effective thickness of the diffusion layer, L_d, may be estimated from the radius growth distance that is influenced by the diffusion layer (i.e., during which growth occurs at the lower rate). Thus, L_d is obtained from the radial growth distance measured at the intersection of two growth lines for old spherulites, as indicated in Figure 6-4. Figure 6-6 shows that, for different resins, under the same crystallization conditions, L_d increases, as the short chain branching content (SCBC) increases. As SCBC or short chain branching degree (D_{branch}) increases, the average size of ethylene sequences between two comonomers decreases; thus, the amount of UCES increases, and L_d increases.

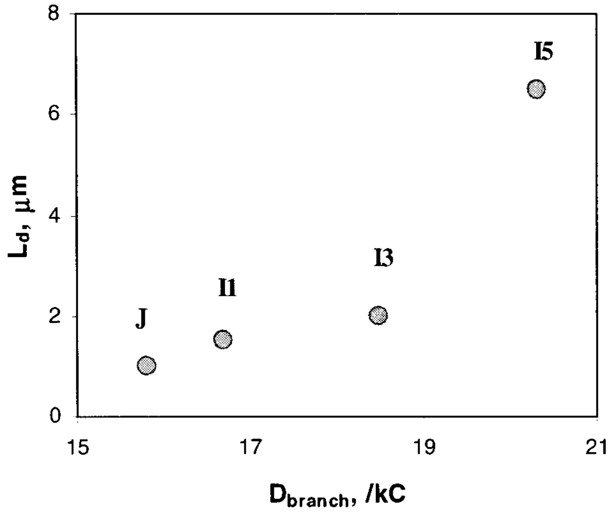

Figure 6-6 The thickness of diffusion layer for different resins
T_{1c} = 109°C in regime II, T_{2c} = 100°C in regime III and t_{1c} = 2 hrs for 2-step experiments.

6.3.3 Crystallization kinetics in non-linear crystallization processes

According to the above discussion, when the crystallization temperature is lower than a certain value, the diffusion layer can be neglected. Under such conditions, the concentration of UCES (CUCES) in the whole melt phase is uniform. Thus, Eq.(6-1) may be used to evaluate the spherulitic growth kinetics during the linear stage of T_{1c}.[5] The same approach is employed in this study to analyze the growth rate, G_2, in the 2nd crystallization step at T_{2c}. The required parameters for the LLDPE systems employed are specified as follows: T_m^0 = 145.5°C,[18] Q_D^* = 24 kJ/mol,[19] b_0 = 0.415 nm, ΔH_u = 8.106 kJ/mol (CH_2CH_2), and σ = 11.8m J/m^2.[2]

6.3.3.1 Spherulitic growth rate in the 2nd crystallization step, G_2

The diffusion layer is not important for resin J at T_{1c} = 108°C, since the diffusion layer is not observed when the crystallization temperature is lowered to T_{2c} (100 or 104°C),. Plots of spherulitic radius vs. the 2nd step crystallization time are shown in Figure 6-7. The spherulitic growth behavior in the 2nd crystallization step remains linear. So, after the 1st crystallization step, the growth behavior is still in regime III under the experimental conditions employed.

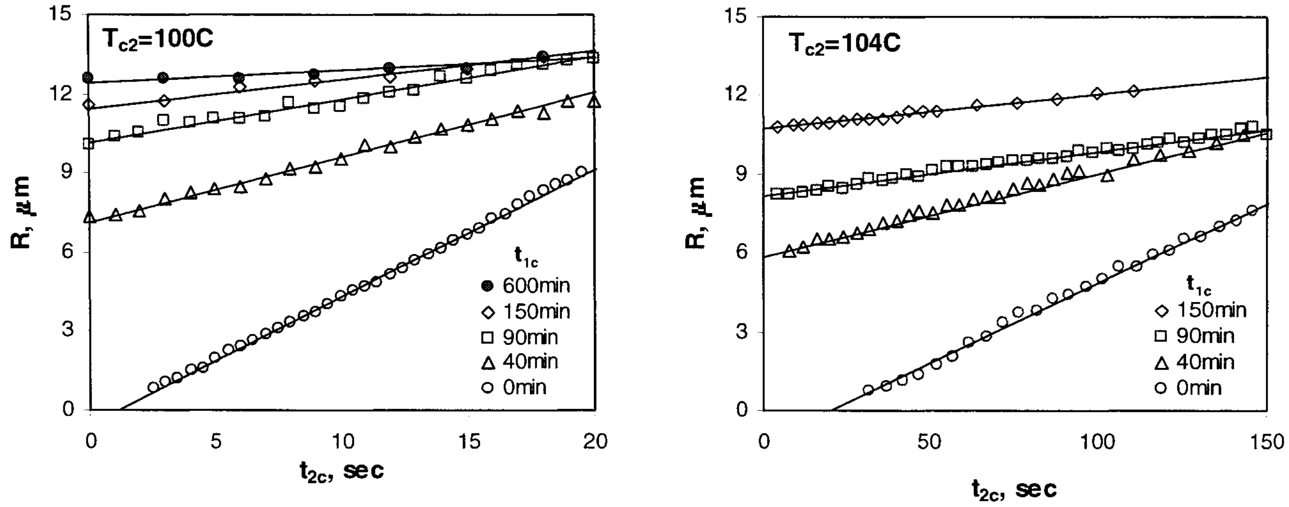

(a) T_{2c} =100°C (b) T_{2c} =104°C

Figure 6-7 The linear growth behavior in isothermal crystallization after different t_{1c} at T_{1c} 108°C for resin J

The plots of G_2 vs. the crystallization time at T_{1c}, t_{1c}, are shown in Figure 6-8 for resin J at T_{1c} = 108°C. The results for T_{2c} (100 and 104°C) are shown, respectively, in Figure 6-8(a) and Figure 6-8(b). G_2 depends strongly on t_{1c}. As t_{1c} increases, G_2 decreases, following a sigmoid curve. G_2 decreases slowly, for t_{1c} less than 20 minutes, then it decreases rapidly between 20 and 100 mins, and it decreases slowly at longer times, possibly approaching a constant value. For comparison, the one-step isothermal experimental results at 108°C are also shown in Figure 6-8(c). The growth rates were calculated from the derivative of the curve of radius vs. time. The spherulitic growth rate decreases, as the crystallization time increases, due to the non-linear growth behavior.

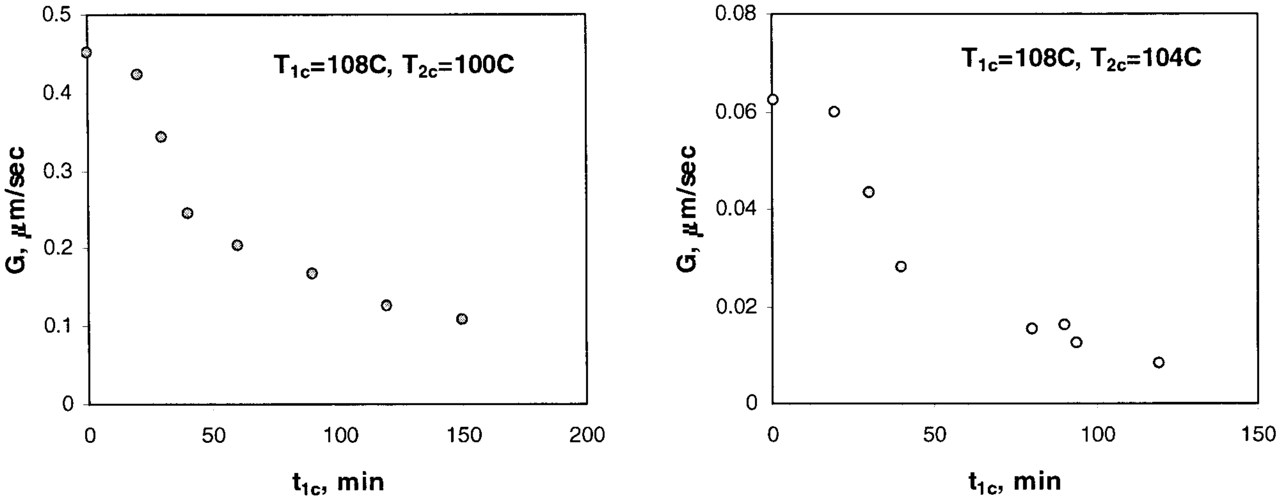

(a) T_{2c} 100°C (b) T_{2c} 104°C

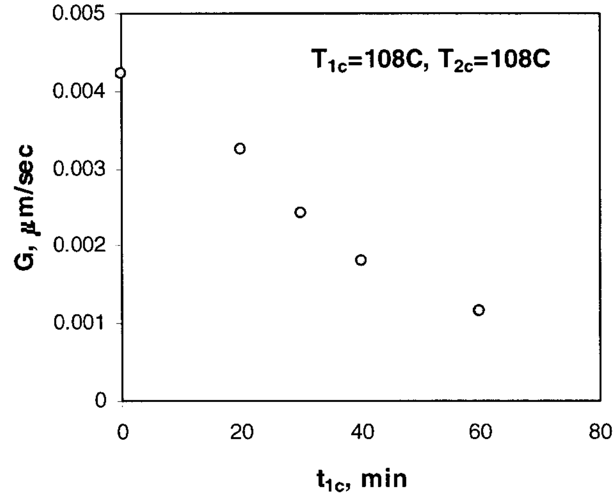

(c) T_{2c} 108°C (1-step isothermal experiment)

Figure 6-8 G_{2c} vs. t_{1c} for resin J

T_{1c}, is 108°C; T_{2c} are 100, 104, and 108°C, respectively.

6.3.3.2 Time dependence of $T_m^{C,n*}$

During the non-linear crystallization process, the concentration of crystallizable ethylene sequences (CCES) in the melt phase decreases with time, because the comonomer content or the short chain branching content (SCBC) in the melt phase increases. Therefore, the melting temperature T_m^{C,n^*} of the crystal stem with the maximum possible length (n^*) decreases, as t_{1c} increases. T_m^{C,n^*} in the melt phase and G_2 depend on t_{1c} at a specific T_{1c}. The values of T_m^{C,n^*} at different t_{1c} may be calculated, if the basal surface free energy is considered to be independent of the crystallization process ($\sigma_e = 5.2$ kJ/mol of m.s.u. for resin J[5]). This is possible by employing Eq.(6-1) to analyze plots of $\ln G + Q_D^*/RT_c$ vs. $1/(T_c\Delta Tf)$ and G_2. The results are shown in Figure 6-9.

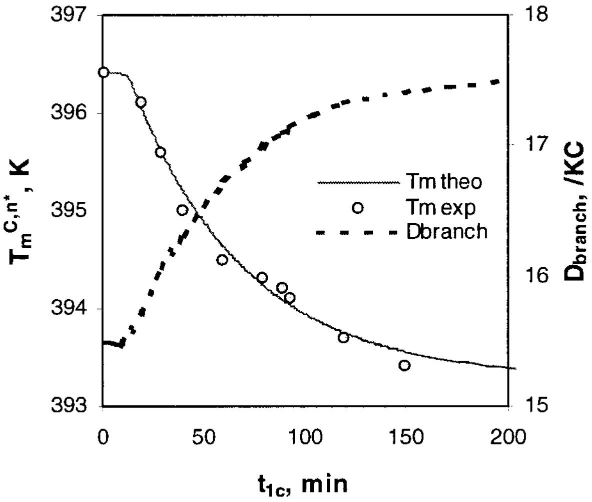

Figure 6-9 T_m^{C,n^*} and D_{branch} (SCBC) vs. t_{1c} at 108°C for resin J

Dots: experimental data; Solid curve: the five-parameter sigmoid equation, $(T_m^{C,n^*})^\infty$ = 393.3K, $a = 3.12$, $b = 0.96$, $c = 0.017$, $t_0 = 12.8$ min, and $R^2 = 0.985$.

Figure 6-9 shows that, as t_{1c} increases, T_m^{C,n^*} decreases slowly initially, then it decreases rapidly in the middle region, and finally it decreases slowly again. An empirical five-parameter sigmoid equation is proposed to fit the experimental values of T_m^{C,n^*} under the experimental conditions employed in this study:

$$T_m^{C,n^*} = \left(T_m^{C,n^*}\right)^\infty + \frac{a}{\left(1+\exp\left(\frac{t-t_0}{b}\right)\right)^c} \qquad (6\text{-}5)$$

where $(T_m^{C,n*})^\infty$, a, b, c and t_0 are empirical constants that depend on material and processing history. $(T_m^{C,n*})^\infty$ is the value of $T_m^{C,n*}$, as t_{1c} approaches infinity. It depends on T_{1c} and the molecular structure. If the basal surface free energy is considered to be constant, the SCBC in the melt phase at different t_{1c} can also be calculated according to Eq.(6-4). The results are also shown in Figure 6-9, indicating the number of branches per 1000 backbone carbons, D_{branch}. The dependence of SCBC in the melt phase on t_{1c} is almost the inverse of the dependence of $T_m^{C,n*}$ on t_{1c}. When t_{1c} is less than 20 mins, the diffusion effect is very small. The CUCES or SCBC in the melt phase increases slowly, because the amount of untrapped UCES is small. Also, $T_m^{C,n*}$ decreases slowly. As more untrapped UCES diffuse into the melt phase, the SCBC increases rapidly. Also, $T_m^{C,n*}$ decreases rapidly. After the CUCES or SCBC increases to a certain value, the concentration of crystallizable ethylene sequences (CCES) is so small that diffusion of CES to the crystal surface becomes limited. At long crystallization times, the CUCES or SCBC approaches a constant value, $D_{branch} = 17.66$ per 1000 backbone carbons, under the experimental conditions employed. $T_m^{C,n*}$ also approaches a constant value, $(T_m^{C,n*})^\infty$. $(T_m^{C,n*})^\infty = 120.1^\circ C$ (393.3K), at $T_{1c} = 108^\circ C$ for resin J.

The above discussion has dealt mainly with homogeneous LLDPE (m-LLDPE resin J). Similar results were obtained for heterogeneous LLDPE. The parameters of Eq.(6-5) for ZN-LLDPE resin H at T_{1c} =118 and 120°C (regime IM) are listed in Table 6-2.

Table 6-2 Some temperature characteristics and parameters of the empirical equation for m-LLDPE resin J and ZN-LLDPE resin H

Material	$T_m^{C,n*}$ (°C)	T_{cf} (°C)	$T_m^{C,n*}-T_{cf}$	T_{1c} (°C)	$(T_m^{C,n*})^\infty$ (°C)	$(T_m^{C,n*})^\infty-T_{1c}$	a	b	c	t_0 (min)
J (I0)	123.2	111.0	12.2	108.0	120.1	12.1	3.12	0.96	0.0017	12.8
H	127.8	120.0	7.8	118.0	125.8	7.8	7.85	7.00	0.0017	38.0
H	127.8	120.0	7.8	120.0	127.8	7.8	5.50	7.00	0.0017	50.0

T_{cf} is the highest isothermal experimental crystallization temperature.[5]

Parameter c was found to be the same (0.0017) for all the conditions in Table 6-2. It seems to be independent of resin type and T_{1c}. Parameter b is the same for resin H at different T_{1c},. However, it is much higher than that for resin J. A high value of a is associated with low T_{1c}, as indicated by the results for resin H at different T_{1c}.

Resin J did not exhibit any solid phase during one-step isothermal experiments at T_c higher than 111°C.[5] This temperature is considered to be the highest isothermal experimental crystallization temperature, T_{cf}. The corresponding degree of supercooling is 12.2. For a non-linear isothermal growth process at T_{1c}, it is possible to estimate $\left(T_m^{C,n^*}\right)_{T_{1c}}^{\infty}$, as indicated above. Table 6-2 suggests that $\left[\left(T_m^{C,n^*}\right)_{T_{1c}}^{\infty} - T_{1c}\right]$ is equal to the degree of supercooling at T_{cf} (i.e., $\left|T_m^{C,n^*} - T_{cf}\right|$). This observation appears to be valid under three conditions reported in Table 6-2.

6.3.3.3 Crystallization kinetics

Eq.(6-1) may be used to evaluate the spherulitic growth kinetics, when the growth behavior is non-linear at high crystallization temperatures. This requires knowledge of the variation of T_m^{C,n^*} with time, according to Eq.(6-5). Figure 6-10 shows the analysis results at three different T_{2c} (100, 104 and 108°C), For $T_{1c} = 108$°C for m-LLDPE resin J. Figure 6-11 shows the analysis results at different T_{2c}, and different T_{1c} (118 and 120°C) for ZN-LLDPE resin H. In order to demonstrate explicitly the influence of the variability of T_m^{C,n^*} with t_{1c}, the x-axis in these figures is defined as $T_m^{C,n^*}/(T_c \Delta T f)$.

Figure 6-10 and Figure 6-11 show that the crystallization kinetics of non-linear isothermal spherulitic growth are in good agreement with the MHL theoretical curves, which were based on the one-step isothermal crystallization behavior in the linear growth stage.[5] This supports the validity of Eq.(6-1) to describe the non-linear spherulitic crystallization kinetics with time dependence, by consideration of T_m^{C,n^*} as a function of t_{1c}. The above conclusion is valid only when the diffusion layer between the solid and melt phases is negligible.

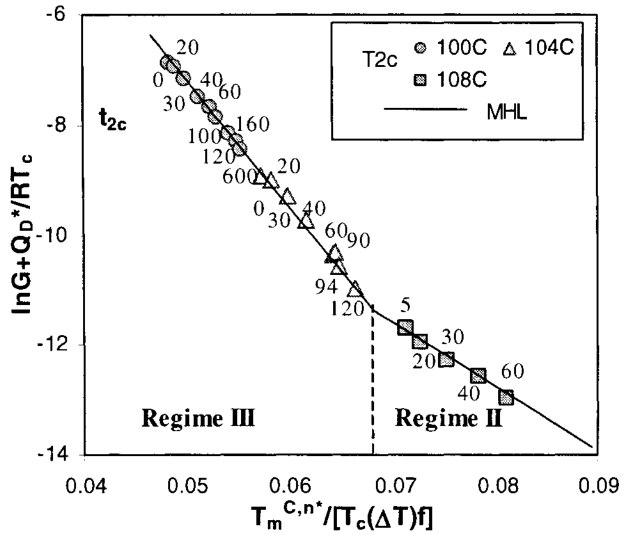

Figure 6-10 The application of the MHL equation to the crystallization kinetics of non-linear spherulitic growth for resin J

T_{1c} = 108°C, T_{2c} = 100, 104, and 108°C as indicated, t_{1c} is marked near each point in minutes for the 2nd step crystallization processes.

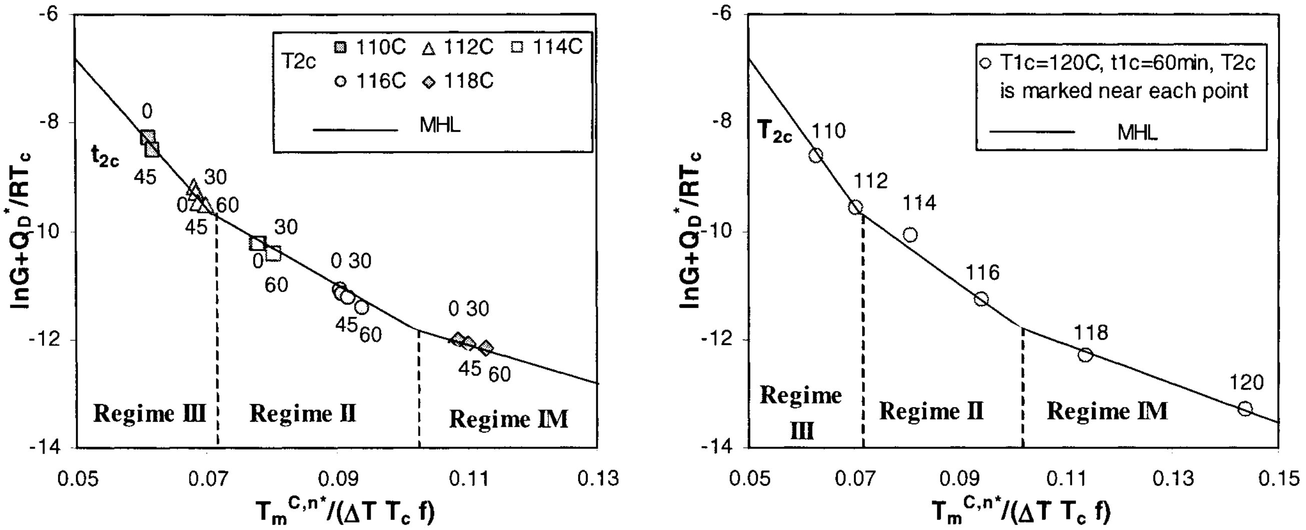

(a) T_{1c}=118°C and different t_{1c}, and different T_{2c} (b) T_{1c} =120°C and t_{1c} =60min, and different T_{2c}

Figure 6-11 The application of the MHL equation to the crystallization kinetics of non-linear spherulitic growth for resin H

Figure 6-10 shows that during the 2nd step (T_{2c} = 100 and 104°C), the spherulitic growth remains linear (Figure 6-7) and continues to be in regime III, while crystallization growth at 108°C follows regime II behavior. Figure 6-11 shows a similar pattern. If the values of T_{2c} are in regime IM (118°C), regime II (114 and 116°C), or regime III (110 and 112°C), the crystallization behavior remains in these respective regimes as in isothermal experiments. Therefore, the 1st step crystallization process does not seem to change the MHL regime for the second crystallization temperature.

6.4 Conclusions

The modified Hoffman-Lauritzen (MHL) equation indicates that non-linear spherulitic growth behavior occurs in regimes II and IM for LLDPEs. During non-linear growth processes, the concentration of uncrystallizable ethylene sequences (CUCES) in the melt phase increases with time. The diffusion layer plays an important role at high crystallization temperatures and in polymers with high short chain branching content (SCBC).

When the diffusion layer is not important, the crystallization kinetics can be described by the MHL expression. This is true for both one-step and two-step crystallization processes. As t_{1c} increases, the spherulitic growth rate decreases. This is due to the reduction of crystallizable ethylene sequences (CES) in the melt phase, which leads to a lowering of the melting temperature of the crystal stem with the maximum possible length, $T_m^{C,n*}$, in the melt phase. An empirical equation is proposed to describe the evolution of $T_m^{C,n*}$ in the non-linear growth region.

6.5 References

1 Hoffman JD, Davis GT, Lauritzen JI. In: Hannay NB. Editor, Treatise on Solid State Chemistry, Vol. 3, New York: Plenum Press, 1976 (Chapter 7).

2 Hoffman JD, Miller RL. Polymer 1997, 38:3151.

3 Phillips PJ. Polym Prepr (Am Chem Soc Div Polym Chem) 1979, 20:483.

4 Kamal MR, Feng L, Huang T. Can J Chem Eng 2002, 80: 432.

5 Feng L, Kamal MR. Polym Eng Sci 2004, accepted for publication (see Chapter 5 in this thesis).

6 Keith HD, Padden FJ. Jr. J Appl Phys 1964, 35:1286.

7 Okada T, Saito H, Inoue T. Macromolecules 1990, 23:3865.

8 Okada T, Saito H, Inoue T. Polymer 1993, 34:4752.

9 Okada T, Saito H, Inoue T. Polymer 1994:35:5699.

10 Wu L, Lisowski M, Talibuddin S, Runt J. Macromolecules 1999, 32:1576.

11 Saito H, Okada T, Hamane T, Inoue T. Macromolecules 1991, 24:4446.

12 Lambert WS, Phillips PJ. Macromolecules 1994, 27:3537.

13 Rodriguez-Arnold J, Bu Z, Cheng SZD, Hsieh ET, Johnson TW, Geerts RG, Palackal SJ, Hawley GR, Welch MB. Polymer 1994 35:5194.

14 Abo el Maaty MI, Hosier IL, Bassett DC. Macromolecules 1998, 31:153.

15 Abo el Maaty MI, Bassett DC, Olley RH, Jääskeläinen P. Macromolecules 1998, 31:7800.

16 Feng L, Kamal MR. Can J Chem Eng 2004, accepted for publication (see Chapter 3 in this thesis).

17 Alamo RG, Mandelkern L. Thermochim Acta 1994, 238:155.

18 Mandelkern L, Alamo RG. In: Mark JE. Editor, Physical Properties of Polymers Handbook, American Institute of Physics, New York: Woodbury, 1996 (Chapter11).

19 Fletcher DP, Klein J. Polym Commun 1985, 26:2.

Chapter 7

7 Crystallization and Melting Behavior of Linear Low-density Polyethylene Resins

The crystallization behavior of homogeneous and heterogeneous linear low-density polyethylenes (LLDPE) was investigated by evaluating the characteristics of melting traces obtained by differential scanning calorimetry (DSC). Based on the isothermal experimental results, the concept of the effective nucleation induction time is suggested. In the initial crystallization stage, the Avrami equation in conjunction with the effective induction time can be used to successfully describe the overall crystallization kinetics. Avrami exponents are 2, 1.5, and 1 were found to apply in regimes III, II, and IM, respectively, as identified by the modified Hoffman-Lauritzen (MHL) equation. The kinetic parameters estimated from evaluating the linear crystallization behavior during spherulitic growth experiments analysis using polarized light microscopy (PLM) are in agreement with the overall crystallization kinetic parameters obtained from DSC experiments.

7.1 Introduction

Polymer molecular structural characteristics and processing conditions have significant effects on the crystallization behavior of semicrystalline polymers, linear low-density polyethylene (LLDPE) has complex molecular structural characteristics, reflected by molecular weight and short chain branching characteristics. Basically, there are two types of LLDPE, which depend on the catalysts used, i.e., homogeneous LLDPEs with metallocene catalyst (m-LLDPE), and heterogeneous LLDPEs with Ziegler-Natta catalyst (ZN-LLDPE). Various studies have been reported regarding the behavior of m-LLDPEs,[1,2,3,4] ZN-LLDPE,[5,6,7] and their blends.[8] Moreover, a generalized melting temperature equation was proposed for random copolymers with excluded comonomers, and applied it to homogeneous LLDPEs.[9] Subsequently, it was extended and applied to heterogeneous LLDPE copolymers.[10] The crystal size distribution[11] and the melting temperature distribution[12] were estimated from differential scanning calorimetry (DSC) melting traces for LLDPEs, and a method to determine the crystal size number distribution was proposed. It was observed that the effect of molecular weight is smaller than that due to short chain branching. When the molecular weight is high, its effect may be neglected,[9] and short chain branching is the dominant factor.[9,13]

In this paper, the crystallization behavior of homogeneous and heterogeneous LLDPEs is studied, from the melting traces obtained after different crystallization times, under isothermal crystallization conditions. The Avrami expression[14,15,16] is employed to analyze overall crystallization behavior from DSC traces in the initial isothermal crystallization stage (primary crystallization process). Finally, the results are compared with data regarding the linear crystallization behavior observed in from polarized light microscopy (PLM) experiments.[10]

7.2 Experimental

7.2.1 Materials

The LLDPE resins, employed in this study, were provided by Nova Chemicals Inc. (Calgary, Canada) in pellet form. They included two experimental m-LLDPEs (referred to as resins I and J), and one ZN-LLDPE (resin G). The comonomer in all the LLDPE resins is 1-octene. The material characteristics are listed in Table 7-1; Nova Chemicals Inc. provided the molecular structural parameters. The short chain branching contents (SCBC) were measured by nuclear magnetic resonance (NMR), and the number and weight average molecular weights, M_n and M_w, respectively, were measured by gel permeation chromatography (GPC). The short chain branching polydispersities were calculated from the traces of temperature rising elution fractionation (TREF). $T_{el,W}$ and $T_{el,N}$ are defined as the weight and number average elution temperatures, respectively. The melting temperature of the crystal stem with the maximum possible length n^*, T_m^{C,n^*}, the basal surface free energy, σ_e, the regime transition temperatures between regimes III and II, $T_{III\text{-}II}$, and between regimes II and IM, $T_{II\text{-}IM}$, were estimated from the modified Hoffman-Lauritzen secondary nucleation crystallization kinetics analysis for the LLDPEs under study.[9,10]

Table 7-1 Polymer characteristics

Resin	Type [a]	D_{Branch} (/1000C)	M_n (kg/mol)	M_w (kg/mol)	T_m^{C,n^*} (°C)	σ_e (J/mol)	$T_{el,W}/T_{el,N}$-1 ×100	$T_{II\text{-}IM}$ (°C)	$T_{III\text{-}II}$ (°C)
G	ZN	15.8	23.1	98.6	130.7	2730	5.42	122.0	116.5
J	m	15.8	38.2	70.2	123.2	5200	0.64	-	107.1
I7	mb (0.7 I wt)	22.1	25.1	58.1	120.1	3920	2.59	-	103.3
I	m	24.8	21.9	52.9	113.5	4660	1.78	100.8	93.9

a: ZN is ZN-LLDPE, and m is m-LLDPE, and mb is blend of m-LLDPE resins I and J

The m-LLDPE blends are intermolecular heterogeneous and intramolecular homogeneous. Their molecular characteristics estimated from those of pure m-LLDPEs.

One m-LLDPE Blend (blend I7) was selected for this study. It was prepared using a solvent method.[11] After resins I and J (7:3 weight ratio) were dissolved thoroughly and stirred in xylene (1%w/v) at 120°C for around 2 hour, the blend was immediately precipitated in a large amount of cold methanol. After filtering, the blend was dried under vacuum at about 50°C for more than one week. The molecular structural parameters were calculated based on those of pure resins.

7.2.2 Differential scanning calorimetry

Thermal analysis was performed in a Perkin-Elmer Pyris-1 differential scanning calorimetry (DSC) apparatus, with an ice bath. Calibrations were carried out for the lag, temperature, and heat of fusion before the experiments. The temperature and the heat of fusion were calibrated with pure indium (T_{onset} = 156.60°C, ΔH_f = 28.45 J/g). All DSC samples were compressed into 0.3 mm thick film at 180°C. The specimen weight varied from 4 to 8 mg. The specimens were placed in the aluminum pan and heated to 180°C, kept at this temperature for 10 min to remove thermal memory effects, and quenched to the specified temperatures at 60°C/min for isothermal experiments. After certain crystallization times, they were heated to 180°C at 10C°C/min. The contribution due to the effects of the aluminum pan on the DSC curves was subtracted from each measurement. All measurements were performed under nitrogen.

7.2.2.1 Nonisothermal stage in the initial isothermal process

The fast cooling rate could not be followed exactly under the experimental conditions employed, since the sample temperature lagged slightly behind the set program controlled temperature during the quenching process. Therefore, at the beginning of the isothermal stage, the isothermal condition could not be accurately attained. Figure 7-1 shows the heat flow rate, and temperature plotted against crystallization time. As can be seen, a stable crystallization temperature could not be achieved until 0.3 min, after which, the real isothermal crystallization time started. The corresponding heat flows showed high negative values, which are related to the effects of the heat capacity and perhaps the nonisothermal crystallization. The latter is more obvious at low crystallization temperatures. Because the initial point of the crystallization peak was overlapped by other information, some crystallization already appeared in blend I7 crystallized isothermally at 96°C, before the temperature reached the set isothermal crystallization temperature (see Figure 7-1). Therefore, in order to analyze the isothermal crystallization behavior accurately, the effects of the nonisothermal stage need to be removed. The delay time is about 0.3 min, under these experimental conditions; therefore, the experimental results before 0.3 min cannot directly be used in the analysis. At high crystallization temperatures, the delay time needs not be considered, because the normal nucleation induction time is of much larger duration. However, at low crystallization temperatures, delay time becomes significant and should be considered when the normal nucleation induction time is less than or about equal to the delay time, and non-isothermal crystallization has already taken place.

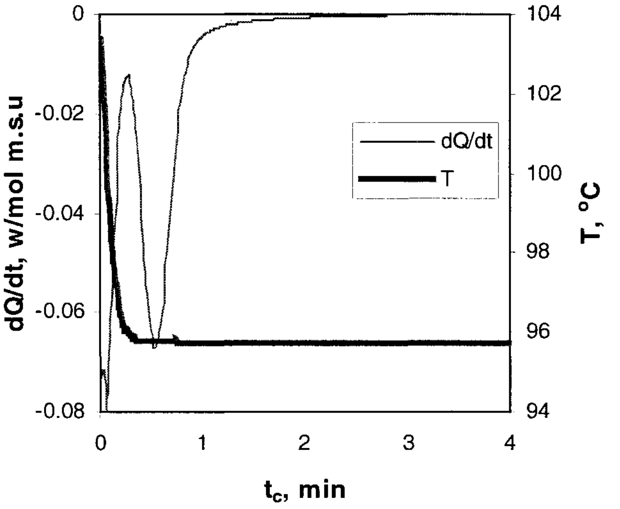

Figure 7-1 Isothermal crystallization curves after quenching from 180°C at 60°C/min for m-LLDPE blend I7 at 96°C.

7.3 Results and Discussion

7.3.1 Crystallization traces

Polymer crystallization is a complex process. Basically, it may include primary crystallization and secondary crystallization. Primary crystallization is a process in which molecular chains or segments (parts of a chain) are extracted from the melt phase and regularly arranged into the crystal phase. At the same time, polymer chains or segments are also possibly irregularly fixed among the crystals. Then, an amorphous phase also forms. Secondary crystallization refers to the rearrangement of irregular polymer chains or segments that are left in the amorphous phase into the crystals. It could be due to the perfection of original crystals, the length increase of original crystals, and the formation of new crystals.[17] Under the experimental conditions employed in this study, the perfection effect is relatively small, thus, secondary crystallization effects are mainly due to the length increase of old crystal and the formation of new crystals.

Three regimes can be clearly observed, by employing the modified Hoffman-Lauritzen (MHL) expression, under the experimental conditions employed.[10] These regimes will be referred to as III, II, and IM. In the following discussion, the crystallization and corresponding melting behavior of the three different types of LLDPE (m-LLDPE, m-LLDPE blend, and ZN-LLDPE) are evaluated. Because it takes extreme long time for DSC experiments in regime IM, only resin I is evaluated in this study.

7.3.1.1 Crystallization traces for different types of LLDPEs

The crystallization traces at the different temperatures are shown in Figure 7-2 for m-LLDPE resin I, Figure 7-3 for m-LLDPE resin J, Figure 7-4 for m-LLDPE blend I7, and Figure 7-5 for ZN-LLDPE resin G. The dots represent the points when the spherulites have finished their growth, in polarized light microscopy (PLM) experiments,[10] at the corresponding isothermal crystallization temperature. At that time, all spherulites in the field of view appear to impinge on each other. The crystallization traces for different types of LLDPEs exhibit various common features. In regimes III and II, only one crystallization minimum is observed for each individual crystallization trace. As the temperature increases, the crystallization trace becomes broad, and the crystallization time at the peak position, t_{p_DSC}, increases.

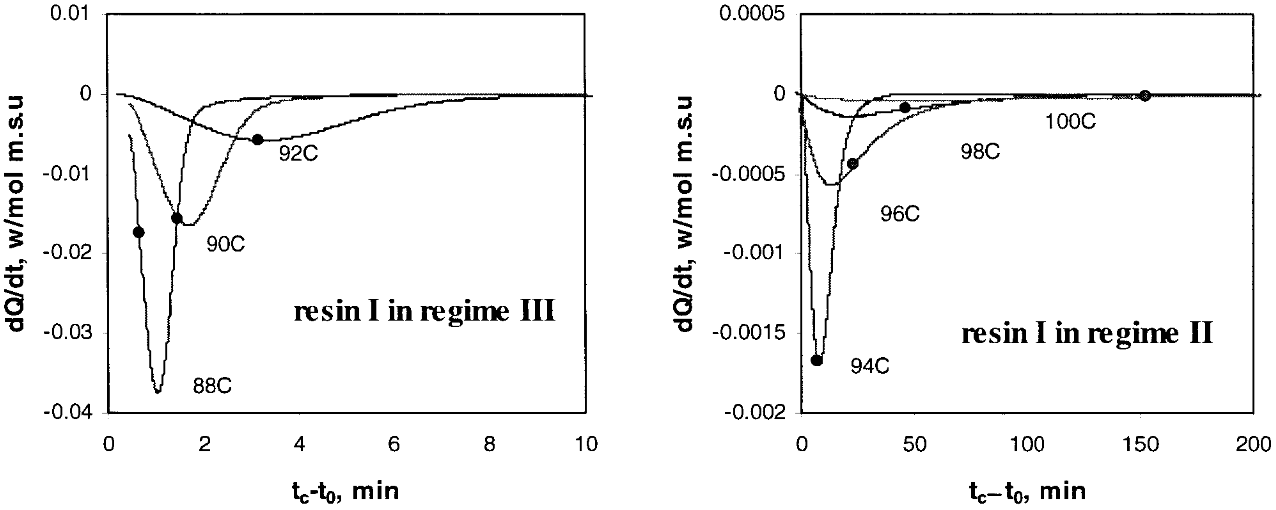

(a) regime III

(b) regime II

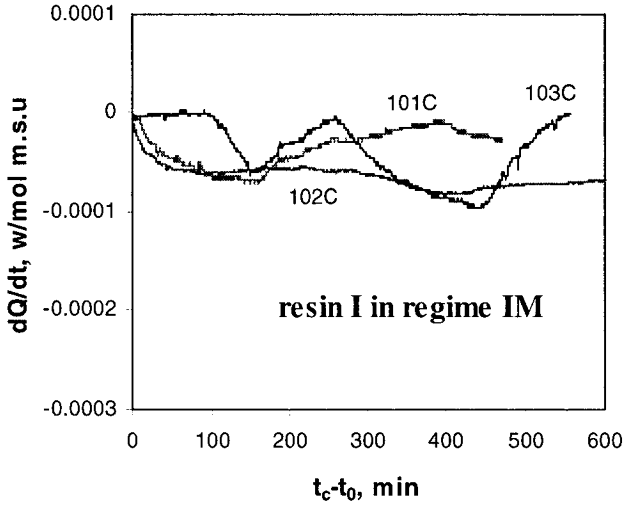

(c) regime IM

Figure 7-2 The crystallization traces at different temperatures for m-LLDPE resin I

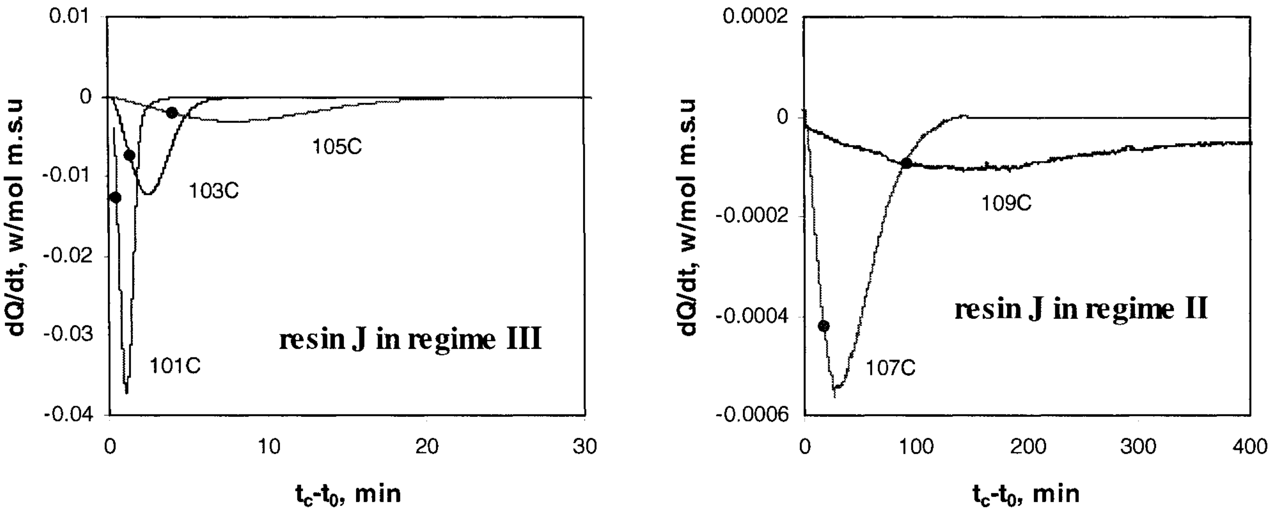

(a) regime III (b) regime II

Figure 7-3 The crystallization traces at different temperatures for m-LLDPE resin J

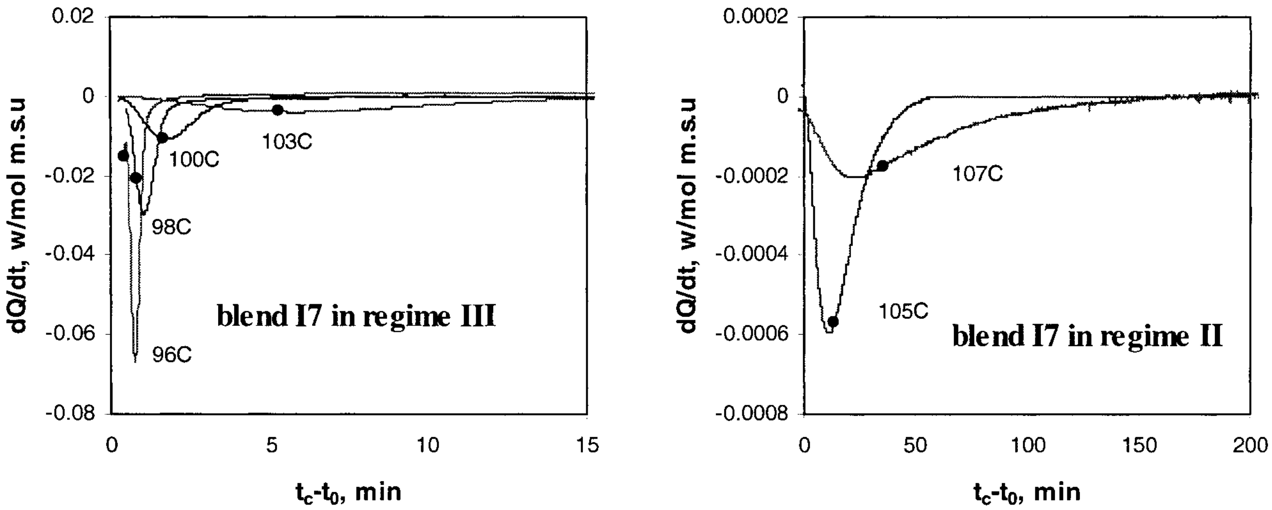

(a) regime III (b) regime II

Figure 7-4 The crystallization traces at different temperatures for m-LLDPE blend I7

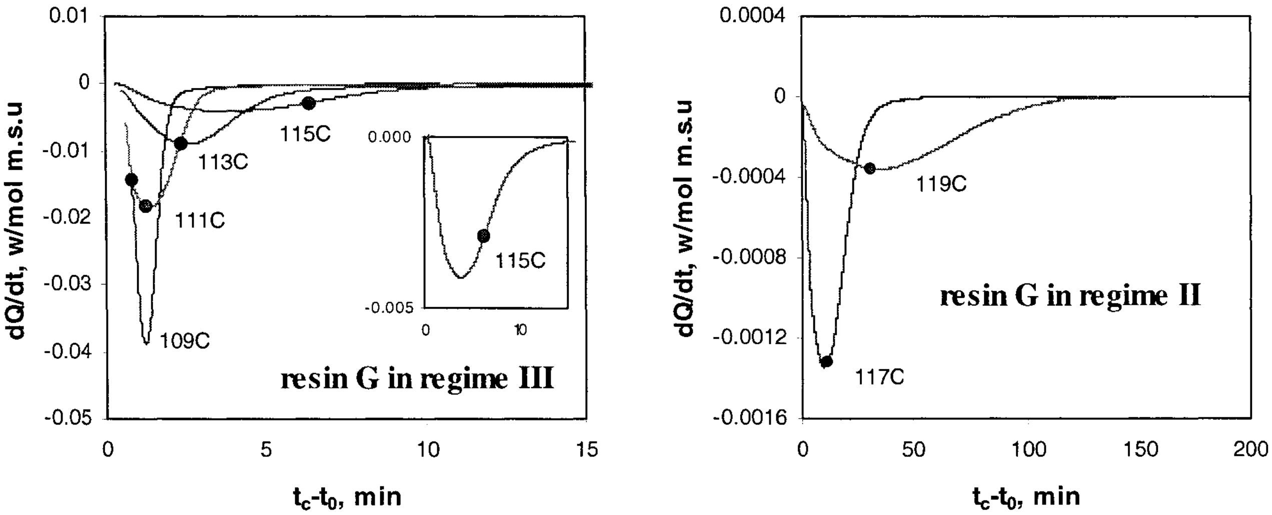

(a) regime III (b) regime II

Figure 7-5 The crystallization traces at different temperatures for ZN-LLDPE resin G

As shown in Figure 7-2(a) to Figure 7-5(a), in regime III, the crystallization curves are almost symmetrical about the peak positions. The m-LLDPEs curves for individual resins I, and J, and blend I7 have the highest symmetry, while that for ZN-LLDPE resin G has the lowest. A shoulder can be clearly seen on the left side of the crystallization trace for ZN-LLDPE, indicating that, as the short chain branching distribution (SCBD) broadens, the crystallization peak symmetry in regime III decreases.

In regime II, the crystallization curves are not symmetric, and a discernible tail appears in Figure 7-2(b) to Figure 7-5(b). As the temperature increases, the tail becomes longer.

In regime IM, the crystallization traces do not exhibit definite single-peak characteristics, as shown in Figure 7-2(c). It will be shown below that this behavior can be explained by changes in crystallization kinetics. Because the Avrami exponent in this regime is 1, crystallization peaks are not expected to appear; the explanation for this behavior is given in detail later in discussion. Another factor could be due to significant interference from experimental noise. Because the crystallinity, in this case, is very small, the signal for the heat flow is very weak. Thus, the crystallization curves oscillated, and system noise cannot be neglected.

7.3.1.2 Crystallization peak time and spherulitic growth time

The experimental results of polarized light microscopy,[10] provide data regarding spherulitic growth time, t_{fs_PLM}. The data are represented by the dots in the corresponding isothermal crystallization traces, shown previously in Figure 7-2 to Figure 7-5. During the complete crystallization process, the spherulites undergo various stages of development. When the crystallization time reaches a value t_{fs_PLM}, primary crystallization is completed. The remaining part of the crystallization peak after t_{fs_PLM}, is then due to secondary crystallization. This part of the crystallization curve is not small. Thus, secondary crystallization respects a significant part of the crystallization process.

In regime III, t_{fs_PLM} appears before the peak position, t_{p_DSC}, for all resins. Hence, most of the crystallization process occurs during secondary crystallization. In regime II, for m-LLDPE resin I and m-LLDPE blend I7, t_{fs_PLM} appears after t_{p_DSC}. Because the spherulites show non-linear growth behavior in this regime, the spherulitic growth rate decreases, as the crystallization time increases. It takes much more time to finish the primary crystallization process. For ZN-LLDPE resin G and m-LLDPE resin J, t_{fs_PLM} appears before t_{p_DSC}. This behavior could be due to their relatively low (15.8 /kC) short chain branching content (SCBC). The non-linear spherulitic growth behavior is not so obvious as for resin I and blend I7, which have higher SCBC values (24.8 /kC, and 22.1/kC, respectively).

Figure 7-6 shows a comparison between t_{fs_PLM} and t_{p_DSC} at different crystallization temperatures in regimes III and II for the different type of LLDPEs. Interestingly, for resin I and blend I7, the dependences of measured t_{fs_PLM} and t_{p_DSC} on the crystallization temperature can satisfactorily be represented by linear exponent characteristics, as shown in Figure 7-6(a) and Figure 7-6(b). Where the lines intersect is the transition temperature between regimes III and II. However, results for resins J and G, show a different behavior. For resin G, the dependence of t_{fs_PLM} and t_{p_DSC} on the crystallization temperature is approximately the same, but the data do not completely agree with the fitted exponent curves over all the range of temperatures considered (Figure 7-6(c)). For resin J, the distributions do not intersect, with t_{fs_PLM} always lower than t_{p_DSC} (Figure 7-6 (d)).

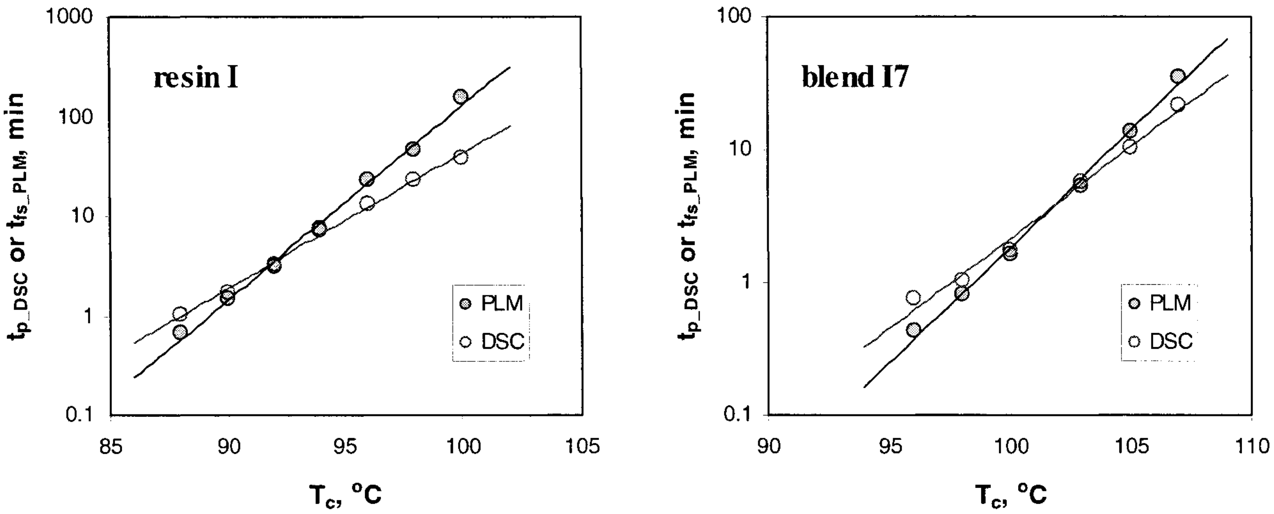

(a)) m-LLDPE resin I

(b)) m-LLDPE blend I7

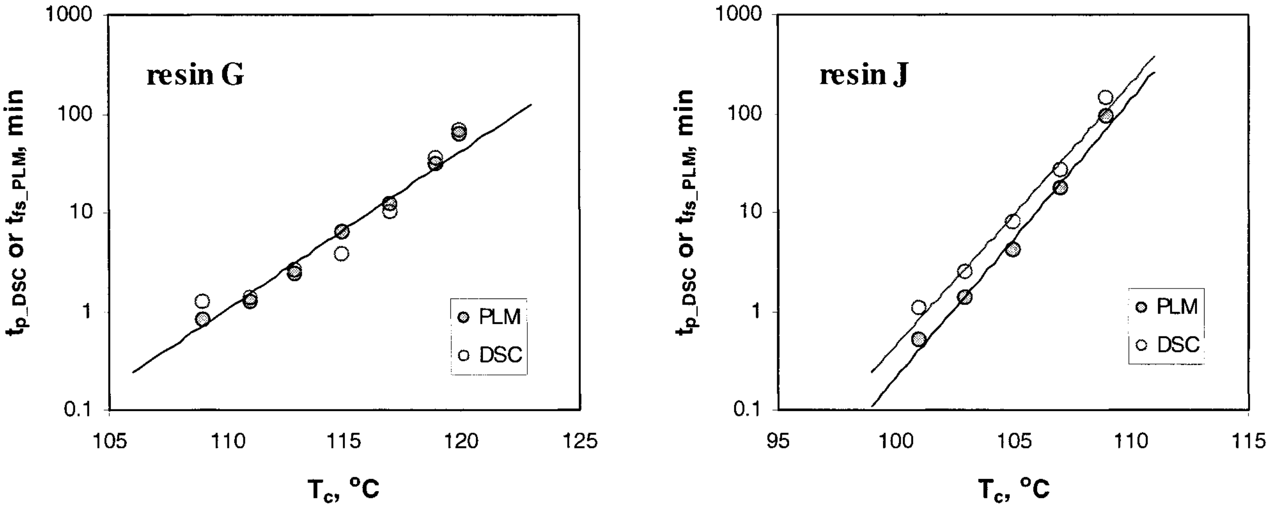

(c) ZN-LLDPE resin G

(d)) m-LLDPE resin J

Figure 7-6 Comparison of the crystallization peak time and the spherulite growth time Dots: experimental results, lines: exponent fitted curves.

7.3.2 Melting traces

For the isothermal crystallization process, several factors affect the initial crystallization curve, such as, the nonisothermal crystallization, heat capacity, and nucleation induction time. It is difficult, therefore, to estimate accurately the value of the crystallinity directly from the crystallization curve in the initial stage of the isothermal process, especially at low crystallization temperatures. In addition, heat flow is very weak, especially when the crystallization temperature is high (in regime IM), and system noise could be a major factor that cannot be neglected. As a result, it is difficult to obtain precise information directly from the crystallization curve. Alternatively, the melting curve is used to study the crystallization characteristics. The heat of fusion from the heating curve is calculated after a certain isothermal crystallization time, and this is assumed to be equal to the heat of fusion of the material crystallized during the previous crystallization experiment. In this case, the reorganization effects, such as melting-recystallization-remelting (MRR) and crystalline multiphase-transformation, are assumed to be small and are neglected.[11]

7.3.2.1 Melting traces in regime III

Typical results of the melting traces after different crystallization times in regime III are shown in Figure 7-7 for m-LLDPE (a) resin I at 90°C, and (b) resin J at 103°C; Figure 7-8 for m-LLDPE blend I7 at (a) 96°C, and (b) 98°C; and Figure 7-9 for ZN-LLDPE resin G at (a) 109°C, and (b) 113°C. The values of t_{fs_PLM}, and t_{p_DSC} were not corrected for nucleation induction time. Although only one peak appeared in the crystallization traces as shown earlier, multiple peaks were observed in the melting traces. Thus, at least two crystal populations with different size (distributions) coexist in the crystal phase.[11] Here, the multiple peaks are classified into two groups. The peaks in the high and low melting temperature ranges are called the H-peak and the L-peak, respectively, and their corresponding peak positions are called T_{mph} , and T_{mpl}, , respectively. For the different types of LLDPEs, the low temperature range only includes one L-peak, while the high temperature range could include two H-peaks, Figure 7-9 (a).

For all the LLDPEs, the melting traces show similar features, from the beginning of crystallization to full spherulite growth. Initially, only the H-peak is observed with no L-peak, as also observed in crystallization traces. As the crystallization times increase, the L-peak appears with increasing intensity, while the intensity of the H-peak also increases slowly. When the corresponding crystallization peak time is reached, the L-peak can be clearly observed. After this peak, the intensity of the H-peak increases very slowly, then, both the intensity of the L-peak heat flux and the L-peak temperature position keep increasing together, with the slowly rising H-peak.

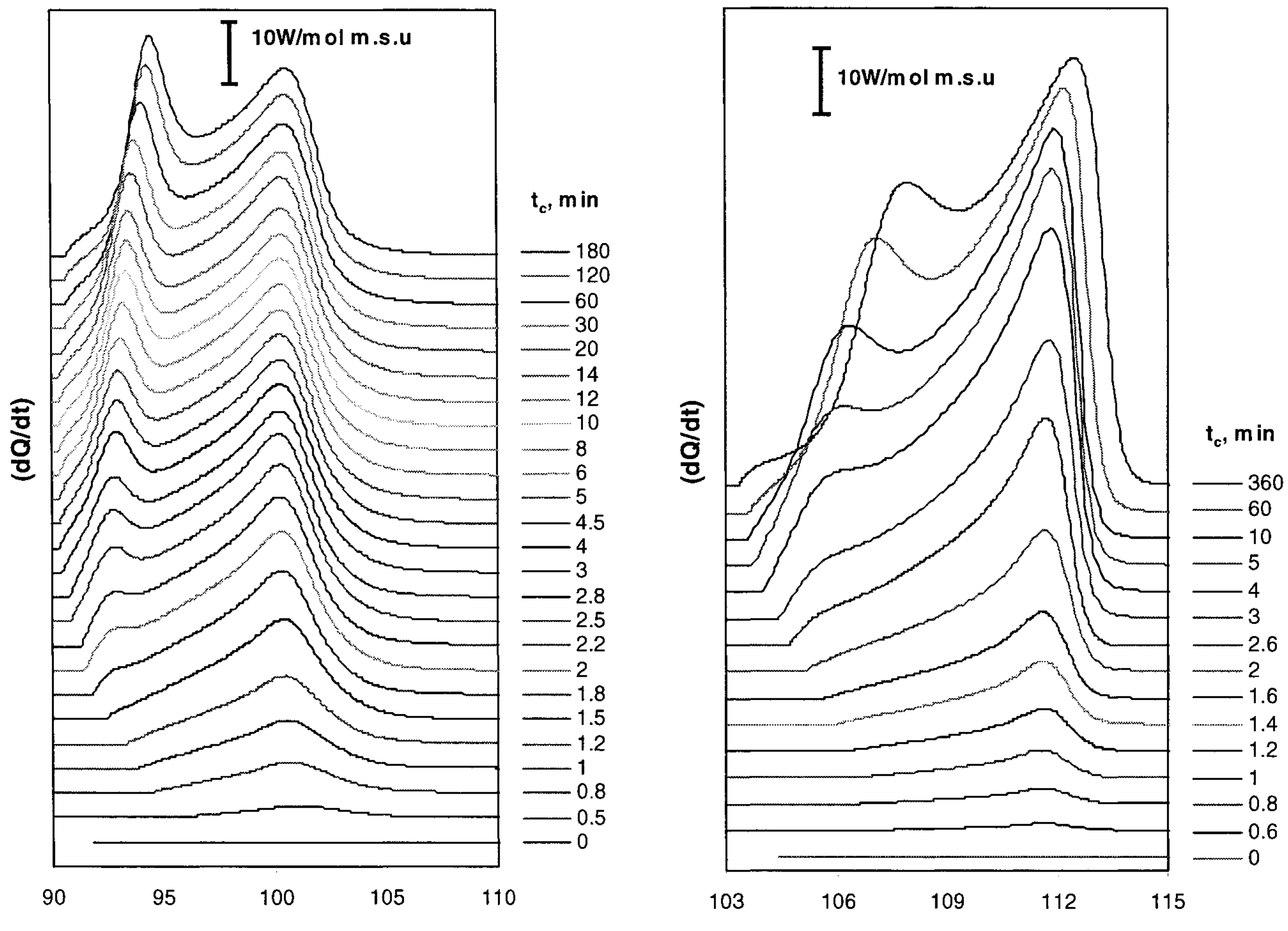

(a) resin I at 90°C
t_{fs_PLM} = 1.5min, t_{p_DSC} = 1.7min

(b) resin J at 103°C
t_{fs_PLM} = 1.3min, t_{p_DSC} = 2.5min

Figure 7-7 The melting traces after different crystallization times in regime III for m-LLDPEs

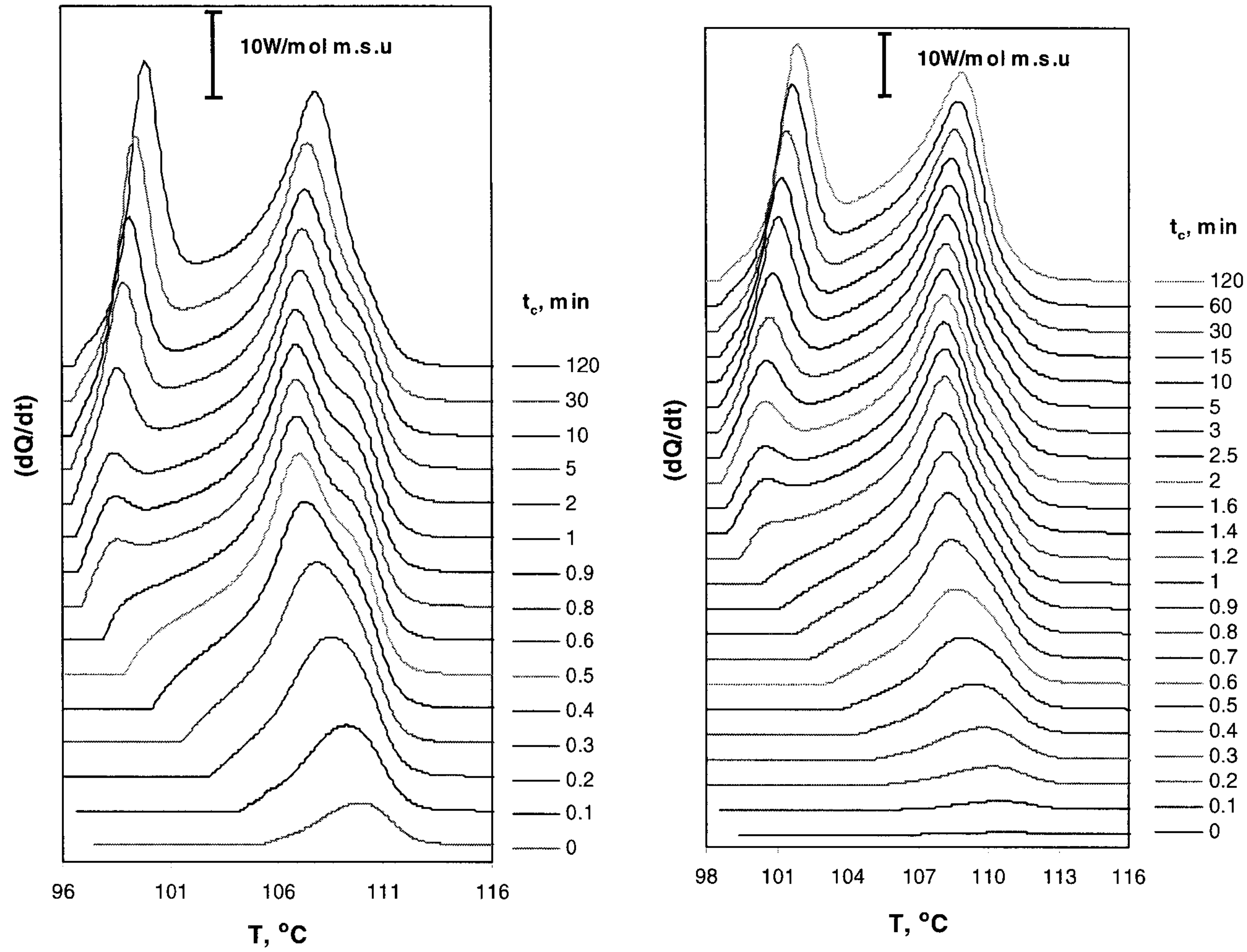

(a) 96°C, t_{fs_PLM} = 0.4min, t_{p_DSC} = 0.6min (b) 98°C, t_{fs_PLM} = 0.8min, t_{p_DSC} =1.0min

Figure 7-8 The melting traces after different crystallization times in regime III for m-LLDPE blend I7

The main difference between the various types of LLDPE is the multiple-peak behavior in the high temperature range. For m-LLDPE resins I and J, as shown in Figure 7-7, there is only one H-peak. For m-LLDPE blend I7, the distribution includes a shoulder in the high temperature position, as shown in Figure 7-8, and hence, appears to have multiple peaks. This shoulder disappears gradually, as the crystallization time increases. The shoulder is more easily observed at the low crystallization temperature (96°C), Figure 7-8(a), than at the high crystallization temperature (98°C), Figure 7-8(b). For ZN-LLDPE, Figure 7-9, the multiple H-peak behavior in the high temperature zone is more pronounced. At the low crystallization temperature (109°C), two H-peaks can be clearly seen, Figure 7-9(a). At the high crystallization temperature (113°C), the traces show only a small shoulder. As the crystallization time increases, the multiple peaks gradually combine into one peak. The multiple-peak behavior does not appear in the homogeneous m-LLDPEs, because their molecular heterogeneity, i.e., multiple ethylene sequence populations, is relatively low. Since the ZN-LLDPE resin G has a higher molecular heterogeneity (a broader short chain branching distribution) than m-LLDPE blend I7, the multiple-peak behavior is more prominent in resin G than in blend I7. Thus, for these experimental conditions covered in this work, the multiple-peak behavior in the high temperature range appears in heterogeneous LLDPEs at a low crystallization temperatures and after a short crystallization time.

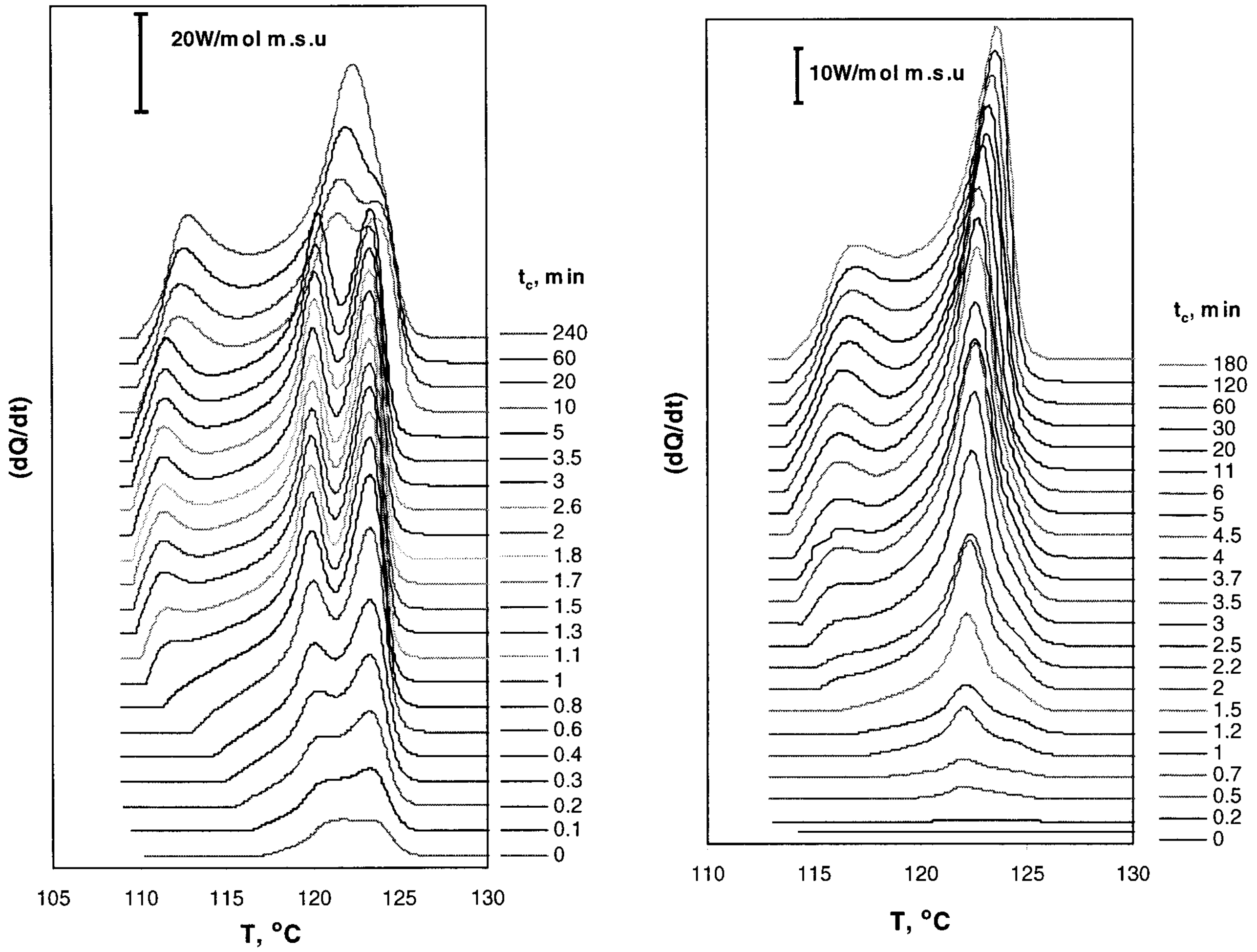

(a) 109°C, t_{fs_PLM} =0.3min, t_{p_DSC} =0.8min (b) 113°C, t_{fs_PLM} =2.4min, t_{p_DSC} =2.5min

Figure 7-9 The melting traces after different crystallization times in regime III for ZN-LLDPE resin G

As previously noted from crystallization traces, in regime III, the primary crystallization process (spherulite growth process) terminates, before crystallization heat flux reaches its maximum value, The H-peak relates to the spherulite crystals, which crystallize from the melt phase. They are the product of the primary crystallization process. The crystals corresponding to the L-peak mainly crystallize from the solidified amorphous part in the spherulites. They are the product of one of the secondary crystallization processes: the new crystal formation. As the crystallization time continuously increases, the increasing length of original crystals makes the melting peak position move to the higher temperatures, for both the H-peak and the L-peak temperatures.

The relative intensity of the L-peak in the final crystallization stage is dependent on the short chain branching content (SCBC) and the crystallization temperature. It is smaller for LLDPE with lower SCBC. Hence, resins G and J (15.8/mC) have lower relative intensities of the L-peaks than resin I (24.8/kC) and blend I7 (22.1/kC). The relative intensities of the L-peak in the final crystallization stage increase, as the crystallization temperature increases (compare curves in Figure 7-8(a) and (b), and in Figure 7-9(a) and (b)). Because the L-peak corresponds to secondary crystallization behavior, the final intensity is higher, as the amount of solidified amorphous parts after primary crystallization increases. As the crystallization temperature decreases and the SCBC increases, much more crystalline ethylene sequences are involved in the solidified amorphous part. Thus, the effect of secondary crystallization (the new crystal formation) increases, accompanied by an increase in relative intensity of the L-peak.

7.3.2.2 Melting traces in regime II

Typical results of the melting traces obtained after different crystallization times in regime II are shown in Figure 7-10 for m-LLDPE (a) resin I at 96°C and (b) resin J at 109°C, and in Figure 7-11 for (a) m-LLDPE blend I7 at 107°C and (b) for ZN-LLDPE resin G at 98°C. The values of t_{fs_PLM}, t_{p_DSC} were not corrected for the nucleation induction times. Although only one peak appeared in their crystallization traces, Figure 7-2 to Figure 7-5, multiple peaks were observed in the melting traces, as already seen for regime III. The peaks appeared at almost the same time from the initial crystallization stage. Therefore, the spherulitic crystals possibly include two populations with different crystal sizes from the H- and L-peak temperature ranges.

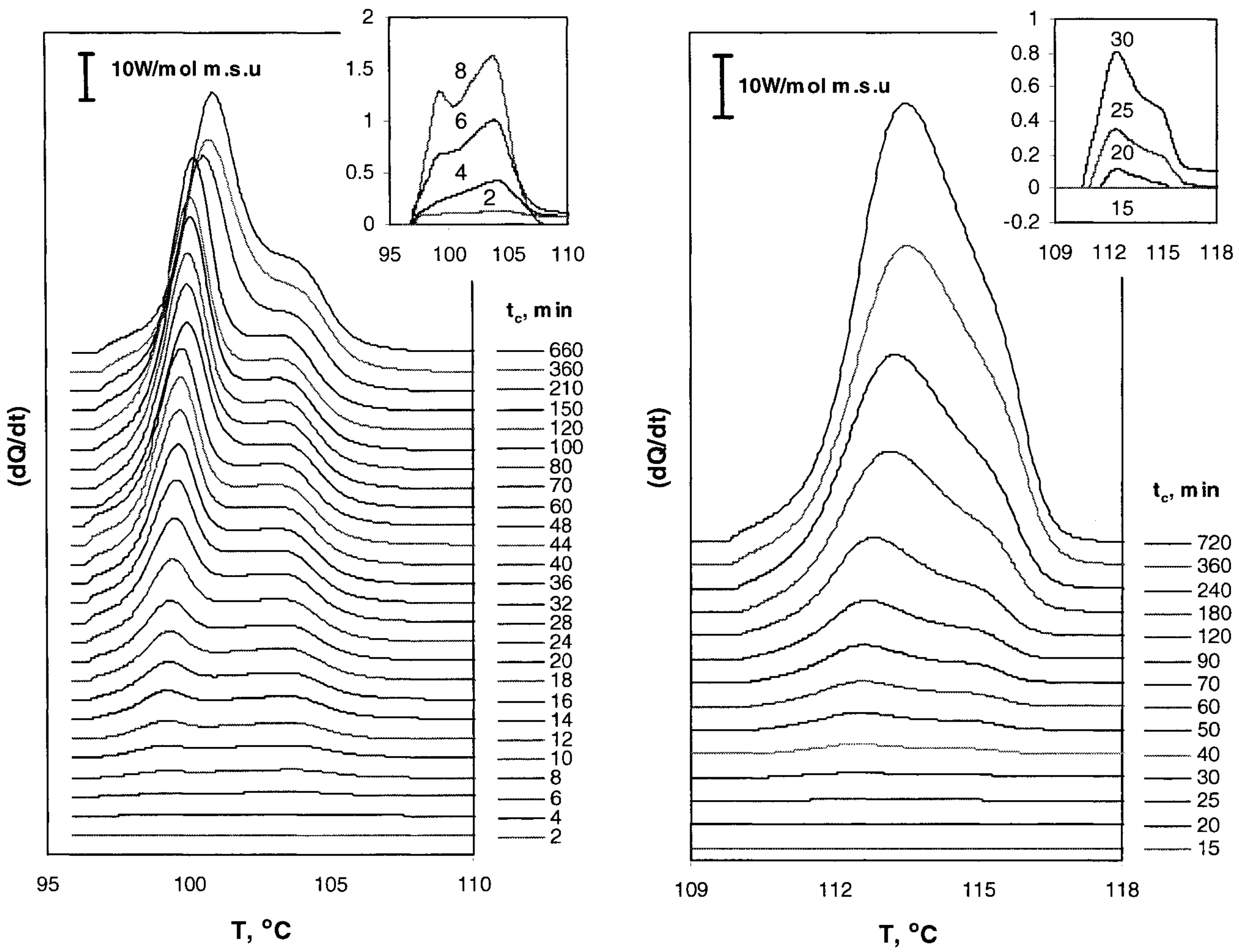

(a) resin I at 96°C
t_{fs_PLM} = 25.1 min, t_{p_DSC} = 14.6 min

(b) resin J at 109°C
t_{fs_PLM} = 110.1 min, t_{p_DSC} = 161.6 min

Figure 7-10 The melting traces in regime II after different crystallization times for m-LLDPEs

In the initial stages of the isothermal crystallizations, the spherulites grew almost linearly in the polarized microscopy experiments,[10] and both H- and L- peaks appeared in the DSC melting traces. After primary crystallization (spherulite growth completed), the overall crystallization process is not yet finished, and both the H and L peaks keep increasing. The changes of melting curves with the crystallization times in regime II are more pronounced than in regime III. Therefore, Both the formation of new crystals and the increase of length of old crystals are significant in regime II. Therefore, secondary crystallization in regime II is more pronounced than in regime III. This is also confirmed in the crystallization traces, where the tails of the profiles in regime II are longer than those in regime III.

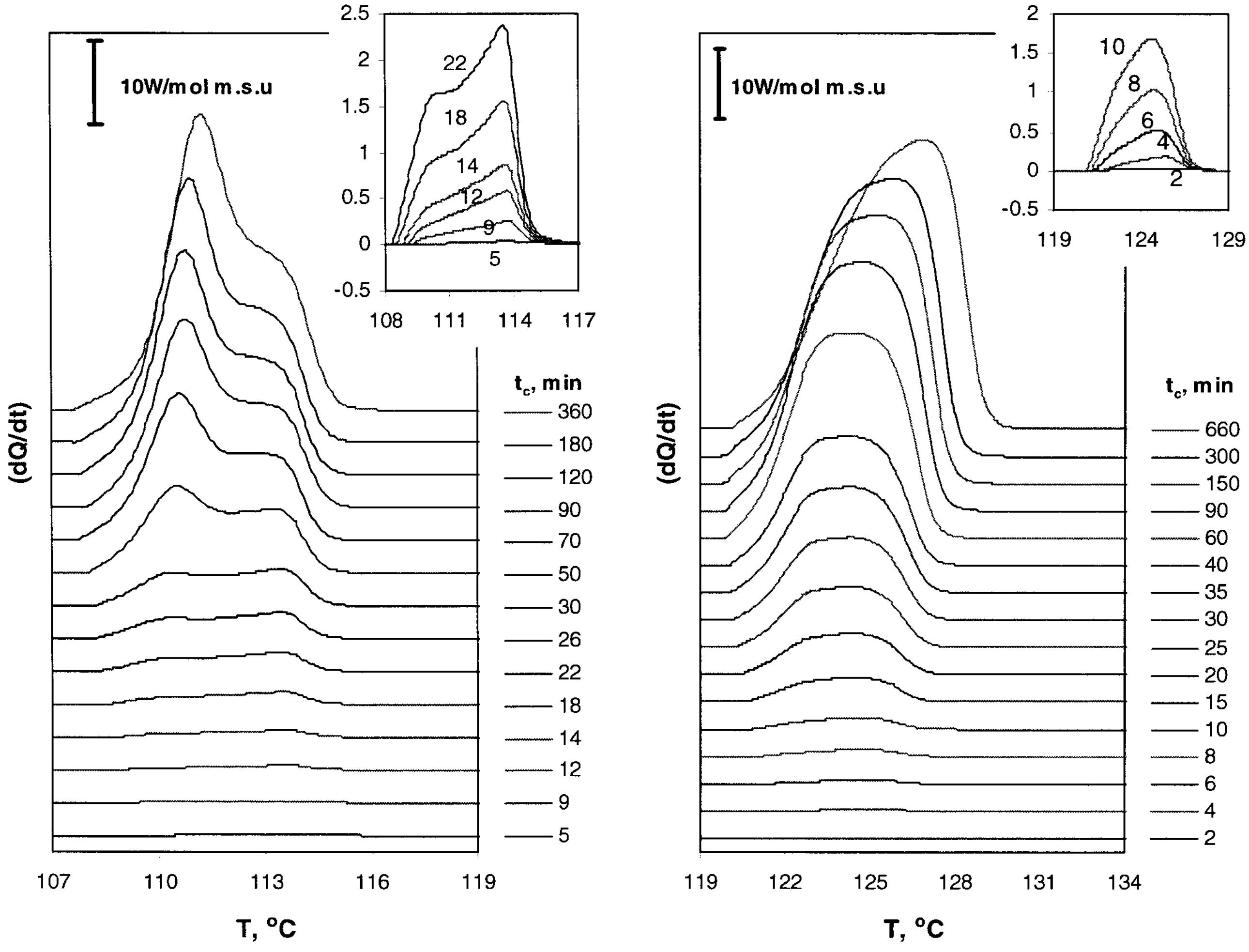

(a) m-LLDPE blend I7 at 107°C
t_{fs_PLM} = 40.5 min, t_{p_DSC} = 26.3 min

(b)) ZN-LLDPE resin G at 119°C
t_{fs_PLM} = 31.5 m, t_{p_DSC} = 35.4 min

Figure 7-11 The melting traces after different crystallization times in regime II

7.3.2.3 Melting traces in regime IM

Typical results of the melting traces obtained after different crystallization times in regime IM are shown in Figure 7-12(c) for m-LLDPE at 102°C. Although, it is very difficult to identify crystallization peak(s), Figure 7-2(c), the melting traces also include two peaks, as in regimes III and II. For the same crystallization time, both the H- and L-peaks appear. Thus, it is possible that the primary crystallization produces two groups of crystals with different crystal sizes, as those in regime II. As the crystallization time, t_c, increases, the area and position of the H- and L-peaks increase. Because a large amount of ethylene sequences are involved in the solidified amorphous part during the primary crystallization process, the L-peak is much stronger than the H-peak.

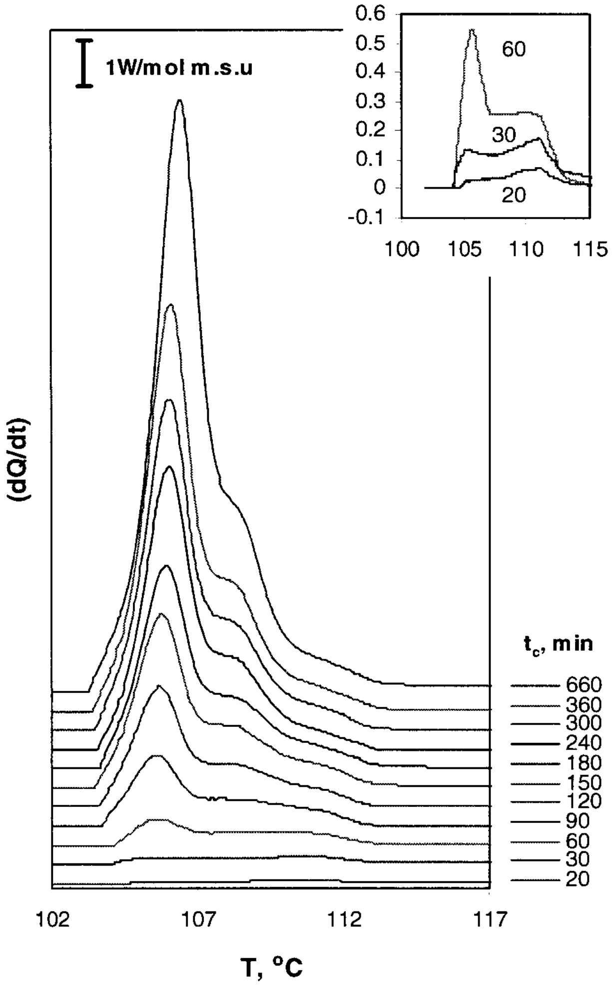

Figure 7-12 The melting traces after different crystallization times in regime IM for m-LLDPE resin I at 102°C.

7.3.2.4 Melting peak positions

As discussed above, two types of melting peaks (the H- and L-peaks) strongly depend on the crystallization temperature and time. The plots of the melting peak position versus the crystallization time at different isothermal crystallization temperatures are shown in Figure 7-13 for m-LLDPE resin I, Figure 7-14 for m-LLDPE resin J, Figure 7-15 for m-LLDPE blend I7, and Figure 7-16 for ZN-LLDPE resin G.

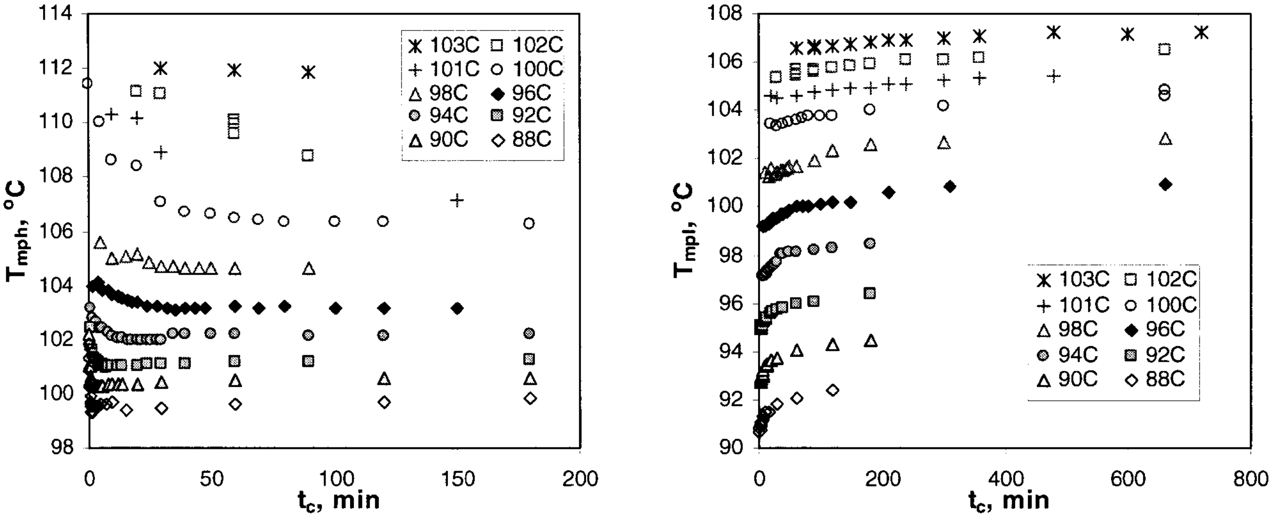

(a) H-peak position (b) L-peak position

Figure 7-13 The melting peak positions in melting traces at different crystallization times and temperatures for m-LLDPE resin I ($T_{II\text{-}IM}$= 100.8°C, $T_{III\text{-}II}$= 93.9°C)

The results show that the temperature effect is very significant. As the isothermal crystallization temperature rises, both the H-peak position, T_{mph}, and the L- peak position, T_{mpl}, increase. Because the H- and L-peak positions are related to the corresponding isothermal crystallization temperature, the L-peak position at the high crystallization temperature is possibly higher than the H-peak position at the low crystallization temperature. This behavior is shown in Figure 7-13 where the L-peak positions in regime IM are higher than the H-peak positions in regime II. However, in the same MHL regime, the L-peak position at the highest crystallization temperature is generally lower than the H-peak position at the lowest crystallization temperature, as shown in the figures.

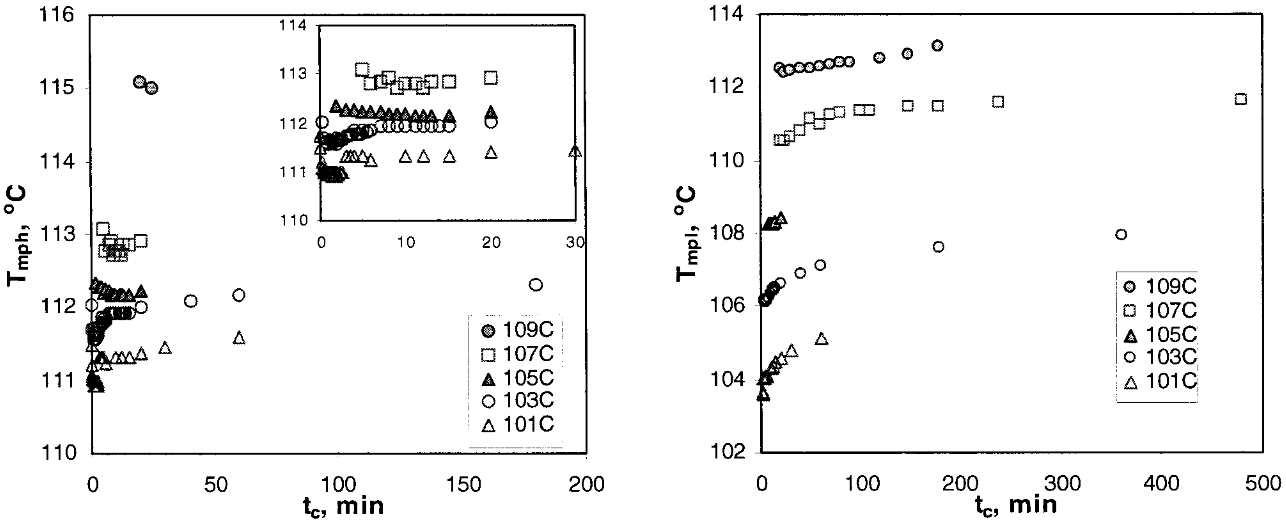

(a) H-peak position (b) L-peak position

Figure 7-14 The melting peak positions in melting traces at different crystallization times and temperatures for m-LLDPE resin J ($T_{III\text{-}II}$= 107.1°C)

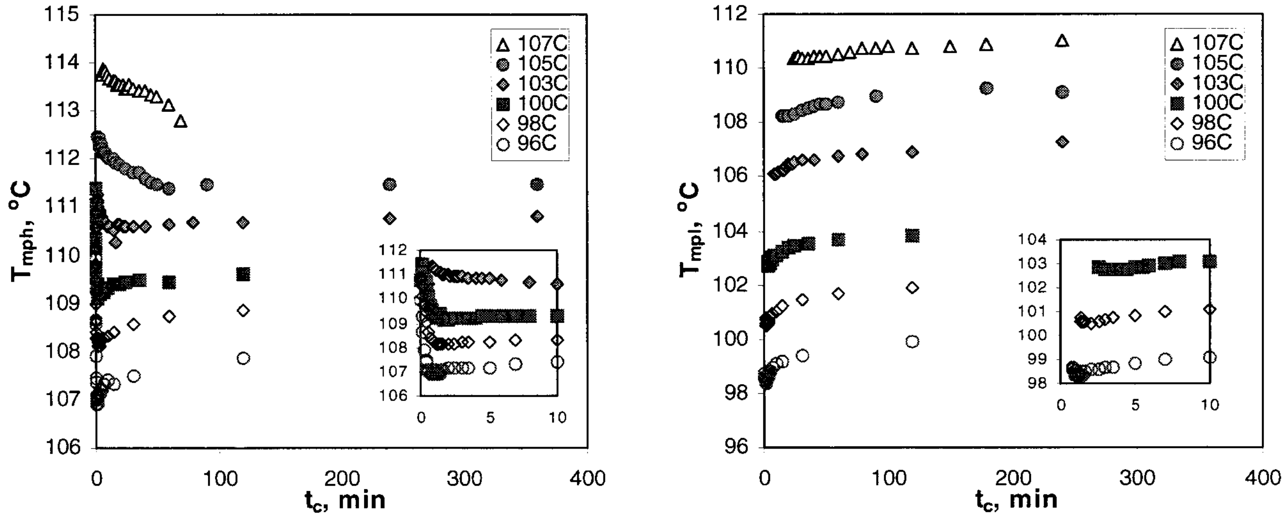

(a) H-peak position (b) L-peak position

Figure 7-15 The melting peak positions in melting traces at different crystallization times and temperatures for m-LLDPE blend I7 ($T_{III\text{-}II}$= 103.3°C)

For resin G, the effects of the melting temperature on the melting traces are more complex. In regime II, the multiple peaks are combined into one broad peak. Thus, no L-peak appears in Figure 7-16(b) for regime II. At low crystallization temperature in regime

III (109 and 111°C), two H-peaks are observed, as well as the L-peak. As shown in the figures inserted in Figure 7-16(a), the high H-peak almost does not vary as the crystallization time increases. Interestingly, their values are between those of the H-peak of isothermal crystallization traces at 115 and 117°C. If the transition temperature between regime III and II for resin G, $T_{III\text{-}II}$, 116.5°C is used as the isothermal crystallization temperature, the H-peak position is expected to be equal to the value of the high H-peak at 109 and 111°C.

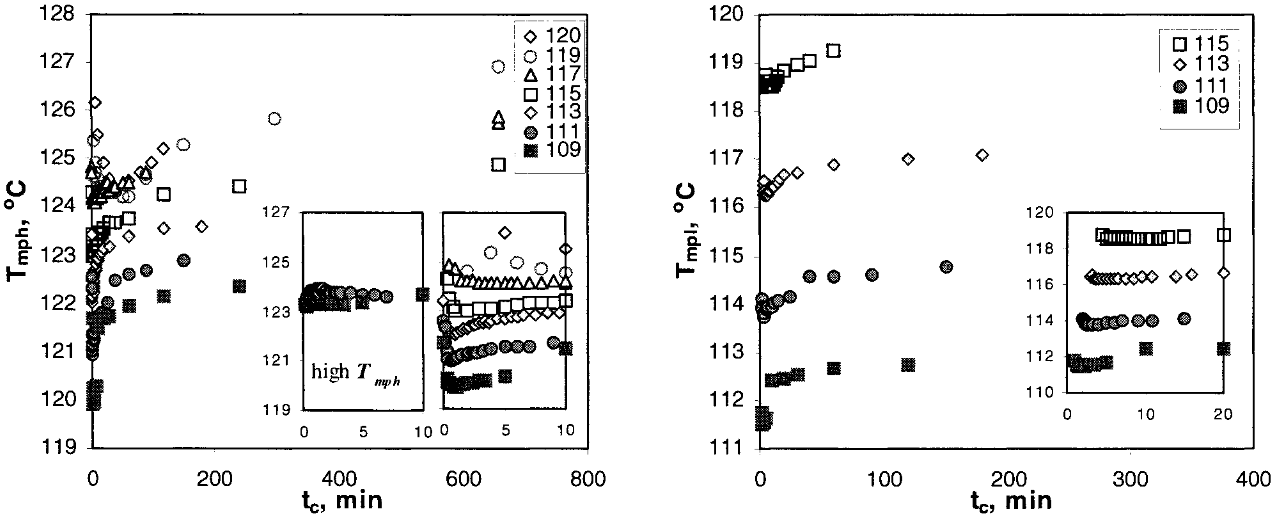

(a) H-peak position (b) L-peak position

Figure 7-16 The melting peak positions in melting traces at different crystallization times and temperatures for ZN-LLDPE resin G ($T_{III\text{-}II}$= 116.5°C)

For (a): low H-peaks at 109 and 111°C; the left inserted figure is for high H-peaks at 109 and 111°C.

The effects of the crystallization time on the melting positions are complex. For the H-peak position, T_{mph}, the tendencies are shown in Figure 7-13(a) for m-LLDPE resin I, Figure 7-14(a) for m-LLDPE resin J, Figure 7-15(a) for m-LLDPE blend I7, and Figure 7-16(a) for ZN-LLDPE resin G. Initially, T_{mph} decreases, as t_c increases. Because the longer ethylene sequences are easier to form the crystals, in the initial stages under isothermal crystallization conditions. Moreover, some may be crystallized during the cooling process (nonisothermal crystallization). They show high melting temperatures.

After the stable isothermal crystallization is reached, the normal crystalline ethylene sequences crystallize. Then, T_{mph} decreases slightly and tends to the minimum value at the end of the primary crystallization. After primary crystallization finishes, T_{mph} increases slightly, because of secondary crystallization due to the length of original crystals.

The tendencies for the L-peak position, T_{mpl}, are shown in Figure 7-13 (b) for m-LLDPE resin I, Figure 7-14 (b) for m-LLDPE resin J, Figure 7-15(b) for m-LLDPE blend I7, and Figure 7-16 (b) for ZN-LLDPE resin G. the relations are slightly different in the different regimes. In regime III (low temperature), as t_c increases, T_{mpl} increases and tends to a constant value. In regimes II and IM (high temperatures), after a slight decrease initially, T_{mpl} follows the same pattern as in regime III: as t_c increases, T_{mpl} increases and tends to a constant value. As discussed above, the T_{mpl} peaks provide information regarding primary and secondary crystallization in regimes II and IM. The initial small decrease of T_{mpl} are assumed to relate the primary crystallization, as shown in the behavior of T_{mph}, because the longer ethylene sequences are crystallized first. As t_c increases, the secondary crystallization prevails. The increase of original crystals (related to T_{mpl}) results into the increase of T_{mpl}. In regime III, the T_{mpl} peaks are mainly related to secondary crystallization. Therefore, the initially slightly decrease of T_{mpl} does not happen.

7.3.3 Induction time

The application of the Avrami expression[14,15,16] is generally effective in describing the overall crystallization kinetics. However, because it does not take into consideration secondary crystallization effects, it is useful only in the initial stages of crystallization The Avrami equation has the following form:

$$X(t) = 1 - \exp\left[-k(T)(t - t_0)^n\right] \tag{7-1}$$

where X is the crystallinity, t_0 is the induction time, and n and k are crystallization constants. A plot of $\ln[-\ln(1-X)]$ vs. $\ln(t-t_0)$, can be used to determine the coefficients n

and k. The crystallization constant k contains cumulative information about the entire crystallization curve at T_c, and it can provide quantitative kinetic information about the crystallization mechanism. The Avrami exponent, n, depends on the growth geometry behavior, and the crystallization nucleation and growth mechanisms.[17] The induction time, t_0, is an important factor in determining overall crystallization kinetics. It is easy to identify in a slowly developing crystallization curve. However, under fast crystallization conditions, it is very difficult to identify, because it is significantly affected by several factors.

Because of energy barrier effects, some time is required to form the nucleation sites, even for the heterogeneous nucleation process. Thus, a normal nucleation induction time, τ_0, is observed. For materials that crystallize slowly, τ_0 can be clearly identified in the isothermal crystallization curve. At a high crystallization temperature, even for materials that crystallize fast, it is possible to measure τ_0. In order to obtain the real crystallization time, τ_0 should be subtracted from the apparent crystallization time.

For materials that crystallize fast, such as polyethylene and polypropylene, it is possible that they undergo some nonisothermal crystallization during quenching, before they reach the specified isothermal temperature, as shown in Figure 7-1. If the crystallization temperature is low, even for materials that crystallize slowly, nonisothermal crystallization can also be observed. Since the Avrami expression is generally applicable only in the initial stages of crystallization, it is necessary to make corrections for this effect. τ_1 is defined to deal with the quenching effect. It refers to the isothermal crystallization time that would produce the same crystallinity obtained during the quenching (cooling) process. τ_1 should be added to the apparent isothermal crystallization time. It is very difficult to identify τ_1 individually. So, it is considered that for the purposes of the present work, the use of an effective crystallization induction time, t_0, is sufficient. This time t_0 is defined as follows: $t_0=\tau_0-\tau_1$. The use of such an effective induction time may lead to a negative value, especially for materials that crystallize fast at low crystallization temperatures.

The experimental results in the initial crystallization stages were fitted to the Avrami expression with the effective nucleation induction time, t_0. The crystallinity employed was the absolute value. The heat of fusion of the 100 percent ethylene crystals was assumed to be 297 J/g.[18] Because the LLDPE branches are excluded from the crystal lattices, the heat of fusion of pure material excludes the contribution of the short chain branching part. The results of the Avrami expression are shown in Figure 7-17. In the initial crystallization stage of all resin samples, the modified Avrami expression appears satisfactorily describe the overall primary crystallization kinetics. However, the same relationship cannot be applied to the secondary crystallization part.

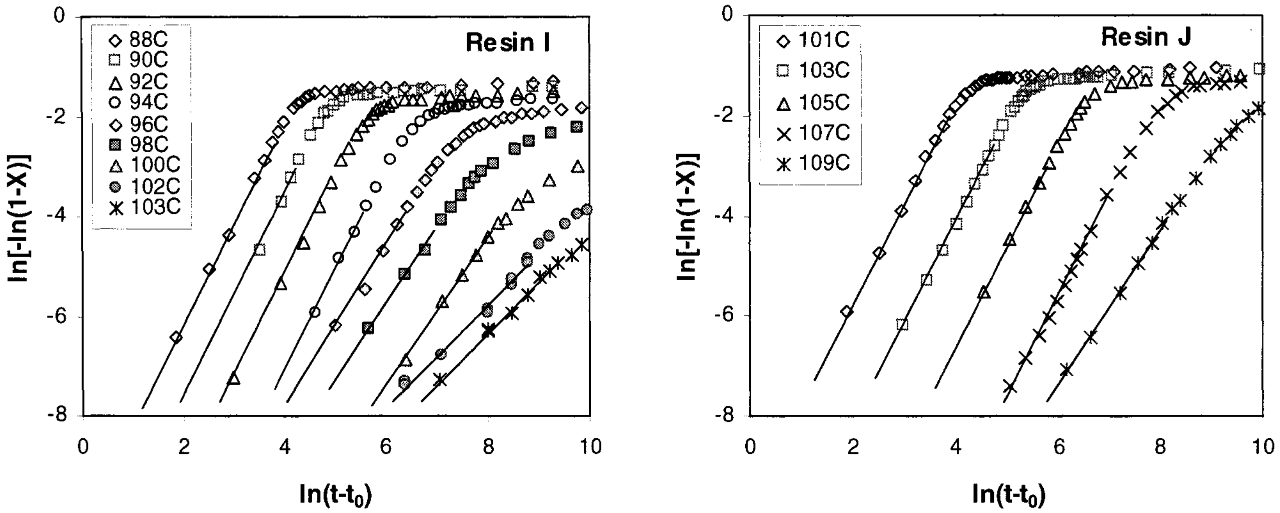

(a) m-LLDPE resin I (b) m-LLDPE resin J

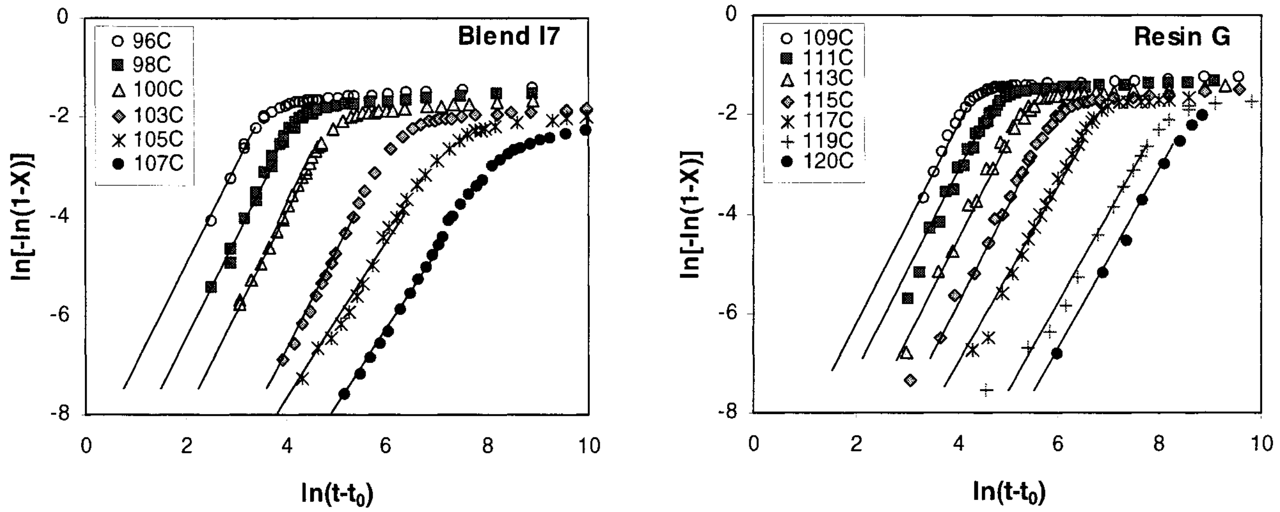

(c) m-LLDPE blend I7 (d)) ZN-LLDPE resin G

Figure 7-17 Plots of $\ln[-\ln(1-x)]$ versus $\ln(t-t_0)$ for isothermal crystallization

The fitting parameters of the Avrami expression are plotted against crystallization temperature in Figure 7-18. All three types of the LLDPEs show similar tendencies. The Avrami crystallization constant, K ($= \sqrt[n]{k}$), decreases, as the crystallization temperature increases. At low crystallization temperature, the effective crystallization time, t_0, shows negative values, because of the aspects considered above. As the isothermal crystallization temperature increases, t_0 increases dramatically.

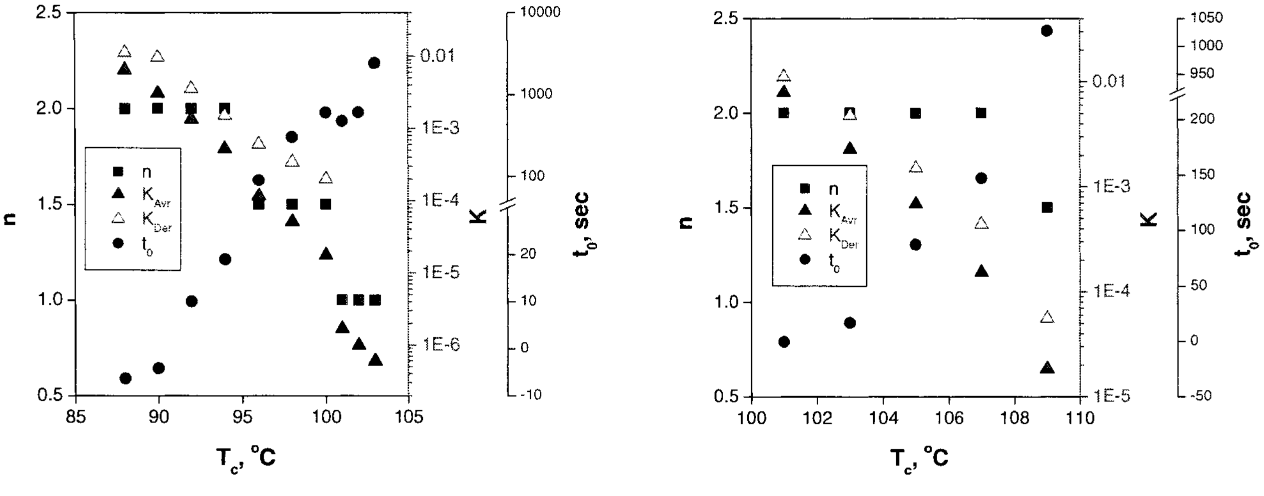

(a) m-LLDPE resin I (b) m-LLDPE resin J

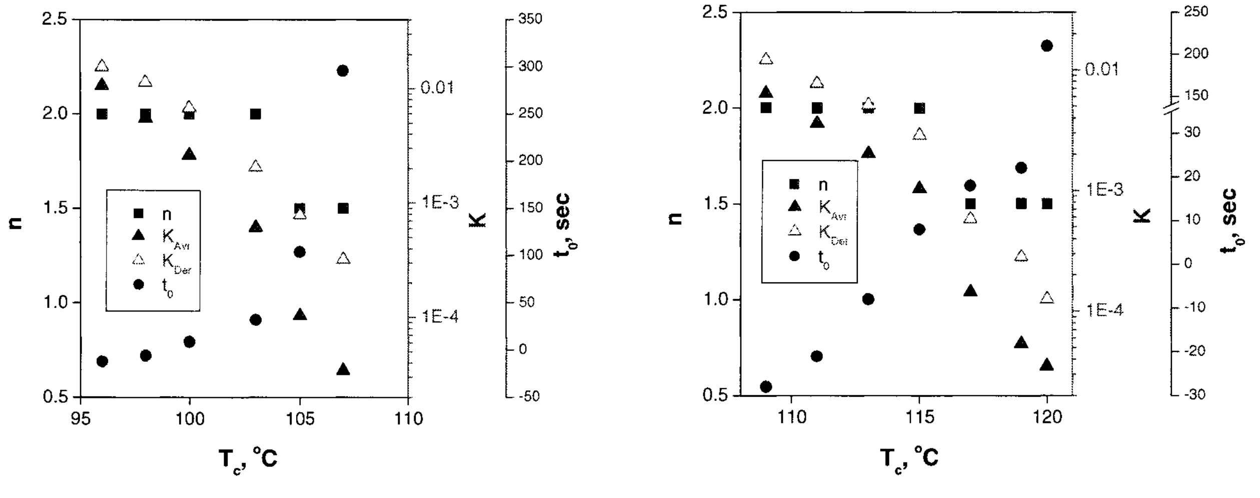

(c) m-LLDPE blend (d) ZN-LLDPE resin G

Figure 7-18 The Avrami constants, and total crystallization induction time plotted against crystallization temperature

The Avrami exponent, n, reflects the regime behavior, under the experimental conditions employed. Exponent values are 2, 1.5 and 1, for regimes III, II, and IM, respectively. Therefore, crystallization growth appears to involve the formation of disc and sphere morphology, and possibly a mixture of discs and circular rods. The value of the exponent is determined by interfacial or diffusion mechanisms, and possibly a mixture of these two mechanisms.[17] It should be recalled that non-linear growth behavior was observed in microscopy experiments in regimes II and IM, under the experimental conditions employed.[10]

7.3.4 Comparison between the linear and overall crystallization kinetics

The linear crystallization kinetics can be described by the modified Hoffman-Lauritzen (MHL) expression:[10]

$$G = G_0 \exp\left[-\frac{Q_D^*}{RT_c}\right]\exp\left[-K_{Mg}\left(\frac{T_m^{C.n^*}}{T_c\Delta Tf}\right)\right] \qquad (7\text{-}2)$$

where $\Delta T = T_m^{C.n^*} - T_c$. The plots of $\ln G + Q_D^*/RT_c$ vs. $T_m^{C,n^*}/(T_c\,\Delta T f)$ are straight lines. $K_{MgIII} = K_{MgI} = \frac{4b_0\sigma\sigma_e}{k\Delta H_u}$ for regimes I and III, and $K_{MgII} = \frac{2b_0\sigma\sigma_e}{k\Delta H_u}$ for regime II. For calculations, parameter values are: T_m^0 = 145.5°C,[19] Q_D^* = 5736 cal/mol,[20] b_0 = 0.415 nm, ΔH_u= 8.106 kJ/mol (CH_2CH_2), σ = 10.2 J/mol.[18]

The concentration of crystallizable ethylene sequences may be considered constant during the early crystallization stage for each of regimes. Therefore, For heterogeneous nucleation crystallization, the spherulitic growth rate can be taken as a constant in the initial crystallization stage, even if spherulites actually show overall non-linear growth behavior in regimes II and IM. The Avrami expression can be applied in the following form:

$$X(t) = 1 - \exp\left[-\dot{N}g(Gt)^n\right] = 1 - \exp\left[-\left(\dot{N}gG^n\right)t^n\right] \qquad (7\text{-}3)$$

where g is a geometric factor, and $\dot{N}$ is the nucleation density (for the heterogeneous nucleation process, it is a constant). Thus,

$$K = \sqrt[n]{k} = \sqrt[n]{\dot{N}g}G \tag{7-4}$$

Figure 7-19 shows a comparison between the results obtained from the Avrami's overall kinetics and those based on Eq.(7-2). The results from the linear and the overall crystallization kinetics show very good agreement. Therefore, under the experimental conditions employed, the overall crystallization kinetics described by the Avrami expression and the linear crystallization kinetics, described by Eq.(7-2), show the same behavior in the initial crystallization stage (the primary crystallization process).

The values of the shift factors, A ($= -\frac{\ln(\dot{N}g)}{n}$), used to be superimpose both sets of data are listed in Table 7-2. In regimes III, II, and IM, the values of A are represented by A_{III}, (A_{III}+A_{II}), and (A_{III}+A_{II}+A_{IM}), respectively. For different materials, the values of A_{III} are different. From the values of A_{III}, it is possible to estimate the relative spherulite size. A high value indicates low nucleation density; so, a large spherulitic size is expected. Polarized light microscopy results confirm this behavior. Resin G has the largest average spherulitic size (radius 30.1μm), followed by resin J (8.0μm) and resin I (7.7μm), with blend I7 having the smallest average size (6.5μm). Because the values of A_{II} and A_{IM} only reflect the differences among the geometric factors in the different regimes, they have the same values, even for different materials, as shown in Table 7-2.

Table 7-2 The shift factors "*A*"

Resin	A_{III}	A_{II}	A_{IM}
G	-9.2	1.0	-
J	-10.0	1.0	-
I	-10.3	1.0	2.0
I7	-10.6	1.0	-

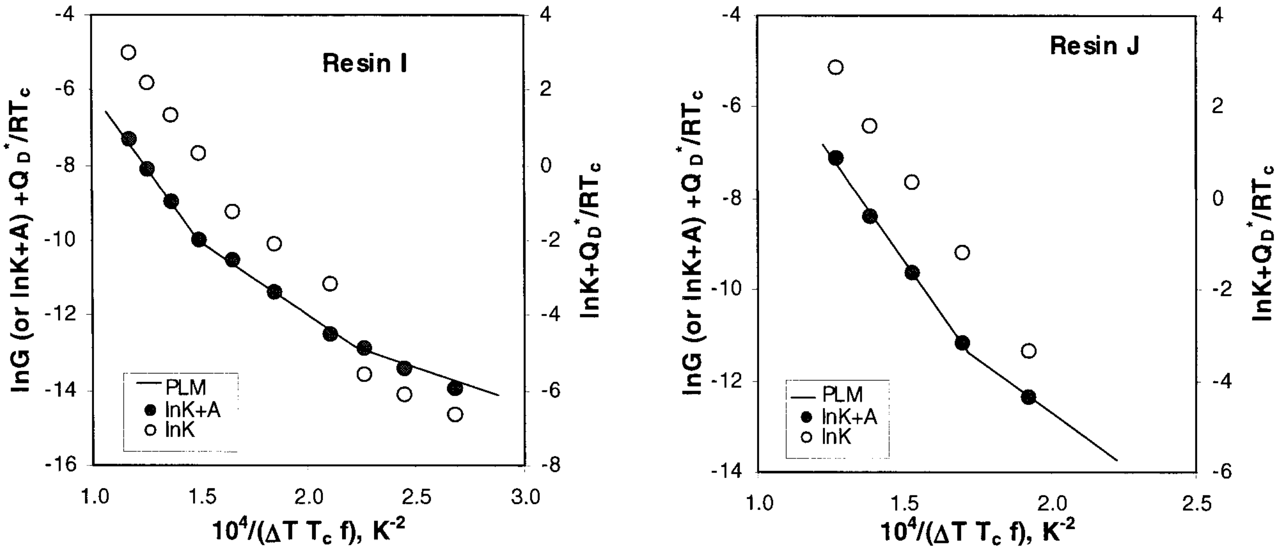

(a) m-LLDPE resin I

(b) m-LLDPE resin J

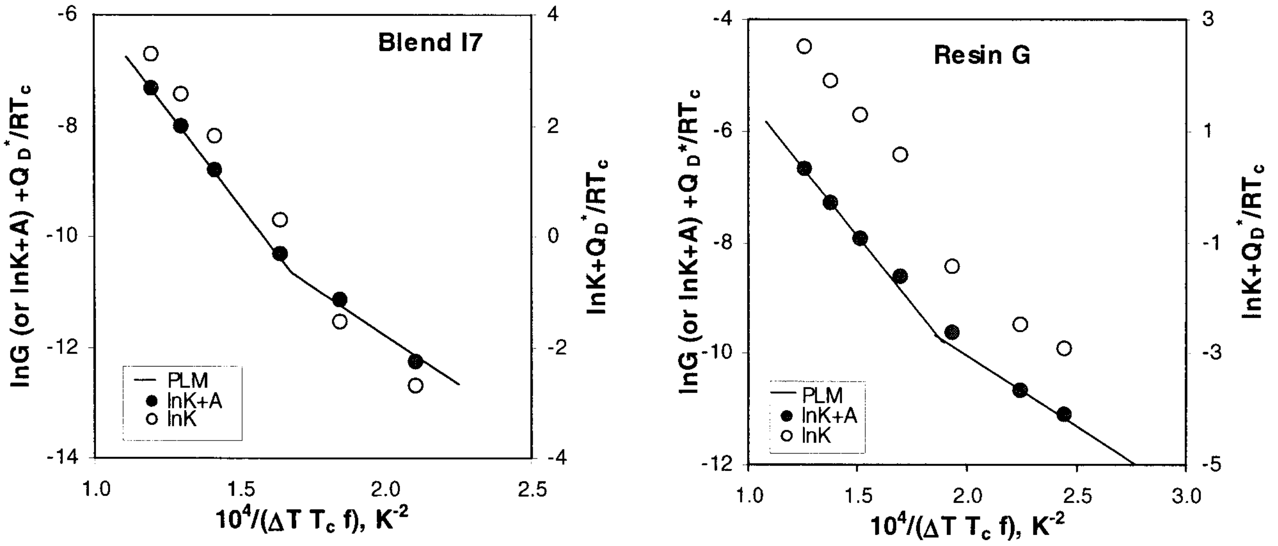

(c) m-LLDPE blend I7

(d) ZN-LLDPE resin G

Figure 7-19 Comparison between the overall and linear crystallization kinetics

7.3.5 Avrami crystallization constants and crystallization peaks

The crystallization rate constant can be estimated from the isothermal crystallization peak position. If the secondary crystallization is neglected, according to Eq.(7-1), the second derivative of crystallinity with respect to crystallization time is equal to zero at the crystallization peak position. Then, if *n* is not equal to 1:

$$k(T) = \frac{n-1}{n\left(t_{peak} - t_0\right)^n} \qquad (7\text{-}5)$$

where t_{peak} is the crystallization time at the peak position of the isothermal crystallization curve. When n is equal to 1, the only result for k is zero. This means that no peaks appear in the crystallization curves. As discussed above, in regimes III and II, one clear peak was observed in each crystallization trace, but in regime IM (as shown in Figure 7-2(c)), no clear crystallization peak could be found.

Although Eq.(7-5) can be used to predict the Avrami crystallization constant, it did produce satisfactory results in this study, because crystallization peak positions are significantly affected by secondary crystallization, under the experimental conditions employed. As shown in Figure 7-18, the Avrami crystallization constants estimated from the crystallization peak position using Eq.(7-5), K_{Der}, are much higher than those obtained using the primary crystallization analysis directly by the Avrami expression.

7.4 Conclusions

Under the experimental conditions employed, the crystallization traces show a clear peak in regimes III and II. Secondary crystallization is significant, because spherulite growth finishes before the crystallization peak. In regime IM, no clear peaks can be identified in the crystallization traces, because the Avrami exponent is 1 in this regime.

Multiple peaks appear in the melting traces after certain crystallization times at specified isothermal crystallization temperatures. Basically, they can be grouped into the H- and L-peaks. In regime III, a single H-peak seems to correspond to the primary crystallization crystal, i.e., spherulitic crystals, in the initial crystallization stage. For heterogeneous LLDPEs, at low crystallization temperature, two such peaks are observed. As both the crystallization temperature and crystallization time increase, these combine into one peak. The formation of the L-peak is due to secondary crystallization. In regimes II and IM, it is difficult to identify the crystals from the primary or secondary crystallization processes. Both the H- and L-peak positions depend on the crystallization temperature and time.

When the Avrami expression is applied to describe the overall crystallization kinetic, the nucleation induction time has to consider the effects of the nonisothermal crystallization, the size of heterogeneous nucleation agents, as well as the normal nucleation induction time. The Avrami expression with an effective induction time can explain the overall crystallization kinetics for the three different types of LLDPEs. The Avrami exponents in the regimes III, II, and IM are 2, 1.5, and 1, respectively. The Avrami crystallization constants superimpose to the linear crystallization kinetics by employing a shift factor.

7.5 References

1 Peeters M, Goderis B, Vonk C, Reynaers H, Mathot V. J Polym Sci, B: Polym Phys 1997, 35:2689.

2 Peeters M, Goderis B, Reynaers H, Mathot V. J Polym Sci, B: Polym Phys 1999, 37:83.

3 Clas SD, McFaddin DC, Russell KE, Scammell-Bullock MV, Peat IR. J Polym Sci, A: Polym Chem 1987, 25:3105.

4 Mathot VBF, Pijpers MFJ. J Appl Polym Sci 1990, 39:979.

5 Schouterden P, Groenickx G, Van der Heijden B, Jansen F. Polymer 1987, 28:2099.

6 Wilfong DL, Knight GW. J Polym Sci, B: Polym Phys 1990, 28:861.

7 Defoor F, Groeninckx G, Reynaers H, Schouterden P, Van der Heijden, B. Polymer 1992, 33:3878.

8 Zhang M, Lynch DT, Wanke SE. Polymer 2001, 42:3067.

9 Kamal MR, Feng L, Huang T. Can J Chem Eng 2002, 80: 432.

10 Feng L, Kamal MR. Polym Eng Sci 2004, accepted for publication (see Chapter 5 in this thesis).

11 Feng L, Kamal MR. Can J Chem Eng 2004, accepted for publication (see Chapter 3 in this thesis).

12 Feng L, Kamal MR. Themochim Acta 2004, submitted for publication (see Chapter 4 in this thesis).

13 Alamo RG, Viers BD, Mandelkern L. Macromolecule 1993, 26:5740.

14 Avrami M. J Chem Phys 1939, 7:1103

15 Avrami M. J Chem Phys 1940, 8:212.

16 Avrami M. J Chem Phys 1941, 9:177.

17 Schultz JM. Polymer Crystallization: the Development of Crystalline Order in Thermoplastic Polymers, Oxford, New York: Oxford University Press, 2001 (Chapter 9).

18 Hoffman JD, Miller RL. Polymer 1997, 38:3151.

19 Mandelkern L, Alamo RG. In: Mark JE. Editor, Physical Properties of Polymers Handbook, American Institute of Physics, New York: Woodbury, 1996 (Chapter11).

20 Fletcher DP, Klein J. Polym Commun 1985, 26:2.

Chapter 8

8 Study on Morphology of Linear Low-Density Polyethylene with Polarized Light Microscopy

This study shows that, as the crystallization temperature increases, the morphology of linear low-density polyethylene (LLDPE) changes from non-ring-banded spherulites, to ring-banded spherulites, and sometimes to irregular structures with rough ring bands. The above morphologies were observed in regimes IIIA, III, II, and IM, respectively, as identified by the modified Hoffman-Lauritzen secondary nucleation growth mechanism. The ring-banded spherulite structure is more obvious in LLDPEs with high short chain branching content and low short chain branching polydispersity. The ring-banded distance shows the same linear dependence on the crystallization temperature in regimes III and II, but not in regime IM. Possibly, the morphology undergoes lamellar twist and rotation in regimes III and II, while undergoing lamellar (bundle) branching in regime IM. Because the growth habit of the spherulite is 3-dimensional, spherulites tend to deteriorate away from the spherulitic centers in regime II.

8.1 Introduction

The crystalline morphology of semi-crystalline polymers depends on their molecular structural properties and the crystallization processing conditions. The morphological characteristics of polyethylenes correspond to the regime behavior, according to the Hoffman-Lauritzen (HL) secondary nucleation mechanism.[1,2]

The original HL equation was proposed for linear crystalline polymers. For homopolymers, the melting temperature for perfect crystals or for molecular length crystals ($T_m^{C,\infty}$) is used as the reference melting temperature. For copolymers with excluded comonomers, such as linear low-density polyethylene (LLDPE), the melting temperature for perfect crystals of copolymers based on the Flory's expression[3] ($T_m^{C,\infty}$) is usually used. However, $T_m^{C,\infty}$ refers to a hypothetical state: the perfect crystal. There is a large difference between $T_m^{C,\infty}$ and the melting temperature for the maximum possible length crystals for copolymers with excluded comonomers ($T_m^{C,n*}$).[4] As reported elsewhere,[5] the use of $T_m^{C,\infty}$ does not lead to differentiation of the various regimes and leads to overestimation of the basal surface free energy. On the other hand, the application of $T_m^{C,n*}$, as the reference melting temperature for the degree of supercooling, produces more reasonable results.

In this paper, the optical morphological characteristics of LLDPEs are studied, in the different regimes identified according to the modified HL expression.[5] The dependence of the ring-banded distance on the crystallization temperature and molecular structure is also discussed.

8.2 Experimental

8.2.1 Materials

The characteristics of the polyethylene resins used in this work are summarized in Table 8-1.[5,6] They were provided by Nova Chemical Inc. (Calgary, Canada) in pellet form, including two experimental metallocene catalyzed LLDPEs (m-LLDPE resins I and J), and three experimental Ziegler-Natta catalyzed LLDPEs (ZN-LLDPE resins H, C, and G).

Table 8-1 Polymer molecular characteristics

Material	Com[a]	Type[b]	SCBC (/1000C)	M_n (kg/mol)	M_w (kg/mol)	σ_e (J/mol)[c]	$T_{el,W}/T_{el,N}$-1 (×100)[d]	$T_{II\text{-}IM}$ (°C)[e]	$T_{III\text{-}II}$ (°C)[e]
H	B	ZN	18.9	29.5	123.0	3060	3.16	118.0	112.5
C	H	ZN	18.87	33.3	102.0	2340	6.47	122.5	118.5
G	O	ZN	15.8	23.1	98.6	2730	5.42	122.0	116.5
J (I0)	O	m	15.8	38.2	70.2	5200	0.64	-	107.1
I1	O	mb (0.1 I wt)	16.7	35.5	68.5	4870	1.25	-	107.2
I3	O	mb (0.3 I wt)	18.5	31.2	65.0	4300	2.13	-	105.8
I5	O	mb (0.5 I wt)	20.3	27.9	61.5	3970	2.58	-	107.6
I7	O	mb (0.7 I wt)	22.1	25.1	58.1	3920	2.59	-	103.3
I9	O	mb (0.9 I wt)	23.9	22.9	54.6	4300	2.16	103.0	96.0
I (I10)	O	m	24.8	21.9	52.9	4660	1.78	100.0	93.9

a: *Com* is comonomer; B is butene, H is hexene, and O is octene.

b: ZN is ZN-LLDPE, and m is m-LLDPE, and mb is m-LLDPE blend.

c: The basal surface free energies were calculated from the modified Hoffman-Lauritzen secondary nucleation crystallization kinetics analysis for LLDPEs.[5]

d: The short chain branching polydispersities are calculated from TREF results.[5] It is represented by $(T_{el,W}/T_{el,N} - 1)\times 100$. $T_{el,W}$ and $T_{el,N}$ are defined as the weight and number average elution temperatures, respectively.

e: The regime transition temperatures from regime III to II, $T_{III\text{-}II}$, and from regime II to IM, $T_{II\text{-}IM}$, were based on the modified Hoffman-Lauritzen expression.[5]

The molecular structural parameters were also provided by Nova Chemical Inc. The short chain branching contents (SCBC) were measured by nuclear magnetic resonance (NMR), molecular weights by gel permeation chromatography (GPC), and the short chain branching polydispersities (SCBP) were determined by temperature rising elution fractionation (TREF). Five blends of m-LLDPE resins I and J (blends I1, I3, I5, I7, and I9) were prepared by the solvent-mixing method.[6] Thus, three different groups of LLDPEs were used in this study, i.e., heterogeneous LLDPE resins (ZN-LLDPE), homogeneous LLDPE resins (m-LLDPE), and heterogeneous inter-molecular and homogeneous intra-molecular LLDPE resins (mb-LLDPE). The blend characteristics were weighted averages based on the properties of the pure m-LLDPE resins.

8.2.2 Polarized light microscopy (PLM) with a hot stage

A thin film specimen was fixed on a circular microscopic glass cover. Then, the glass cover was placed on a hot stage (Linkam TH600). The hot stage was used in conjunction with a polarized light microscope (Olympus BH-2), equipped with a digital camcorder system (SONY DXC-950/1). The temperature precision was 0.1degree. The film specimen was heated to 180°C and kept for 10min to remove thermal history effects. Subsequently, the melted film was quenched to the set crystallization temperature, and kept at that temperature until the crystallization process was terminated. The quenching rate was about 130°C/min, which was achieved by direct flow of compressed air through the hot stage sample holder. The spherulitic growth with time was recorded and saved in a computer by the Linkam software. The whole experimental process was conducted under nitrogen atmosphere.

8.3 Results and Discussion

8.3.1 A Modification of Hoffman-Lauritzen Expression

In order to adapt the Hoffman-Lauritzen (HL) expression to the crystallization of copolymers with excluded comonomers, it was modified by replacing the equilibrium melting temperature for perfect crystals, T_m^0 ($T_m^{C,\infty}$), with T_m^{C,n^*}, the melting temperature of the crystal stem with the maximum possible length, n^*.[5] The modified Hoffman-Lauritzen expression becomes:

$$G = G_0 \exp\left[-\frac{Q_D^*}{RT_c}\right]\exp\left[-\frac{K_{Mg}}{T_c\left(T_m^{C,n^*}-T_c\right)f}\right] \qquad (8\text{-}1)$$

G refers the spherulitic radial growth rate; G_0 is a pre-exponential parameter containing quantities not strongly dependent on the temperature; the first exponential term refers to the transportation across the interface of crystals and melts; the second term represents the deposition of crystal stems; Q_D^* is the diffusion activation energy; T_c refers to the crystallization temperature; and $\Delta T = T_m^{C.n*} - T_c$ is the degree of supercooling; f = $2T_c/(T_m^0+T_c)$ is a correction factor for the variation in the heat of fusion with temperature. Plots of $\ln(G)+Q_D^*/RT_c$ versus $1/(T_c\Delta Tf)$ are straight lines. The slopes are the nucleation constant, K_{Mg}, corresponding to the net activation energy for layer growth. In regimes III and I,

$$K_{MgIII} = K_{MgI} = \frac{4b_0\sigma\sigma_e}{k\Delta H_u} T_m^{C.n^*} \tag{8-2}$$

and in regime II,

$$K_{MgII} = \frac{2b_0\sigma\sigma_e}{k\Delta H_u} T_m^{C.n^*} \tag{8-3}$$

where σ and σ_e are, respectively, the lateral and basal (folding) surface free energies, k is Boltzmann's constant, b_0 is the layer thickness, and ΔH_u is the heat of fusion. For polyethylenes, T_m^0 = 145.5°C,[7] Q_D^* = 24 kJ/mol,[8] b_0 = 0.415 nm, ΔH_u = 8.1 kJ/mol monomer structural unit (m.s.u., CH_2CH_2), σ = 10.2 mJ/m^2.[1]

Eq.(8-1) was applied to evaluate the spherulitic growth behavior of the above LLDPE resins. The resins exhibited three regimes: regimes III, II, and IM, as the crystallization temperature increased (the degree of supercooling decreased), under the experimental conditions employed.[5]

8.3.2 Crystalline Morphology of LLDPEs

The crystallization temperature has a significant effect on the crystalline morphological characteristics. Generally, as the crystallization temperature increases, the spherulitic morphology deteriorates. The morphological characteristics for different types of LLDPEs in different regimes are discussed below.

8.3.2.1 Morphology of ZN-LLDPEs

On applying the MHL analysis for the ZN-LLDPEs, three regimes (regimes III, II and IM) were clearly observed, under the experimental conditions employed.[5] In different regimes, different crystalline morphologies are observed. The morphological characteristics in different regimes are shown in Figure 8-1 for ZN-LLDPE resin G (with octene comonomer, 15/kC), Figure 8-2 for ZN-LLDPE resin H (with butene comonomer, 18.9/kC), and Figure 8-3 for ZN-LLDPE resin C (with hexene comonomer, 18.87/kC).

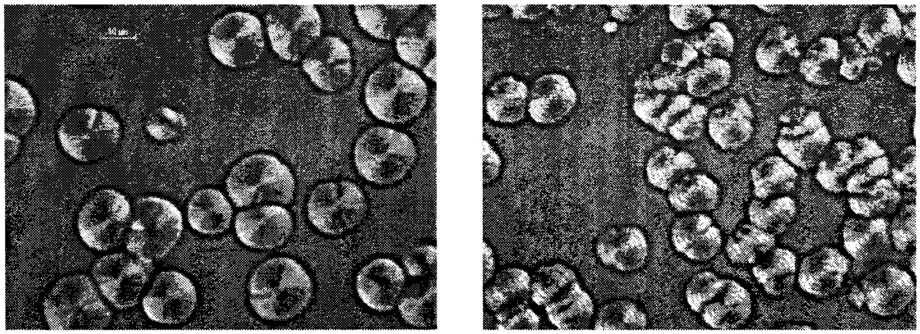

(a) 106°C, regime III (b) 113°C, regime III

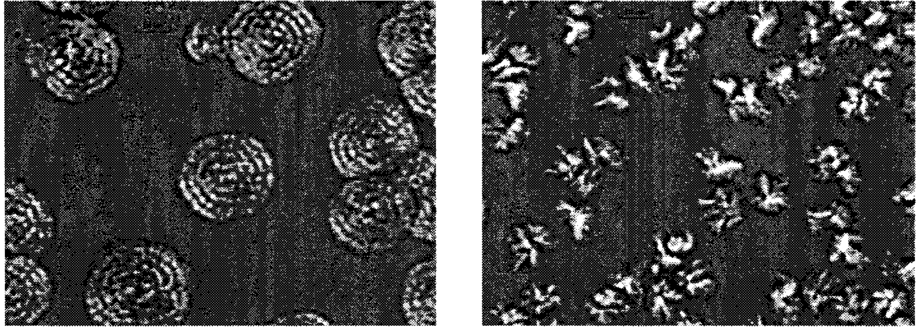

(c) 117°C, regime II (d) 123°C, regime IM

Figure 8-1 The morphologies of resin G in different regimes

The dependence of the morphological characteristics on the crystallization temperature (regime) is similar for different ZN-LLDPEs. Under the experimental conditions employed in this study, three typical morphologies are obtained, as the crystallization temperature increases: spherulite without ring bands, ring-banded spherulite, and irregular morphology.

For resins G and H, when the crystallization temperature is relatively low in regime III, no clear ring bands can be observed in the spherulites, as shown Figure 8-1(a) and Figure 8-2(a). This could be due to the ring band distance being too small to be identified by PLM, or that no ring bands are formed at low crystallization temperatures. For resin C, however, as the crystallization temperature increases, the ring-banded structure is gradually formed, as can be seen in Figure 8-1(b) for resin G, Figure 8-2(b) for resin H, and Figure 8-3(a) for resin C. In regime II, the ring-banded spherulite is the typical morphology, as shown in Figure 8-1(c), Figure 8-2(c), and Figure 8-3(b) for resins G, H, and C, respectively. The ring-banded distance decreases, as the crystallization temperature decreases. As the crystallization temperature continues to increase, regime IM with only irregular morphology is observed, as shown in Figure 8-1(d), Figure 8-2(d) and Figure 8-3(c) for resins G, H, and C, respectively.

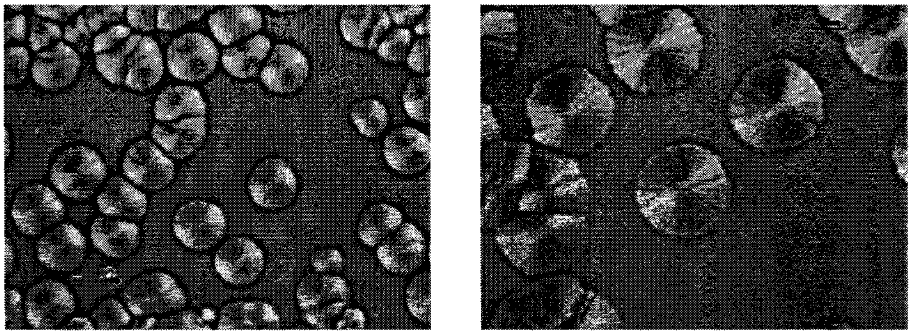

(a) 104°C, regime III (b) 110°C, regime III

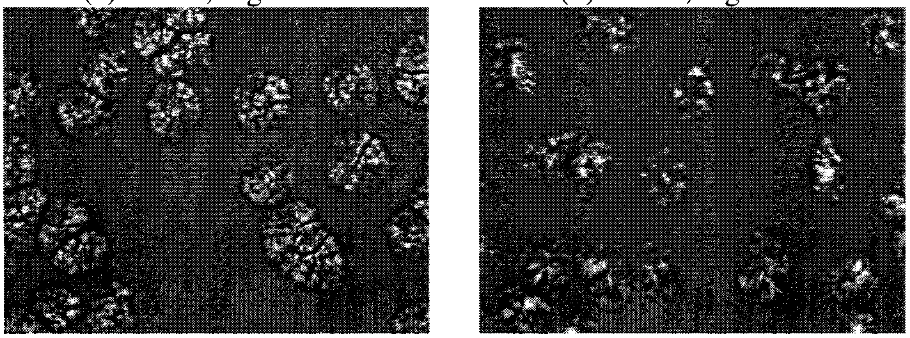

(c) 116°C, regime II (d) 120°C, regime IM

Figure 8-2 The morphologies of resin H in different regimes

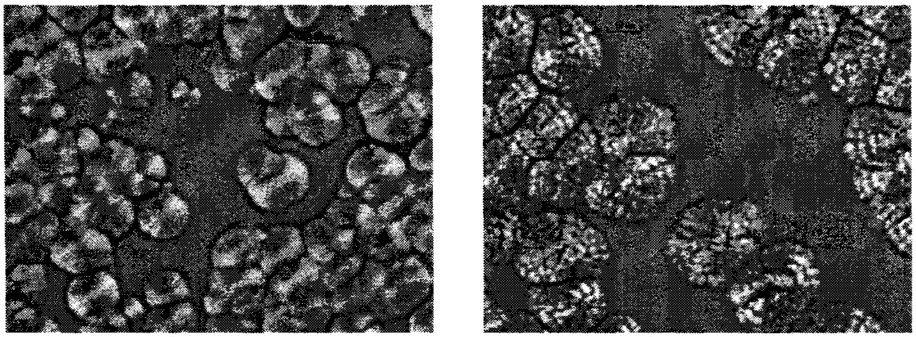

(a) 112°C, regime III (b) 119°C, regime II

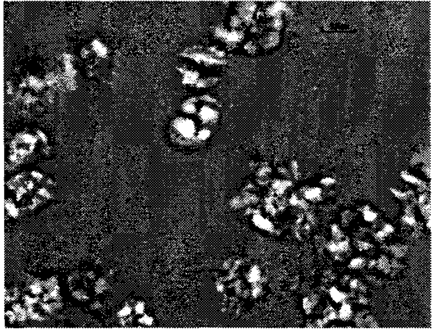

(c) 123°C, regime IM

Figure 8-3 The morphologies of resin C in different regimes

8.3.2.2 Morphology of m-LLDPEs

For m-LLDPE resin J (octene comonomers, 15.8/kC), the morphological characteristics in different regimes are shown in Figure 8-4. Under the experimental conditions employed, only regimes III and II were observed.[5] In regime III, the spherulites do not have any ring bands, as shown in Figure 8-4(a). In regime II, the ring-banded spherulites can be observed, as shown in Figure 8-4(b). Some spherulites become irregular during crystallization because of the three-dimensional growth.

The m-LLDPE resin I (octene comonomers, 24.8/kC) has a higher short chain branching content than resin J. The morphological characteristics in different regimes are shown in Figure 8-5. All three regimes appear in resin I, under the experimental conditions used.[5] However, the ring-banded spherulites do not appear over the whole experimental crystallization temperature range. In regimes III and II, regular non-ring-banded spherulites are observed, as in Figure 8-5(a) and Figure 8-5 (b). In the regime II, some spherulites become irregular during isothermal crystallization, as in the case of resin J. In regime IM, the morphology is irregular, as shown in Figure 8-5(c).

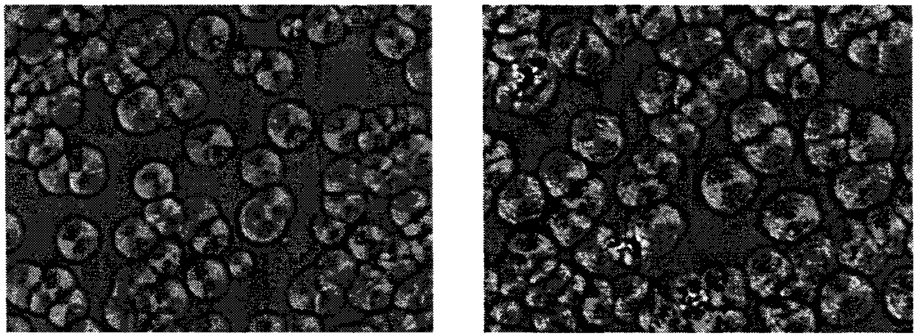

(a) 100°C, regime III (b) 111°C, regime II

Figure 8-4 The morphologies of resin J in different regimes

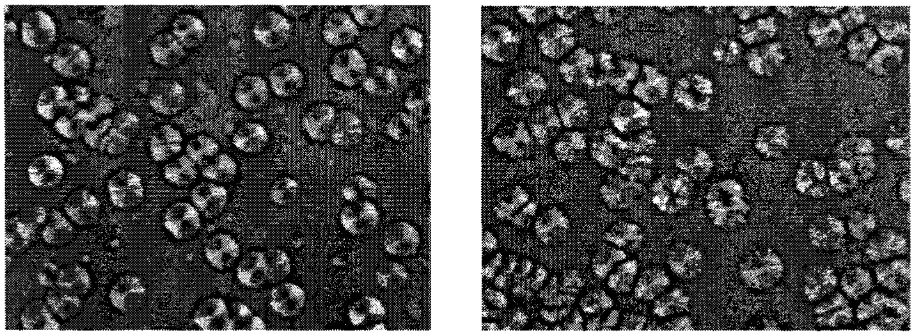

(a) 90°C, regime III (b) 94°C, regime II

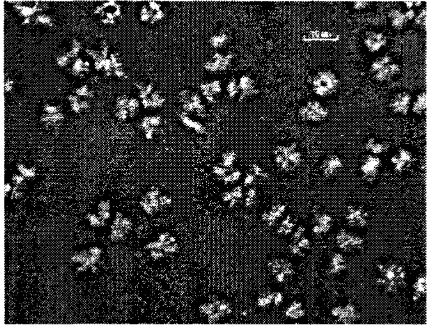

(c) 100°C, regime IM

Figure 8-5 The morphologies of resin I in different regimes

8.3.2.3 Morphology of m-LLDPE blends

Blends of m-LLDPEs are solvent-mixed using the m-LLDPE resins I and J. They have similar optical morphological characteristics. Figure 8-6 shows the morphological characteristics in different regimes for blend I1 (10% resin I weight fraction, octene comonomers, 16.7/kC). Under the experimental conditions employed, only regimes III and II were observed.[5] In regime III, in the low temperature range, the spherulites do not show any ring bands, Figure 8-6(a). In the high temperature range of regime III and regime II, ring-banded spherulites are observed, as shown in Figure 8-6(b) and Figure 8-6(c), respectively. Some spherulites become irregular during crystallization in regime II (Figure 8-6(c)), as already observed with the pure m-LLDPE resins.

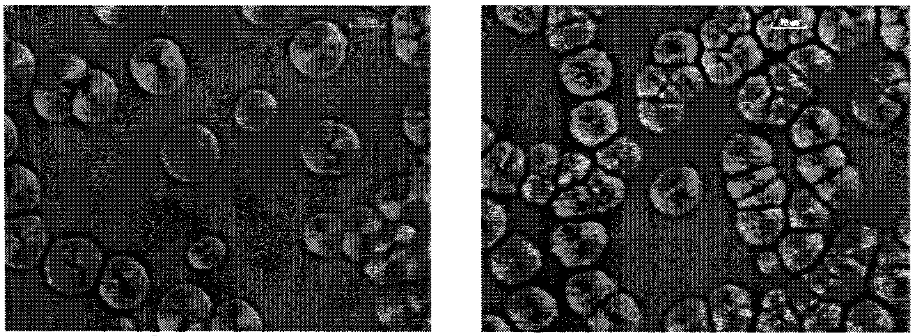

(a) 98°C, regime III (b) 104°C, regime III

(c) 108°C, regime II

Figure 8-6 The morphologies of blend I1 in different regimes

For Blends I3, I5, and I7, only regimes III and II were observed, under the experimental conditions employed.[5] They show the same crystallization morphological characteristics as Blend I1. For Blend I9, regime IM was also observed,[5] together with irregular ring-banded characteristics, as shown in Figure 8-7.

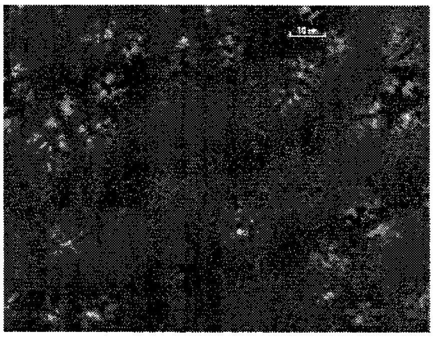

Figure 8-7 The morphology of blend I9 at 105°C, in regime IM.

8.3.3 Ring-banded spherulitic morphology

For different LLDPEs, the temperature ranges, in which the ring-banded spherulites were observed, are shown in Figure 8-8. The experimental isothermal crystallization temperature range, the regime transition temperature,[5] and the short chain branching polydispersity (SCBP) are also included. The experimental crystallization temperatures for different resins were mainly determined by the crystalline spherulitic growth rate. The spherulitic growth rates generally varied from 0.001 to 1μm/sec,[5] because of the limitations of the experimental arrangement employed.[5] However, the corresponding crystallization temperature ranges were totally different for different materials, because of the differences of their molecular structural characteristics, especially the differences of the short chain branching characteristics.

For the experimental conditions employed, ring-banded spherulites did not appear in m-LLDPE resin I over the whole experimental crystallization temperature range. They were observed in the other resins, generally seen in regimes III and II, but only for blend I9 in regime III. For ZN-LLDPE resin H and m-LLDPE blend I9, some rough ring-banded structural characteristics were also seen in regime IM.

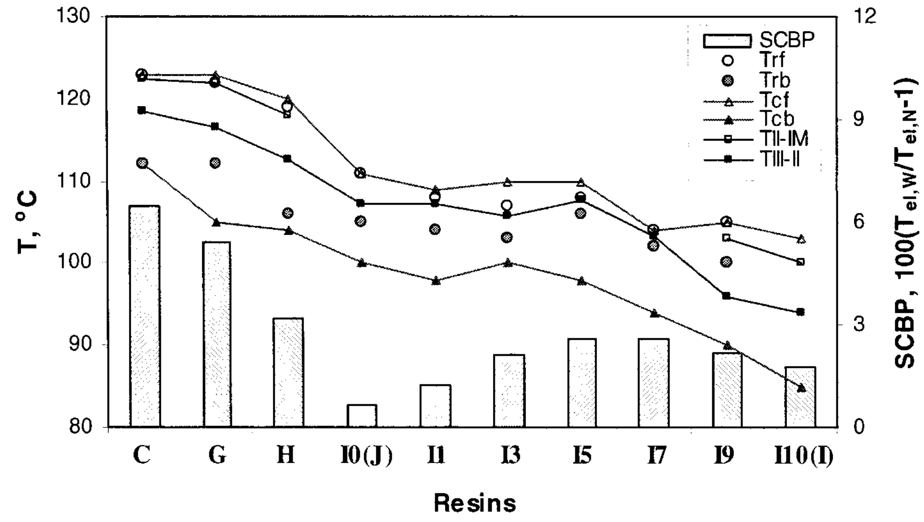

Figure 8-8 Characteristic temperatures and SCBP for different LLDPEs.

T_{rb} and T_{rf} refer to the lowest and highest temperatures, respectively, at which the ring-banded spherulites were observed, under the experimental conditions employed.

T_{cb} and T_{cf} are the lowest and highest experimental crystallization temperatures, respectively.

$T_{II\text{-}IM}$ and $T_{III\text{-}II}$ refer to the regime transition temperatures from regimes II to IM and from regimes III to II, respectively.[5]

SCBP is described by the TREF experimental results, and, $T_{el,W}$ and $T_{el,N}$ are defined as the weight and number average elution temperatures, respectively.[5]

The results indicate that the probability of appearance of ring-banded spherulites in LLDPEs depends on the short chain branching content (SCBC) and short chain branching polydispersity (SCBP). As SCBP increases, the probability increases. For examples, for ZN-LLDPE resin G (SCBC = 15.8/kC, SCBP = 5.42) and m-LLDPE resin J (15.8/kC, 0.64), resin G has a larger crystallization temperature range ($[T_{rb}\text{-}T_{rf}]$ = 10°C = [112-122°C]), in which the ring-banded spherulites are observed, than resin J (6°C = [105-111°C]), because SCBP of resin G is much higher than that in resin J, as can be seen in Figure 8-8. Also, the ring-banded distances of resin G are much larger than those of resin J at the same supercooling degree, Figure 8-9(a). Although ZN-LLDPE resins H (18.9/kC, 3.16), C (18.87/kC, 6.47), and m-LLDPE blend I3 (18.5/kC, 2.13) have similar SCBC, the ring-banded spherulites were observed over the whole experimental crystallization temperature range for resin C ($[T_{rb}\text{-}T_{rf}]/[T_{cb}\text{-}T_{cf}]$ = 11/11 = [112-123°C]/[112-123°C]), a partial range for resin H (13/16 = [106-119°C]/[104-120°C]), and a narrower range for blend I3 (4/10 = [103-107°C]/[100-110°C]). Resin C has the highest SCBP, resin H has an intermediate SCBP, and blend I3 has the lowest polydispersity, as shown in Figure 8-8. Figure 8-9(b) shows that the ring-banded characteristics become more obvious (the ring-banded distance, D_{rb}, increases) as the SCBP increases. However, this tendency is not as large as shown in Figure 8-9(a), possibly, because the SCBC is higher for the materials in Figure 8-9(b) than for those in Figure 8-9(a), and also because the commoners are different for the materials in Figure 8-9(b). The comonomers are butene-1, hexene-1, and octene-1 for resin H, resin C and blend I3, respectively. As the comonomer size decreases, the ring-banded characteristic becomes less obvious (the ring-banded distance, D_{rb}, decreases).

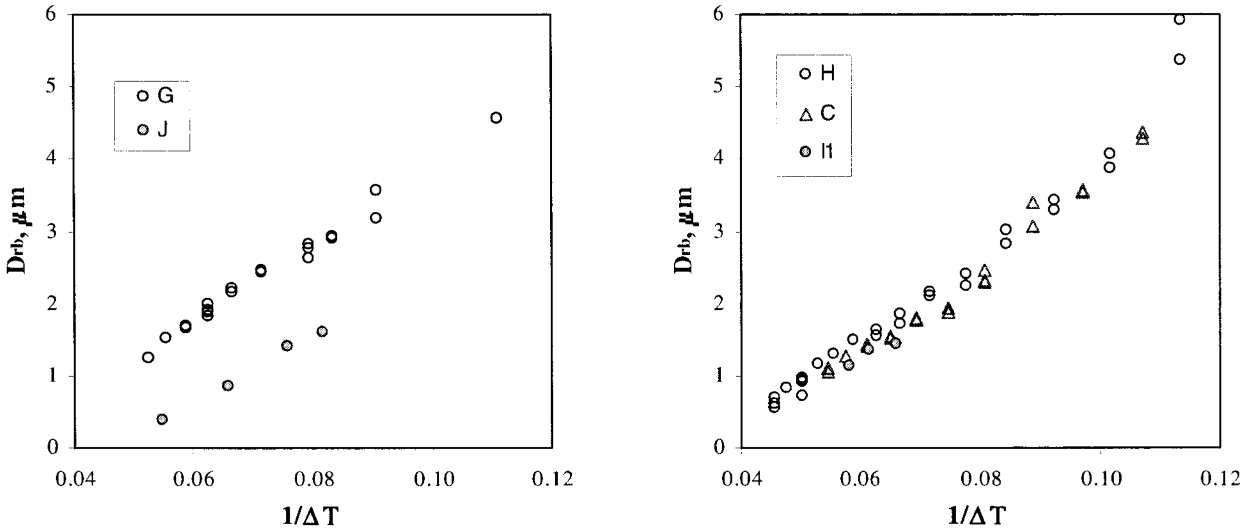

(a) resins G and J (b) resins H, C and blend I1

Figure 8-9 The plots of ring-banded distance versus reciprocal supercooling degree

Figure 8-8 shows that as the SCBC increases, the probability of appearance of the ring-banded spherulites decreases. For example, although the SCBP of m-LLDPE resin I is higher than that of m-LLDPE resin J, the ring-banded spherulites could be observed in resin J but not in resin I. This is because resin I (24.8/kC) has much higher SCBC than resin J (15.4/kC). Furthermore, although m-LLDPE blend I3 and I7 have similar SCBP, blend I3 has a larger crystallization temperature range ($[T_{rb}\text{-}T_{rf}]/[T_{cb}\text{-}T_{cf}]$ = 4/10 = [103-

107°C]/[100-110°C]), in which the ring-banded spherulites could be observed, than blend I7 (2/10 = [102-104°C]/[94-104°C], because blend I7 (22.1/kC) has a higher SCBC than blend I3 (18.5/kC).

8.3.4 Ring-banded distances in different MHL regimes

Eq.(8-1) is used to discuss the ring-banded distance, D_{rb}. Typical experimental results are shown in Figure 8-10 for resin H. In regimes III and II, the measured ring-banded distances can be fitted with one straight line for each individual LLDPE. Thus, the same mechanism seems to be operative for the formation of the ring-banded structure in regimes III and II. However, the data in regime IM deviate from the straight line. The experimental distances observed in regime IM are much higher than those obtained by extrapolation of the straight lines for the material, as can be seen in Figure 8-10. Thus, the ring-banded structure in regime IM appears to follow a different mechanism.

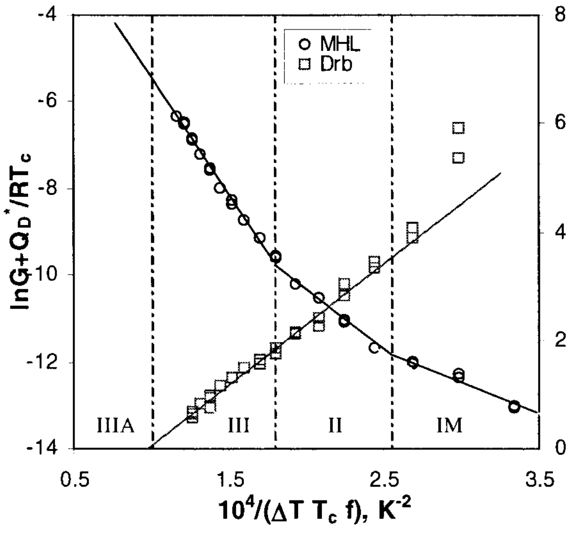

Figure 8-10 The ring-banded distances in the different MHL regimes for resin H

If the straight lines fitted over regimes III and II are extended to $D_{rb}=0$, that is, the start of the no ring-banded spherulite region, the corresponding temperatures can be calculated, and these are shown in Figure 8-11. This temperature is identified as the transition temperature between regime IIIA and normal regime III, $T_{IIIA\text{-}III}$. When the crystallization temperature is below $T_{IIIA\text{-}III}$, the crystalline morphology does not exhibit ring-banded spherulitic structure. In Figure 8-8, some of the lowest crystallization temperatures at which ring-banded structure was observed, T_{rb}, are higher than $T_{IIIA\text{-}III}$, under the experimental conditions employed. In such cases, non-ring-banded structure was observed between $T_{IIIA\text{-}III}$ and T_{rb}. It is possible that under these experimental conditions, there is a transition temperature range in which ring-banded structure develops. Alternatively, the microscope magnification does not provide sufficient resolution to observe the ring-banded behavior.

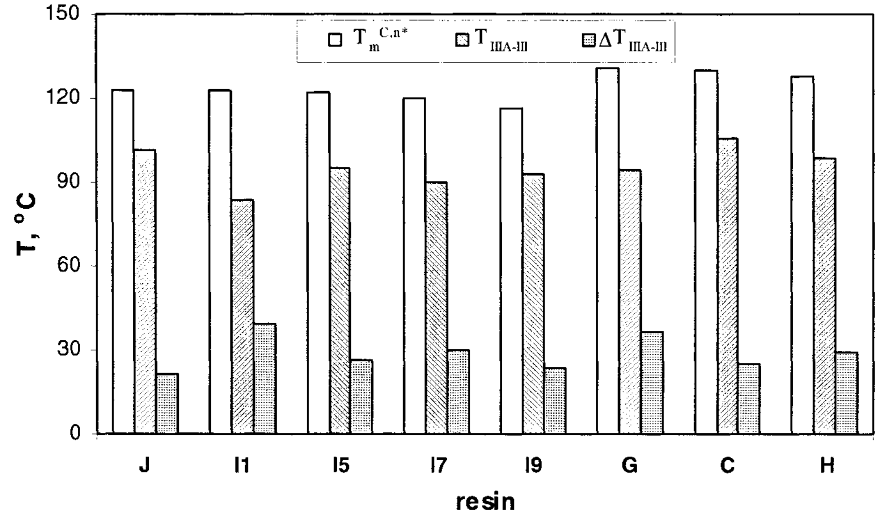

Figure 8-11 The transition temperatures between spherulites without and with ring bands in regime III for some resins, which are deducted from the MHL expression.

8.3.4.1 Twist mechanism in regimes III and II

The regular ring-banded structure, which appears in regimes III and II, might be controlled by the lamellar twist mechanism. If the crystals rotate regularly about an axis orienting along the spherulite radius, the ring-banded spherulites appear.[9,10] The rotation is accompanied by the twist of lamellae along the spherulite radius.[11] The period of the twist (the ring-banded distance) decreases, as the supercooling degree increases (the crystallization temperature decreases)[12] and as the concentration of uncrystallizable part increases.[13] For LLDPE resins, the concentration of the uncrystallizable part depends on the crystallization temperature and the short chain branching characteristics. The concentration of the uncrystallizable part rises, as the crystallization temperature increases and as the SCBC increases.

For polyethylenes, a twisting mechanism, that produces ring-banded structure, occurs only in S- and C-profile lamellae.[11] The basal surfaces in these lamellae provide enough space to hold adjacent folding loops. A flat basal surface can hold the loops, if the folding loops are loose. Thus, it is not necessary to form S- and C-profile lamellae, and no ring-banded structure appears. Furthermore, if the crystal stem size is not uniform in the same crystal lamella, a rough basal surface appears, then, the surface area is possibly sufficient to hold folding loops. Under these conditions, non-ring-banded structure appears.

At low temperature, because the molecular chain mobility is too slow to fold tightly, the secondary nucleation is the sole method for crystal growth. Therefore, ethylene sequences are roughly packed into crystal lattices, with few tight folding loops. No S- and C-lamellae appear, then spherulites without ring bands are observed in regime IIIA, as indicated in Figure 8-10. As the temperature increases, the molecular chain mobility increases, and the part of tightly folding loops increases. Therefore, S- and C-profile lamellae appear, and the ring-banded spherulites are observed. As the temperature increases, so also does the crystal size, and then, the rotation period (ring-banded distance).

The regular tightly folding loops appear only in ethylene sequences. When the folding loops include branches, they cannot fold tightly, but loosely, because branches need more space. As the SCBC increases, the average length of ethylene sequences decreases. When ethylene sequences are not long enough to fold once, no S- and C-profile lamellae can form. Thus, no ring-banded structure appears, as observed in the m-LLDPE resin I. As the SCBP increases, the concentration of long ethylene sequences, possibly also increases. Thus, the content of tightly folding loops increases, and it is more likely to observe ring-banded spherulites.

8.3.4.2 Branching mechanism in regime IM

The rough ring-banded structure in regime IM is different from that in regimes III and II, and possibly relates to the branching mechanism.[14] Lamellar branching appears, only when there is enough free space. The lamellar growth direction is along the radial direction for spherulitic structure. The free space (without lamellae) between lamellae increases, as the spherulitic size increases. If the spherulitic growth rates are the same along all radial direction, the free spaces between lamellae are also the same. Thus, the branching points occur at similar distance from the spherulitic center. Ring-banded-like structure appears. The evolution of the crystallization morphology for resin H in regime IM (at 119°C) is shown in Figure 8-12. In the initial stages, the morphology was irregular; it exhibited some lamellar (bundle) branches, as shown in Figure 8-12(a). As the crystallization time increased, the morphology developed into ring-banded structure, because of the lamellar branching, as shown in Figure 8-2(b). However, because of the concentration fluctuations of crystallizable ethylene sequences in front of the crystals, the regular and concentric ring-banded spherulites are not observed clearly. Also, the typical spherulitic Maltese cross structure is not obvious.

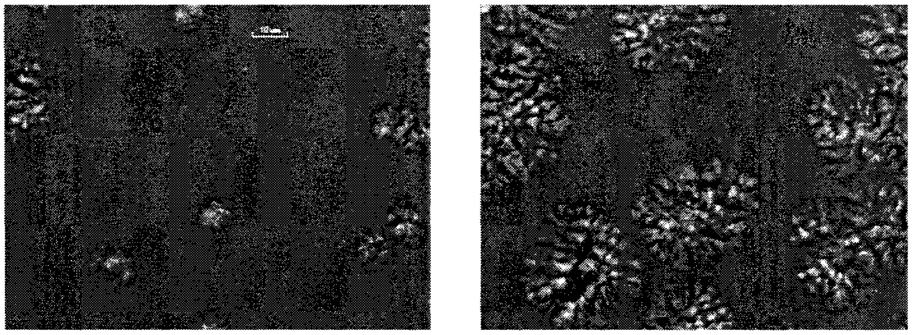
(a) 43min (b) 167min

Figure 8-12 The irregular ring-banded spherulitic morphology in regime IM for resin H at 119°C

8.3.5 The 3-dimensional growth behavior

In regime II, in the early crystallization stage, all spherulites show a regular structure. As the crystallization time increases, some of them become irregular, starting at the centers.

Typical irregular spherulites are shown in Figure 8-13(a) for m-LLDPE resin J at 109.3°C, (b) for ZN-LLDPE resin G at 120°C, and (c) for m-LLDPE blend I1 at 108°C. The irregular spherulites are caused by the 3-D growth characteristics. According to the overall crystallization kinetics for LLDPEs, the Avrami exponent is 2 in regime II.[5] Thus, the growth habit is a 3-dimensional sphere structure.[5,15]

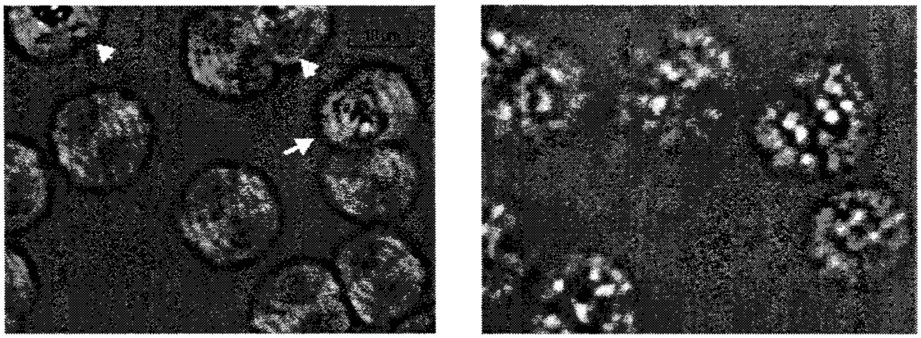

(a) m-LLDPE resin J at 109.3°C (b) ZN-LLDPE resin G at 120°C

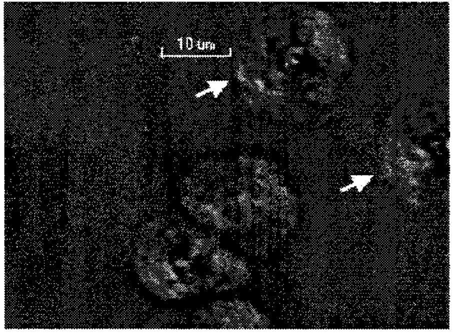

(c) m-LLDPE blend I1 at 108°C

Figure 8-13 3-Dimensional characteristic of spherulites for different types of LLDPEs in regime II

Arrows in (a) and (c) refer to the 3-D irregularized spherulites.

For 2-dimensional spherulitic discs, the thickness along the radial direction is approximately the same. For perfect 3-D spherulites, under 2-D observation, the thickness is the largest at the sphere centers, then it decreases along the radial direction, and becomes the lowest at the spherulite boundary. Under the experimental conditions employed, perfect 3-D spheres could not be formed, because of the restriction due to sample thickness. There was no glass cover on the top of the film samples. Thus, it was possible that the thickness in the whole sample was not uniform, or that the sample surface became rough during the crystallization process. If some spherulites were located in regions with a relatively large thickness, they could grow along the normal direction, as well as along the surface direction, and the 3-D sphere structure would appear. However, Because of the sample thickness restriction, the spheres could not be perfectly formed. Therefore, the typical morphology is as shown in Figure 8-13. The 3-D growth characteristic appears first in the spherulite center, and then extends gradually to the whole spherulite. As sample thickness increases, the number of irregular spherulites increases. No irregular spherulites were produced in the very thin samples sandwiched between the two glass covers. Therefore, the formation of irregular spherulites appears to be related to the 3-D growth behavior.

In order to confirm that the appearance of irregular spherulites is due to 3-D growth behavior rather than to degradation effects, the same samples, which had already shown irregular spherulites and finished crystallization, were subjected to new experiments again, in which the crystallization temperatures were in regime III (without irregular spherulites at all). Their morphological characteristics and growth rates were almost the same as those obtained with fresh specimens. Therefore, under the experimental conditions employed, the specimens did not degrade, and the irregular spherulites that were observed could not be attributed to degradation. The irregular spherulite formation is most likely due to the 3-D growth behavior.

8.4 Conclusions

For the experimental conditions employed, the following crystalline morphologies were observed: spherulites without ring bands, ring-banded spherulites, and irregular structures. The above morphologies were obtained in the low crystallization temperature range of regime IIIA, in the slightly high crystallization temperature range of regime III and in the whole range of regime II, and in regime IM, respectively. The application of Eq.(8-1) seems to indicate accurately the transitions between the above regimes.

The probability of appearance of ring-banded spherulites in LLDPEs increases, as the short chain branching content (SCBC) decreases, and as the short chain branching polydispersity (SCBP) increases. The ring-banded structure follows the lamellar twisting mechanism in regimes III and II, but a lamellar (bundle) branching mechanism is observed in regime IM.

In regime II, some irregular spherulites appear during the crystallization process. This seems to be due to the effect of the 3-dimensional growth behavior, because the crystalline structure follows a spherulite growth habit in this regime, according to the value of the Avrami exponent.

8.5 References

1 Hoffman JD, Miller RL. Polymer 1997, 38:3151.

2 Armistead JP, Hoffman JD. Macromolecules 2002, 35:3895.

3 Flory PJ. Trans Faraday Soc 1955, 51:847.

4 Kamal MR, Feng L, Huang T. Can J Chem Eng 2002, 80:432.

5 Feng L, Kamal MR. Polym Eng Sci 2004, accepted for publication (see Chapter 5 in this thesis).

6 Feng L, Kamal MR. Can J Chem Eng 2004, accepted for publication (see Chapter 3 in this thesis).

7 Mandelkern L, Alamo RG. In: Mark JE. Editor, Physical Properties of Polymers Handbook, American Institute of Physics, New York: Woodbury, 1996 (Chapter11).

8 Fletcher DP, Klein J. Polym Commun 1985, 26:2.

9 Keller A. J Polym Sci 1955, 17:351.

10 Keith HD, Padden Jr. FJ. J Polym Sci 1959, 39:101.

11 Bassett DC, Hodge AM. Polymer 1978, 19:469.

12 Lindenmeyer PH, Holland VF. J Appl Phys 1964, 35:55.

13 Li W, Yan R, Jiang B. Polymer 1992, 33:889.

14 Briber RM, Khoury FJ. Polym Sci, B: Polym Phys 1993, 31:1253.

15 Flory PJ, McIntyre AC. J Polym Sci 1955, 18:592.

Chapter 9

9 General Conclusions, Contributions to Original Knowledge, and Suggestions for Future Work

9.1 General Conclusions

1) A general treatment is proposed leading to a melting temperature equation to calculate melting temperature characteristics of homopolymers and compolymers. The equation provides a basis for the calculation of the melting temperature of crystal stems with the infinite crystal size, $T_m^{C,\infty}$, the melting temperature of crystal stems with the maximum possible size (n^*), $T_m^{C,n*}$, and the melting temperature of crystal stem with the actual crystal size (n), $T_m^{C,n}$, for copolymers with excluded comonomers. It is proposed that $T_m^{C,n*}$ should be the basis for estimating the degrees of supercooling and superheating. With proper assumptions, the equation leads to the Gibbs-Thomson equation for homopolymers and of a modified form of the Gibbs-Thomson equation for copolymers. Experimental data from the literature regarding

the melting behavior of linear low-density polyethylene (LLDPE) confirm the validity of the proposed equation.

2) Using the above melting temperature equation, a calculation method is described to estimate the crystal size number and weight distributions and melting temperature polydispersity from DSC melting traces. The proposed method provides a realistic estimation of crystal size distribution for finite-length crystals, with due consideration to the contribution of the basal surface free energy to the heat of fusion. DSC and SAXS experimental results for different types of polyethylenes, including high-density polyethylene (HDPE), Ziegler-Natta-based LLDPE (ZN-LLDPE), metallocene-based LLDPE (m-LLDPE), and m-LLDPE blend, were analyzed, using the proposed distribution form. The results suggest that the proposed melting temperature equation can be extended to non-homogeneous copolymers with excluded comonomers, by treating them as blends of homogeneous ethylene sequences.

3) A modified form of the Hoffman-Lauritzen (HL) equation is proposed for copolymers by replacing the equilibrium melting temperature, T_m^0, by $T_m^{C,n*}$. The modified Hoffman-Lauritzen equation (MHL) provides satisfactory description of the spherulitic growth kinetics for m-LLDPEs, m-LLDPE blends, and ZN-LLDPEs. The regime behavior was observed and analyzed according to the MHL equation. The application of the MHL equation seems to indicate accurately the transitions between regimes. In addition to regimes III and II, a special regime (regime IM) was observed for ZN-LLDPEs, m-LLDPE resin I, and a m-LLDPE blend. Non-linear growth behavior of spherulites was observed in regimes II and IM.

4) Non-linear growth behavior and morphological characteristics may be explained by the crystallization growth habits and mechanisms indicated by the Avrami exponents, as obtained from bulk crystallization kinetics experiments. The basal surface free energy is strongly dependent on the short chain branching characteristics, as qualitatively indicated by temperature rising elution fractionation (TREF) results.

5) During non-linear growth processes (in regimes II and IM), the concentration of uncrystallizable ethylene sequences (CUCES) in the melt phase increases with time.

The diffusion layer plays an important role at high crystallization temperatures and in polymers with high short chain branching content (SCBC). The reduction of crystallizable ethylene sequences (CES) in the melt phase leads to a lowering of the melting temperature of the crystal stem with the maximum possible length, T_m^{C,n^*}, in the melt phase. An empirical equation is proposed to describe the evolution of T_m^{C,n^*} in the non-linear growth region, when the diffusion layer is not important. The non-linear spherulitic growth crystallization kinetics can be described by the MHL expression by employing a variable T_m^{C,n^*}.

6) The Avrami expression with an effective induction time can explain the overall crystallization kinetics for the three different types of LLDPEs. The Avrami exponents in the regimes III, II, and IM are 2, 1.5, and 1, respectively. The Avrami crystallization rate constants, *K*, are proportional to the linear crystallization rate, *G*. The proportionality constants depend on the crystallization regime. Multiple peaks appear in the melting traces after certain crystallization times at specified isothermal crystallization temperatures. Basically, they can be grouped into the H- and L-peaks. In regime III, a single H-peak seems to correspond to the primary crystallization, i.e., spherulitic crystals, in the initial crystallization stage. The formation of the L-peak is due to secondary crystallization. In regimes II and IM, it is difficult to distinguish the crystals from the primary or secondary crystallization processes. Both the H- and L-peak positions depend on the crystallization temperature and time.

7) The crystalline morphologies show spherulites without ring bands, ring-banded spherulites, and irregular structures. The above morphologies were obtained in the low crystallization temperature range of regime IIIA, in the slightly high crystallization temperature range of regime III and in the whole range of regime II, and in regime IM, respectively. The probability of appearance of ring-banded spherulites in LLDPEs increases, as the short chain branching content (SCBC) decreases, and as the short chain branching polydispersity (SCBP) increases. The ring-banded structure follows the lamellar twisting mechanism in regimes III and II, but a lamellar (bundle) branching mechanism is observed in regime IM.

9.2 Contributions to Original Knowledge

1) An equation is derived and proposed to describe the melting temperature characteristics of homopolymers and copolymers with excluded comonomers. It incorporates the effects of comonomer volume, crystal length, folding surface free energy and enthalpy of fusion.
2) The proposed equation is used, along with melting traces obtained by differential scanning calorimetry (DSC), to estimate the crystal size number distributions.
3) New melting temperature parameters are proposed to relate the melting temperature characteristics to the crystal size number distributions.
4) A modified Hoffman-Lauritzen (MHL) expression is proposed for the linear crystallization kinetics by replacing the equilibrium melting temperature, T_m^0, with the melting temperature of the crystal stem with the maximum possible length, $T_m^{C,n*}$.
5) The MHL expression is used to analyze non-linear growth crystallization kinetics by employing a variable $T_m^{C,n*}$.

9.3 Suggestions for Future Work

1) This research dealt with LLDPE polymers. Theoretical analyses and experimental methods may be modified and expanded for the study of other copolymers with excluded comonomers, such as polypropylene copolymer systems.
2) The proposed melting temperature equation in this study is restricted to copolymers with excluded comonomers. Also, it does not consider the lateral surface free energy. Possible extensions could deal with copolymers having included comonomers and non-lamellar structural crystals.
3) In order to understand the whole crystallization process, the secondary crystallization kinetics needs to be studied in more detail for LLDPE systems.

Bibliography

Abo el Maaty MI, Hosier IL, Bassett DC. "A Unified Context for Spherulitic Growth in Polymers", *Macromolecules*, **1998**, 31(1), 153-157.

Abo el Maaty MI, Bassett DC, Olley RH, Jääskeläinen P. "On Cellulation in Polyethylene Spherulites", *Macromolecules*, **1998**, 31(22), 7800-7805.

Alamo R, Mandelkern L. "Origins of Endothermic Peaks in Differential Scanning Calorimetry", *Journal of Polymer Science, Part B: Polymer Physics*, **1986**, 24(9), 2087-105.

Alamo RG, Mandelkern L. "Thermodynamic and Structural Properties of Ethylene Copolymers", *Macromolecules*, **1989**, 22(3), 1273-7.

Alamo RG, Mandelkern L. "The Crystallization Behavior of Random Copolymers of Ethylene", *Thermochimica Acta*, **1994**, 238(1-2), 155-201.

Alamo RG, Viers BD, Mandelkern L. "Phase Structure of Random Ethylene Copolymers: A Study of Counit Content and Molecular Weight as Independent Variables", *Macromolecules*, **1993**, 26(21), 5740-7.

Alberola N, Cavaille J, Perez J. "Mechanical Spectrometry of Alpha Relaxations of High-Density Polyethylene", *Journal of Polymer Science, Part B: Polymer Physics*, **1990**, 28(4), 569-86.

Alizadeh A, Richardson L, Xu J, McCartney S, Marand H, Cheung W, Chum S. "Influence of Structural and Topological Constraints on the Crystallization and Melting Behavior of Polymers. 1. Ethylene/1-Octene Copolymers", *Macromolecules*, **1999**, 32(19), 6221-6235.

Androsch R, Blackwell J, Chvalun SN, Wunderlich B. "Wide- and Small-Angle X-ray Analysis of Poly(ethylene-co-octene). *Macromolecules*", **1999**, 32(11), 3735-3740.

Androsch R, Wunderlich B. "Analysis of the Degree of Reversibility of Crystallization and Melting in Poly(ethylene-co-1-octene)", *Macromolecules*, **2000**, 33(24), 9076-9089.

Androsch R. "Melting and Crystallization of Poly(ethylene-co-octene) Measured by Modulated DSC and Temperature-Resolved X-ray Diffraction", *Polymer*, **1999**, 40(10), 2805-2812.

Armistead JP, Hoffman JD. "Direct Evidence of Regimes I, II, and III in Linear Polyethylene Fractions As Revealed by Spherulite Growth Rates", *Macromolecules*, **2002**, 35(10), 3895-3913.

Avrami M. "Kinetics of Phase Change. I. General Theory", *Journal of Chemical Physics*, **1939**, 7, 1103-12.

Avrami M. "Kinetics of Phase Change. II. Transformation-Time Relations for Random Distribution of Nuclei", *Journal of Chemical Physics*, **1940**, 8, 212-24.

Avrami M. "Granulation, Phase Change and Microstructure. Kinetics of Phase Change. III." *Journal of Chemical Physics*, **1941**, 9, 177-84.

Bassett DC, Vaughan AS. "On the Lamellar Morphology of Melt-Crystallized Isotactic Polystyrene", *Polymer*, **1985**, 26(5), 717-25.

Bassett DC, Hodge AM. "On Lamellar Organization in Banded Spherulites of Polyethylene", *Polymer*, **1978**, 19(4), 469-72.

Baur H, Baltorowicz M. "Influence of Sequence-Length Distribution on the Melting End Point of Copolymers", *Makromolekulare Chemie*, **1966**, 98 297-301.

Bensason S, Minick J, Moet A, Chum S, Hiltner A, Baer E. "Classification of Homogeneous Ethylene-Octene Copolymers Based on Comonomer Content", *Journal of Polymer Science, Part B: Polymer Physics*, **1996**, 34(7), 1301-15.

Bensason S, Nazarenko S, Chum S, Hiltner A, Baer E. "Blends of Homogeneous Ethylene-Octene Copolymers", *Polymer*, **1997**, 38(14), 3513-20.

Bensason S, Stepanov EV, Chum S, Hiltner A, Baer E. "Deformation of Elastomeric Ethylene-Octene Copolymers", *Macromolecules*, **1997**, 30(8), 2436-44.

Bergmann K, Nawotki K. "New Interpretation of the Broad-Line Nuclear Magnetic Resonance Spectra of Linear Polyethylene", *Kolloid Zeitschrift & Zeitschrift fuer Polymere*, **1967**, 219(2), 132-44.

Blundell DJ. "Models for Small-Angle X-ray Scattering from Highly Dispersed Lamellae", *Polymer*, **1978,** 19(11), 1258-66.

Bodor G, Dalcolmo HJ, Schroter O. "Structural and Property Correlations of Ethylene-α-Olefin Copolymers", *Colloid and Polymer Science*, **1989**, 267(6), 480-93.

Briber RM, Khoury F. "The Morphology of Poly(vinylidene fluoride) Crystallized from Blends of Poly(vinylidene fluoride) and Poly(ethyl acrylate)", *Journal of Polymer Science, Part B: Polymer Physics*, **1993**, 31(10), 1253-72.

Broadhurst MG. Broadhurst, Martin G. "Analysis of the Solid-Phase Behavior of the Normal Paraffins", *Journal of Research of the National Bureau of Standards*, **1962**, A66(3), 241-9.

Bunn CW. "Chemical Crystallography:An Introduction to Optical and X-ray Methods", 2nd ed. Publisher: Clarendon Press (Oxford Press), **1961**.

Clas SD, McFaddin DC, Russell KE, Scammell-Bullock MV, Peat IR. "Melting Points of Homogeneous Random Copolymers of Ethylene and 1-Alkenes", *Journal of Polymer Science, Part A: Polymer Chemistry*, **1987**, 25(11), 3105-15.

Crist B, Claudio ES. "Isothermal Crystallization of Random Ethylene-Butene Copolymers: Bimodal Kinetics", *Macromolecules*, **1999**, 32(26), 8945-51.

Crist B, Howard PR. "Crystallization and Melting of Model Ethylene-Butene Copolymers", *Macromolecules*, **1999**, 32(9), 3057-67.

Crist B, Mirabella FM. "Crystal Thickness Distributions from Melting Homopolymers or Random Copolymers", *Journal of Polymer Science, Part B: Polymer Physics*, **1999**, 37(21), 3131-40.

Crist B, Morosoff N. "Small-Angle X-ray Scattering of Semicrystalline Polymers. II. Analysis of Experimental Scattering Curves", *Journal of Polymer Science, Polymer Physics Edition*, **1973**, 11(6), 1023-45.

Crist B. "Thermodynamics of Statistical Copolymer Melting", *Polymer*, **2003**, 44(16), 4563-72.

Crist B. "Small-Angle X-ray Scattering of Semicrystalline Polymers. I. Existing Models", *Journal of Polymer Science, Polymer Physics Edition*, **1973**, 11(4), 635-61.

Defoor F, Groeninckx G, Reynaers H, Schouterden P, Van der Heijden, B. "Molecular, Thermal, and Morphological Characterization of Narrowly Branched Fractions of 1-Octene Linear Low-Density Polyethylene. 3. Lamellar and Spherulitic Morphology", *Macromolecules*, **1993**, 26(10), 2575-82.

Defoor F, Groeninckx G, Reynaers H, Schouterden P, Van der Heijden, B. "Molecular, Thermal, and Morphological Characterization of Narrowly Branched Fractions of 1-Octene Linear Low-Density Polyethylene. 1. Molecular and Thermal Characterization", *Polymer*, **1992**, 33(18), 3878-83.

Dietz W. Dietz, W. "Spherulitic Growth in Polymers", *Colloid and Polymer Science*, **1981**, 259(4), 413-29.

Eng LM, Fuchs H, Jandt KD, Petermann J. "Chain Folding of Polyethylene Observed by SFM", *Helvetica Physica Acta*, **1992**, 65(6), 870-1.

Evans RD, Mighton HR, Flory PJ. "Crystallization in High Polymers. V. Dependence of Melting Temperatures of Polyesters and Polyamides on Composition and Molecular Weight", *Journal of the American Chemical Society*, **1950**, 72, 2018-27.

Fatou JG, Marc C, Mandelkern L. "The Crystallization Kinetics of Low-Molecular-Weight Polyethylene Fractions", *Polymer*, **1990**, 31(5), 890-8.

Fatou JG, Marc C, Mandelkern L. "The Influence of Molecular Weight on the Regime Crystallization of Linear Polyethylene", *Polymer*, **1990**, 31(9), 1685-93.

Fatou JG. In: Vasile C, Seymour RB. Editors, "Handbook of Polyolefins: Synthesis and Properties", New York: Marcel-Dekker, **1993**.

Feng L, Kamal MR. "Distributions of Crystal Size from DSC Melting Traces for Polyethylenes", *The Canadian Journal of Chemical Engineering* **2004**, accepted for publication. (see Chapter 3 in this thesis).

Feng L, Kamal MR. "Melting Temperature Characteristics for Polyethylenes from Crystal Size Distribution", *Themochimica Acta* **2004**, submitted for publication. (see Chapter 4 in this thesis).

Feng L, Kamal MR. "Spherulitic Crystallization Behavior of Linear Low-Density Polyethylene", *Polymer Engineering and Science* **2004**, accepted for publication. (see Chapter 5 in this thesis).

Feng L, Kamal MR. "Crystallization and Melting Behavior of Homogeneous and Heterogeneous Linear Low-density Polyethylenes", *Polymer Engineering and Science* **2004**, submitted for publication. (see Chapter 7 in this thesis).

Feng L, Kamal MR. "Study on Morphology of Linear Low-Density Polyethylene with Polarized Light Microscopy", *Polymer* **2004**, submitted for publication. (see Chapter 8 in this thesis).

Fletcher DP, Klein J. "Temperature Dependence of the Diffusion Coefficient of Entangled Linear and Star-Branched Polymers", *Polymer Communications*, **1985**, 26(1), 2-4.

Flory PJ. "Thermodynamics of Crystallization in High Polymers. IV. A Theory of Crystalline States and Fusion in Polymers, Copolymers, and Their Mixtures with Diluents", *Journal of Chemical Physics*, **1949**, 17, 223-40.

Flory PJ, Mandelkern L, Hall HK. "Crystallization in High Polymers. VII. Heat of Fusion of Poly-(N,N'-sebacoylpiperazine) and Its Interaction with Diluents", *Journal of the American Chemical Society*, **1951**, 73, 2532-8.

Flory PJ, McIntyre AC. "Mechanism of Crystallization in Polymers", *Journal of Polymer Science*, **1955**, 18, 592-4.

Flory PJ, Vrij A. "Melting Points of Linear-Chain Homologs. The Normal Paraffin Hydrocarbons", *Journal of the American Chemical Society*, **1963**, 85(22), 3548-53.

Flory PJ. "Theory of Crystallization in Copolymers", *Transactions of the Faraday Society*, **1955**, 51, 848-57.

Francuskiewicz F. "Polymer Fractionation", Berlin: Springer-Verlag, **1994**.

Fu Q, Chiu FC, McCreight KW, Guo M, Tseng WW, Cheng SZD, Keating MY, Hsieh ET, DesLauriers PJ. "Effects of the Phase-Separated Melt on Crystallization Behavior and Morphology in Short Chain Branched Metallocene Polyethylenes", *Journal of Macromolecular Science, Physics*, **1997**, B36(1), 41-60.

Goldbeck-Wood G, Sadler DM. "A Rate Theory Model of Copolymer Crystallization", *Polymer Communications*, **1990**, 31(4), 143-6.

Goldbeck-Wood G. "On the Melting-Point Depression of Copolymer Crystals", *Polymer*, **1992**, 33(4), 778-82.

Haudin JM, Monasse E. "Crystallization Mechanisms and Relevant Theories", *NATO Science Series, Series E: Applied Sciences*, **2000**, 370(*Structure Development during Polymer Processing*), 93-112.

Hauser G, Schmidtke J, Strobl GR. "The Role of Co-Units in Polymer Crystallization and Melting: New Insights from Studies on Syndiotactic Poly(propene-co-octene)", *Macromolecules*, **1998**, 31(18), 6250-58.

Heck B, Hugel T, Iijima M, Strobl G. "Steps in the Formation of the Partially Crystalline State", *Polymer*, **2000**, 41(25), 8839-48.

Helfand E, Lauritzen JI. Jr. "Theory of copolymer crystallization", *Macromolecules* **1973**, 6(4), 631-8.

Hoffman JD, Davis GT, Lauritzen JI. In: Hannay NB. Editor, "Treatise on Solid State Chemistry", Vol. 3, New York: Plenum Press, **1976** (Chapter 7).

Hoffman JD, Frolen LJ, Ross GS, Lauritzen JI. "On the Growth Rate of Spherulites and Axialites from the Melt in Polyethylene Fractions: Regime I and Regime II Crystallization", *Journal of Research of the National Bureau of Standards, Section A: Physics and Chemistry*, **1975**, 79A(6), 671-99.

Hoffman JD, Guttman CM, DiMarzio EA. "On the Problem of Crystallization of Polymers from the Melt with Chain Folding", *Faraday Discussions of the Royal Society of Chemistry*, **1979**, Volume Date 1980, 68(Organ. Macromol. Condens. Phase), 177-97.

Hoffman JD, Lauritzen JI. Jr. "Crystallization of Bulk Polymers with Chain Folding: Theory of Growth of Lamellar Spherulites. *Journal of Research of the National Bureau of Standards*, **1961**, 65A 297-336.

Hoffman JD, Miller RL. "Test of the Reptation Concept: Crystal Growth Rate as a Function of Molecular Weight in Polyethylene Crystallized from the Melt", *Macromolecules*, **1988**, 21(10), 3038-51.

Hoffman JD, Miller RL. "Test of the Reptation Concept: Crystal Growth Rate as a Function of Molecular Weight in Polyethylene Crystallized from the Melt [Erratum to Document Cited in CA109(20):171221w]", *Macromolecules*, **1990**, 23(14), 3544.

Hoffman JD, Miller RL. "Kinetics of Crystallization from the Melt and Chain Folding in Polyethylene Fractions Revisited: Theory and Experiment", *Polymer*, **1997**, 38(13), 3151-3212.

Hoffman JD, Weeks JJ. "Rate of Spherulitic Crystallization with Chain Folds in Polychlorotrifluoroethylene", *Journal of Chemical Physics*, **1962**, 37, 1723-41.

Hoffman JD, Weeks JJ. "Melting Process and Equilibrium Melting Temperature of Poly(chlorotrifluoroethylene)", *Journal of Research of the National Bureau of Standards*, **1962**, 66A(1), 13-28.

Hoffman JD. "Regime III Crystallization in Melt-Crystallized Polymers: the Variable Cluster Model of Chain Folding", *Polymer*, **1983**, 24(1), 3-26.

Hoffman JD. "Transition from Extended-Chain to Once-Folded Behaviour in Pure n-Paraffins Crystallized from the Melt", *Polymer*, **1991**, 32(15), 2828-41.

Hosoda S, Kojima K, Furuta M. "Morphological Study of Melt-Crystallized Linear Low-Density Polyethylene by Transmission Electron Microscopy", *Makromolekulare Chemie*, **1986**, 187(6), 1501-14.

Hosoda S. "Structural Distribution of Linear Low-Density Polyethylenes", *Polymer Journal (Tokyo, Japan)*, **1988**, 20(5), 383-97.

Huang J, Prasad A, Marand H. "Study of the Temperature Dependence of Isothermal Spherulitic Growth Rate Data for Poly(pivalolactone) in Blends with Poly(vinylidene fluoride): A Link between Coherent Secondary Nucleation Theory and Mixing Thermodynamics", *Polymer*, **1994**, 35(9), 1896-908.

Illers KH. "Degradation of Melt-Crystallized Polyethylene by Nitric Acid", *Makromolekulare Chemie*, **1968**, 118 88-127.

Imuta J, Kashiwa N. In: Vasile, C. Editor, "Handbook of Polyolefins", New York: Marcel-Dekker Press, **2000**, p.71-88.

Jackson JF, Mandelkern L, Long OC. "Solubility of Crystalline Polymers. I. Polyethylene Fractions Crystallized in Bulk", *Macromolecules*, **1968**, 1(3), 218-23.

Jackson JF, Mandelkern L. "Solubility of Crystalline Polymers. II. Polyethylene Fractions Crystallized from Dilute Solutions", *Macromolecules*, **1968**, 1(6), 546-54.

Jandt KD, Buhk M, Miles MJ. Petermann J. "Shish-Kebab Crystals in Polyethylene Investigated by Scanning Force Microscopy", *Polymer*, **1994**, 35(11), 2458-62.

Janeschitz-Kriegl H, Fleischmann E, Geymayer W. In: Karger-Kocsis I. Editor, "Polypropylene: Structure, Blends, and Compositions", London: Chapman and Hall, **1995** (Chapter1).

Jokela K, Väänänen A, Torkkeli M, Starck P, Serimaa R, Löfgren B, Seppälä J. "Differential Scanning Calorimetry, Small-Angle X-ray Scattering, and Wide-Angle X-ray Scattering on Homogeneous and Heterogeneous Ethylene-α-Copolymers", *Journal of Polymer Science, Part B: Polymer Physics*, **2001**, 39(16), 1860-1875.

Kamal MR, Feng L, Huang T. "A Generalized Equation for the Prediction of Melting Temperatures of Homopolymers and Copolymers", *The Canadian Journal of Chemical Engineering*, **2002**, 80(3), 432-442.

Kamal MR, Feng L. "Non-linear Crystalline Spherulitic Growth Behavior for Linear Low-Density Polyethylene", *International Polymer Processing* **2004**, accepted for publication. (see Chapter 6 in this thesis).

Kamide K, Ohno K, Kawai T. "Equilibrium Melting Temperature of Polyethylene with Finite Chain Length", *Makromolekulare Chemie*, **1970**, 37, 1-7

Keller A. "Spherulitic Structure of Crystalline Polymers. II. The Problem of Molecular Orientation in Polymer Spherulites", *Journal of Polymer Science*, **1955**, 17 351-64.

Keith HD, Padden FJ. "A Phenomenological Theory of Spherulitic Crystallization", *Journal of Applied Physics*, **1963**, 34(8), 2409-21.

Keith HD, Padden FJ. Jr. "Spherulitic Crystallization from the Melt. II. Influence of Fractionation and Impurity Segregation on the Kinetics of Crystallization", *Journal of Applied Physics*, **1964**, 35(4), 1286-96.

Keith HD, Padden FJ., Jr. "The Optical Behavior of Spherulites in Crystalline Polymers. I. Calculation of Theoretical Extinction Patterns in Spherulites with Twisting Crystalline Orientation", *Journal of Polymer Science*, **1959**, 39, 101-22.

Keresztury G, Földes E. "On the Raman Spectroscopic Determination of Phase Distribution in Polyethylene", *Polymer Testing*, **1990**, 9(5), 329-39.

Kim MH, Phillips PJ, Lin JS. "The Equilibrium Melting Points of Random Ethylene-Octene Copolymers: A Test of the Flory and Sanchez-Eby Theories", *Journal of Polymer Science, Part B: Polymer Physics*, **2000**, 38(1), 154-170.

Kim MH, Phillips PJ. "Nonisothermal Melting and Crystallization Studies of Homogeneous Ethylene/α-Olefin Random Copolymers", *Journal of Applied Polymer Science*, **1998**, 70(10), 1893-1905.

Kim SP, Kim SC. "Crystallization Kinetics of Poly(ethylene terephthalate). Part I. Kinetic Equation with Variable Growth Rate", *Polymer Engineering and Science*, **1991**, 31(2), 110-15.

Kuwabara K, Kaji H, Horii F, Bassett DC, Olley RH. "Solid-State 13c Nmr Analyses of the Crystalline-Noncrystalline Structure for Metallocene-Catalyzed Linear Low-Density Polyethylene", *Macromolecules*, **1997**, 30(24), 7516-21.

Lambert WS, Phillips PJ. "Crystallization Kinetics of Low Molecular Weight Fractions of Branched Polyethylenes", *Macromolecules*, **1994**, 27(13), 3537-42.

Lambert WS, Phillips PJ. "Crystallization Kinetics of Fractions of Branched Polyethylenes: 2. Effect of Molecular Weight", *Polymer*, **1996**, 37(16), 3585-91.

Lauritzen JI, Hoffman JD. "Extension of Theory of Growth of Chain-Folded Polymer Crystals to Large Undercoolings", *Journal of Applied Physics*, **1973**, 44(10), 4340-52.

Lauritzen JI. Jr., Hoffman JD. "Theory of Formation of Polymer Crystals with Folded Chains in Dilute Solution", *Journal of Research of the National Bureau of Standards*, **1960**, 64A(1), 73-102.

Lee YD, Phillips PJ, Lin JS. "The Influence of Crystallinity Distribution on Small-Angle X-ray Scattering from Semicrystalline Polymers", *Journal of Polymer Science, Part B: Polymer Physics*, **1991**, 29(10), 1235-54.

Li W, Yan R, Jiang B. "The Ring-Banded Spherulite Structure of Poly(ε-Caprolactone) in Its Miscible Mixtures with Poly(Styrene-Co-Acrylonitrile)", *Polymer*, **1992**, 33(4), 889-92.

Lindenmeyer PH, Holland VF. "Relationship between Molecular Weight, Radial-Growth Rate, and the Width of the Extinction Bands in Polyethylene Spherulites", *Journal of Applied Physics*, **1964**, 35(1), 55-8.

Lovinger AJ, Davis DD, Padden FJ. Jr. "Kinetic Analysis of the Crystallization of Poly(p-phenylene sulfide)", *Polymer*, **1985**, 26(11), 1595-604.

Lu L, Alamo RG, Mandelkern L. "Lamellar Thickness Distribution in Linear Polyethylene and Ethylene Copolymers", *Macromolecules*, **1994**, 27(22), 6571-6.

Maderek E, Strobl GR. "Crystallization and Melting Behavior of Fractions of Branched Polyethylene. 1. Preparation and Characterization of Fractions", *Makromolekulare Chemie*, **1983**, 184(12), 2553-61.

Maderek E, Strobl GR. "Crystallization and Melting Behavior of Fractions of Branched Polyethylene. II. Dilatometric and Small Angle X-ray Scattering Study on the Molecular Weight Dependence of Isothermal Crystallization", *Colloid and Polymer Science*, **1983**, 261(6), 471-6.

Malkin AY, Beghishev VP, Kipin IA, Bolgov SA. "General Treatment of Polymer Crystallization Kinetics. Part 1. A New Macrokinetic Equation and Its Experimental Verification", *Polymer Engineering and Science*, **1984**, 24(18), 1396-401.

Malkin AY, Beghishev VP, Kipin IA, Andrianova ZS. "General Treatment of Polymer Crystallization Kinetics. Part 2. The Kinetics of Nonisothermal Crystallization", *Polymer Engineering and Science*, **1984**, 24(18), 1402-8.

Mandelkern L, Alamo RG. In: Mark JE. Editor, "Physical Properties of Polymers Handbook", American Institute of Physics, New York: Woodbury, **1996** (Chapter11).

Mandelkern L, Flory PJ. "Melting and Glassy-State Transitions in Cellulose Esters and Their Mixtures with Diluents", *Journal of the American Chemical Society*, **1951**, 73, 3206-12.

Mandelkern L, Stack GM. "Equilibrium Melting Temperature of Long-Chain Molecules", *Macromolecules*, **1984**, 17(4), 871-8.

Mandelkern L. "Crystallization of Polymers", New York: McGraw-Hill, **1964**.

Mandelkern L. "Crystallization Kinetics in High Polymers. II. Polymerdiluent Mixtures", *Journal of Applied Physics*, **1955**, 26, 443-51.

Marega C, Marigo A, Cingano G, Zannetti R, Paganetto G. "Small-Angle X-ray Scattering from High-Density Polyethylene: Lamellar Thickness Distributions", *Polymer*, **1996**, 37(25), 5549-57.

Marigo A, Zannetti R, Milani F. "A Small- And Wide-Angle X-ray Scattering Study of 1-Butene LLDPE Obtained by Metallocene and Ziegler-Natta Catalysis", *European Polymer Journal*, **1997**, 33(5), 595-8.

Mathot VBF. In: Mathot VBF. Editor, "Calorimetry and Thermal Analysis of Polymers", New York: Hanser Publishers, **1994** (Chapter 9).

Mathot VBF, Pijpers MFJ. "Molecular Structure, Melting Behavior, and Crystallinity of 1-Octene-Based Very Low Density Polyethylenes (VLDPEs) as Studied by Fractionation and Heat Capacity Measurements with DSC", *Journal of Applied Polymer Science*, **1990**, 39(4), 979-94.

McFaddin DC, Russell KE, Wu G, Heyding RD. "Characterization of Polyethylenes by X-ray Diffraction and Carbon-13 NMR: Temperature Studies and the Nature of the Amorphous Halo", *Journal of Polymer Science, Part B: Polymer Physics*, **1993**, 31(2), 175-83.

McMaster TJ, Hobbs JK, Barham PJ, Miles MJ. "AFM Study of In Situ Real Time Polymer Crystallization and Spherulite Structure", *Probe Microscopy*, **1997**, 1(1), 43-56.

Minick J, Moet A, Hiltner A, Baer E, Chum SPJ. "Crystallization of Very Low Density Copolymers of Ethylene With α-Olefins", *Journal of Applied Polymer Science*, **1995**, 58(8), 1371-84.

Mirabella FM. "Correlation of the Melting Behavior and Copolymer Composition Distribution of Ziegler-Natta-Catalyst and Single-Site-Catalyst Polyethylene Copolymers", *Journal of Polymer Science, Part B: Polymer Physics*, **2001**, 39(22), 2800-18.

Mirabella FM. "Crystallization and Melting of Narrow Composition Distribution Polyethylenes: Investigation and Implications of Crystal Thickening", *Journal of Polymer Science, Part B: Polymer Physics*, **2003**, 41(3), 235-46.

Mizushima S, Shimanouchi T. "Raman Frequencies of n-Paraffin Molecules", *Journal of the American Chemical Society*, **1949**, 71, 1320-4.

Monrabal B. "Crystallization Analysis Fractionation: A New Technique for the Analysis of Branching Distribution in Polyolefins", *Journal of Applied Polymer Science*, **1994**, 52(4), 491-9.

Muller AJ, Hernandez ZH, Arnal ML, Sanchez JJ. "Successive Self-Nucleation/Annealing (Ssa). A Novel Technique to Study Molecular Segregation during Crystallization", *Polymer Bulletin (Berlin)*, **1997**, 39(4), 465-72.

Nakamura K, Watanabe T, Katayama K. Amano T. "Nonisothermal Crystallization of Polymers. I. Relation between Crystallization Temperature, Crystallinity, and Cooling Conditions", *Journal of Applied Polymer Science*, **1972**, 16(5), 1077-91.

Okada T, Saito H, Inoue T. "Nonlinear Crystal Growth in the Mixture of Isotactic Polypropylene and Liquid Paraffin", *Macromolecules*, **1990**, 23(16), 3865-8.

Okada T, Saito H, Inoue T. "Kinetics of Crystal Growth in Mixtures of Isotactic Polypropylene and Liquid Paraffin", *Polymer*, **1993**, 34(22), 4752-5.

Okada T, Saito H, Inoue T. "Kinetic Studies of Crystallization in Mixtures of Isotactic Polystyrene and Atactic Polystyrene", *Polymer*, **1994**, 35(26), 5699-705.

Ozawa T. "Kinetics of Nonisothermal Crystallization", *Polymer*, **1971**, 12(3), 150-8.

Peacock AJ. "Handbook of Polyethylene: Structures, Properties, and Applications", New York: Maecel-Dekker Press, **2000**.

Peeters M, Goderis B, Vonk C, Reynaers H, Mathot V. "Morphology of Homogeneous Copolymers of Ethene and 1-Octene. I. Influence of Thermal History on Morphology", *Journal of Polymer Science, Part B: Polymer Physics*, **1997**, 35(16), 2689-713.

Peeters M, Goderis B, Reynaers H, Mathot V. "Morphology of Homogeneous Copolymers of Ethene and 1-Octene. II. Structural Changes on Annealing". *Journal of Polymer Science, Part B: Polymer Physics*, **1999**, 37(1), 83-100.

Phillips PJ, Vatansever N. "Regime Transitions in Fractions of Cis-Polyisoprene", *Macromolecules*, **1987**, 20(9), 2138-46.

Phillips PJ. "Polymer Crystallization: the Third Regime", *Polymer Preprints (American Chemical Society, Division of Polymer Chemistry)*, **1979**, 20(2), 483-6.

Plummer CJG, Kausch HH. "The Effect of Melting Point Distributions on DSC Melting Peaks", *Polymer Bulletin (Berlin)*, **1996**, 36(3), 355-60.

Plummer CJG, Kausch HH. "Lattice Imaging of Friction Deposited PTFE Films", *Polymer Bulletin (Berlin)*, **1996**, 37(3), 393-397.

Randall JC. "A Review of High-Resolution Liquid Carbon-13 Nuclear Magnetic Resonance Characterizations of Ethylene-Based Polymers", *Journal of Macromolecular Science, Reviews in Macromolecular Chemistry and Physics*, **1989**, C29(2-3), 201-317.

Richardson MT, Flory PJ, Jackson JB. "Crystallization and Melting of Copolymers of Polymethylene", *Polymer*, **1963**, 4(2), 221-36.

Rodriguez-Arnold J, Bu Z, Cheng SZD, Hsieh ET, Johnson TW, Geerts RG, Palackal SJ, Hawley GR, Welch MB. "Crystallization, Melting and Morphology of Syndiotactic Polypropylene Fractions. 2. Linear Crystal Growth Rate and Crystal Morphology", *Polymer*, **1994**, 35(24), 5194-201.

Sadler DM, Gilmer GH. "Rate-Theory Model of Polymer Crystallization", *Physical Review Letters*, **1986**, 56(25), 2708-11.

Saito H, Okada T, Hamane T, Inoue T. "Crystallization Kinetics in the Mixtures of Poly(vinylidene fluoride) and Poly(methyl methacrylate): Two-Step Diffusion Mechanis", *Macromolecules*, **1991**, 24(15), 4446-9.

Sanchez IC, Eby RK. "Thermodynamics and Crystallization of Random Copolymers", *Macromolecules*, **1975**, 8(5), 638-41.

Schouterden P, Groeninckx G, Van der Heijden B, Jansen F. "Fractionation and Thermal Behavior of Linear Low Density Polyethylene", *Polymer*, **1987**, 28(12), 2099-104.

Schultz JM. "Polymer Crystallization: the Development of Crystalline Order in Thermoplastic Polymers", Oxford, New York: Oxford University Press, **2001**.

Schultz JM. "Polymer Materials Science", Englewood Cliffs, NJ: Prentice Hall, **1974**.

Sehanobish K, Patel RM, Croft BA, Chum SP, Kao CI. "Effect of Chain Microstructure on Modulus Of Ethylene-α-Olefin Copolymers", *Journal of Applied Polymer Science*, **1994**, 51(5), 887-94.

Svergun DI, Feigin LA. "X-ray and Neutron Low-Angle Scattering", New York: Plenum Press, **1987**.

Snyder RG, Scherer JR. "Interpretation of Longitudinal-Acoustical-Mode Spectra of Polymers", *Journal of Polymer Science, Polymer Physics Edition*, **1980**, 18(3), 421-8.

Snyder RG, Schlotter NE, Alamo R, Mandelkern L. "Observation of a Conformationally Liquid-Like Component in Crystalline Polyethylene by Raman Spectroscopy", *Macromolecules*, **1986**, 19(3), 621-6.

Soares JBP. "Mathematical Modelling of the Microstructure of Polyolefins Made by Coordination Polymerization: A Review", *Chemical Engineering Science*, **2001**, 56(13), 4131-4153.

Stack GM, Mandelkern L, Kröhnke C, Wegner G. "Melting and Crystallization Kinetics of a High Molecular Weight n-Alkane: C192H386", *Macromolecules*, **1989**, 22(11), 4351-61.

Strobl GR, Hagedorn W. "Raman Spectroscopic Method for Determining the Crystallinity of Polyethylene", *Journal of Polymer Science, Polymer Physics Edition*, **1978**, 16(7), 1181-93.

Svergun DI, Feigin LA. "X-ray and Neutron Low-Angle Scattering", New York: Plenum Press, **1987**.

Tobin MC. "Theory of Phase Transition Kinetics with Growth Site Impingement. I. Homogeneous Nucleation", *Journal of Polymer Science, Polymer Physics Edition*, **1974**, 12(2), 399-406.

Tobin MC. "The Theory of Phase Transition Kinetics with Growth Site Impingement. II. Heterogeneous Nucleation", *Journal of Polymer Science, Polymer Physics Edition*, **1976**, 14(12), 2253-7.

Tobin MC. "Theory of Phase Transition Kinetics with Growth Site Impingement. III. Mixed Heterogeneous-Homogeneous Nucleation and Nonintegral Exponents of the Time". *Journal of Polymer Science, Polymer Physics Edition*, **1977**, 15(12), 2269-70.

Tung LH. "Recording Microdilatometer for the Measurement of Polymer Crystallization Rates". *Journal of Polymer Science, Polymer Physics Edition,* **1967**, 5(1), 391-3.

Turner-Jones A, Aizlewood JM, Beckett DR. "Crystalline Forms of Isotactic Polypropylene", *Makromolekulare Chemie*, **1964**, 75 134-58.

Wagner J, Phillips PJ. "The Mechanism of Crystallization of Linear Polyethylene, and Its Copolymers with Octene, over a Wide Range of Supercoolings", *Polymer*, **2001**, 42(21), 8999-9013.

Varga J. "Supermolecular Structure of Isotactic Polypropylene", *Journal of Materials Science*, **1992**, 27(10), 2557-79.

Villarreal N, Pastor JM, Perera R, Rosales C, Merino JC. "Use of the Raman-Active Longitudinal Acoustic Mode in the Characterization of Reactively Extruded Polyethylenes", *Macromolecular Chemistry and Physics*, **2002**, 203(1), 238-44.

Voigt-Martin IG, Alamo R, Mandelkern L. "A Quantitative Electron Microscopic Study of the Crystalline Structure of Ethylene Copolymers", *Journal of Polymer Science, Part B: Polymer Physics*, **1986**, 24(6), 1283-302.

Voigt-Martin IG, Mandelkern L. "A Quantitative Electron Microscopic Study of the Crystallite Structure of Molecular Weight Fractions of Linear Polyethylene", *Journal of Polymer Science, Polymer Physics Edition*, **1984**, 22(11), 1901-17.

Wendling J, Suter UW. "A New Model Describing the Cocrystallization Behavior of Random Copolymers", *Macromolecules*, **1998**, 31(8), 2516-2520.

Wilfong DL, Knight GW. "Crystallization Mechanisms for LLDPE and Its Fractions", *Journal of Polymer Science, Part B: Polymer Physics*, **1990**, 28(6), 861-70.

Wild L, Ryle T, Knobeloch D, Peat I. "Determination of Branching Distributions in Polyethylene and Ethylene Copolymers", *Journal of Polymer Science, Polymer Physics Edition*, **1982**, 20(3), 441-55.

Wlochowicz A, Eder M. "Distribution of Lamella Thicknesses in Isothermally Crystallized Polypropylene and Polyethylene by Differential Scanning Calorimetry", *Polymer*, **1984**, 25(9), 1268-70.

Wu L, Lisowski M, Talibuddin S, Runt J. "Crystallization of Poly(ethylene oxide) and Melt-Miscible PEO Blends", *Macromolecules*, **1999**, 32(5), 1576-1581.

Wunderlich B, Czornyj G. "A Study of Equilibrium Melting of Polyethylene", *Macromolecules*, **1977**, 10(5), 906-13.

Wunderlich B. "Macromolecular Physics", Vol.3. London: Academic Press, **1980**.

Wunderlich B. "Thermal Analysis of Materials", downloadable: http://web.utk.edu/~athas/courses/ tham99.html

Zhang M, Lynch DT, Wanke SE. "Effect of Molecular Structure Distribution on Melting and Crystallization Behavior of 1-Butene/Ethylene Copolymers", *Polymer*, **2001**, 42(7), 3067-75.

Zhou H, Wilkes GL. "Comparison of Lamellar Thickness and Its Distribution Determined from DSC, SAXS, TEM and AFM for High-Density Polyethylene Films Having a Stacked Lamellar Morphology", *Polymer*, **1997**, 38(23), 5735-47.

Ziabicki A. "An Approximate Theory of Nonisothermal Crystallization of Polymers", *Polimery (Warsaw, Poland)*, **1967**, 12(9), 405-10.

Appendix

GPC and TREF Traces for Blends of Resins I and J

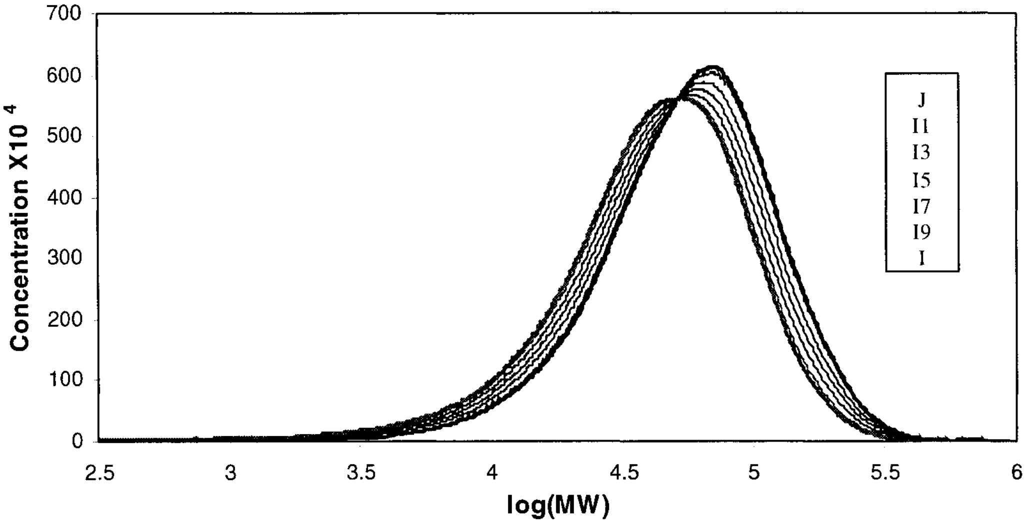

Figure Appendix-1 GPC results of blends of resins I and J

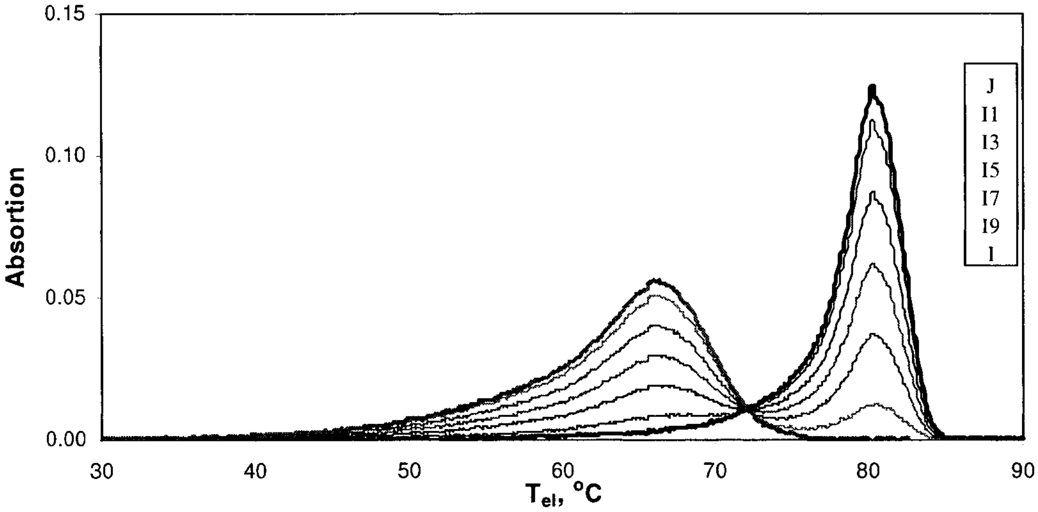

Figure Appendix-2 TREF results of blends of resins I and J